KATHOLIEKE UNIVERSITEIT LEUVEN
FACULTEIT INGENIEURSWETENSCHAPPEN
DEPARTEMENT ELEKTROTECHNIEK
Kasteelpark Arenberg 10, 3001 Leuven (Heverlee)

TRANSMISSION OVER TIME- AND FREQUENCY-SELECTIVE MOBILE WIRELESS CHANNELS

Promotor:
Prof. dr. ir. M. Moonen

Proefschrift voorgedragen tot
het behalen van het doctoraat
in de ingenieurswetenschappen

door

Imad BARHUMI

SEPTEMBER 2005

KATHOLIEKE UNIVERSITEIT LEUVEN
FACULTEIT INGENIEURSWETENSCHAPPEN
DEPARTEMENT ELEKTROTECHNIEK
Kasteelpark Arenberg 10, 3001 Leuven (Heverlee)

TRANSMISSION OVER TIME- AND FREQUENCY-SELECTIVE MOBILE WIRELESS CHANNELS

Jury:
Prof. dr. ir. G. De Roeck, voorzitter
Prof. dr. ir. M. Moonen, promotor
Prof. dr. ir. G. Leus (TU Delft, The Netherlands)
Prof. dr. ir. J. Vandewalle
Prof. dr. ir. G. Gielen
Prof. dr. ir. D. Slock (Institut Eurécom, France)
Prof. dr. ir. M. Moeneclaey (U. Gent)

Proefschrift voorgedragen tot
het behalen van het doctoraat
in de ingenieurswetenschappen

door

Imad BARHUMI

U.D.C. 654.185 SEPTEMBER 2005

D/2005/7515/69

ISBN 90-5682-635-2

DEDICATION

I dedicate this work to my parents
and
to my daughter Ahlam

Acknowledgment

I would like to thank and express my sincere gratitude to all of those who helped me during the PhD journey. Your help made this work possible.

First of all, I would like to thank Prof. Marc Moonen for giving me the opportunity to join his group, for his continuous encouragement, support and for his insightful comments. You have been a great supervisor.

This work would not have been possible without a close collaboration with Prof. Geert Leus. Thank you Geert for sharing your knowledge, for your constructive comments, and for teaching me many of the algebra and matrix tricks. I have learned a lot from you. Thank you also for the nice moments we had together and the nice lunches in via-via. You have been a great friend as well.

I would like to thank the reading committee: Prof Joos Vandewalle, and Prof. Georges Geilen, for their effort and time they invested in proofreading this text. Your comments have added a lot to the final version of the text. I would also like to thank the jury members: Prof. Dirk Slock, Marc Moeneclay, and the chairman Prof. Guido De Roeck. Thank you for agreeing to be on the board of examiners.

To the group at the Katholieke Universtiet Leuven: Hilde Vanhaute, Olivier Rousseux, Raphael Cendrillon, Thomas Klassen, Geert van Meerbergen, Gert Cypers, Koen Van Bleu, Geert Ysebeart, Toon van Waterschoot, Ann Spriet, Geert Rombouts, Simon Doclo, Vincent Lenir, Jan Vangorp, Paschalis Tsiaflakis, Deepak Tandoor, and Matteo Montani. Thank you for the nice memories we had during my PhD journey.

To the Palestinian and Arab friends: Jehad Najjar, Mohammed Benkhedir, Mohammad Saleh, Ahmed Alabadelah, Nurhan Abujidi, Noureddin Moussaif, Ali Jaffari, Mahmoud Barham, and Mazen Al-Shaer. Thank you for your support, for the nice activities and the nice memories we had in Belgium. Your friendship has made life abroad a lot easier.

To the Palestinian European Academic Cooperation in Education (PEACE) programme for their partial financial support of the first 4 years of my PhD.

To my parents and to my sister, thank you for every thing. For your support and the unconditioned love you have given me all over the years. I love you very much.

At last but not least, to my wife, thank you for your patience, for your support and for your enthusiasm.

Abstract

THE wireless communication industry has experienced rapid growth in recent years, and digital cellular systems are currently designed to provide high data rates at high terminal speeds. High data rates give rise to intersymbol interference (ISI) due to so-called multipath fading. Such an ISI channel is called *frequency-selective*. On the other hand, due to terminal mobility and/or receiver frequency offset the received signal is subject to frequency shifts (Doppler shifts). Doppler shift induces *time-selectivity* characteristics. The Doppler effect in conjunction with ISI gives rise to a so-called *doubly selective* channel (frequency- and time-selective). In addition to the channel effects, the analog front-end may suffer from an imbalance between the I and Q branch amplitudes and phases as well as from carrier frequency offset. These analog front-end imperfections then result in an additional and significant degradation in system performance, especially in multi-carrier based transmission techniques.

In this thesis, novel channel estimation and equalization techniques are devised to combat the doubly selective channel effects. Single carrier (SC) transmission techniques and orthogonal frequency division multiplexing (OFDM) transmission techniques are considered.

In the context of *SC transmission*, a set of linear and decision feedback time-varying finite impulse response (FIR) equalizers are proposed to overcome the doubly selective channel effects. The basis expansion model (BEM) is used to approximate the doubly selective channel and to model the time-varying FIR equalizers. By doing so, a complicated time-varying 1-D deconvolution problem is turned into a simpler time-invariant (TI) 2-D deconvolution problem in the TI coefficients of the channel BEM and the time-varying FIR equalizer BEM coefficients. The design criteria considered in this context are the Zero-Forcing (ZF) and the Minimum Mean-Square Error (MMSE) criterion. It is shown that the ZF solution exists when the system has a number of receive antennas equal to the number of transmit antennas plus at least one. Using the MMSE criterion, on the other hand, the time-varying FIR equalizer always exists for any number of receive antennas. This approach is shown to unify and extend the previously proposed equalization techniques for TI channels.

So far, in this approach the doubly selective channel is assumed to be known at the receiver, which is far from practical. To facilitate practical scenarios, channel estimation and direct equalization techniques are also investigated. The proposed techniques range from pilot symbol assisted modulation based techniques to blind and semi-blind techniques.

For *OFDM transmission*, a set of time-domain and frequency domain equalization techniques are proposed. In addition to assuming the channel is rapidly time-varying, the so-called cyclic prefix (CP) length is assumed to be shorter than the channel impulse response length. This assumption introduces interblock interference (IBI), which in conjunction with the Doppler shift induces severe intercarrier interference (ICI). Time-domain equalizers (TEQs) are then needed to shorten the channel to fit within the CP length and to eliminate the channel time-variation. Doing so the TEQ is capable of restoring orthogonality between subcarriers. While the TEQ optimizes the performance on all subcarriers in a joint fashion, an optimal frequency-domain per-tone equalizer (PTEQ), that optimizes the performance on each subcarrier separately, can also be obtained by transferring the TEQ operation to the frequency domain.

Finally, analog front-end impairments may have a big impact on system's performance. In this context, joint channel equalization and compensation techniques are proposed to equalize the channel and compensate for the analog front-end impairments for OFDM transmission over TI channels. The analog front-end impairments treated in this thesis are the in-phase and quadrature-phase (IQ) imbalances and the carrier frequency-offset (CFO). While IQ imbalance causes a mirroring effect, CFO induces ICI. A frequency-domain PTEQ is then proposed to overcome the problems associated with the analog front-end and to equalize the TI channel. The PTEQ is obtained here by transferring two TEQ operations to the frequency domain. One TEQ is applied to the received sequence, and the other one is applied to a conjugated version of the received sequence. Each TEQ is implemented as a time-varying FIR and modeled using the BEM. Once again, the BEM modeling here shows to be efficient to combat the problem of ICI induced due to CFO. Other analog front-end impairments like phase noise, nonlinear power amplifiers, etc. are out of the scope of this thesis.

Glossary

Mathematical Notation

$\mathbf{x}$	vector $\mathbf{x}$
$\mathbf{x}(z)$	vector $\mathbf{x}$, function of the z–transform variable
$[\mathbf{x}]_k$	kth element of vector $\mathbf{x}$
$\mathbf{A}$	matrix $\mathbf{A}$
$\mathbf{A}(z)$	matrix $\mathbf{A}$, function of the z–transform variable
$[\mathbf{A}]_{i,j}$	element on the ith row and jth column of matrix $\mathbf{A}$
$\mathbf{A}^T$	transpose of matrix $\mathbf{A}$
$\mathbf{A}^*$	complex conjugate of matrix $\mathbf{A}$
$\mathbf{A}^H = (\mathbf{A}^*)^T$	Hermitian transpose of matrix $\mathbf{A}$
$\mathbf{A}^{-1}$	inverse of matrix $\mathbf{A}$
$\mathbf{A}^\dagger$	pseudo–inverse of matrix $\mathbf{A}$
$\det \mathbf{A}$	determinant of matrix $\mathbf{A}$
$\mathrm{tr}\{\mathbf{A}\}$	trace of matrix $\mathbf{A}$
$\\|\mathbf{A}\\|$	Frobenius norm of matrix $\mathbf{A}$
$\mathrm{diag}\{\mathbf{x}\}$	square diagonal matrix with vector $\mathbf{a}$ as diagonal
$\mathbf{A} \otimes \mathbf{B}$	Kronecker product of matrix $\mathbf{A}$ and $\mathbf{B}$
$\mathbf{0}_{M \times N}$	$M \times N$ all-zeros matrix
$\mathbf{1}_{M \times N}$	$M \times N$ all-ones matrix
$\mathbf{I}_N$	$N \times N$ Identity matrix
$\boldsymbol{\mathcal{F}}$	Unitary DFT matrix
$\mathcal{F}^{(k)}$	$(k+1)$st row of the DFT matrix $\boldsymbol{\mathcal{F}}$
$\bar{\mathbf{I}}_N$	$N \times N$ anti-diagonal Identity matrix
$\mathbb{R}$	the set of real numbers
$\mathbb{C}$	the set of complex numbers
$\Re\{x\}$	real part of $x \in \mathbb{C}$
$\Im\{x\}$	imaginary part of $x \in \mathbb{C}$
x^*	complex conjugate of x
$\hat{x}$	estimate of x
$\lfloor x \rfloor$	largest integer smaller or equal to $x \in \mathbb{R}$
$\lceil x \rceil$	smallest integer larger or equal to $x \in \mathbb{R}$
$\lvert \cdot \rvert$	absolute value

$\|\| \cdot \|\|_2$	2–norm
$\mathcal{E}\{\cdot\}$	expectation operator
σ_x^2	variance of x
$a \ll b$	a is much smaller than b
$a \gg b$	a is much larger than b
$a \approx b$	a is approximately equal to b

Fixed Symbols

T	sampling time
W	system bandwidth
c	speed of light
f_c	carrier frequency
$\tau_{\max}$	channel maximum delay spread
$f_{\max}$	channel maximum Doppler spread
T_c	channel coherence time
B_c	channel coherence bandwidth
N_r	number of receive antennas
$x(t)$	continuous time baseband transmitted signal
$y^{(r)}(t)$	continuous time baseband received signal at the rth receive antenna
$x[n]$	discrete time baseband transmitted signal
$y^{(r)}[n]$	discrete time baseband received signal at the rth receive antenna
$S_k[i]$	frequency-domain QAM symbols transmitted on the kth subcarrier in the ith OFDM symbol
$Y_k^{(r)}[i]$	frequency-domain received signal at the kth subcarrier in the ith OFDM symbol
$g^{(r)}(t;\tau)$	continuous time impulse response of the doubly selective channel between the transmitter and the rth receive antenna
$g^{(r)}[n;\theta]$	discrete time impulse response of the doubly selective channel between the transmitter and the rth receive antenna
$h^{(r)}[n;\theta]$	BEM approximation of the discrete time impulse response of the doubly selective channel between the transmitter and the rth receive antenna
$h_{q,l}^{(r)}$	coeficient of the qth basis of the lth tap of the time-varying channel between the transmitter and rth receive antenna
$w_{q',l'}^{(r)}$	coeficient of the q'th basis of the l'th tap of the time-varying FIR feedforward filter at the rth receive antenna
$b_{q'',l''}$	coeficient of the q''th basis of the l''th tap of the time-varying FIR feedback filter
N	Data symbol block length
K	The BEM window size (BEM resolution)

L	channel order
L'	feedforward time-varying FIR equalizer order
Q'	feedforward time-varying FIR equalizer number of time-varying basis functions
L''	feedback time-varying FIR equalizer order
Q''	feedback time-varying FIR equalizer number of time-varying basis functions

Acronyms and Abbreviations

1-D	One Dimensional
2-D	Two Dimensional
1G	First Generation Mobile Wireless Systems
2G	Second Generation Mobile Wireless Systems
3G	Third Generation Mobile Wireless Systems
4G	Fourth Generation Mobile Wireless Systems
A/D	Analog–to–Digital converter
ADSL	Asymmetric Digital Subscriber Line
AMPS	Advanced Mobile Phobne Service
B3G	Beyond Third Generation
BDFE	Block Decision Feedback Equalizer
BEM	Basis Expansion Model
BLE	Block Linear Equalizer
BER	Bit Error Rate
CDMA	Code Division Multiple Access
CFO	Carrier Frequency Offset
CP	Cyclic Prefix
CSI	Channel State Information
D/A	Digital–to–Analog converter
D-AMPS	Digital-AMPS
DAB	Digital Audio Broadcasting
DFE	Decision Feedback Equalizer
DFT	Discrete Fourier Transform
DMT	Discrete Multt-Tone
DSP	Digital Signal Processor
DVB	Digital Video Broadcasting
e.g.	`exempli gratia` : for example
EDGE	Enhanced Data rates for GSM Evolution
FEQ	Frequency–domain EQualizer
FFT	Fast Fourier Transform
FIR	Finite Impulse Response filter
FM	Frequency-Modulation

GSM	Global System for Mobile communications
GPRS	General Packet Radio Service
HIPERLAN	HIgh PErformance Radio LAN
Hz	Hertz
IBI	Inter-Block Interference
ICI	Inter-Carrier Interference
IDFT	Inverse Discrete Fourier Transform
i.e.	`id est` : that is
IFFT	Inverse Fast Fourier Transform
IMT	International Mobile Telecommunications
IQ	In-phase and Quadrature-phase
ISI	Inter Symbol Interference
LMS	Least Mean Square adaptive filter
LAN	Local Area Network
LS	Least Squares
MA	Multiply Add
MC	Multi–Carrier
MIMO	Multi–Input Multi–Output system
ML	Maximum Likelihood
MLSE	ML Sequence Estimator
MMSE	Minimum Mean-Square Error
MRE	Mutually Referenced Equalizer
MSE	Mean-Square Error
NMT	Nordic Mobile Telephone
OFDM	Orthogonal Frequency Division Multiplexing
P/S	Parallel–to–Serial converter
PDC	Pacific Digital Cellular
PSAM	Pilot Symbol Assisted Modualtion
PTEQ	Per-Tone EQualizer
QAM	Quadrature Amplitude Modulation
QPSK	Quadrature Phase Shift Keying
RLS	Recursive Least Squares adaptive filter
S/P	Serial–to–Parallel converter
SDFE	Serial DFE
SC	Single Carrier
SIMO	Single–Input Multiple–Output
SISO	Single–Input Single–Output
SLE	Serial Linear Equalizer
SNR	Signal–to–Noise Ratio
SVD	Singular Value Decomposition
TACS	Total Access Communication System
TDMA	Time-Division Multiple Access
TEQ	Time-domain EQualizer
TI	Time-Invariant
TV	Telvision

UEC	Unit Energy Constraint
UMTS	Universal Mobile Telecommunications System
UNC	Unit Norm Constraint
US	Uncorrelated Scattering
VA	Viterbi Algorithm
vs.	versus
W-CDMA	Wideband Code Division Multiple Access
WGN	White Guassian Noise
WLAN	Wireless LAN
WSSUS	Wide Sense Stationary US
ZF	Zero Forcing
ZP	Zero Padding

Contents

Chapter 1

Introduction

OVER the last decade, the mobile wireless telecommunication industry has undergone tremendous changes and experienced rapid growth. As a result of this growth the number of subscribers is expected to exceed 2 billion users by the end of the year 2005. The reason behind this growth is the increasing demand for bandwidth hungry multimedia applications. This demand for even higher data rates at the user's terminal is expected to continue for the coming years as more and more applications are emerging. Therefore, current cellular systems have been designed to provide date rates that range from a few megabits per second for stationary or low mobility users to a few hundred kilobits to high mobility users. This data range is insufficient with respect to the increasing demand for high date rates to high mobility users.

Throughout history, the mobile wireless communications has taken on multiple phases/generations depending on the technology used and services provided. These generations are listed below:

- First generation (1G) cellular systems: 1G mobile communication systems based on analog frequency-modulation (FM) were first deployed in the late 1970s early 1980s. They were used mainly for voice applications. Examples of 1G systems are AMPS in the United States, Nordic mobile telephone system in Scandinavia, TACS in the United Kingdom, and NAMTS in Japan.
- Second generation (2G) cellular systems: 2G systems were still used mainly for voice applications but were based on digital technology, including digital signal processing techniques. Beside voice applications, 2G systems provide data communication services at low data rates. Examples of 2G systems are GSM mainly in Europe, DAMPS, TDMA (IS-54), CDMA (IS-95) in the United States, and PDC in Japan.

Table 1.1: History of mobile wireless systems

Technology	Services	Standard	Data Rate
1G	Analog voice	AMPS, NMT, etc.	1.9kbps
2G	Digital voice, short messages	TDMA, CDMA, GSM	14.4 Kbps
2.5G	Higher Capacity packetized data	GPRS, EDGE	384 kbps
3G	Broadband data	WCDMA, CDMA2000	2Mbps
4G	Multimedia data	?	100 Mbps

- Third generation (3G) cellular systems: 3G systems are currently designed to provide higher quality voice services as well as broadband data capabilities up to 2Mbps. Examples of 3G systems are UMTS, IMT-2000 and CDMA2000.

- The interim step between 2G and 3G is referred to as 2.5G systems: 2.5G systems are designed to provide increased capacity on the 2G channels, and to provide higher data rates for data services up to 384kbps. Examples of 2.5G systems include GPRS, and EDGE.

- Fourth generation (4G) cellular systems: 4G systems are currently under development and will be implemented within the coming 5-10 years (2010-2015). 4G systems are expected to provide high rate multimedia services like live television, video games, etc.

A summary of the mobile wireless evolution is presented in Table 1.1. For further details the reader is referred to the excellent overview of the early generations presented by Hanzo in [51] and references therein, for later generations the reader is referred to [53, 97]. The data rates indicated in this table are for stationary users.

So far, most of the services offered are voice services. With the advent of new generations like 2.5G and 3G systems, new data services have emerged. These include but are not limited to e-mail, file transfers, radio and TV. The expected new data services are highly bandwidth consuming. This results in higher data rate requirements for future systems. In addition to providing high data rate services to stationary and or to low mobility indoor users, the new technologies are expected to provide high data rate applications to high mobility outdoor users.

Concerning data rates versus mobility, the status of current mobile wireless systems is depicted in Figure 1.1. Third generation (3G) wireless systems like UMTS provide the following data rates defined according to the degree of mobility:

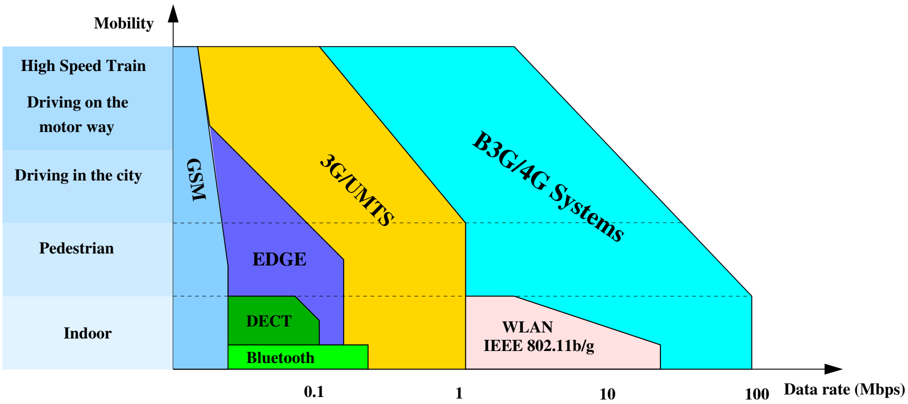

Figure 1.1: User's mobility vs. data rate.

- **Low Mobility**: For limited mobility users and stationary indoor environments, 3G systems provide data rates up to 2 Mbps.
- **Limited Mobility**: For mobile users traveling at speeds less than vehicular speed (120Km/hr) (outdoor to indoor pedestrian), 3G systems provide data rates up to 384 Kbps.
- **High Mobility**: For high mobility users traveling at speeds more than vehicular speed, 3G systems provide data rates up to 144 Kbps.

The current data rates of 3G systems for high mobility users are insufficient for the new emerging high data rate applications. Therefore, providing high data rates for high mobility users is the cornerstone of the future beyond third generation (B3G) and 4G wireless systems. 4G and B3G wireless systems are expected to provide up to 100 Mbps for stationary users and up to 20 Mbps for vehicular speed users[1]. These high data rates are necessary to provide/develop services like live video, mobile games, etc.

Broadcast systems also contribute to the development of the future wireless communication systems. These systems include digital audio broadcasting (DAB) and digital video broadcasting (DVB). So far, these systems have been standardized for stationary users, and the trend towards mobile users and hand held terminals is in progress. Currently, there are efforts to bring DVB to mobile users through the DVB-mobile (DVB-M), and DVB-handheld (DVB-H) standards.

In this thesis we address the problem of robust and reliable transmission techniques to provide high data rate applications to high mobility users. Due

[1]Field trials carried out by Motorola Inc. http:// www.motorola.com using MIMO OFDM.

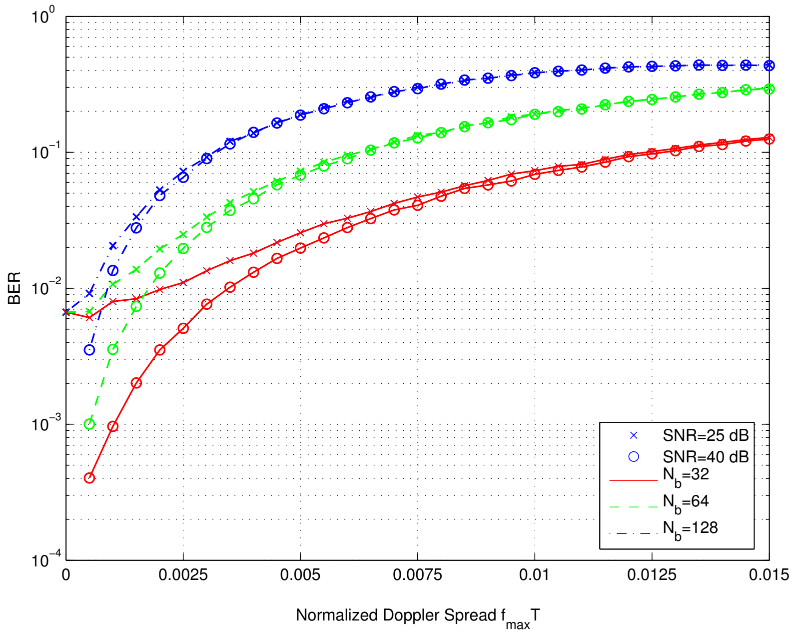

Figure 1.2: BER vs. Normalized Doppler spread for $SNR = 25dB$, and $SNR = 40dB$.

to user's mobility the channel is no longer stationary, and so in addition to the frequency-selectivity characteristics caused by multipath propagation, the channel exhibits time-variant characteristics. In short, this thesis addresses the problem of transmission over time- and frequency-selective fading or the so-called doubly selective channels.

1.1 Problem Statement

In order to provide multimedia applications for mobile users advanced signal processing techniques are necessary. As mentioned earlier, the user's mobility introduces time variations. As the user's mobility increases, the underlying communication channel, which characterizes the link between the transmitter and receiver, becomes more rapidly time-varying. Under high mobility scenarios the assumption that the channel is stationary or block stationary is not valid. What we mean by a block stationary (also referred to as block fading) channel, is that the channel is stationary over a transmission period of a block of symbols and may change independently from block to block. For mobile users this assumption results in performance degradation. This degradation is proportional to the block size and the user's mobility. To explain this we consider the following scenario. Consider transmission over a time-varying flat fading channel (one-tap channel). For demodulation purposes the channel is assumed to be block fading over a period of transmission of N_b symbols. Over each block, the channel state information (CSI) at $N_b/2$ is used to equalize the channel. Assume that QPSK signaling is used, and the system's performance is measured in terms of bit-error rate (BER) versus normalized Doppler spread $f_{\max}T$, where $f_{\max}$ is the maximum Doppler spread (a measure of the channel's time variation, see Chapter 2 for a definition) and T is the sampling time. We ran the simulations for two values of signal-to-noise ratios (SNRs) $SNR = 25\ dB$ and $SNR = 40\ dB$, and considered the following block sizes $N_b = 32, 64, 128$. The simulation results are shown in Figure 1.2. From this figure we draw the following conclusions.

- The system performance experiences significant degradation as the Doppler spread increases.
- For a fixed Normalized Doppler spread $f_{\max}T$, the BER increases as the block size increases.
- A target BER of 10^{-2} (usually used as a benchmark for uncoded transmission) can only be achieved for a limited normalized Doppler spread $f_{\max}T$ that varies with the block size and the operating SNR. The maximum normalized supported Doppler spread decreases by increasing the block size.
- The modeling error (modeling the channel as a block fading over a period of transmitting a block of N_b symbols) becomes more dominant than the system noise as the normalized Doppler spread increases. For example, for $N_b = 32$ and $f_{\max}T \geq 0.0075$, for $N_b = 64$ and $f_{\max}T \geq 0.005$, and for $N_b = 128$ and $f_{\max}T \geq 0.0025$ [2], the BER curve of $SNR = 25\ dB$ coincides with that of $SNR = 40\ dB$. This threshold value decreases significantly when the block size is increased.

This problem also arises in DVB reception for high speed terminals, e.g. for vehicular speeds over motorway or high speed trains ($300 Km/hr$) in Europe and Japan. The following example gives an overview of the system parameters.

Example 1.1 DVB uses MC for transmission implemented using OFDM. For DVB 8K mode with a signal bandwidth of 8MHz over the UHF band from 470-862MHz, the carrier spacing is 1.12kHz. The Doppler spread is around 10% of the carrier spacing for speeds of 120Km/hr and around 20% for speeds

[2] This corresponds to a vehicular speed of v = 180Km/hr, v = 120Km/hr and v = 60Km/hr for GSM carrier f_c = 1800MHz and sampling time $T = 25\mu sec$.

of 300Km/hr. For the 4K and 2K modes, the Doppler spread is less sever due to the wider the carrier spacing. △

Motivated by the degradation in performance of the above system due to the block fading assumption, new channel estimation and equalization techniques are devised. These techniques rely on better channel modeling. More specifically, the basis expansion model (BEM) is used to model (approximate) the doubly selective channel, which subsumes the block fading case. Further, the BEM will be used to design time- and frequency-domain equalizers. By doing so, we show that the proposed techniques unify and extend the previously proposed equalizers for time-invariant (TI) channels.

1.2 Thesis Context

In this thesis we address the problem of transmission over time- and frequency-selective channels. We consider single carrier (SC) systems as well as multicarrier (MC) systems implemented by orthogonal frequency division multiplexing (OFDM). Mainly, we focus on the problem of channel estimation and equalization. The two modes of transmission (SC and OFDM) are presented below.

- **Single Carrier Transmission**
  In SC transmission the high rate data is transmitted on a single carrier. Due to multipath fading, intersymbol interference (ISI) arises, which mainly happens when the channel delay spread is longer than the duration of one transmitted symbol. Higher data rates result in severe ISI. To combat the effects of ISI, equalization techniques must be implemented. Applications that use SC transmission include but not limited to cellular systems (GSM, GPRS, EDGE, etc.) and satellite communications systems.

- **OFDM Transmission**
  In OFDM transmission, the high rate data symbols are simultaneously transmitted on lower rate parallel sub-channels. The bandwidth of each sub-channel is sufficiently narrow so that the frequency response characteristics of the sub-channels are nearly flat. This can be achieved by the DFT/IDFT and insertion of a cyclic prefix (CP). The CP insertion of length equal to or greater than the channel impulse response length converts the linear convolution into a cyclic convolution. The CP in conjunction with the IDFT/DFT allows for a very simple equalization technique based on a one-tap frequency-domain equalizer (1-tap FEQ) [25, 88, 116], provided that the channel is time-invariant (stationary users). The purpose of the 1-tap FEQ is to correct the channel phase and gain on a

particular sub-channel. Applications that use OFDM transmission include DAB, DVB, wireless local area networks (WLANs), etc.

It is important to mention that, CP-based SC transmission systems are equivalent in complexity to OFDM. By utilizing the DFT and IDFT at the receiver, a low complexity frequency-domain equalization can be developed [34].

Throughout this thesis we consider the following scenario:

a) The channel is doubly selective. We assume that the channel is mainly characterized as a time-varying multipath fading channel. The channel time-variation results from the Doppler spread arise due to the user's mobility and/or the carrier frequency offset arises due to the mismatch between the transmitter and receiver local oscillators. The latter case arises due to the use of the cheap Zero-IF receiver which is extensively used and implemented in WLAN systems based on OFDM transmission.

b) The channel is unknown at the transmitter. This assumption is a consequence of the first assumption. Since the channel is rapidly time-varying, feeding back channel estimates mostly results in outdated channel state information (CSI).

c) Single-input multiple-output (SIMO) system. In this thesis we review several equalization techniques considering the SIMO assumption. Extending the results to multiple-input multiple-output (MIMO) systems is rather straightforward. The SIMO case subsumes the single-input single-output (SISO) system. The SIMO assumption is often necessary for the existence of the zero-forcing (ZF) solution.

1.3 Objectives and Solution Approach

The main objective of this thesis is to provide reliable communication (transmission) over rapidly time-varying multipath fading wireless channels. More specifically:

- Develop robust channel equalization techniques for SC as well as for OFDM transmission.
- Develop robust channel estimation/tracking techniques.
- Time-variation also arises due to carrier frequency-offset even if the underlying communication channel is TI. In this thesis we aim at developing algorithms that are capable to combat the effects imposed on the system

due to the analog front-end impairments, especially in OFDM transmission.

For SC transmission over doubly selective channels, the doubly selective channel is first approximated by the BEM, which is shown to accurately approximate the doubly selective channel. Similarly, we rely on the BEM to design the equalizer which is implemented as a time-varying finite impulse response (FIR) filter. The different equalization and channel estimation techniques covered in this thesis range from linear to decision feedback and from blind to pilot symbol assisted modulation techniques.

For OFDM transmission over doubly selective channels, time-domain as well as frequency-domain per-tone equalization techniques are proposed to alleviate the problem of ICI. OFDM transmission is also sensitive to analog front-end impairments such as in-phase and quadrature-phase (IQ) imbalance and carrier frequency-offset (CFO). Joint equalization and compensation techniques are proposed. Other analog front-end impairments like phase noise, power amplifier nonlinearity, etc, are beyond the scope of this thesis.

1.4 Outline of the Thesis and Contributions

An overview of the thesis and its major contributions is now given.

An overview study of the mobile wireless channel is presented in Chapter 2. The mobile wireless channel may generally be characterized as doubly selective, i.e. selective in both time and in frequency. Multipath propagation results in frequency-selectivity. Mobility and/or the carrier frequency offset result in time-selectivity. Multipath propagation results from reflection, diffraction, and scattering of the radiated electromagnetic waves of buildings and other objects that lie in the vicinity of the transmitter and/or the receiver. In this chapter, the main channel parameters of the underlying wireless channel are introduced. We mainly focus on channel parameters that are related to the assumption of wide sense stationary uncorrelated scattering (WSSUS). The basis expansion channel model (BEM) and its relationship to the well known Jakes' channel model is also introduced.

This thesis consists of two parts. The first part discusses SC transmission over doubly selective channels and the second part discusses OFDM transmission over doubly selective channels.

Part I of this thesis investigates *single carrier transmission* over doubly selective channels. Future generation wireless systems are required to provide high data rates to high mobility users. In such scenarios, conventional time-invariant equalization schemes or adaptive schemes, suitable for slowly time-varying channels, are not suitable since the channel may vary significantly from sample to sample. The channel equalization/estimation schemes related to this part are presented in the following chapters.

In **Chapter 3**, we focus on the problem of *linear equalization* of doubly selective channels. We derive the zero forcing (ZF) and minimum mean square-error (MMSE) equalizers. In this chapter we focus on two categories of linear equalizers, the block linear equalizers (BLEs), and serial linear equalizers (SLEs). The SLEs are implemented by time-varying finite impulse response (FIR) filters. While the first type equalizes a block of received samples, the second type operates on a sample by sample basis. However, the design and implementation of the SLEs is done on a block level basis. The publications that are related to this chapter are:

- **I. Barhumi**, G. Leus, and M. Moonen, "Time-Varying FIR Equalization of Doubly-Selective Channels", *IEEE Trans. on Wireless Comm.*, pp. 202-214, vol. 4, no. 1, Jan. 2005.
- **I. Barhumi**, G. Leus and M. Moonen, "Time-Varying FIR Equalization of Doubly-Selective Channels", in the proceedings of the IEEE 2003 International Conference on Communications (ICC'03), 11-15 May, 2003 Anchorage, AK, USA.
- G. Leus, **I. Barhumi** and M. Moonen, "MMSE Time-Varying FIR Equalization of Doubly-Selective Channels", in The IEEE 2003 International Conference on Acoustics, Speech, and Signal Processing (ICASSP'03), Hong Kong, April 6-10, 2003.

In **Chapter 4**, we focus on *decision feedback equalization (DFE)* of doubly selective channels. Similar to Chapter 3, we consider two types of equalizers. First, we focus on block decision feedback equalizers (BDFEs). Second, we propose a serial DFE (SDFE). Unlike linear equalizers, which apply one feedforward filter, DFEs apply two filters; namely a feedforward filter and a feedback filter. For the SDFE, both feedforward and feedback filters are implemented using time-varying FIR filters. The publications that are related to this chapter are:

- **I. Barhumi**, G. Leus and M. Moonen, "Time-Varying FIR Decision Feedback Equalization of Doubly-Selective Channels", in the IEEE 2003 Global Communications Conference (GLOBECOM'03), San Francisco, CA, December 2003.
- G. Leus, **I. Barhumi**, and M. Moonen, "Low-Complexity Serial Equalization of Doubly-Selective Channels", in Sixth Baiona Workshop on Signal Processing in Communications, September 8-10, 2003, Baiona, Spain.

In the previous two chapters we design the equalizers, linear or decision feedback, by considering that the doubly selective channel is perfectly known at the receiver. In **Chapter 5**, we focus on the problem of channel estimation and equalization based on pilot symbol assisted modulation (PSAM) techniques. First, we focus on PSAM-based *channel estimation*, where the estimated BEM coefficients of the channel are then used to design the equalizer (linear and decision feedback). Second, we focus on PSAM-based *direct equalization*. There the BEM coefficients of the equalizer are obtained directly from the pilot symbols. The publications that are related to this chapter are:

- **I. Barhumi**, G. Leus and M. Moonen, "MMSE Estimation of Basis Expansion Models for Rapidly Time-Varying Channels", EUSIPCO 2005, *accepted for publication*. (Also presented at the SPS-DARTs 2005).

Using pure pilot symbols for channel estimation and/or direct equalization can be either skipped resulting in *blind techniques* or combined with blind techniques resulting in *semi-blind techniques* as discussed in **Chapter 6**. The publications that are related to this chapter are:

- **I. Barhumi**, and M. Moonen, "Estimation and Direct Equalization of Doubly Selective Channels", *EURASIP Journal on Applied Signal Processing*, special issue on "Reliable Communications over Rapidly Time-Varying Channels", submitted June, 2005.
- G. Leus, **I. Barhumi**, O. Rousseaux, and M. Moonen, "Direct Semi-Blind Design of Serial Linear Equalizers for Doubly-Selective Channels", in the 2004 IEEE International Conference on Communications (ICC 2004), June 19-24, Paris, France.

Part II of this thesis investigates OFDM transmission over doubly selective channels as well as over TI channels with analog front-end receiver impairments. Similar to the case of SC transmission, conventional time- and frequency-domain equalization techniques can not adequately cope with the challenging problem of equalizing the underlying mobile wireless channel. In OFDM transmission, time-varying channels induce ICI, i.e. the energy of a particular subcarrier is leaked to neighboring subcarriers. Time-domain and/or frequency-domain equalization techniques are needed to cope with the problem of ICI.

In **Chapter 7**, a brief overview of OFDM transmission is given. In this chapter, the OFDM system model is introduced along with the notation that will be used throughout this part. In order to develop equalization techniques, it is important to understand the mechanism of ICI. Therefore, ICI analysis is introduced in this chapter.

In **Chapter 8**, we propose time-domain and frequency-domain per-tone equalization techniques. In addition to the time-variation of the channel, we assume the CP length is shorter than the channel impulse response, which also introduces inter-block interference (IBI). Applications that use OFDM as a transmission technique, such as DVB, encounter long delay multipath channels. Using a CP of length equal to the channel order results in a significant decrease of throughput. In such applications one way to increase transmission throughput is by using a shorter CP length. Hence, equalization techniques are needed to mitigate ICI and IBI. The publications that are related to this chapter are:

- **I. Barhumi**, G. Leus, and M. Moonen, "Time- and Frequency-Domain Per-Tone Equalization for OFDM over Doubly-Selective Channels", *Signal Processing (Elsevier)*, vol. 84/11, pp. 2055-2066, 2004. Special Section Signal Processing in Communications.
- **I. Barhumi**, G. Leus, and M. Moonen, "Equalization for OFDM over Doubly-Selective Channels", *IEEE Transactions on Signal Processing*, accepted February, 2005.
- **I. Barhumi**, G. Leus and M. Moonen, "Combined Channel Shortening and Equalization of OFDM over Doubly-Selective Channels", in the IEEE 2004 International Conference on Acoustics, Speech and Signal Processing (ICASSP 2004), May 17-21, Montreal, Canada. (Invited Paper)
- **I. Barhumi**, G. Leus and M. Moonen, "Frequency-domain Equalization for OFDM over Doubly-Selective Channels", in the 2004 IEEE International Conference on Communications (ICC 2004), 19-24 June, Paris, France.
- **I. Barhumi**, G. Leus and M. Moonen, "Frequency-domain Equalization for OFDM over Doubly-Selective Channels", in Sixth Baiona Workshop on Signal Processing in Communications, September 8-10, 2003, Baiona, Spain.

Not only is OFDM sensitive to channel variations, but also to receiver and/or transmitter analog front-end impairments. In **Chapter 9**, we study OFDM transmission over a time-invariant channel (in this case), but with receiver analog front-end impairments. The analog front-end impairments are IQ imbalance and carrier frequency-offset (CFO). While IQ imbalance results in a mirroring effect, CFO results in ICI. Frequency-domain techniques for joint channel equalization, IQ imbalance and CFO compensation are investigated. The publications that are related to this chapter are:

- **I. Barhumi**, and M. Moonen, "IQ Compensation for OFDM in the presence of CFO and IBI", *IEEE Transactions on Signal Processing*, submitted May, 2005.

- **I. Barhumi**, and M. Moonen, "IQ Compensation for OFDM in the presence of CFO and IBI", ICC, 2006, *to be submitted.*

Besides the material presented in this thesis, we also published or contributed to the following papers during our PhD research period:

- **I. Barhumi**, G. Leus, and M. Moonen, "Optimal Training Design for MIMO OFDM Systems in Mobile Wireless Channels", *IEEE Transactions on Signal Processing*, pp. 1615-1624, vol. 51, no. 6, June 2003.
- **I. Barhumi**, G. Leus and M. Moonen, "Optimal Training Sequences for Channel Estimation in MIMO OFDM Systems in Mobile Wireless Channels", International Zurich Seminar on Broadband Communications, Access, Transmission, Networking (IZS02), February 18-21, 2002, Zurich, Switzerland.
- **I. Barhumi** and M. Moonen, "Optimal Training for Channel Estimation in MIMO OFDM Systems", ProRISC, October 27-31, 2001. Veldhoven, The Netherlands.
- G. Leus, **I. Barhumi** and M. moonen, "Per-Tone Equalization for MIMO OFDM Systems", in the proceedings of the IEEE 2003 International Conference on Communications (ICC'03), 11-15 May, 2003 Anchorage, AK, USA.

Conclusions are drawn and directions for further research are explored in **Chapter 10**.

Chapter 2

Mobile Wireless Channels

2.1 Introduction

IN this chapter, we will give a brief description of the wireless channel that paves the way for further development of the algorithms presented in this dissertation. The underlying study of the statistical models of the wireless channel is essential to analyze and design appropriate signal processing algorithms as needed to provide reliable communication.

In wireless communications the transmitted signal arrives at the receiver along a number of different paths, referred to as multipaths as shown in Figure 2.1. Multipath propagation arises due to reflection, refraction, and scattering of the electromagnetic wave on objects such as buildings, hills, trees, etc. that lie in the vicinity of the transmitter and/or receiver. User mobility (or the relative motion between the transmitter and receiver) and/or carrier frequency offset induce time-variation on the channel. Hence, the wireless channel may generally be characterized as a linear, time-varying multipath fading. Multipath results into spreading of the transmitted signal in time (the so-called intersymbol interference (ISI)), while the time-variation of the channel results into frequency spreading (the so-called Doppler spread) [91, 92]. Mobile channels exhibit frequency selectivity characteristics due to multipath fading, as well as time-variant characteristics due to the Doppler shift. This results in time- and frequency-selective a.k.a doubly selective channels[1].

This chapter is organized as follows. The system model is introduced in Section 2.2. The channel parameters are introduced in Section 2.3. The different

[1] The doubly selective channel may also be referred to as time-dispersive frequency-selective, or doubly-dispersive channel.

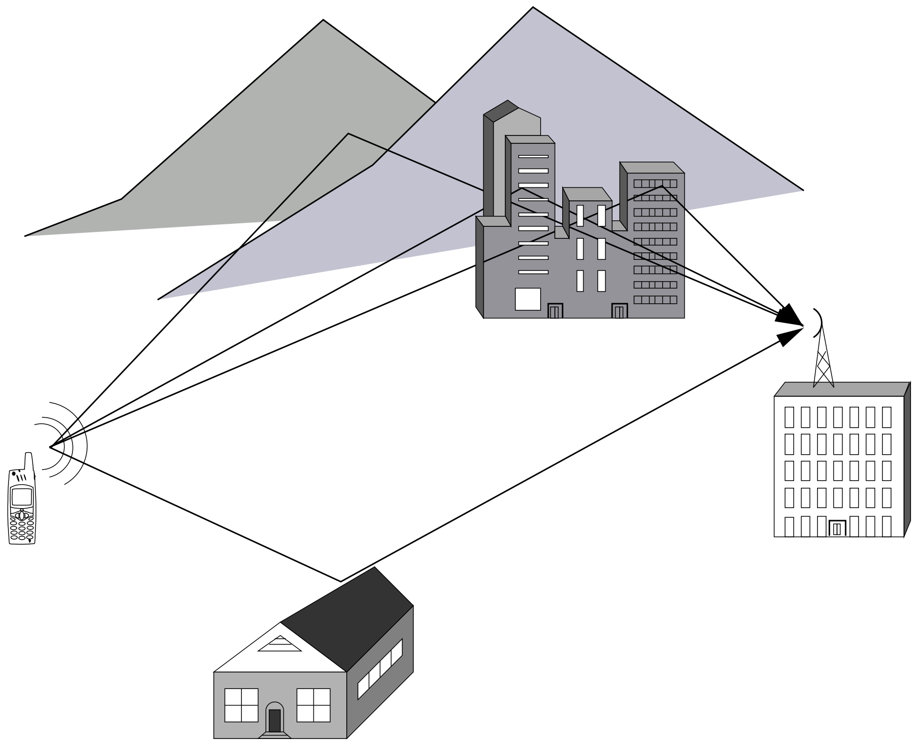

Figure 2.1: The user signal experiences multipath propagation.

channel models are discussed in Section 2.4. In Section 2.5 we introduce the discrete-time channel model. The basis expansion channel model (BEM) is introduced in Section 2.6. Finally, we summarize in Section 2.7

2.2 System Model

In this section we describe the baseband equivalent continuous-time system model. The baseband equivalent discrete-time system will be treated in a later section.

The system under consideration is depicted in Figure 2.2. We assume a single-input multiple-output (SIMO) system, where N_r receive antennas are used. The channel is assumed to be doubly selective. The input-output relationship of the continuous-time linear time-varying channel with additive noise can be written as

$$y^{(r)}(t) = \int_{-\infty}^{\infty} x(t-\tau) g^{(r)}(t;\tau) \mathrm{d}\tau + v^{(r)}(t), \tag{2.1}$$

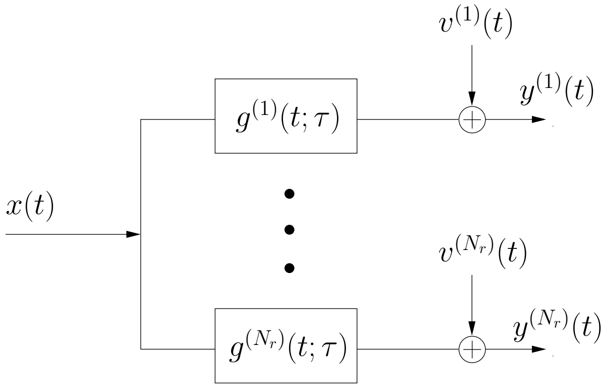

Figure 2.2: SIMO system model.

where $x(t)$ is the channel input, $y^{(r)}(t)$ is the received signal at the rth receive antenna, $g^{(r)}(t;\tau)$ is the impulse response of the doubly selective channel from the transmitter to the rth receive antenna, and $v^{(r)}(t)$ is the additive noise at the rth receive antenna. $g^{(r)}(t;\tau)$ can be thought of as the impulse response of the system (the channel linking the transmitter and the rth receive antenna) at a fixed time t.

The dual input-output relationship in the frequency-domain can also be derived. To do so we first introduce the following functions which equivalently describe the time-varying channel.

1. Time-varying transfer function $G^{(r)}(t;f)$ as

$$G^{(r)}(t;f) = \int_{-\infty}^{\infty} g^{(r)}(t;\tau)e^{-j2\pi f\tau}\mathrm{d}\tau.$$

   The time-varying transfer function is obtained by the Fourier transform of the time-varying channel with respect to the time-delay τ, i.e. $g^{(r)}(t;\tau) \overset{\mathcal{F}_\tau}{\rightarrow} G^{(r)}(t;f)$. This function represents the frequency response of the time-varying channel at fixed time t. In the special case when the channel is time-invariant, this reduces to the usual frequency response.

2. The output Doppler spread is obtained by the Fourier transform of the time-varying transfer function $G^{(r)}(t;f)$ as

$$D^{(r)}(\nu;f) = \int_{-\infty}^{\infty} G^{(r)}(t;f)e^{-j2\pi\nu t}\mathrm{d}t.$$

We define $Y^{(r)}(f)$ as the the Fourier transform of the received signal at the rth receive antenna, and $X(f)$ as the Fourier transform of the input signal. The dual input-output relationship in the frequency domain can be then expressed as

$$Y^{(r)}(f) = \int_{-\infty}^{\infty} D^{(r)}(f-\nu;\nu)X(\nu)\mathrm{d}\nu + V^{(r)}(f),$$

where $V^{(r)}(f)$ denotes the Fourier transform of the additive noise signal at the rth receive antenna.

2.3 Channel Parameters

The time-varying multipath fading channel in wireless communications is often modeled as a wide sense stationary uncorrelated scattering (WSSUS) channel. The WSSUS model of the wireless channel was first introduced by Bello in [24]. The channel is said to be delay uncorrelated scattering (US) if the different paths of the channel are assumed uncorrelated. Define the channel autocorrelation function $r_h(t_1, t_2; \tau_a, \tau_b)$ as

$$r_h(t_1, t_2; \tau_a, \tau_b) = \frac{1}{2}\mathcal{E}\{g^{(r)*}(t_1; \tau_a)g^{(r)}(t_2; \tau_b)\} \tag{2.2}$$

Note that we dropped the receive antenna index from the autocorrelation function assuming that the different channels associated with the different receive antennas follow the same statistical model. The channel is then delay US if

$$r_h(t_1, t_2; \tau_a, \tau_b) = r_h(t_1, t_2; \tau_a)\delta(\tau_a - \tau_b).$$

In addition, the channel is said to be wide sense stationary (WSS) if

$$r_h(t_1, t_2; \tau) = r_h(\Delta t; \tau),$$

where $\Delta t = t_2 - t_1$. Hence, the autocorrelation function of the WSSUS channel is represented by its correlation function $r_h(\Delta t; \tau)$.

Equivalently, the WSSUS channel can be characterized by the following correlation function [84]:

$$\phi(\Delta t; \Delta f) = \frac{1}{2}\mathcal{E}\{G^{(r)*}(t; f)G^{(r)}(t + \Delta t; f + \Delta f)\},$$

where the delay US is replaced by the frequency US.

An important function that can be derived from the function $\phi(\Delta t; \Delta f)$ is the scattering function $S(\tau; \lambda)$. The scattering function is a measure of the power spectrum of the channel at time delay τ and frequency offset λ. The scattering function is obtained by taking the double Fourier transform of the autocorrelation function as [84]:

$$S(\tau; \lambda) = \int_{-\infty}^{\infty}\int_{-\infty}^{\infty} \phi(\Delta t; \Delta f)e^{-j2\pi\lambda\Delta t}e^{j2\pi\tau\Delta f}\mathrm{d}\Delta t\ \mathrm{d}\Delta f. \tag{2.3}$$

The delay power spectrum can then be obtained by averaging the scattering function over λ:

$$S_\tau(\tau) = \int_{-\infty}^{\infty} S(\tau;\lambda)\mathrm{d}\lambda.$$

Similarly; the Doppler power spectrum is obtained by averaging the scattering function over τ:

$$S_f(\lambda) = \int_{0}^{\infty} S(\tau;\lambda)\mathrm{d}\tau.$$

The maximum *delay spread* $\tau_{\max}$ of the channel is then defined as the range of values over which the delay power spectrum $S_\tau(\tau)$ is nonzero, and the maximum *Doppler spread* $f_{\max}$ is defined as the range of values over which the Doppler power spectrum $S_f(\lambda)$ is nonzero.

The *channel coherence time* T_c is inversely proportional to the channel Doppler spread, i.e. $T_c = 1/f_{\max}$. The channel coherence time is a measure of how rapidly the channel impulse response varies in time. Equally important is the *channel coherence bandwidth* B_c. The channel coherence bandwidth B_c provides a measure of the channel frequency selectivity, i.e. the width of the band of the frequencies which are similarly affected by the channel. The channel coherence bandwidth is inversely proportional to the channel maximum delay spread, $B_c = 1/\tau_{\max}$.

Another important channel parameter is the *spread factor* defined as the product $\tau_{\max} f_{\max}$. It was shown in [59] that if the spread factor $\tau_{\max} f_{\max} \ll 1/2$, the channel impulse response can be easily measured. However, measuring the channel impulse response becomes extremely difficult if not impossible when the spread factor $\tau_{\max} f_{\max} > 1/2$. In the following we briefly discuss the different channel models that arise due to the different channel parameters discussed above.

2.4 Channel Models

The selection of the channel model is linked to the transmitted signal characteristics, mainly based on the relationship between the transmitted signal bandwidth W and the channel coherence bandwidth B_c or equivalently between the the duration of the transmitted symbol T and the channel coherence time T_c. In the following we will give a brief description of the different fading types.

2.4.1 Frequency Non-Selective Fading Channel

Consider the system input-output relationship as in 2.1. Let $X(f)$ denote the frequency-domain representation of the transmitted signal. The noiseless received signal $z^{(r)}(t)$ at the rth receive antenna can be written as

$$z^{(r)}(t) = \int_{-\infty}^{\infty} g^{(r)}(t;\tau)x(t-\tau)\mathrm{d}\tau$$
$$= \int_{-\infty}^{\infty} G^{(r)}(t;f)X(f)e^{j2\pi ft}\mathrm{d}f \tag{2.4}$$

Suppose that the transmitted signal bandwidth W is much smaller than the coherence bandwidth of the channel B_c, i.e. $W \ll B_c$. Then all the frequency components of the transmitted signal $X(f)$ will experience the same attenuation and phase shift. This means that the channel frequency response is fixed over the transmitted signal bandwidth W. Such a channel is called frequency non-selective or frequency flat fading. Hence, for frequency flat fading channels the input-output relationship is reduced to

$$z^{(r)}(t) = G^{(r)}(t;0)\int_{-\infty}^{\infty} X(f)e^{j2\pi ft}\mathrm{d}f$$
$$= G^{(r)}(t;0)x(t)$$
$$= \alpha^{(r)}(t)e^{j\theta^{(r)}(t)}x(t), \tag{2.5}$$

where $\alpha^{(r)}(t)$ represents the time-varying envelop and $\theta^{(r)}(t)$ represents the time-varying phase of the channel impulse response. From (2.5), we see that the frequency flat fading channel can be viewed as a multiplicative channel.

2.4.2 Frequency-Selective Fading Channel

In the previous subsection we have treated the case when the transmitted signal bandwidth is smaller than the coherence bandwidth of the channel resulting into the so-called frequency non-selective or frequency flat fading channel. In this subsection we will treat the case when the transmitted signal bandwidth is larger than the coherence bandwidth of the channel, i.e. when $W \gg B_c$. In this case the different frequency components of the transmitted signal $X(f)$ will experience different gains and phase shifts. In such a case, the channel is called frequency-selective. Contrary to the frequency flat case where the channel consists of one tap, the frequency-selective channel consists of multiple-taps (resolvable multipaths). The multipath components are resolvable if they are separated in delay by $1/W$. $1/W$ can be viewed as the time resolution of the receiver. For frequency-selective fading, the channel maximum delay spread $\tau_{\max}$ is much greater than the time resolution of the receiver $\tau_{\max} \gg 1/W$, and therefore, echoes of the transmitted signal arrive at the receiver causing intersymbol interference (ISI). The signal echoes arrive at the receiver along a number of different resolvable paths (resolvable by the receiver time resolution $1/W$). Hence, the impulse response of the time-varying frequency-selective

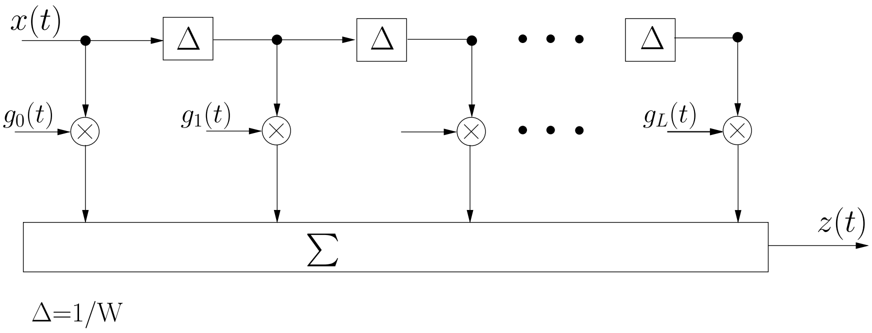

Figure 2.3: Tapped delay line model of frequency-selective channels.

fading channel (or ISI channel) can be written as

$$g^{(r)}(t;\tau) = \sum_{l=0}^{L} g_l^{(r)}(t)\delta(t - l/W), \tag{2.6}$$

where L is the number of resolvable multipath components. Since the channel maximum delay spread is $\tau_{\max}$, and the time resolution of the systems is $1/W$, the number of multipath components L is obtained as

$$L = \lfloor \tau_{\max} W \rfloor.$$

The lth resolvable path $g_l^{(r)}(t)$ of the multipath fading channel is characterized by its time-varying amplitude $\alpha_l^{(r)}(t)$, and its time-varying phase $\theta_l^{(r)}(t)$ and can be written as

$$g_l^{(r)}(t) = \alpha_l^{(r)}(t)e^{j\theta_l^{(r)}(t)}.$$

Therefore, the frequency-selective fading channel may be modeled by a tapped delay line with $L+1$ uniformly spaced taps. The tap spacing between adjacent taps is $1/W$, and each tap is characterized by a complex-valued time-varying gain $g_l^{(r)}(t)$, as shown in Figure 2.3 [84].

The frequency-selective channel reduces to frequency flat if $L = 0$ or the channel maximum delay spread $\tau_{\max}$ is much smaller than the time resolution of the receiver, i.e. $\tau_{\max} \ll 1/W$.

2.4.3 Fast Fading vs. Slow Fading

In our discussion so far we consider the coherence bandwidth B_c of the channel and its impact on the channel frequency selectivity. In this subsection we will consider the channel's coherence time T_c and its impact on the channel time selectivity. The channel time selectivity determines whether the channel is slowly or fast fading.

Small Scale Fading
(Based on multipath time delay spread)

Flat Fading
1. BW of signal < BW of channel ($W < B_c$)
2. Delay spread < symbol period ($\tau_{\max} < T$)

Frequency–Selective Fading
1. BW of signal > BW of channel ($W > B_c$)
2. Delay spread > symbol period ($\tau_{\max} > T$)

Small Scale Fading
(Based on Doppler spread)

Fast Fading
1. High Doppler spread
2. Coherence time < symbol period ($T_c < T$)
3. Channel variations faster than baseband signal variations

Slow Fading
1. Low Doppler spread
2. Coherence time > symbol period ($T_c > T$)
3. Channel variations slower than baseband signal variations

Figure 2.4: Types of small scale fading [86].

In **fast fading**, the channel impulse response changes rapidly within the symbol period T. In other words, the channel's coherence time is smaller than the symbol period. The time coherence of the channel is directly related to the Doppler spread, the larger the Doppler spread the smaller the coherence time and the faster the channel changes within the symbol period of the transmitted signal. Therefore, the transmitted signal is said to experience fast fading if

$$1/W < T_c.$$

In **slow fading**, the channel impulse response changes at a rate much slower than the symbol period of the transmitted signal. In this case the channel may be assumed to be static (invariant) over several symbol periods. Hence, the transmitted signal is said to experience slow fading if

$$1/W > T_c.$$

Note that, characterizing the channel as slow or fast fading does not specify whether the channel is frequency-selective or frequency-flat. The different types of fading are shown in Figure 2.4 adopted from [86].

In Figure 2.5, we depict the different types of the mobile wireless channels. The time-variation of a one tap channel is depicted in Figure 2.5(a). The general doubly selective channel is depicted in Figure 2.5(b) which arises when the channel maximum delay spread $\tau_{\max} \ll 1/W$ and the transmitted signal bandwidth satisfies $1/W < T_c$. In terms of mobility and data rates, this case

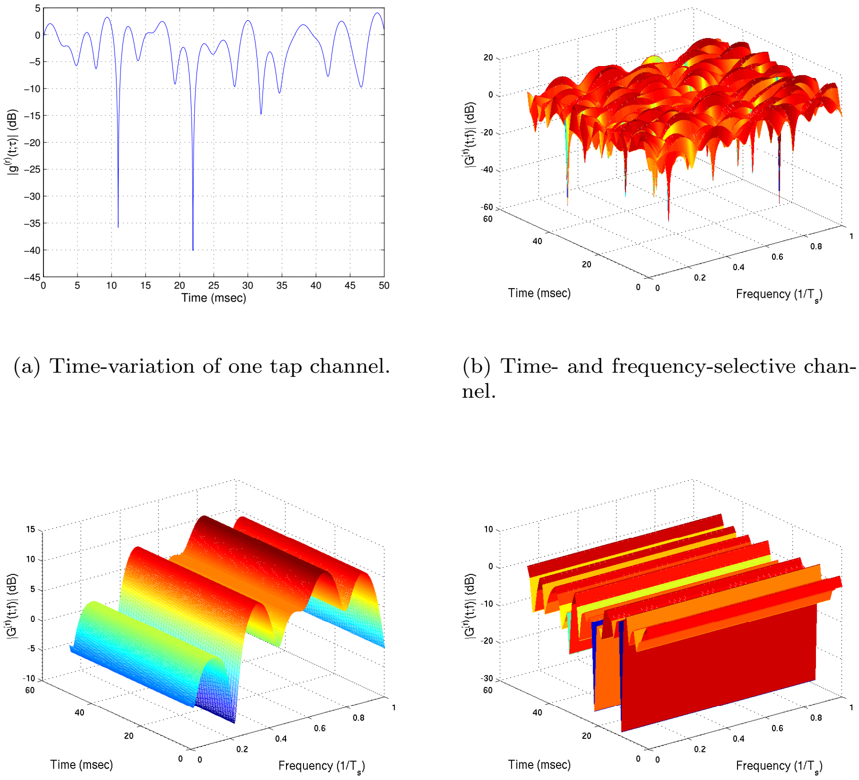

(a) Time-variation of one tap channel.

(b) Time- and frequency-selective channel.

(c) Frequency-selective channel.

(d) Time-selective channel.

Figure 2.5: Fading types in mobile wireless channels.

arises for high mobility high data rate terminals. The frequency-selective case is depicted in Figure 2.5(c). This case arises in general for stationary or low mobility users with high data rate terminals. The time-selective channel is finally depicted in Figure 2.5(d) which arises for high mobility users with low data rate terminals.

2.4.4 Doppler Spread and Time-Selective Fading Channels

The channel is said to be time non-selective if it is time-invariant. Similarly, the channel is said to be time-selective if it is time variant. Channel time-variation results due to the relative motion between the receiver and the transmitter and/or the motion of the surrounding which in turn results in a Doppler shift. The Doppler shift is a measure of the relative frequency shift between the transmitted signal and the received signal. For a mobile moving at a constant speed v and an angle of arrival ϕ, the Doppler shift f_d is given by

$$f_d = \frac{v}{\lambda}\cos\phi = \frac{v}{c} f_c \cos\phi,$$

where λ is the wavelength, c is the speed of light, and f_c is the carrier frequency.

In multipath communications the transmitted signal arrives at the receiver along multiple resolvable paths. Each resolvable path, however, consists of a superposition of a large number of scatterers (rays) that arrive at the receiver almost simultaneously with a common propagation delay. Each of these rays is characterized by its own complex gain and frequency-offset. Hence, we can write the lth resolvable path of the multipath channel characterizing the link between the transmitter and the rth receive antenna as

$$g_l^{(r)}(t) = \sum_{\mu} G_{l,\mu}^{(r)} e^{j2\pi f_{\max}\cos\phi_{l,u}^{(r)} t}, \tag{2.7}$$

where the maximum Doppler spread is obtained as

$$f_{\max} = \frac{v}{c} f_c.$$

For example, for a system with carrier frequency $f_c = 900\ MHz$, and a vehicle speed $v = 120\ Km/hr$, the maximum Doppler spread is $f_{\max} = 100\ Hz$.

Accordingly, the channel time-selectivity is determined by the Doppler shift. The higher the Doppler shift, the faster the channel varies over time, and vice versa.

The time correlation of the multipath channel is often used to characterize how fast the channel changes over time. According to the model described in (2.7), the time correlation of the lth tap of the multipath fading channel can be obtained as[2]:

$$\begin{aligned} r_h(t; t+\tau) &= \mathcal{E}\left\{ g_l^{(r)}(t+\tau) g_l^{(r)*}(t) \right\} \\ &= \mathcal{E}\left\{ \sum_{\mu} G_{l,\mu}^{(r)} e^{j2\pi f_{\max}\cos\phi_{l,u}^{(r)}(t+\tau)} \sum_{\mu'} G_{l,\mu'}^{(r)*} e^{-j2\pi f_{\max}\cos\phi_{l,u'}^{(r)} t} \right\}. \end{aligned} \tag{2.8}$$

When there is a large number of scatterers , the central limit theorem (CLT) leads to a Gaussian process model for the channel impulse response. Assuming a zero-mean Gaussian process, the envelope of the channel impulse response

[2] The analysis done in this section assumes WSSUS (see Section 2.3).

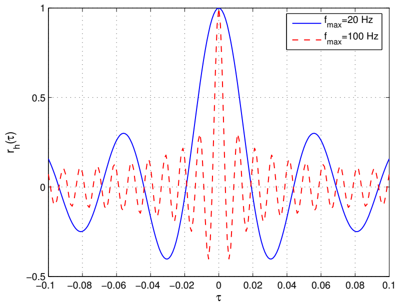

(a) Channel autocorrelation function.

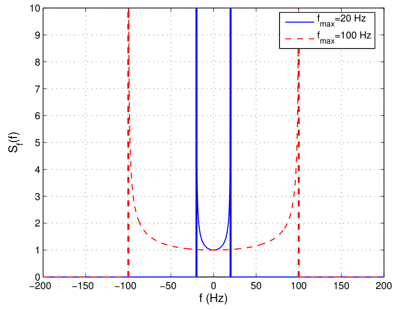

(b) Doppler power spectrum.

Figure 2.6: The channel autocorrelation function and Doppler power spectrum.

at any time instant has a Rayleigh probability distribution and the phase is uniformly distributed in the interval $[0, 2\pi]$. Define the envelope of the lth tap of the multipath channel as $R = |g_l^{(r)}(t)|$, the probability distribution of the random variable R is given according to the Rayleigh probability distribution function:

$$p_R(r) = \frac{r}{\Omega_l^2} e^{-r^2/\Omega_l^2} \qquad r \geq 0,$$

where $\Omega_l^2 = \mathcal{E}\{R^2\}$ represents the average power of the lth tap that may vary from tap to tap according to the power delay profile of the multipath fading channel[3]. It is assumed that the different scattering rays are independent, such that $\mathcal{E}\{G_{l,\mu}^{(r)} G_{l,\mu'}^{(r)}\} = \mathcal{E}\{|G_{l,\mu}^{(r)}|^2\}\delta(\mu - \mu')$. Hence, the autocorrelation function $r_h(t; t+\tau)$ can be written as

$$\begin{aligned} r_h(t; t+\tau) &= \sum_{\mu} \mathcal{E}\left\{|G_{l,\mu}|^2\right\} \mathcal{E}\left\{e^{-j2\pi f_{\max} \cos\phi_{l,\mu}^{(r)} \tau}\right\} \\ &= \Omega_l^2 \frac{1}{2\pi} \int_0^{2\pi} e^{-j2\pi f_{\max} \cos\phi_{l,\mu}^{(r)} \tau} \mathrm{d}\phi \\ &= \Omega_l^2 J_0(2\pi f_{\max} \tau), \end{aligned} \tag{2.9}$$

where J_0 is the zeroth order Bessel function of the first kind. The Doppler power spectrum can therefore be obtained by taking the Fourier transform of the autocorrelation function as

$$S_f(f) = \begin{cases} \frac{\Omega_l^2}{\sqrt{1 - (\frac{f}{f_{\max}})^2}} & |f| \leq f_{\max} \\ 0 & |f| > f_{\max} \end{cases}$$

[3]Throughout this thesis we assume a uniform power delay profile, i.e. all taps have the same average power.

The channel autocorrelation and Doppler power spectrum are shown in Figure 2.6.

2.5 Discrete-Time Channel Model

In digital communication systems, the transmitted signal consists of discrete symbols that are sampled at the symbol rate T and pulse shaped with the transmit filter $g_{tr}(t)$. This pulse shaping operation at the transmitter is usually referred to as digital-to-analog conversion (D/A). Hence, the baseband transmitted signal can be written as

$$x(t) = \sum_{k=-\infty}^{\infty} x[k] g_{tr}(t - kT), \tag{2.10}$$

where $x[k]$ is the kth transmitted symbol (possibly complex) transmitted at a rate of $1/T$ symbols/s.

The transmitted signal is then convolved with the time-varying physical channel $g_{ch}^{(r)}(t;\tau)$, corrupted by the additive noise $v^{(r)}(t)$, and finally filtered with the receive filter $g_{rec}(t)$. Hence, we can write the input-output relationship as

$$\begin{aligned} y^{(r)}(t) = & \sum_{k=-\infty}^{\infty} x[k] g^{(r)}(t; t - kT) + v^{(r)}(t) \\ & \sum_{k=-\infty}^{\infty} x[k] \int_{-\infty}^{\infty} g_{ch}^{(r)}(t;\theta)\psi(t - kT - \theta)\mathrm{d}\,\theta + v^{(r)}(t) \end{aligned} \tag{2.11}$$

where $\psi(t)$ is the overall impulse response of the transmit and receive filters $\psi(t) = g_{tr}(t) \star g_{rec}(t)$.

The received signal is then sampled at the symbol rate T[4]. The discretization operation at the receiver is normally referred to as analog-to-digital conversion (A/D). Define $y^{(r)}[n] = y^{(r)}(nT)$, the discrete-time input-output relationship can be written as

$$\begin{aligned} y^{(r)}[n] &= \sum_{k=-\infty}^{\infty} x[k] \int_{-\infty}^{\infty} g_{ch}^{(r)}(nT;\theta)\psi((n-k)T - \theta)\mathrm{d}\,\theta + v^{(r)}(nT) \\ &= \sum_{k=-\infty}^{\infty} x[k] g^{(r)}[n; n-k] + v^{(r)}[n], \end{aligned} \tag{2.12}$$

[4]Temporal oversampling is also possible here to obtain a SIMO system. In this thesis we consider the use of multiple receive antennas. Assuming temporal oversampling, to some degree, is equivalent to using multiple receive antennas, where the number of equivalent receive antennas is equal to the oversampling factor.

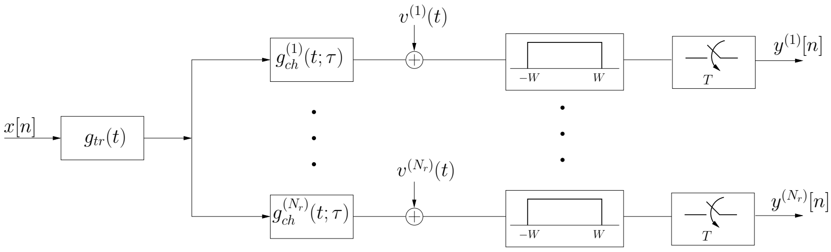

Figure 2.7: System diagram of the discrete-time baseband equivalent communication system.

where $v^{(r)}[n]$ is the discrete-time additive noise at the rth receive antenna. The discrete-time baseband communication systems is shown in Figure 2.7.

Assuming an ideal pulse shaping filter $\psi(t) = \text{sinc}(\pi t/T)$, then $g^{(r)}[n;\nu]$ is obtained as

$$g^{(r)}[n;\nu] = \int_{-\infty}^{\infty} g_{ch}^{(r)}(nT;\tau)\text{sinc}(\pi(\nu T - \tau)/T)\text{d}\tau. \tag{2.13}$$

For large bandwidth channels, (2.13) can be well approximated as

$$g^{(r)}[n;\nu] = g_{ch}^{(r)}(nT;\nu T), \tag{2.14}$$

which corresponds to sampling the time-varying physical channel in the time domain as well as in the lag dimension.

For causal doubly selective channels with finite maximum delay spread $\tau_{\max}$ and order $L = \lfloor \tau_{\max}/T \rfloor$, the input-output relationship (2.12) can be written as

$$y^{(r)}[n] = \sum_{l=0}^{L} g^{(r)}[n;l]x[n-l] + v^{(r)}[n]. \tag{2.15}$$

Note that if $g^{(r)}[n;l] = g_l^{(r)}\ \forall n$, then (2.15) yields a time-invariant frequency-selective channel and the input-output relation becomes:

$$y^{(r)}[n] = \sum_{l=0}^{L} g_l^{(r)} x[n-l] + v^{(r)}[n]. \tag{2.16}$$

On the other hand if $L = 0$, (2.15) yields a time-selective channel with an input-output relation

$$y^{(r)}[n] = g^{(r)}[n]x[n] + v^{(r)}[n]. \tag{2.17}$$

2.6 Basis Expansion Channel Model (BEM)

In the previous sections we have given a brief description of the mobile wireless channel. We have shown that the mobile wireless channel can be characterized as a time-varying multipath fading channel, and that each resolvable path consists of a superposition of a large number of independent scatterers (rays) that arrive at the receiver almost simultaneously. This is referred to as *Jakes' channel model* [56]. In this model the variation of each tap can be simulated as

$$g^{(r)}[n;l] = \sum_{\mu=0}^{Q_J-1} G_{l,\mu}^{(r)} e^{j2\pi f_{\max} T \cos\phi_{l,\mu}^{(r)} n}, \tag{2.18}$$

where:

- Q_J is the number of scatterers,
- $G_{l,\mu}^{(r)}$ is the complex gain of the μth ray of the lth tap,
- $\phi_{l,\mu}^{(r)}$ is the direction of arrival angle of the μth ray of the lth tap, and is a uniformly distributed random variable in $[0, 2\pi]$.

This model, however, is obtained by sampling $g_l^{(r)}(t)$ in (2.7) with the symbol period T . In this model, a huge number of parameters need to be identified and/or equalized (e.g. $Q_J = 400$), which is prohibitive if not impossible in practical systems. This motivates us to search for alternative models with fewer parameters and get enough accuracy to model the real world channel. A model that satisfies these requirement is the basis expansion model (BEM)[102, 46, 79, 89]. In the BEM the time-varying channel taps are expressed as a superposition of a finite number complex exponential basis functions. The BEM makes it feasible to obtain an accurate model of the time-varying channel with a smaller number of parameters by modeling the time-varying channel over a limited time-window. The obtained coefficients may change from window to window as will be clear later.

In the BEM the lth tap of the time-varying channel between the transmitter and the rth receive antennas at time index n is written as

$$h^{(r)}[n;l] = \sum_{q=-Q/2}^{Q/2} h_{q,l}^{(r)} e^{j\omega_q n} \tag{2.19}$$

where $Q+1$ is the number of complex exponential basis functions with frequencies $\{\omega_q\}$. Note the relation with Jakes' channel model with $\omega_q = 2\pi v/\lambda \cos\phi_q$ for sufficiently large Q.

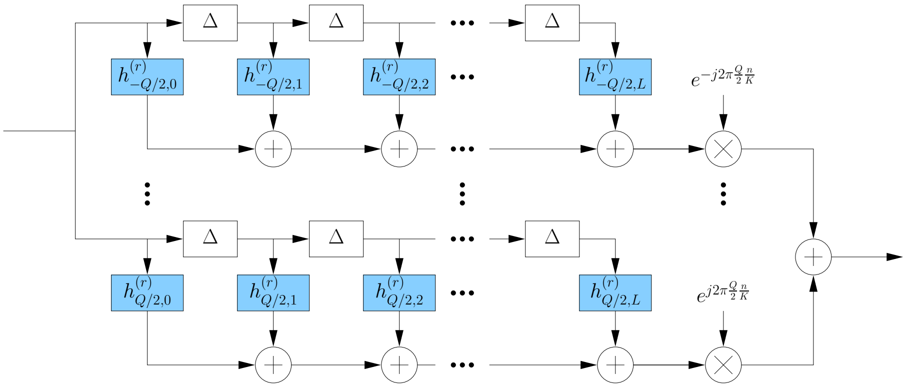

Figure 2.8: Block diagram of BEM channel realization.

In this work, we use the BEM of [89, 77, 69], which has been shown to accurately model realistic channels. In this BEM (which we simply call *the BEM* from now on), the channel is modeled as a time-varying FIR filter, where each tap is expressed as a superposition of complex exponential basis functions with frequencies on a DFT grid, as described next.

Let us first make the following assumptions:

A1) The delay spread is bounded by τ_{max};

A2) The Doppler spread is bounded by f_{max}.

Under assumptions A1) and A2), it is possible to accurately model the doubly-selective channel $g^{(r)}[n;\theta]$ for $n \in \{0, 1, \ldots, N-1\}$ as

$$h^{(r)}[n;l] = \sum_{q=-Q/2}^{Q/2} e^{j2\pi qn/K} h^{(r)}_{q,l}, \quad \text{for } l \in \{0, \cdots, L\}, \tag{2.20}$$

where N is the period of transmission of concern, and $K \geq N$ is the BEM resolution, and L and Q satisfy the following conditions:

C1) $LT \geq \tau_{max}$;

C2) $Q/(KT) \geq 2f_{max}$,

In this expansion model, L represents the discrete delay spread (expressed in multiples of T, the delay resolution of the model), and $Q/2$ represents the discrete Doppler spread (expressed in multiples of $1/(KT)$, the Doppler resolution of the model). Note that the coefficients $h^{(r)}_{q,l}$ remain invariant for

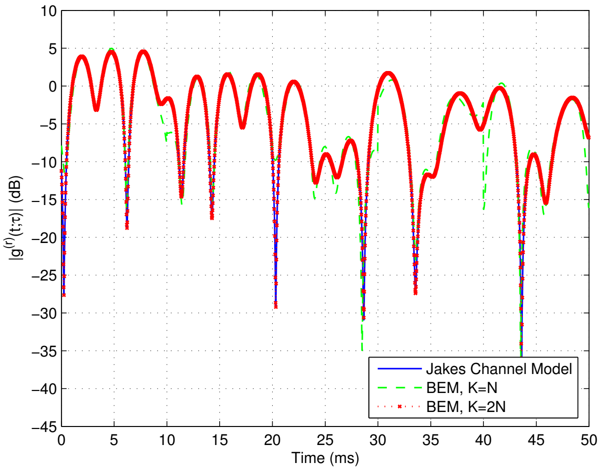

(a) Fitting Jakes' model with the BEM.

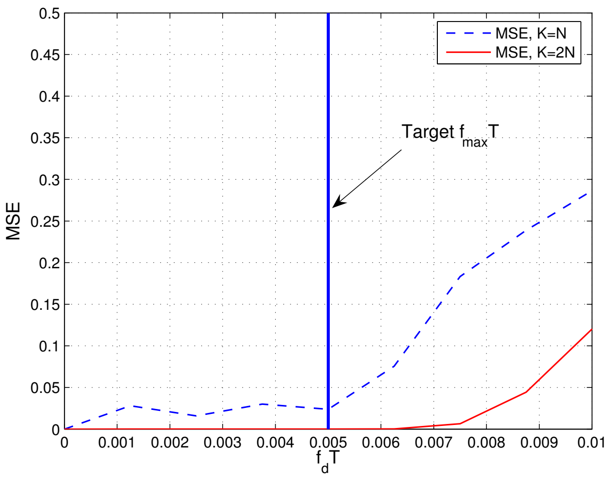

(b) Channel MSE vs the normalized Doppler spread.

Figure 2.9: BEM vs. Jakes' channel model.

$n \in \{0, 1, \ldots, N-1\}$, and hence are the BEM coefficients of interest. Under this BEM the time-varying channel is modeled as shown in Figure 2.8.

The input-output relation under the BEM assumption for $n \in \{0, \ldots, N-1\}$can be written as

$$y^{(r)}[n] = \sum_{l=0}^{L} \sum_{q=-Q/2}^{Q/2} h_{q,l}^{(r)} e^{j2\pi qn/K} x[n-l] + v^{(r)}[n]. \tag{2.21}$$

It is useful to introduce the block version of (2.21). Define $\mathbf{y}^{(r)} = [y^{(r)}[0], \cdots, y^{(r)}[N-1]]^T$, the input-output relation (2.21) on the block level formulation can be written as

$$\mathbf{y}^{(r)} = \sum_{q=-Q/2}^{Q/2} \mathbf{D}_q \mathbf{H}_q^{(r)} \mathbf{x} + \mathbf{v}^{(r)}, \tag{2.22}$$

where $\mathbf{D}_q = \mathrm{diag}\{[1, \cdots, e^{j2\pi q(N-1)/K}]\}$, $\mathbf{H}_q^{(r)}$ is an $N \times (N+L)$ Toeplitz matrix with first row $[h_{q,L}^{(r)}, \cdots, h_{q,0}^{(r)}, \mathbf{0}_{1\times(N-1)}]$, and first column $[h_{q,L}^{(r)}, \mathbf{0}_{1\times(N-1)}]^T$, $\mathbf{x} = [x[-L], \cdots, x[N-1]]^T$, and $\mathbf{v}^{(r)} = [v^{(r)}[0], \cdots, v^{(r)}[N-1]]^T$.

2.6.1 BEM vs. Jakes Model

In this subsection we will examine how accurate the BEM is to approximate the doubly selective channel. In other words, how accurately can the BEM capture the time variation of realistic channels. In this dissertation we will consider the well-known and widely accepted Jakes' model to simulate realistic channels. For our validation process we consider the following channel setup:

- sampling time $T = 25\mu sec$,
- carrier frequency $f_c = 1800MHz$ (GSM carrier),
- maximum mobile speed $v = 120Km/hr$,
- the corresponding maximum Doppler frequency $f_{\max} = 200Hz$,
- realistic channel model according to Jakes' model with $Q_J = 400$ scatterers,
- approximate the realistic channel over a time-window $N = 400$,
- the BEM resolution $K = N$ and $K = 2N$,
- the number of time-varying basis functions $Q = 2\lceil K f_{\max} T \rceil$. Hence, $Q = 4$ for $K = N$, and $Q = 8$ for $K = 2N$.

For simplicity we consider the time-variation of a one-tap channel. We assume the time-varying Jakes' channel is known, and the BEM coefficients are then

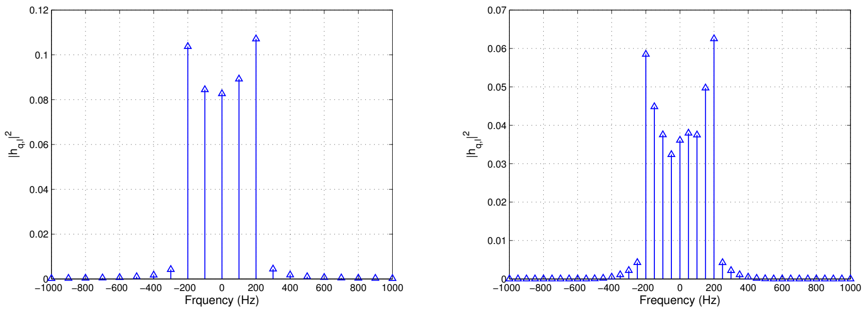

(a) Power Spectrum Density of the BEM coefficients $K = N$.

(b) Power Spectrum Density of the BEM coefficients $K = 2N$.

Figure 2.10: Power Spectrum Density of the BEM coefficients.

obtained by least-squares (LS) fitting. Assume that the lth tap of the time-varying channel is known $\mathbf{g}_l^{(r)} = [g^{(r)}[0,l], \cdots, g^{(r)}[N-1,l]]^T$ where $g^{(r)}[k,l]$ is the lth tap at time index k generated according to Jakes' model as

$$g^{(r)}[k,l] = \sum_{\mu=0}^{Q_J-1} G_{l,\mu}^{(r)} e^{j2\pi f_{\max} T \cos \phi_{l,\mu}^{(r)} k}.$$

The BEM coefficients of the lth tap $\mathbf{h}_l^{(r)} = [h_{-Q/2,l}^{(r)}, \cdots, h_{Q/2,l}^{(r)}]^T$ are then obtained by LS fitting as

$$\mathbf{h}_l^{(r)} = \mathcal{L}_K^{\dagger} \mathbf{g}_l^{(r)},$$

where $\mathcal{L}_K$ is an $N \times (Q+1)$ matrix with the $(q+Q/2+1)$th column given by $[1, e^{j2\pi q/K}, \cdots, e^{j2\pi q(N-1)/K}]^T$.

In Figure 2.9(a), one realization of the Jakes' channel model is plotted. We also plot the BEM fitting for the case of $K = N$, and $K = 2N$. From this figure we verify that the BEM accurately approximates the realistic Jakes' model especially for the case where the BEM resolution is twice the window size ($K = 2N$).

In general, we design the communication system for a target maximum Doppler spread. In this sense we examine the mean square error (MSE) channel estimate between the BEM and Jakes' model as a function of the normalized Doppler spread $f_d T$. This MSE channel estimate actually reflects the modeling error between the BEM and Jakes' model. As shown in Figure 2.9(b), the MSE channel estimate is very small as long as the maximum Doppler spread is lower than the designated Doppler spread. In other words, the MSE channel estimate is very low as long as $f_d \leq f_{\max}$.

The power spectrum density (PSD) of the BEM coefficients is shown in Figure 2.10. From this figure we draw the following observations.

- Both Figures 2.10(a) and 2.10(b) resemble the power spectrum density of Jakes' model (at discrete frequencies shown in Figure 2.6(b)).
- The number of BEM coefficients Q given by $Q = 2\lceil K f_{\max} T \rceil$ is quite accurate. In both figures the power spectrum of coefficients beyond this number is very small and can be neglected.

2.7 Summary

In this chapter, we have shown that the mobile wireless channel may generally be characterized as doubly selective, i.e. selective in both time and frequency. Frequency-selectivity is caused by multipath propagation which introduces intersymbol interference (ISI). Multipath propagation results from reflection, diffraction, and scattering of the radiated electromagnetic waves of buildings and other objects that lie in the vicinity of the transmitter and/or receiver. In this chapter, the main channel parameters of the underlying wireless channel have been introduced. We have mainly focused on the channel parameters that are related to the assumption of wide sense stationary uncorrelated scattering (WSSUS). The basis expansion channel model (BEM) and its relationship to the well known Jakes' channel model has also been introduced. Finally, we have concluded with the validation of the BEM compared with the more realistic Jakes' model.

Part I

Single Carrier Transmission over Time- and Frequency-Selective Fading Channels

In single carrier (SC) transmission data symbols are transmitted using one carrier over the available bandwidth. This is in contrast to multi-carrier (MC) systems, where the available bandwidth is divided into narrow band sub-channels. Multipath fading can cause echoes from a particular data symbol to interfere with adjacent symbols causing intersymbol interference (ISI). To combat the problem of ISI, equalizers are needed to recover the transmitted symbols. If the multipath fading channel is time-invariant (TI), TI equalizers are utilized to compensate for ISI. For time-varying multipath fading channels, TI equalizers are not adequate to compensate for the problem of ISI. For slowly time-varying channels, adaptive algorithms can be invoked in order to provide the equalizer the means of adapting its coefficients. However, for rapidly time-varying channels, adaptive algorithms are not fast enough to provide the equalizer the means to adapt its coefficients.

Equalizers can be classified according to their structure, namely as linear or decision feedback equalizers. Equalizers can also be classified according to the optimization criterion. In this sense, equalizers can be classified as zero-forcing (ZF)[5], when a zero-forcing solution is sought, or minimum mean-square error (MMSE) when the equalizer optimizes the mean-square error (MSE) of the symbol estimate, or maximum likelihood (ML) when the maximum likelihood sequence estimation criterion is utilized.

In the context of linear equalization of TI channels, MMSE and ZF equalizers are investigated in [50, 38]. Decision feedback equalizers (DFE) developed by using previously detected symbols to compensate for ISI are discussed in [80, 23]. Utilizing finite impulse response filters for DFEs is investigated in [5]. Maximum likelihood sequence estimation (MLSE) for data transmission over TI channels with ISI is introduced in [58, 124].

Adaptive techniques for channel estimation or equalization are developed to combat the problem of ISI over slowly time-varying channels. The adaptive algorithms range from the least mean-squares (LMS) algorithm [117, 72, 73], to the recursive least squares (RLS) algorithm or Kalman filtering algorithm [40, 63, 64, 39].

For fast flat-fading channels, polynomial fitting of the 1-tap time-varying channel is used to predict the channel as proposed in [26]. Extending polynomial fitting over the whole packet (or using a sliding window approach) to time-varying frequency-selective channels is investigated in [27]. A maximum likelihood sequence estimation based on the Viterbi algorithm (VA) is studied in [36]. However, the ML approach turns out to be very complex to implement.

In this Part of this thesis we investigate single carrier transmission over doubly selective channels. Future generations wireless (B3G and 4G) systems are required to provide high data rates to high mobility users. For such scenarios,

[5] ZF means that ISI is completely eliminated.

conventional TI equalization schemes or adaptive schemes that are suitable for slowly time-varying channels are not suitable since the channel may vary significantly from sample to sample. In this part, we present channel equalization and estimation schemes as follows.

In **Chapter 3** we focus on the problem of linear equalization of doubly selective channels. We mainly will derive the ZF and MMSE equalizers. In this chapter we will focus on two categories of linear equalizers. Namely, block linear equalizers (BLEs), and serial linear equalizers (SLEs), implemented using time-varying FIR filters. While the first type equalizes a block of received samples, the second type operates on a sample by sample basis. However, the design and implementation of SLEs is done on a block-by-block basis. This material has been published as: [20, 13, 66].

In **Chapter 4**, we focus on the case of decision feedback equalization of doubly selective channels. Similar to Chapter 3, we consider two types of equalizers. First, we focus on block decision feedback equalizers (BDFEs). Second, we propose a serial DFE (SDFE). Unlike linear equalizers which apply one feedforward filter, DFEs apply two filters; a feedforward filter and a feedback filter. Similar to the SLE, the feedforward and feedback filter of the SDFE are implemented using time-varying FIR filters. This material has been published as: [12, 65].

In chapters 3 and 4 we design the equalizers (linear or decision feedback) assuming the doubly selective channel is perfectly known at the receiver. In **Chapter 5**, we focus on the problem of channel estimation and direct equalization based on pilot symbol assisted modulation (PSAM) techniques. This material has been published as: [19, 18].

Using pure pilot symbols for channel estimation and/or direct equalization can actually either be skipped, resulting into blind techniques, or combined with blind techniques resulting into semi-blind techniques as discussed in **Chapter 6**. This material has been published as: [18, 67].

Chapter 3

Linear Equalization of SC Transmission over Doubly Selective Channels

3.1 Introduction

IN this chapter we focus on the problem of equalization for single carrier (SC) transmission over doubly selective channels. We namely focus on the type of linear equalization techniques considering the zero-forcing (ZF) and minimum mean square error (MMSE) criterion.

For frequency-selective channels, equalizers have been extensively studied in literature, where both block and serial equalizers are developed. We may distinguish between these two types as follows. In terms of the ZF solution existence, block linear equalizers (BLEs) for frequency-selective channels only require a single receive antenna [116]. However, they are usually complex to design and to implement. Complex to design because they require an inversion of a large matrix, and complex to implement because a multiplication with a large matrix is required. However, since a frequency-selective channel can be diagonalized by means of the discrete Fourier transform (DFT) in conjunction with the insertion of a cyclic prefix with proper length, the design and implementation complexity can be reduced, at the cost of a slight decrease in performance. On the other hand, serial linear equalizers (SLEs), more specifically finite impulse response (FIR) equalizers, for frequency-selective channels generally require at least two receive antennas for the ZF solution to exist, but allow for a flexible tradeoff between complexity and performance [107, 93].

Recently, equalizers have also been developed for doubly selective channels [75] where TI equalizers are proposed to combat the doubly selective channel. This approach results in the fact that a ZF solution only exists when the number of receive antennas is greater than or equal to the number of basis functions used to accurately approximate the doubly selective channels. Therefore, a different approach will be developed here. As for frequency-selective channels, BLEs for doubly selective channels only require a single receive antenna for the ZF solution to exist. However, since a doubly selective channel cannot be diagonalized by means of a channel independent transformation (such as the DFT), they can not be simplified, and hence, they are always complex to design and implement. This motivates us to look at SLEs, more specifically FIR equalizers, for doubly selective channels, which we expect to allow for a flexible tradeoff between complexity and performance.

In this chapter, we introduce time-varying FIR equalizers for doubly selective channels. We use a basis expansion model (BEM) to approximate the doubly selective channel and to design the time-varying FIR equalizer. This allows us to turn a complicated equalization problem (a time-varying 1-D deconvolution problem) into an equivalent simpler equalization problem (a TI 2-D deconvolution problem), containing only the BEM coefficients of both the doubly selective channel and the time-varying FIR equalizer. We focus on the MMSE as well as the ZF solution. It turns out that time-varying FIR equalizers generally require at least two receive antennas for the ZF solution to exist. However, this is generally much lower than the number of receive antennas TI FIR equalizers require. Decision feedback time-varying FIR equalizers will be treated in Chapter 4.

In this chapter, we consider a non-precoded transmission scheme as well as precoded block transmission techniques. In particular we consider zero padding based and cyclic prefix based block transmission schemes. Note also that more elaborated precoded transmission schemes have recently been developed for doubly selective channels to improve performance [77]. However, these schemes usually apply a complex block equalizer at the receiver. These schemes are outside the scope of this thesis.

This chapter is organized as follows. In Section 3.2, the system model is reviewed. We then introduce block linear equalization in Section 3.3. Serial linear equalizers implemented by time-varying FIR filters are discussed in Section 3.4. Equalization for block transmission techniques is discussed in Section 3.5. Section 3.6 compares block linear equalization and SLE techniques with respect to the existence of the ZF solution as well as complexity. In Section 3.7, we compare through computer simulations the performance of block linear equalizers and time-varying FIR equalizers. Finally, our conclusions are drawn in section 3.8.

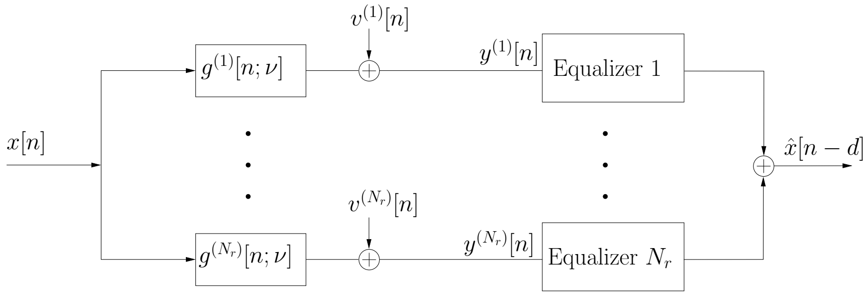

Figure 3.1: Linear Equalizer block diagram.

3.2 System model

The system under consideration is depicted Figure 3.1. We assume a single-input multiple-output (SIMO) system with N_r receive antennas[1].

For completeness here we rewrite the input-output relationship (2.15):

$$y^{(r)}[n] = \sum_{l=0}^{L} g^{(r)}[n;l]x[n-l] + v^{(r)}[n]. \tag{3.1}$$

On each receive antenna we apply an equalizer. An estimate of the transmitted symbol is then obtained by combining the outputs of the equalizers on the different receive antennas. Our estimate here is subject to some decision delay d. Using the BEM to approximate the doubly selective channel $g[n;l]$ for $n \in \{0, 1, \ldots, N-1\}$, we obtain the following relationship:

$$y^{(r)}[n] = \sum_{l=0}^{L} \sum_{q=-Q/2}^{Q/2} e^{j2\pi qn/K} h_{q,l}^{(r)} x[n-l] + v^{(r)}[n]. \tag{3.2}$$

In the following we will develop the block version of the input-output relationships which will be the basis for designing the different equalizers developed in the subsequent sections of this chapter.

Block Data Model

We define the $(N+L) \times 1$ symbol block as $\mathbf{x} = [x[-L], \ldots, x[N-1]]^T$, and the $N \times 1$ received sample block at the rth receive antenna as $\mathbf{y}^{(r)} = [y^{(r)}[0], \ldots, y^{(r)}[N-1]]^T$. Finally $\mathbf{v}^{(r)}$ is similarly defined as $\mathbf{y}^{(r)}$. The received block at the rth receive antenna $\mathbf{y}^{(r)}$ can then be written as:

$$\mathbf{y}^{(r)} = \mathbf{H}^{(r)}\mathbf{x} + \mathbf{v}^{(r)}. \tag{3.3}$$

[1]The extension to multiple-input multiple-output (MIMO) systems is straightforward.

The block channel matrix characterizing the link between the transmitter and the rth receive antenna $\mathbf{H}^{(r)}$ is an $N \times (N+L)$ Toeplitz matrix given by:

$$\mathbf{H}^{(r)} = \sum_{l=0}^{L} \sum_{q=-Q/2}^{Q/2} h_{q,l}^{(r)} \mathbf{D}_q \mathbf{Z}_l, \tag{3.4}$$

where $\mathbf{D}_q = \text{diag}\{[1, \cdots, e^{j2\pi q(N-1)/K}]^T\}$, and $\mathbf{Z}_l$ is the $N \times (N+L)$ Toeplitz matrix defined as $\mathbf{Z}_l = [\mathbf{0}_{(L-l)\times N}, \mathbf{I}_N, \mathbf{0}_{l\times N}]$. Substituting (3.4) in (3.3), we arrive at:

$$\mathbf{y}^{(r)} = \sum_{l=0}^{L} \sum_{q=-Q/2}^{Q/2} h_{q,l}^{(r)} \mathbf{D}_q \mathbf{Z}_l \mathbf{x} + \mathbf{v}^{(r)}. \tag{3.5}$$

Stacking the N_r (number of receive antennas) received sample blocks: $\mathbf{y} = [\mathbf{y}^{(1)T}, \ldots, \mathbf{y}^{(N_r)T}]^T$, we finally obtain:

$$\mathbf{y} = \mathbf{H}\mathbf{x} + \mathbf{v},$$

where $\mathbf{v}$ is similarly defined as $\mathbf{y}$, and $\mathbf{H} = [\mathbf{H}^{(1)T}, \ldots, \mathbf{H}^{(N_r)T}]^T$. In the following, we assume perfect channel knowledge at the receiver. In practice, the BEM coefficients have to be estimated. This can be done blindly [46, 68] or by training [78]. This generally requires the channel to be under-spread, i.e., the product of the delay spread $\tau_{\max}$ (or L) and the Doppler spread $f_{\max}$ (or $Q/2$) to be smaller than $1/2$ (or $N/2$) [59, 76]. However, under the assumption of perfect channel knowledge, the channel spread factor does not play any role in our equalizer design.

3.3 Block Linear Equalization

In this section, we review block linear equalizers (BLEs). We focus on the minimum mean-square error (MMSE) and zero-forcing (ZF) BLEs[2].

The idea is to apply an $N \times N$ BLE $\mathbf{W}^{(r)}$ on the rth receive antenna, as depicted in Figure 3.2, in order to estimate $\mathbf{x}_* = [x[0], \ldots, x[N-1]]^T$ as

$$\begin{aligned}\hat{\mathbf{x}}_* &= \sum_{r=1}^{N_r} \mathbf{W}^{(r)} \mathbf{y}^{(r)} \\ &= \Big(\sum_{r=1}^{N_r} \mathbf{W}^{(r)} \mathbf{H}^{(r)}\Big)\mathbf{x} + \sum_{r=1}^{N_r} \mathbf{W}^{(r)} \mathbf{v}^{(r)}, \end{aligned} \tag{3.6}$$

[2]ISI is completely eliminated in the ZF solution if the underlying communication channel follows perfectly the BEM. In our case, the true channel is first approximated using the BEM, which is then used to design the equalizer (block or serial) to equalize the true channel. Therefore, ZF in the sense of eliminating completely ISI is not truly achieved.

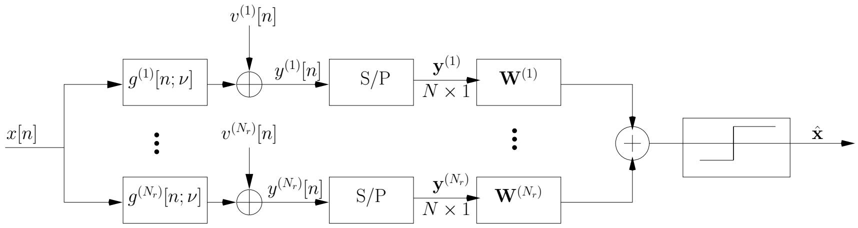

Figure 3.2: Block linear equalization

where $\hat{\mathbf{x}}_* = [\hat{x}[0], \ldots, \hat{x}[N-1]]$ with $\hat{x}[n]$ an estimate for $x[n]$ for $n \in \{0, \cdots, N-1\}$, assuming the transmitted sequence edges ($x[n]$ for $n \in \{-L, \cdots, -1\}$) are taken care of either by being estimated in a previous block or by applying a block transmission technique such as zero-padding or cyclic prefix that takes care of the so-called inter-block interference (IBI), as will be explained later.

Defining $\mathbf{W} = [\mathbf{W}^{(1)}, \ldots, \mathbf{W}^{(N_r)}]$, we obtain

$$\hat{\mathbf{x}}_* = \mathbf{W}\mathbf{y} = \mathbf{W}\mathbf{H}\mathbf{x} + \mathbf{W}\mathbf{v}. \tag{3.7}$$

We will now design BLEs according to the MMSE and ZF criteria.

3.3.1 Minimum Mean-Square Error BLE

The MMSE BLE is determined as

$$\mathbf{W}_{MMSE} = \arg\min_{\mathbf{W}} \mathcal{E}\{\|\hat{\mathbf{x}}_* - \mathbf{x}_*\|^2\},$$

which leads to [62]

$$\mathbf{W}_{MMSE} = \mathbf{R}_{\tilde{x}}^H \mathbf{H}^H (\mathbf{H}\mathbf{R}_x\mathbf{H}^H + \mathbf{R}_v)^{-1} \tag{3.8a}$$

$$= \mathbf{R}_{\tilde{x}}^H \mathbf{R}_x^{-1} \left(\mathbf{R}_x^{-1} + \mathbf{H}^H\mathbf{R}_v^{-1}\mathbf{H}\right) \mathbf{H}^H \mathbf{R}_v^{-1}, \tag{3.8b}$$

where $\mathbf{R}_x = \mathcal{E}\{\mathbf{x}\mathbf{x}^H\}$ is the input source symbol covariance matrix, $\mathbf{R}_{\tilde{x}} = \mathcal{E}\{\mathbf{x}\mathbf{x}_*^H\}$, and $\mathbf{R}_v = \mathcal{E}\{\mathbf{v}\mathbf{v}^H\}$ is the noise covariance matrix. Note that (3.8b) is obtained from (3.8a) by applying the matrix inversion lemma [3].

For a white input source and white noise (i.e. $\mathbf{R}_x = \sigma_s^2\mathbf{I}_{N+L}$, $\mathbf{R}_{\tilde{x}} = \sigma_s^2\mathbf{Z}_0^H$, and $\mathbf{R}_v = \sigma_s^2\mathbf{I}_N$), (3.8b) becomes:

$$\mathbf{W}_{MMSE} = \mathbf{Z}_0(\mathbf{H}^H\mathbf{H} + \frac{\sigma_n^2}{\sigma_s^2}\mathbf{I}_{N+L})^{-1}\mathbf{H}^H. \tag{3.9}$$

[3] $\left(\mathbf{A} - \mathbf{B}\mathbf{D}^{-1}\mathbf{C}\right)^{-1} = \mathbf{A}^{-1} + \mathbf{A}^{-1}\mathbf{B}\left(\mathbf{D} - \mathbf{C}\mathbf{A}^{-1}\mathbf{B}\right)^{-1}\mathbf{C}\mathbf{A}^{-1}$

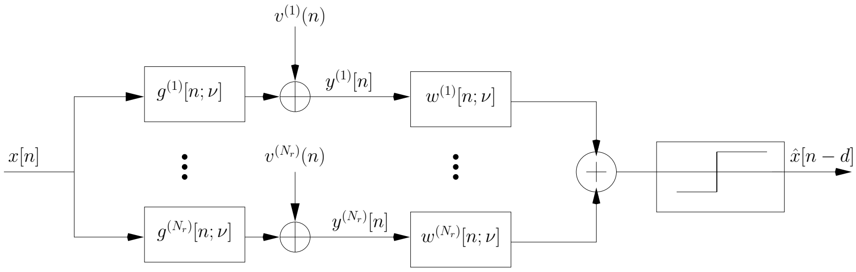

Figure 3.3: Serial linear equalization

3.3.2 Zero-Forcing BLE

From (3.7) an (unbiased) ZF solution is obtained if

$$\mathbf{W}\mathbf{H} = \mathbf{Z}_0. \tag{3.10}$$

Assuming that $\mathbf{H}$ is of full column rank[4], a simple ZF solution is:

$$\mathbf{W}_{ZF} = \mathbf{Z}_0(\mathbf{H}^H\mathbf{H})^{-1}\mathbf{H}^H. \tag{3.11}$$

However, this does not necessarily lead to the minimum norm ZF solution, which is obtained by minimizing the quadratic cost function

$$\min_{\mathbf{W}} \mathbf{W}^H\mathbf{R}_v^{-1}\mathbf{W}$$

subject to (3.10) (see [60]), or equivalently by setting the signal power to infinity in the MMSE solution (see (3.8b)). This leads to [62]

$$\mathbf{W}_{ZF} = \mathbf{Z}_0(\mathbf{H}^H\mathbf{R}_v^{-1}\mathbf{H})^{-1}\mathbf{H}^H\mathbf{R}_v^{-1}. \tag{3.12}$$

Note that (3.12) reduces to (3.11) in the white noise case.

3.4 Serial Linear Equalization

In the previous section we derived the block version of the equalizer considering the MMSE and ZF criterion. In this section, we derive the serial linear equalizer (SLE) considering the ZF and MMSE criterion as well. The SLE consists of a time-varying FIR filter. In other words we apply a time-varying FIR equalizer

[4] A full column rank $\mathbf{H}$ is obtained for the SIMO case ($N_r \geq 2$ receive antenna). However, for the SISO case, this is untrue unless we apply some redundant precoding techniques like zero-padding or cyclic prefix as will be discussed later.

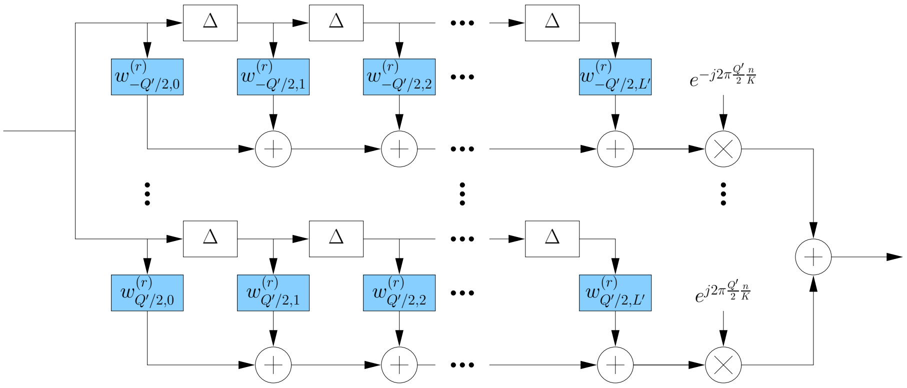

Figure 3.4: Block diagram of BEM realization of the time-varying FIR equalizer.

$w^{(r)}[n;\nu]$ on the rth receive antenna, as depicted in Figure 3.3. We estimate $x[n]$ for $n \in \{0, 1, \ldots, N-1\}$ subject to some decision delay d as:

$$\hat{x}[n-d] = \sum_{r=1}^{N_r} \sum_{\nu=-\infty}^{\infty} w^{(r)}[n;\nu] y^{(r)}[n-\nu]. \tag{3.13}$$

Since the doubly selective channel $g^{(r)}[n;\nu]$ was approximated by the BEM, it is also convenient to design the time-varying FIR equalizer $w^{(r)}[n;\nu]$ using the BEM. This approach will allow us to turn a complicated equalizer design problem into an equivalent simpler equalizer design problem, containing only the BEM coefficients of both the doubly selective channel and the time-varying FIR equalizer. As we explain next, it will allow us to convert a complicated time-varying 1-D deconvolution problem into an equivalent simpler TI 2-D deconvolution problem.

More specifically, we design each time-varying FIR equalizer $w^{(r)}[n;\nu]$ for $n \in \{0, 1, \ldots,$
$N-1\}$ to have $L'+1$ taps, where the time-variation of each tap is modeled by $Q'+1$ complex exponential basis functions with frequencies on the same DFT grid as for the channel, i.e. the time-varying FIR equalizer at the rth receive antenna $w^{(r)}[n;\nu]$ is modeled at time index n as:

$$w^{(r)}[n;l'] = \sum_{q'=-Q'/2}^{Q'/2} w_{q',l'}^{(r)} e^{j2\pi q' n/K}, \tag{3.14}$$

Note that a similar equalizer structure has been proposed in [46, Sec. V.B], but there the authors did not use a model for the time-variation of the different equalizer taps. Note that the time-varying FIR filter in (3.14) has the same structure as the BEM channel in (2.20). Therefore, the time-varying FIR filter is designed (realized) as in Figure 2.8 with L, Q, and $h_{q,l}^{(r)}$ replaced by L', Q', and $w_{q',l'}^{(r)}$, respectively as shown in Figure 3.4.

Using the BEM to design the time-varying FIR filter, an estimate of $x[n]$ subject to some decision delay d for $n \in \{0, 1, \dots, N-1\}$ can be obtained as:

$$\hat{x}[n-d] = \sum_{l'=0}^{L'} \sum_{q'=-Q'/2}^{Q'/2} e^{j2\pi q'n/K} w_{q',l'}^{(r)} y^{(r)}[n-l']. \tag{3.15}$$

Note that for this type of equalizers the decision delay is limited to $0 \leq d \leq L + L' + 1$.

Instead of continuing to work on the sample level, it is more convenient to switch to the block level at this point. This will more clearly reveal the structure we impose on the time-varying FIR filter. On the block level, (3.15) corresponds to estimating the transmitted block $\mathbf{x}_*$ subject to some decision delay ($\mathbf{x}_* = [x[-d], \dots, x[N-d-1]]^T$) as in (3.6), but now with $\mathbf{W}^{(r)}$ constrained to:

$$\mathbf{W}^{(r)} = \sum_{l'=0}^{L'} \sum_{q'=-Q'/2}^{Q'/2} w_{q',l'}^{(r)} \mathbf{D}_{q'} \mathbf{Z}_{l'}. \tag{3.16}$$

An estimate of $\mathbf{x}_*$ is then obtained as

$$\begin{aligned}\hat{\mathbf{x}}_* = &\sum_{r=1}^{N_r} \sum_{q'=-Q'/2}^{Q'/2} \sum_{l'=0}^{L'} w_{q',l'}^{(r)} \mathbf{D}_{q'} \mathbf{Z}_{l'} \sum_{q=-Q/2}^{Q/2} \sum_{l=0}^{L} h_{q,l}^{(r)} \bar{\mathbf{D}}_q \bar{\mathbf{Z}}_l \mathbf{x} \\ &+ \sum_{r=1}^{N_r} \sum_{q'=-Q'/2}^{Q'/2} \sum_{l'=0}^{L'} w_{q',l'}^{(r)} \mathbf{D}_{q'} \mathbf{Z}_{l'} \mathbf{v}^{(r)},\end{aligned} \tag{3.17}$$

with $\hat{\mathbf{x}}_* = [\hat{x}[-d], \dots, \hat{x}[N-d-1]]^T$, redefined here due to the decision delay d, and $\mathbf{v}^{(r)} = [v^{(r)}[-L'], \dots, v^{(r)}[N-1]]^T$.

Note that due to the fact that the SLE operates on the received sequence in a serial fashion, and the time-varying FIR filter is of order L', we redefine $\mathbf{x}$ as $\mathbf{x} = [x[-L-L'], \dots, x[N-1]]^T$, which is different than the definition introduced while discussing the BLEs. Accordingly, we redefine the matrices $\mathbf{Z}_{l'}$, $\bar{\mathbf{Z}}_l$, $\mathbf{D}_{q'}$, and $\bar{\mathbf{D}}_q$ as follows:

$$\begin{aligned}\mathbf{Z}_{l'} &= [\mathbf{0}_{N\times(L'-l')}, \mathbf{I}_N, \mathbf{0}_{N\times l'}] & \bar{\mathbf{Z}}_l &= [\mathbf{0}_{(N+L')\times(L-l)}, \mathbf{I}_{(N+L)}, \mathbf{0}_{(N+L')\times l}] \\ \mathbf{D}_{q'} &= \mathrm{diag}\{[1, \dots, e^{j2\pi q'(N-1)/K}]^T\} & \bar{\mathbf{D}}_q &= \mathrm{diag}\{[1, \dots, e^{j2\pi q(N+L'-1)/K}]^T\}\end{aligned}$$

Defining $p = q + q'$, $k = l + l'$, and using the following property

$$\mathbf{Z}_{l'} \bar{\mathbf{D}}_q = e^{j2\pi q(L'-l')/K} \mathbf{D}_q \mathbf{Z}_{l'},$$

(3.17) can be rewritten as:

$$\hat{\mathbf{x}}_* = \sum_{p=-(Q+Q')/2}^{(Q+Q')/2} \sum_{k=0}^{L+L'} f_{p,k} \mathbf{D}_p \tilde{\mathbf{Z}}_k \mathbf{x} + \sum_{r=1}^{N_r} \sum_{q'=-Q'/2}^{Q'/2} \sum_{l'=0}^{L'} w_{q',l'}^{(r)} \mathbf{D}_{q'} \mathbf{Z}_{l'} \mathbf{v}^{(r)}, \quad (3.18)$$

where we have introduced the 2-dimensional function

$$f_{p,k} = \sum_{r=1}^{N_r} \sum_{q'=-Q'/2}^{Q'/2} \sum_{l'=0}^{L'} e^{-j2\pi(p-q')(L'-l')/K} w_{q',l'}^{(r)} h_{p-q',k-l'}^{(r)}, \quad (3.19)$$

and $\tilde{\mathbf{Z}}_k = [\mathbf{0}_{N\times(L+L'-k)}, \mathbf{I}_N, \mathbf{0}_{N\times k}]$. It will be useful to rewrite (3.18) in a matrix-vector form as

$$\hat{\mathbf{x}}_* = (\mathbf{f}^T \otimes \mathbf{I}_N)\mathbf{A}\mathbf{x} + \sum_{r=1}^{N_r} (\mathbf{w}^{(r)T} \otimes \mathbf{I}_N)\mathbf{B}^{(r)}\mathbf{v}^{(r)}, \quad (3.20)$$

where $\mathbf{f} = [f_{-(Q+Q')/2,0}, \ldots, f_{-(Q+Q')/2,L+L'}, \ldots, f_{(Q+Q')/2,L+L'}]^T$, $\mathbf{w}^{(r)} = [w_{-Q'/2,0}^{(r)}, \ldots, w_{-Q'/2,L'}^{(r)}, \ldots, w_{Q'/2,L'}^{(r)}]^T$ and the matrices $\mathbf{A}$ and $\mathbf{B}^{(r)}$ are defined as

$$\mathbf{A} = \begin{bmatrix} \mathbf{D}_{-(Q+Q')/2} \tilde{\mathbf{Z}}_0 \\ \vdots \\ \mathbf{D}_{-(Q+Q')/2} \tilde{\mathbf{Z}}_{L+L'} \\ \vdots \\ \mathbf{D}_{(Q+Q')/2} \tilde{\mathbf{Z}}_{L+L'} \end{bmatrix}, \quad \mathbf{B}^{(r)} = \begin{bmatrix} \mathbf{D}_{-Q'/2} \mathbf{Z}_0 \\ \vdots \\ \mathbf{D}_{-Q'/2} \mathbf{Z}_{L'} \\ \vdots \\ \mathbf{D}_{Q'/2} \mathbf{Z}_{L'} \end{bmatrix}.$$

Note that $\mathbf{B}^{(r)}$ does not depend on r. However, when different equalizer orders and delays would be selected for the different receive antennas, $\mathbf{B}^{(r)}$ would depend on r. We can further rewrite (3.20) as

$$\hat{\mathbf{x}}_* = (\mathbf{f}^T \otimes \mathbf{I}_N)\mathbf{A}\mathbf{x} + (\mathbf{w}^T \otimes \mathbf{I}_N)\mathbf{B}\mathbf{v}, \quad (3.21)$$

where

$$\mathbf{w} = [\mathbf{w}^{(1)T}, \ldots, \mathbf{w}^{(N_r)T}]^T,$$

and the matrix $\mathbf{B}$ is defined as

$$\mathbf{B} = \begin{bmatrix} \mathbf{B}^{(1)} & & \\ & \ddots & \\ & & \mathbf{B}^{(N_r)} \end{bmatrix}.$$

The term in $f_{p,k}$ (see (3.19)) corresponding to the rth receive antenna is related to a 2-dimensional convolution of the BEM coefficients of the doubly selective channel for the rth receive antenna and the BEM coefficients of the time-varying FIR equalizer for the rth receive antenna. This allows us to derive a linear relationship between $\mathbf{f}$ and $\mathbf{w}$, as discussed next.

We first define the $(L'+1) \times (L'+L+1)$ block Toeplitz matrix

$$\mathcal{T}_{l,L'+1}(h_{q,l}^{(r)}) = \begin{bmatrix} h_{q,0}^{(r)} & \dots & h_{q,L}^{(r)} & & 0 \\ & \ddots & & \ddots & \\ 0 & & h_{q,0}^{(r)} & \dots & h_{q,L}^{(r)} \end{bmatrix}.$$

We then define $\boldsymbol{\mathcal{H}}_q^{(r)} = \boldsymbol{\Omega}_q \mathcal{T}_{l,L'+1}(h_{q,l}^{(r)})$, where $\boldsymbol{\Omega}_q = \mathrm{diag}\{[e^{-j2\pi qL'/K}, \dots, 1]^T\}$, and introduce the $(Q'+1)(L'+1) \times (Q+Q'+1)(L+L'+1)$ block Toeplitz matrix

$$\mathcal{T}_{q,Q'+1}(\boldsymbol{\mathcal{H}}_q^{(r)}) = \begin{bmatrix} \boldsymbol{\mathcal{H}}_{-Q/2}^{(r)} & \dots & \boldsymbol{\mathcal{H}}_{Q/2}^{(r)} & & \mathbf{0} \\ & \ddots & & \ddots & \\ \mathbf{0} & & \boldsymbol{\mathcal{H}}_{-Q/2}^{(r)} & \dots & \boldsymbol{\mathcal{H}}_{Q/2}^{(r)} \end{bmatrix}.$$

Introducing the notation $\boldsymbol{\mathcal{H}}^{(r)} = \mathcal{T}_{q,Q'+1}(\boldsymbol{\mathcal{H}}_q^{(r)})$ and defining the matrix $\boldsymbol{\mathcal{H}} = [\boldsymbol{\mathcal{H}}^{(1)T}, \dots, \boldsymbol{\mathcal{H}}^{(N_r)T}]^T$, we can then derive from (3.19) that:

$$\mathbf{f}^T = \mathbf{w}^T \boldsymbol{\mathcal{H}}. \tag{3.22}$$

Substituting (3.22) in (3.21) finally leads to

$$\hat{\mathbf{x}}_* = (\mathbf{w}^T \boldsymbol{\mathcal{H}} \otimes \mathbf{I}_N)\mathbf{A}\mathbf{x} + (\mathbf{w}^T \otimes \mathbf{I}_N)\mathbf{B}\mathbf{v}. \tag{3.23}$$

Based on this equation, we will now design time-varying FIR equalizers according to the MMSE and ZF criteria.

3.4.1 Minimum Mean-Square Error SLE

The BEM coefficients of the MMSE time-varying FIR filter are determined as

$$\mathbf{w}_{MMSE} = \arg\min_{\mathbf{w}} \mathcal{E}\{\|\hat{\mathbf{x}}_* - \mathbf{x}_*\|^2\}. \tag{3.24}$$

Using (3.23), the MSE can be written as

$$\begin{aligned} \mathcal{E}\{\|\hat{\mathbf{x}}_* - \mathbf{x}_*\|^2\} = {} & \mathrm{tr}\left\{(\mathbf{w}^T \boldsymbol{\mathcal{H}} \otimes \mathbf{I}_N)\mathbf{A}\mathbf{R}_x\mathbf{A}^H(\boldsymbol{\mathcal{H}}^H\mathbf{w}^* \otimes \mathbf{I}_N)\right\} \\ & + \mathrm{tr}\left\{(\mathbf{w}^T \otimes \mathbf{I}_N)\mathbf{B}\mathbf{R}_v\mathbf{B}^H(\mathbf{w}^* \otimes \mathbf{I}_N)\right\} \\ & - 2\Re\left\{\mathrm{tr}\left\{(\mathbf{w}^T \boldsymbol{\mathcal{H}} \otimes \mathbf{I}_N)\mathbf{A}\mathbf{R}_{\tilde{x}}\right\}\right\} + \mathrm{tr}\left\{\mathbf{R}_{\tilde{x}}\right\}, \end{aligned} \tag{3.25}$$

where $\mathbf{R}_{\tilde{x}} = \mathcal{E}\{\mathbf{x}_*\mathbf{x}_*^H\}$. Let us now introduce the following properties:

$$\mathrm{tr}\{(\mathbf{a}^T \otimes \mathbf{I}_N)\mathbf{V}\} = \mathbf{a}^T \mathrm{subtr}\{\mathbf{V}\}, \tag{3.26}$$

$$\mathrm{tr}\{(\mathbf{a}^T \otimes \mathbf{I}_N)\mathbf{U}(\mathbf{a}^* \otimes \mathbf{I}_N)\} = \mathbf{a}^T \mathrm{subtr}\{\mathbf{U}\}\mathbf{a}^*, \tag{3.27}$$

for an arbitrary $k \times 1$ vector $\mathbf{a}$, arbitrary $kN \times N$ matrix $\mathbf{V}$, and arbitrary $kN \times kN$ matrix $\mathbf{U}$. subtr$\{\cdot\}$ splits the matrix up into $N \times N$ sub-matrices and replaces each sub-matrix by its trace [5]. Hence, subtr$\{\cdot\}$ reduces the row and column dimension by a factor N. The MSE can then be written as:

$$\mathcal{E}\{\|\hat{\mathbf{x}}_* - \mathbf{x}_*\|^2\} = \mathrm{tr}\left\{\mathbf{R}_{\tilde{x}}\right\} + \mathbf{w}^T\boldsymbol{\mathcal{H}}\mathbf{R}_A\boldsymbol{\mathcal{H}}^H\mathbf{w}^* + \mathbf{w}^T\mathbf{R}_B\mathbf{w}^* - 2\Re\left\{\mathbf{w}^T\boldsymbol{\mathcal{H}}\mathbf{r}_A\right\} \tag{3.28}$$

where $\mathbf{r}_A = \mathrm{subtr}\{\mathbf{A}\mathbf{R}_{\tilde{x}}\}$, $\mathbf{R}_A = \mathrm{subtr}\{\mathbf{A}\mathbf{R}_x\mathbf{A}^H\}$, and $\mathbf{R}_B = \mathrm{subtr}\{\mathbf{B}\mathbf{R}_v\mathbf{B}^H\}$. The BEM coefficients of the MMSE time-varying FIR filter are now obtained by solving $\partial\mathcal{E}\{\|\hat{\mathbf{x}}_* - \mathbf{x}_*\|^2\}/\partial\mathbf{w} = \mathbf{0}$, which leads to

$$\begin{aligned}
\mathbf{w}_{MMSE}^T &= \mathbf{r}_A^H\boldsymbol{\mathcal{H}}^H(\boldsymbol{\mathcal{H}}\mathbf{R}_A\boldsymbol{\mathcal{H}}^H + \mathbf{R}_B)^{-1} && \text{(3.29a)}\\
&= \mathbf{r}_A^H\mathbf{R}_A^{-1}(\boldsymbol{\mathcal{H}}^H\mathbf{R}_B^{-1}\boldsymbol{\mathcal{H}} + \mathbf{R}_A^{-1})^{-1}\boldsymbol{\mathcal{H}}^H\mathbf{R}_B^{-1}, && \text{(3.29b)}\\
&= \mathbf{e}_d^T(\boldsymbol{\mathcal{H}}^H\mathbf{R}_B^{-1}\boldsymbol{\mathcal{H}} + \mathbf{R}_A^{-1})^{-1}\boldsymbol{\mathcal{H}}^H\mathbf{R}_B^{-1}, && \text{(3.29c)}
\end{aligned}$$

where (3.29b) is again obtained from (3.29a) by applying the matrix inversion lemma, and (3.29c) is obtained from (3.29b) by using the fact that $\mathbf{r}_A^H\mathbf{R}_A^{-1} = \mathbf{e}_d^T$, where $\mathbf{e}_d$ is a $(Q + Q' + 1)(L + L' + 1) \times 1$ unit vector with the 1 in the $((Q + Q')(L + L' + 1)/2 + d + 1)$st position. Substituting (3.29c) in (3.28), we can now write the MSE of the MMSE SLE as

$$\begin{aligned}
MSE_{MMSE} &= \mathbf{e}_d^T\Big(\mathbf{R}_A - \mathbf{R}_A\boldsymbol{\mathcal{H}}^H\mathbf{R}_B^{-1}\boldsymbol{\mathcal{H}}(\boldsymbol{\mathcal{H}}^H\mathbf{R}_B^{-1}\boldsymbol{\mathcal{H}} + \mathbf{R}_A^{-1})^{-1}\Big)\mathbf{e}_d\\
&= \mathbf{e}_d^T(\mathbf{R}_A^{-1} + \boldsymbol{\mathcal{H}}^H\mathbf{R}_B^{-1}\boldsymbol{\mathcal{H}})^{-1}\mathbf{e}_d && \text{(3.30)}
\end{aligned}$$

Note that we have used the fact that $\mathrm{tr}\{\mathbf{R}_{\tilde{x}}\} = \mathbf{e}_d^T\mathbf{R}_A\mathbf{e}_d$.

3.4.2 Zero-Forcing SLE

From (3.23), an (unbiased) ZF solution is obtained if

$$(\mathbf{w}^T\boldsymbol{\mathcal{H}} \otimes \mathbf{I}_N)\mathbf{A} = \tilde{\mathbf{Z}}_d, \tag{3.31}$$

[5] Let $\mathbf{A}$ be the $pN \times qN$ matrix: $\mathbf{A} = \begin{bmatrix} \mathbf{A}_{11} & \dots & \mathbf{A}_{1q} \\ \vdots & \ddots & \vdots \\ \mathbf{A}_{p1} & \dots & \mathbf{A}_{pq} \end{bmatrix}$, where $\mathbf{A}_{ij}$ is the (i, j)th $N \times N$ sub-matrix of $\mathbf{A}$. The $p \times q$ matrix subtr$\{\mathbf{A}\}$ is then given by: $\mathrm{subtr}\{\mathbf{A}\} = \begin{bmatrix} \mathrm{tr}\{\mathbf{A}_{11}\} & \dots & \mathrm{tr}\{\mathbf{A}_{1q}\} \\ \vdots & \ddots & \vdots \\ \mathrm{tr}\{\mathbf{A}_{p1}\} & \dots & \mathrm{tr}\{\mathbf{A}_{pq}\} \end{bmatrix}$

which is equivalent to

$$\mathbf{w}^T \boldsymbol{\mathcal{H}} = \mathbf{e}_d^T.$$

Therefore, a simple ZF is obtained as

$$\mathbf{w}_{ZF}^T = \mathbf{e}_d^T \left(\boldsymbol{\mathcal{H}}^H \boldsymbol{\mathcal{H}}\right)^{-1} \boldsymbol{\mathcal{H}}^H. \tag{3.32}$$

However, this does not necessarily lead to the minimum norm ZF solution, which is obtained by minimizing the quadratic cost function

$$\min_{\mathbf{w}} \mathbf{w}^T \mathbf{R}_B \mathbf{w}^* \quad \text{subject to} \quad \mathbf{w}^T \boldsymbol{\mathcal{H}} = \mathbf{e}_d^T.$$

which is again equivalently obtained by setting the signal power equal to infinity in the MMSE solution (see (3.29c)). This leads to

$$\mathbf{w}_{ZF}^T = \mathbf{e}_d^T (\boldsymbol{\mathcal{H}}^H \mathbf{R}_B^{-1} \boldsymbol{\mathcal{H}})^{-1} \boldsymbol{\mathcal{H}}^H \mathbf{R}_B^{-1}. \tag{3.33}$$

By setting the signal power to infinity in (3.30), we obtain the MSE of the ZF time-varying FIR equalizer:

$$MSE_{ZF} = \mathbf{e}_d^T (\boldsymbol{\mathcal{H}}^H \mathbf{R}_B^{-1} \boldsymbol{\mathcal{H}})^{-1} \mathbf{e}_d \tag{3.34}$$

3.5 Equalization with Block Transmission Techniques

In our discussion so far we considered serial transmission where no structure is imposed on the transmitted sequence, and therefore inter-block interference (IBI) is typically present. In this section we focus on block transmission techniques for two reasons. First, block transmission techniques have been proposed to overcome the edge effect, i.e. to overcome the problem of IBI. Second, in our equalizer design we rely on the BEM to approximate the doubly selective channel and to design the equalizer. In this BEM model, we fit the model over a block of symbols, and the model coefficients may change from block to block. Therefore, it is more convenient to consider block transmission techniques. In this section we will focus on zero-padding (ZP) based block transmission, and cyclic-prefix (CP) based block transmission techniques.

In block transmission techniques the transmitted sequence is parsed into blocks of size N each. A CP or ZP of length ν is appended at the top of each block as explained in Figure 3.5. For channels with order L, a CP or ZP of length $\nu \geq L$ is sufficient to eliminate IBI. Bearing this in mind we will develop equalization techniques (block and serial) for these types of transmission.

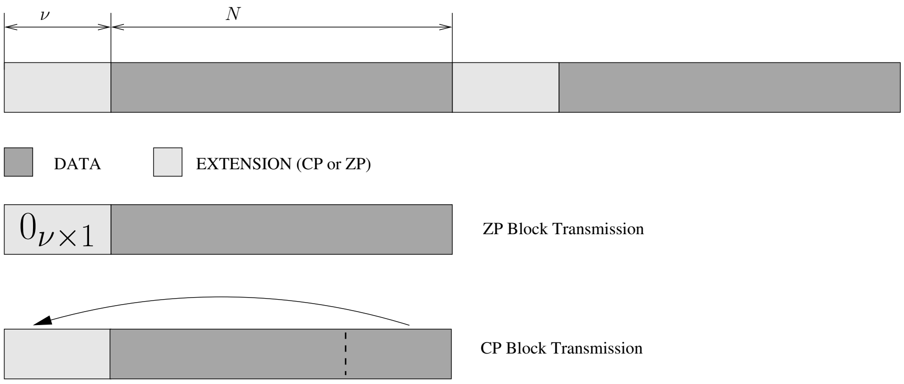

Figure 3.5: The transmitted sequence for CP/ZP-based block transmission.

3.5.1 BLE for Block Transmission

ZP-Based Block Transmission

In ZP-based block transmission trailing zeros of length ν are appended at the top of the transmitted block as explained in Figure 3.5. For this type of transmission the input-output relationship is written as:

$$\mathbf{y} = \bar{\mathbf{H}}\mathbf{x} + \mathbf{v}. \tag{3.35}$$

where $\bar{\mathbf{H}} = [\bar{\mathbf{H}}^{(1)T}, \ldots, \bar{\mathbf{H}}^{(N_r)T}]^T$, with $\bar{\mathbf{H}}^{(r)}$ given by:

$$\bar{\mathbf{H}}^{(r)} = \sum_{-Q/2}^{Q/2} \mathbf{D}_q \bar{\mathbf{H}}_q^{(r)}, \tag{3.36}$$

where $\bar{\mathbf{H}}_q^{(r)}$ is an $N \times N$ Toeplitz matrix given by:

$$\bar{\mathbf{H}}_q^{(r)} = \begin{bmatrix} h_{q,0}^{(r)} & 0 & & \cdots & & 0 \\ \vdots & \ddots & \ddots & & & \\ h_{q,L}^{(r)} & & \ddots & \ddots & & \vdots \\ 0 & \ddots & & \ddots & \ddots & \\ \vdots & \ddots & \ddots & & \ddots & 0 \\ 0 & \cdots & 0 & h_{q,L}^{(r)} & \cdots & h_{q,0}^{(r)} \end{bmatrix}.$$

Hence the **MMSE equalizer** obtained in (3.8a) and (3.8b) reduces to:

$$\begin{aligned} \mathbf{W}_{MMSE,zp} &= \mathbf{R}_x \bar{\mathbf{H}}^H (\bar{\mathbf{H}} \mathbf{R}_x \bar{\mathbf{H}}^H + \mathbf{R}_v)^{-1} \\ &= (\bar{\mathbf{H}}^H \mathbf{R}_v^{-1} \bar{\mathbf{H}} + \mathbf{R}_x^{-1})^{-1} \bar{\mathbf{H}}^H \mathbf{R}_v^{-1}, \end{aligned}$$

and the **ZF solution** can then be obtained; assuming full column rank $\bar{\mathbf{H}}$, as[6]:

$$\mathbf{W}_{ZF,zp} = (\bar{\mathbf{H}}^H \mathbf{R}_v^{-1} \bar{\mathbf{H}})^{-1} \bar{\mathbf{H}}^H \mathbf{R}_v^{-1},$$

which is obtained by setting the signal power to infinity. It can be easily shown that this solution corresponds to solving the following optimization problem [60]:

$$\min_{\mathbf{W}} \mathbf{W}^H \mathbf{R}_v \mathbf{W} \quad \text{subject to} \quad \mathbf{W}\bar{\mathbf{H}} = \mathbf{I}_N.$$

For a white data source and white noise ($\mathbf{R}_x = \sigma_s^2 \mathbf{I}$, and $\mathbf{R}_v = \sigma_n^2 \mathbf{I}$), the MMSE and ZF equalizers can be written as:

$$\begin{aligned} \mathbf{W}_{MMSE,zp} &= (\bar{\mathbf{H}}^H \bar{\mathbf{H}} + \frac{\sigma_n^2}{\sigma_s^2} \mathbf{I}_N)^{-1} \bar{\mathbf{H}}^H \\ \mathbf{W}_{ZF,zp} &= (\bar{\mathbf{H}}^H \bar{\mathbf{H}})^{-1} \bar{\mathbf{H}}^H. \end{aligned}$$

CP-Based Block Transmission

For the case of CP-based block transmission techniques, the same analysis is applied as the ZP-based block transmission technique except for the definition of the matrix $\bar{\mathbf{H}}_q^{(r)}$, which is now defined as:

$$\bar{\mathbf{H}}_q^{(r)} = \begin{bmatrix} h_{q,0}^{(r)} & 0 & \dots & 0 & h_{q,L}^{(r)} & \dots & h_{q,1}^{(r)} \\ \vdots & \ddots & & & & \ddots & \vdots \\ \vdots & & \ddots & & & & h_{q,L}^{(r)} \\ h_{q,L}^{(r)} & & & \ddots & & & \\ 0 & \ddots & & & \ddots & & \vdots \\ \vdots & \ddots & \ddots & & & \ddots & \\ 0 & \dots & 0 & & h_{q,L}^{(r)} & \dots & h_{q,0}^{(r)} \end{bmatrix}.$$

The full column rank requirement here happens with probability one for time-varying channels as well as for TI channels. For time-varying channels, the conditions that violate the full column rank property are not known yet, and still under investigation. However, the full column rank property is violated for TI channels when the TI channel has zeros on the DFT grid (i.e. when the channel experiences deep fades).

[6] The full column rank property is achieved here for the case of SISO systems with probability 1. For the TI case the full column rank property is always satisfied.

3.5.2 SLE for Block Transmission

ZP-Based Block Transmission

For the ZP-based block transmission, the time-varying FIR filter is cleared over each block. This process corresponds to appending L' zeros at the top of each received block. In this case the time-varying FIR equalizer at the rth receive antenna is restricted to:

$$\mathbf{W}^{(r)} = \sum_{l'=0}^{L} \sum_{q'=-Q'/2}^{Q'/2} w_{q',l'}^{(r)} \mathbf{D}_{q'} \mathbf{Z}_{l'},$$

with $\mathbf{Z}_{l'}$ is an $N \times N$ lower triangular Toeplitz matrix with the first column $[\mathbf{0}_{1\times l'}, 1, \mathbf{0}_{1\times(N-l'-1)}]^T$. Taking the decision delay d into account, we redefine the transmitted block to count for this decision as $\mathbf{x} = [\mathbf{x}_*^T, \mathbf{0}_{1\times d}]^T$, where $\mathbf{x}_* = [x[0], \ldots, x[M-1]]^T$ with $M = N - d$. A relation between $\mathbf{x}$ and $\mathbf{x}_*$ is obtained as:

$$\mathbf{x} = \bar{\mathbf{T}}_{zp} \mathbf{x}_*,$$

where $\bar{\mathbf{T}}_{zp} = [\mathbf{I}_M, \mathbf{0}_{M\times d}]^T$. Hence, the received sequence at the rth receive antenna can be written as:

$$\mathbf{y}^{(r)} = \sum_{l=0}^{L} \sum_{q=-Q/2}^{Q/2} h_{q,l}^{(r)} \mathbf{D}_q \mathbf{Z}_l \bar{\mathbf{T}}_{zp} \mathbf{x}_* + \mathbf{v}^{(r)}, \tag{3.37}$$

An estimate of $\mathbf{x}_*$ is then obtained as

$$\begin{aligned}\hat{\mathbf{x}}_* = {} & \mathbf{R}_{zp} \sum_{r=1}^{N_r} \sum_{q'=-Q'/2}^{Q'/2} \sum_{l'=0}^{L'} w_{q',l'}^{(r)} \mathbf{D}_{q'} \mathbf{Z}_{l'} \sum_{q=-Q/2}^{Q/2} \sum_{l=0}^{L} h_{q,l}^{(r)} \mathbf{D}_q \mathbf{Z}_l \bar{\mathbf{T}}_{zp} \mathbf{x}_* \\ & + \mathbf{R}_{zp} \sum_{r=1}^{N_r} \sum_{q'=-Q'/2}^{Q'/2} \sum_{l'=0}^{L'} w_{q',l'}^{(r)} \mathbf{D}_{q'} \mathbf{Z}_{l'} \mathbf{v}^{(r)},\end{aligned} \tag{3.38}$$

where $\mathbf{R}_{zp} = [\mathbf{0}_{M\times d}, \mathbf{I}_M]$. Defining $p = q+q'$, $k = l+l'$, and using the property $\mathbf{Z}_{l'} \mathbf{D}_q = e^{-j2\pi q l'/N} \mathbf{D}_q \mathbf{Z}_{l'}$, (3.38) can be rewritten as

$$\hat{\mathbf{x}}_* = \mathbf{R}_{zp} \sum_{p=-(Q+Q')/2}^{(Q+Q')/2} \sum_{k=0}^{L+L'} f_{p,k} \mathbf{D}_p \mathbf{Z}_k \bar{\mathbf{T}}_{zp} \mathbf{x}_* + \mathbf{R}_{zp} \sum_{r=1}^{N_r} \sum_{q'=-Q'/2}^{Q'/2} \sum_{l'=0}^{L'} w_{q',l'}^{(r)} \mathbf{D}_{q'} \mathbf{Z}_{l'} \mathbf{v}^{(r)}, \tag{3.39}$$

where

$$f_{p,k} = \sum_{r=1}^{N_r} \sum_{q'=-Q'/2}^{Q'/2} \sum_{l'=0}^{L'} e^{-j2\pi(p-q')l'/N} w_{q',l'}^{(r)} h_{p-q',k-l'}^{(r)}. \tag{3.40}$$

Next, we rewrite (3.39) as

$$\begin{aligned}\hat{\mathbf{x}}_* &= (\mathbf{f}^T \otimes \mathbf{I}_M)\tilde{\mathbf{A}}\mathbf{x}_* + \sum_{r=1}^{N_r}(\mathbf{w}^{(r)T} \otimes \mathbf{I}_M)\tilde{\mathbf{B}}\mathbf{v}^{(r)} \\ &= (\mathbf{f}^T \otimes \mathbf{I}_M)\tilde{\mathbf{A}}\mathbf{x}_* + (\mathbf{w}^T \otimes \mathbf{I}_M)(\mathbf{I}_{N_r} \otimes \tilde{\mathbf{B}})\mathbf{v}, \qquad (3.41)\end{aligned}$$

the matrices $\tilde{\mathbf{A}}$ and $\tilde{\mathbf{B}}$ in (3.41) are $\tilde{\mathbf{A}} = (\mathbf{I}_{(Q+Q'+1)(L+L'+1)} \otimes \mathbf{R}_{zp})\mathbf{A}\bar{\mathbf{T}}_{zp}$ and $\tilde{\mathbf{B}} = (\mathbf{I}_{(Q'+1)(L'+1)} \otimes \mathbf{R}_{zp})\mathbf{B}$, respectively. In a similar way, we can derive a linear relationship between $\mathbf{f}$, $\mathbf{w}$ and $\boldsymbol{\mathcal{H}}$ as in (3.22). Hence, the MMSE and ZF solutions can be similarly derived as before.

The **MMSE solution** is obtained as

$$\begin{aligned}\mathbf{w}_{MMSE,zp}^T &= \mathbf{r}_A^H\boldsymbol{\mathcal{H}}^H\left(\boldsymbol{\mathcal{H}}\mathbf{R}_A\boldsymbol{\mathcal{H}}^H + (\mathbf{I}_{N_r} \otimes \mathbf{R}_B)\right)^{-1} \\ &= \mathbf{e}_d^T\left(\boldsymbol{\mathcal{H}}^H(\mathbf{I}_{N_r} \otimes \mathbf{R}_B)^{-1}\boldsymbol{\mathcal{H}} + \mathbf{R}_A^{-1}\right)^{-1}\boldsymbol{\mathcal{H}}^H(\mathbf{I}_{N_r} \otimes \mathbf{R}_B)^{-1},\end{aligned}$$

where $\mathbf{r}_A$, $\mathbf{R}_A$ and $\mathbf{R}_B$ are similarly defined as before but replacing $\mathbf{A}$ with $\tilde{\mathbf{A}}$ and $\mathbf{B}$ with $\tilde{\mathbf{B}}$.

The corresponding **ZF solution** is obtained by setting the source power equal to infinity

$$\mathbf{w}_{ZF,zp}^T = \mathbf{e}_d^T(\boldsymbol{\mathcal{H}}^H(\mathbf{I}_{N_r} \otimes \mathbf{R}_B)^{-1}\boldsymbol{\mathcal{H}})^{-1}\boldsymbol{\mathcal{H}}^H(\mathbf{I}_{N_r} \otimes \mathbf{R}_B)^{-1},$$

When $M \gg L$, i.e. when the edge effects can be ignored, it can be shown that $\mathbf{R}_A \approx M\mathbf{I}_{(Q+Q'+1)(L+L'+1)}$ and $\mathbf{R}_B \approx M\mathbf{I}_{(Q'+1)(L'+1)}$, which simplifies the expressions.

CP-Based Block Transmission

For the CP-based block transmission a CP of length L' is added to the top of the received sequence to enforce a cyclic convolution. In this case the time-varying FIR filter at the rth receive antenna is restricted to:

$$\mathbf{W}^{(r)} = \sum_{l'=0}^{L}\sum_{q'=-Q'/2}^{Q'/2} w_{q',l'}^{(r)}\mathbf{D}_{q'}\mathbf{Z}_{l'},$$

with $\mathbf{Z}_{l'}$ is an $N \times N$ circulant matrix with $[\mathbf{Z}_l]_{n,n'} = \delta_{(n-n'-l') \bmod N}$. The same analysis can be done for this case resulting into the same expressions. Note here that the decision delay results into a cyclic shift of the received sequence, and therefore no special structure is required here to count for this delay. The same expressions as for the ZF case can be obtained for the ZF and MMSE solutions. The only difference will be in the definitions of $\tilde{\mathbf{A}}$ and

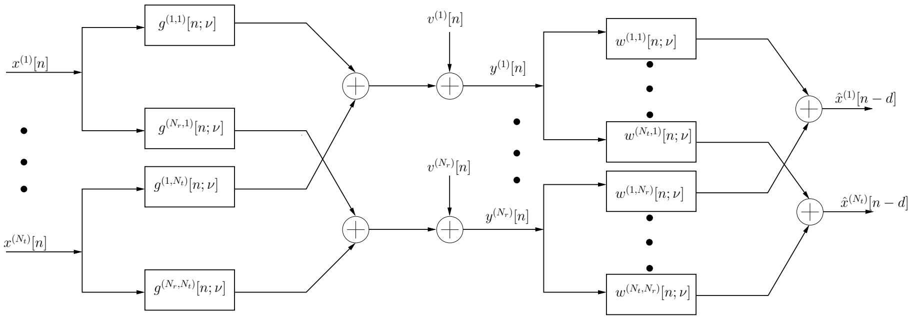

Figure 3.6: MIMO system model.

$\tilde{\mathbf{B}}$, or consequently in the definition of $\mathbf{R}_A$ and $\mathbf{R}_B$. Setting the appropriate definitions the MMSE and ZF solutions can be written as

$$\begin{aligned}\mathbf{w}_{MMSE,cp}^T &= \mathbf{e}_d^T \left(\boldsymbol{\mathcal{H}}^H(\mathbf{I}_{N_r}\otimes\mathbf{R}_B)^{-1}\boldsymbol{\mathcal{H}}+\mathbf{R}_A^{-1}\right)^{-1}\boldsymbol{\mathcal{H}}^H(\mathbf{I}_{N_r}\otimes\mathbf{R}_B)^{-1}\\ \mathbf{w}_{ZF,cp}^T &= \mathbf{e}_d^T(\boldsymbol{\mathcal{H}}^H(\mathbf{I}_{N_r}\otimes\mathbf{R}_B)^{-1}\boldsymbol{\mathcal{H}})^{-1}\boldsymbol{\mathcal{H}}^H(\mathbf{I}_{N_r}\otimes\mathbf{R}_B)^{-1}. \end{aligned} \tag{3.42}$$

Note here that for white data and noise with variances σ_s^2 and σ_n^2, respectively, it is easy to show that $\mathbf{R}_A = N\mathbf{I}_{(Q+Q'+1)(L+L'+1)}$ and $\mathbf{R}_B = N\mathbf{I}_{N_r(Q'+1)(L'+1)}$ for $K = N$, where we used the fact that $\mathrm{tr}\{\mathbf{Z}_l\mathbf{D}_p\mathbf{Z}_{l'}\} = N\delta_{l-l'}$. Hence, the BEM coefficients of the MMSE time-varying FIR equalizer reduce to

$$\mathbf{w}_{MMSE,cp}^T = \mathbf{e}_d^T(\boldsymbol{\mathcal{H}}^H\boldsymbol{\mathcal{H}}+\sigma_n^2/\sigma_s^2\mathbf{I}_{(Q+Q'+1)(L+L'+1)})^{-1}\boldsymbol{\mathcal{H}}^H, \tag{3.43}$$

and the ZF solution in (3.42) reduces to

$$\mathbf{w}_{ZF,cp}^T = \mathbf{e}_d^T(\boldsymbol{\mathcal{H}}^H\boldsymbol{\mathcal{H}})^{-1}\boldsymbol{\mathcal{H}}^H. \tag{3.44}$$

3.5.3 Extension to MIMO Systems

In this subsection, we will show that the extension to multi-input Multi-output (MIMO) systems is straightforward. The system model is shown in Figure 3.6, where N_t transmit antennas and N_r receive antennas are assumed. The received block at the rth receive antenna is now written as

$$\mathbf{y}^{(r)} = \sum_{t=1}^{N_t}\sum_{l=0}^{L}\sum_{q=-Q/2}^{Q/2} h_{q,l}^{(r,t)}\bar{\mathbf{D}}_q\bar{\mathbf{Z}}_l\mathbf{x}^{(t)} + \mathbf{v}^{(r)}. \tag{3.45}$$

where $h_{q,l}^{(r,t)}$ is the qth bases of the lth tap of the time-varying channel between the rth receive antenna and tth transmit antenna, and $\mathbf{x}^{(t)}$ is the tth antenna transmitted block. At each receive antenna a bank of N_t equalizers is used. The output of the corresponding filter are combined to estimate the transmitted block on a particular antenna.

An estimate of $\mathbf{x}_*^{(a)}$ is obtained as:

$$\hat{\mathbf{x}}_*^{(a)} = \sum_{r=1}^{N_r} \sum_{q'=-Q'/2}^{Q'/2} \sum_{l'=0}^{L'} w_{q',l'}^{(a,r)} \mathbf{D}_{q'} \mathbf{Z}_{l'} \sum_{t=1}^{N_t} \sum_{q=-Q/2}^{Q/2} \sum_{l=0}^{L} h_{q,l}^{(r,t)} \bar{\mathbf{D}}_q \bar{\mathbf{Z}}_l \mathbf{x}^{(t)} + \sum_{r=1}^{N_r} \sum_{q'=-Q'/2}^{Q'/2} \sum_{l'=0}^{L'} w_{q',l'}^{(a,r)} \mathbf{D}_{q'} \mathbf{Z}_{l'} \mathbf{v}^{(r)}, \quad (3.46)$$

where $w_{q',l'}^{(a,r)}$ is the coefficient of the q'th bases of the l'th tap of the time-varying FIR filter corresponding to the rth receive antenna and the ath transmit antenna.

Briefly, we can define the 2-dimensional function that corresponds to the ath transmit antenna as

$$f_{p,k}^{(a,t)} = \sum_{r=1}^{N_r} \sum_{q'=-Q'/2}^{Q'/2} \sum_{l'=0}^{L'} e^{-j2\pi(p-q')(L'-l')/K} w_{q',l'}^{(a,r)} h_{p-q',k-l'}^{(r,t)}. \quad (3.47)$$

Defining $\mathbf{f}^{(a,t)} = [f_{-(Q+Q')/2,0}^{(a,t)}, \ldots, f_{-(Q+Q')/2,L+L'}^{(a,t)}, \ldots, f_{(Q+Q')/2,L+L'}^{(a,t)}]^T$, $\mathbf{f}^{(a)} = [\mathbf{f}^{(a,1)T}, \ldots, \mathbf{f}^{(a,N_t)T}]^T$, $\mathbf{w}^{(a,r)} = [w_{-Q'/2,0}^{(a,r)}, \ldots, w_{Q'/2,L'}^{(a,r)}]^T$, and finally $\mathbf{w}^{(a)} = [\mathbf{w}^{(a,1)T}, \ldots, \mathbf{w}^{(a,N_r)T}]^T$. We can derive a relation between $\mathbf{f}^{(a)}$ and $\mathbf{w}^{(a)}$ as explained next.

First, define the $(L'+1) \times (L'+L+1)$ block Toeplitz matrix as

$$\mathcal{T}_{l,L'+1}(h_{q,l}^{(r,t)}) = \begin{bmatrix} h_{q,0}^{(r,t)} & \ldots & h_{q,L}^{(r,t)} & & \mathbf{0} \\ & \ddots & & \ddots & \\ \mathbf{0} & & h_{q,0}^{(r,t)} & \ldots & h_{q,L}^{(r,t)} \end{bmatrix},$$

then define $\boldsymbol{\mathcal{H}}_q^{(r,t)} = \boldsymbol{\Omega}_q \mathcal{T}_{l,L'+1}(h_{q,l}^{(r,t)})$. Introducing the $(Q'+1)(L'+1) \times (Q+Q'+1)(L+L'+1)$ block Toeplitz matrix

$$\mathcal{T}_{q,Q'+1}(\boldsymbol{\mathcal{H}}_q^{(r,t)}) = \begin{bmatrix} \boldsymbol{\mathcal{H}}_{-Q/2}^{(r,t)} & \ldots & \boldsymbol{\mathcal{H}}_{Q/2}^{(r,t)} & & \mathbf{0} \\ & \ddots & & \ddots & \\ \mathbf{0} & & \boldsymbol{\mathcal{H}}_{-Q/2}^{(r,t)} & \ldots & \boldsymbol{\mathcal{H}}_{Q/2}^{(r,t)} \end{bmatrix},$$

and the definitions $\boldsymbol{\mathcal{H}}^{(r,t)} = \mathcal{T}_{q,Q'+1}(\boldsymbol{\mathcal{H}}_q^{(r,t)})$, $\boldsymbol{\mathcal{H}}^{(t)} = [\boldsymbol{\mathcal{H}}^{(1,t)T}, \ldots, \boldsymbol{\mathcal{H}}^{(N_r,t)T}]^T$ and $\boldsymbol{\mathcal{H}} = [\boldsymbol{\mathcal{H}}^{(1)T}, \ldots, \boldsymbol{\mathcal{H}}^{(N_t)T}]^T$, we can derive from (3.47) that

$$\mathbf{f}^{(a)T} = \mathbf{w}^{(a)T} \boldsymbol{\mathcal{H}}. \quad (3.48)$$

For a ZF solution to exist we require that $\boldsymbol{\mathcal{H}}$ is of column rank. For sufficiently large L' and Q', a necessary condition to have full column rank $\boldsymbol{\mathcal{H}}$ is that the number of receive antennas is greater than the number of transmit antenna, i.e. $N_r > N_t$, and Q' and L' are chosen to satisfy the inequality $N_r(Q'+1)(L'+1) \geq N_t(Q+Q'+1)(L+L'+1)$.

3.6 Discussion and Comparisons

3.6.1 Existence of ZF Solution

The existence of the ZF BLE in (3.11) or (3.12) requires that $\mathbf{H}$ has full column rank, which requires that the number of receive antennas $N_r \geq 2$. This, however, is different when block transmission techniques are used (ZP or CP). For block transmission techniques, the ZF solution exists when the matrix $\bar{\mathbf{H}}$ is of full column rank, which happens with probability one regardless of the N_r. Note that, for a TI channel $\bar{\mathbf{H}}$ is always of full column rank for ZP-based block transmission, and of full column rank with probability one for CP-based block transmission. For CP-based block transmission, the matrix $\bar{\mathbf{H}}$ violates the full column rank property when the channel experiences deep fades (i.e. the channel has zeros on the DFT grid).

On the other hand, the existence of the ZF SLE equalizer requires that $\boldsymbol{\mathcal{H}}$ has full column rank, which happens with probability one when $\boldsymbol{\mathcal{H}}$ has at least as many rows as columns, i.e., when $N_r(Q'+1)(L'+1) \geq (Q+Q'+1)(L+L'+1)$, which can always be obtained with a sufficiently large Q' and L' if $N_r \geq 2$. A more detailed existence result follows from a result for the existence of a ZF TI FIR equalizer of a purely frequency-selective multiple-input multiple-output (MIMO) channel [1], since we can view $\boldsymbol{\mathcal{H}}$ as the channel matrix related to the purely frequency-selective MIMO channel $\boldsymbol{\mathcal{H}}_q = [\boldsymbol{\mathcal{H}}_q^{(1)T}, \ldots, \boldsymbol{\mathcal{H}}_q^{(N_r)T}]^T$ of order Q ($q \in \{-Q/2, \ldots, Q/2\}$), which has $(L+L'+1)$ inputs and $N_r(L'+1)$ outputs. The following proposition gives a set of sufficient conditions for $\boldsymbol{\mathcal{H}}$ to be of full column rank [1]:

Theorem 3.1 *The matrix $\boldsymbol{\mathcal{H}}$ has full column rank if:*

C1) $Q' \geq Q(L+L'+1)$*;*

C2) $\boldsymbol{\mathcal{H}}(z) = \sum_{q=-Q/2}^{Q/2} \boldsymbol{\mathcal{H}}_q z^{-q}$ *has full column rank* $\forall z \notin \{0, \infty\}$*;*

C3) $\boldsymbol{\mathcal{H}}_{-Q/2}$ *and* $\boldsymbol{\mathcal{H}}_{Q/2}$ *have full column rank.*

The second and third conditions, which require $N_r(L'+1) \geq L+L'+1$, are usually known as the irreducible and column reduced condition, respectively.

Note that condition C1 puts a rather tough constraint on Q'. However, the conditions are sufficient and not necessary. In any case, as said before, $\boldsymbol{\mathcal{H}}$ has full column rank with probability one when $N_r(Q'+1)(L'+1) \geq (Q+Q'+1)(L+L'+1)$, which can always be obtained with a sufficiently large Q' and L' if $N_r \geq 2$. This can be easily seen by solving for Q' for a fixed L' as

$$Q' \geq \frac{Q(L+L'+1)}{(N_r-1)(L'+1)-L} - 1, \quad Q' \geq 0. \tag{3.49}$$

(3.49) implies the following necessary (not necessarily sufficient) conditions:

1. $N_r \geq 2$
2. $L'+1 > \frac{L}{N_r-1}$

In a similar fashion, we can solve for L' for a fixed Q' as

$$L' \geq \frac{L(Q+Q'+1)}{(N_r-1)(Q'+1)-Q} - 1, \quad L' \geq 0. \tag{3.50}$$

(3.50) implies the following necessary (not necessarily sufficient) conditions:

1. $N_r \geq 2$
2. $Q'+1 > \frac{Q}{N_r-1}$

For $N_r = 2$ receive antennas, $L = 3$ and $Q = 4$, the solution region of (3.49)/(3.50) is shown in Figure 3.7, where the dots represent the possible solution pairs (Q', L').

Note that existence is not an issue when an MMSE SLE is considered. However, it is clear that the performance of the MMSE equalizer will improve when it is designed in such a way that the corresponding ZF equalizer exists.

3.6.2 Complexity

In this section, we will compare the complexity of the BLE with the complexity of the SLE proposed in this chapter. Two types of complexity can be considered: the design complexity and the implementation complexity. The bock size N will play an important role in these complexity types. In general, we assume that N is large enough such that blind channel estimation performs well or the overhead of the training symbols for training based channel estimation does not decrease the data rate too much, which basically means that the channel should be far under-spread, i.e., $LQ \ll N$.

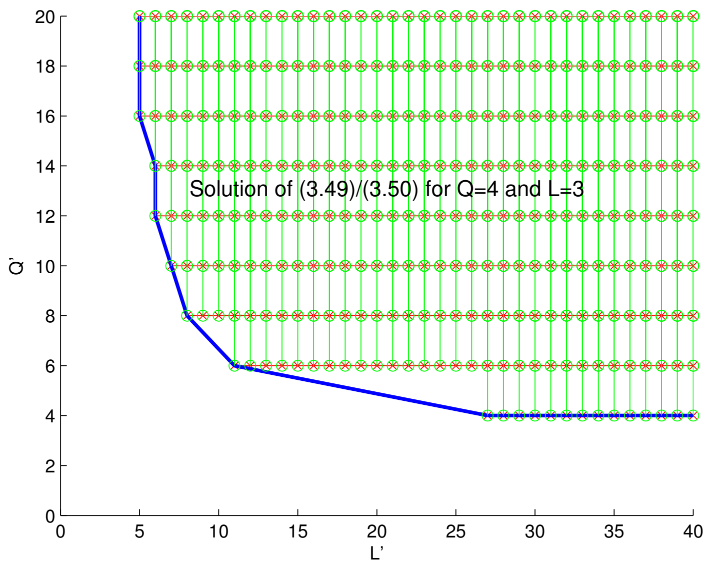

Figure 3.7: Solution Region for (3.49)/(3.50) for $L = 3$, $Q = 4$, and $N_r = 2$ receive antennas

Design complexity: The design complexity is the complexity associated with computing the equalizer. To design the BLE, we have to compute the inverse of an $N \times N$ matrix. This requires $\mathcal{O}(N^3)$ flops. On the other hand, to design the SLE, we have to compute the inverse of a $A \times A$ matrix, where $A = (Q+Q'+1)(L+L'+1)$. This requires $\mathcal{O}(A^3)$ flops. Assuming the channel is far under-spread and L' and Q' are not much larger than L and Q, we may assume that A is less than the block size N, and thus the design complexity of the SLE is lower than the design complexity of the BLE.

Implementation complexity: The implementation complexity (run-time complexity) is computed as the number of multiply-add (MA) operations required to estimate the transmitted block. For the BLE, estimating the transmitted block requires N^2 MA operations per receive antenna. On the other hand, for the SLE, estimating the transmitted block requires $N(Q'+1)(L'+1)$ MA operations per receive antenna. Again, assuming the channel is far under-spread and L' and Q' are not much larger than L and Q, we may assume that $(Q'+1)(L'+1)$ is less than the block size N, and thus the implementation complexity of the SLE is lower than the implementation complexity of the BLE.

Note that our simulation results indicate that in order to obtain a performance close to the performance of the BLE, we do not have to take L' and Q' much larger than L and Q (at least as far as the practical MMSE case is concerned).

As indicated above, in this case the proposed approach leads to a lower design and implementation complexity.

3.6.3 Unifying Framework

In this subsection, we show that the time-varying FIR equalizer proposed in this chapter unifies and extends many previously proposed serial linear equalization approaches.

First of all, TI FIR equalization of a purely frequency-selective channel ($Q = 0$ and $Q' = 0$) and time-varying 1-tap FIR equalization of a purely time-selective channel ($L = 0$ and $L' = 0$) can be viewed as special cases of our approach. In the first case, the existence of the ZF solution requires $L' \geq \lceil \frac{L}{Nr-1} - 1 \rceil$, which coincides with the result obtained in [93]. In the second case, the existence of a ZF solution requires $Q' \geq \lceil \frac{Q}{Nr-1} - 1 \rceil$, which is a novel observation.

It is also worth to note that our framework encompasses equalization of doubly selective channels using a TI FIR equalizer or a time-varying 1-tap FIR equalizer, provided enough receive antennas are available. For $N_r > Q + 1$ it is possible to perfectly equalize a doubly selective channel with a TI FIR equalizer ($Q' = 0$) if we choose $L' \geq \lceil \frac{(Q+1)L}{N_r-(Q+1)} - 1 \rceil$. This result coincides with the result obtained in [75]. On the other hand, for $N_r > L + 1$, it is possible to perfectly equalize a doubly selective channel with a time-varying 1-tap FIR equalizer ($L' = 0$) if we choose $Q' \geq \lceil \frac{(L+1)Q}{N_r-(L+1)} - 1 \rceil$, which is again a novel observation.

3.7 Simulations

In our simulations, we investigate the performance of the ZF and the MMSE BLEs as well the performance of the ZF and the MMSE SLEs. For the case of ZF SLE, we consider a SIMO system with $N_r = 2$, 3, 4, and 6 receive antennas, while for the case of MMSE SLE, we consider a single-input single-output (SISO) system as well as a SIMO system with $N_r = 2$, and 4 receive antennas. Other parameters of the system are listed as follows:

- Doppler spread $f_{\max} = 100$ Hz (corresponds to a speed of $120 Km/hr$ over the 900 MHz GSM band);
- delay spread $\tau_{\max} = 75$ μs;
- block size $N = 800$;
- a BEM resolution K is considered as $K = PN$ with $P = 1, 2$;

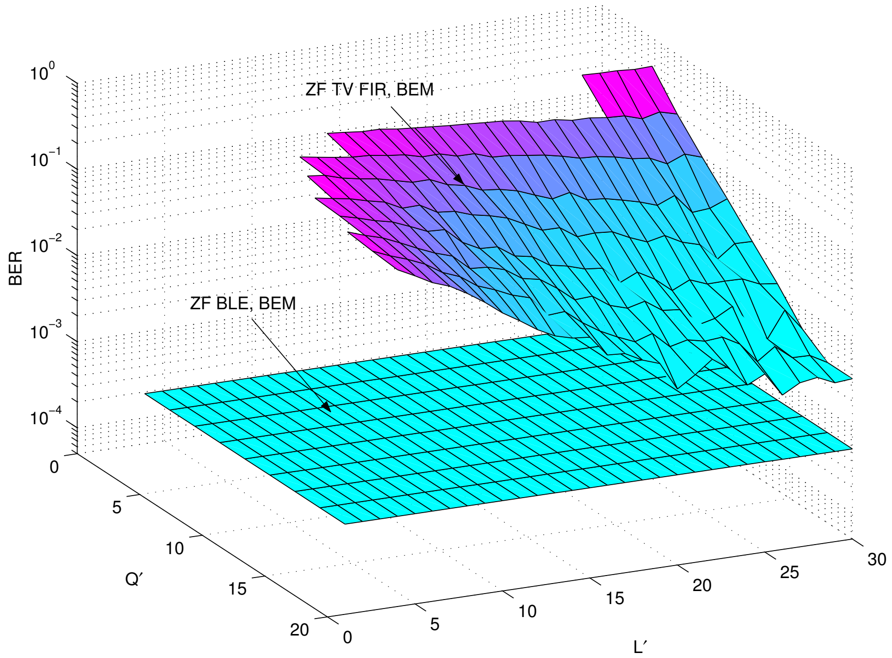

Figure 3.8: BER as a function of (Q', L') for $N_r = 2$ receive antennas using a ZF time-varying FIR equalizer at an SNR of 16 dB.

- symbol/sample period $T = 25$ μs;
- discrete Doppler spread $Q/2 = \lceil f_{\max} KT \rceil$, which leads to $Q = 4$ for $K = N$ and $Q = 8$ for $K = 2N$;
- discrete delay spread $L = 3$.

The channel taps are first simulated as i.i.d. random variables, correlated in time with a correlation function according to Jakes' model $r_h(\tau) = J_0(2\pi f_{\max}\tau)$, where J_0 is the zeroth-order Bessel function of the first kind . This channel model is used to generate the channel output sequences. The doubly selective channel is then approximated by the BEM. We only assume the knowledge of the BEM coefficients of the channel at the receiver, and not the knowledge of the true Jakes' channel, which can never be obtained in practice. We use these BEM coefficients to design the BLE as well as the SLE to equalize the true Jakes' channel model rather than the approximated one. We consider ZP-based as well as CP-based block transmission techniques.

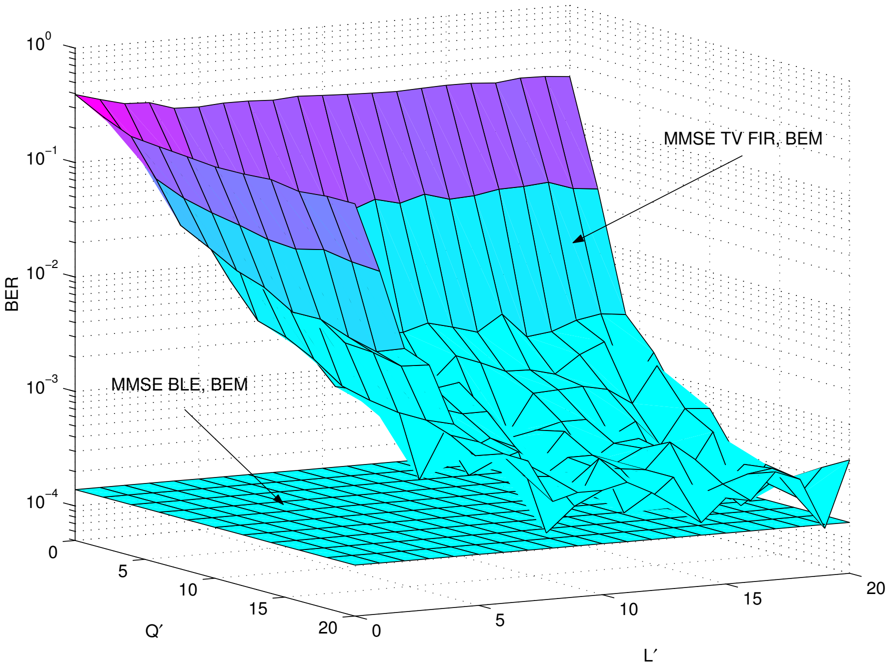

Figure 3.9: BER as a function of (Q', L') for $N_r = 2$ receive antennas using an MMSE time-varying FIR equalizer at an SNR of 16 dB.

In all simulations, QPSK signaling is used and the synchronization delay is chosen as $d = \lfloor \frac{L+L'}{2} \rfloor + 1$. The performance is measured in terms of bit error rate (BER) vs. signal-to-noise ratio (SNR). We compare the performance of the SLE (ZF and MMSE) with the performance of the BLE (ZF and MMSE) for both case of $K = N$ and $K = 2N$.

Design parameters: To give a feeling on how to choose the time-varying FIR filter parameters, we measure the performance of the SLE for $N_r = 2$ receive antennas as a function of the time-varying FIR filter design parameters Q' and L' at a fixed SNR of 16 dB. We consider both the ZF and the MMSE cost function, and use the BEM resolution $K = 2N$ to keep the modeling error as small as possible, which is shown to be the case for $K = 2N$ (see Chapter 2). As shown in Figures 3.8 and 3.9, by increasing the equalizer parameters, the performance of the ZF and MMSE SLEs comes closer to the performance of the ZF and MMSE BLEs. One can also observe that a significant gain can be obtained by increasing the time-varying FIR filter parameters up to a certain threshold value at which point the gradient of the BER surface becomes very small. For the ZF case, this point might be too far away to be practical, and

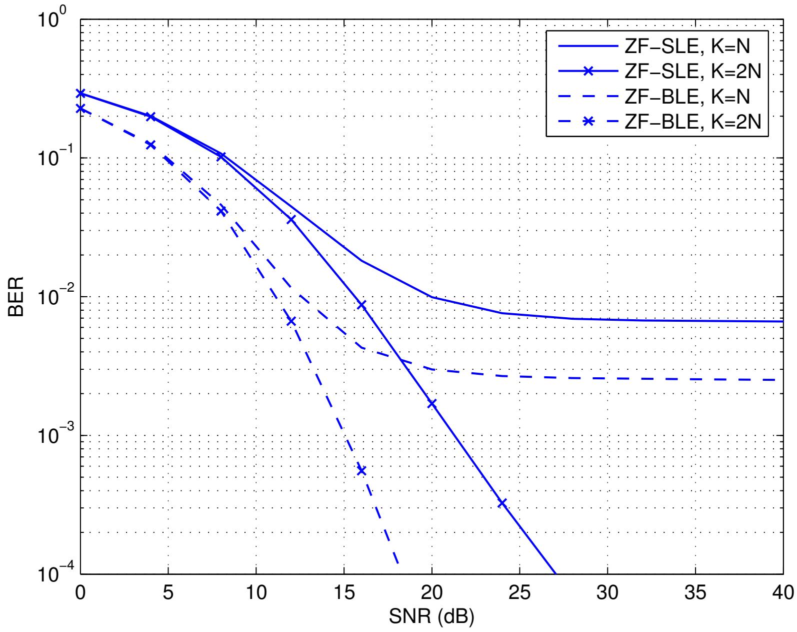

Figure 3.10: BER vs. SNR for ZF receivers ($N_r = 2$ receive antennas).

hence we resort to $Q' = L' = 20$ in the simulations for $N_r = 2$. For the MMSE case, on the other hand, this point is situated around $Q' = L' = 12$, which is what we will use in the simulations for $N_r = 2$. Note that for this channel setup, which is almost symmetric in Q and L, we also observe a performance symmetry in Q' and L', which means that there is no reason to choose Q' different from L'. This motivates us to take $Q' = L'$ in the sequel. The time-varying FIR filter parameters used in the simulations for the SLE case are listed in Table 3.1.

Table 3.1: time-varying FIR equalizer parameters.

	ZF		**MMSE**	
Nr	Q'	L'	Q'	L'
1	NA	NA	20	20
2	20	20	12	12
4	8	8	8	8
6	4	4		

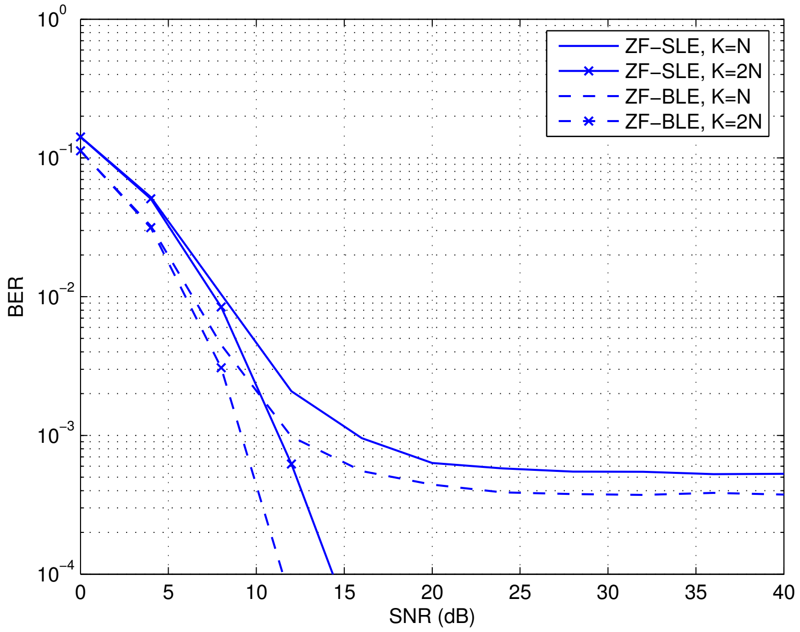

Figure 3.11: BER vs. SNR for ZF receivers ($N_r = 4$ receive antennas).

In the following we consider the performance of the proposed equalizers (SLE and BLE) for ZP-based block transmission technique, while, similar results are obtained considering the CP-based block transmission. For the sake of conciseness we discuss only the ZP-based block transmission results.

For the ZP-based block transmission techniques we consider the ZF as well as the MMSE criterion to design the equalizers.

ZF equalizers: As shown in Figure 3.10, using $N_r = 2$ receive antennas, the ZF-SLE with $Q' = 20$ and $L' = 20$ is outperformed by the ZF-BLE for both cases $K = N$ and $K = 2N$. At a BER of 10^{-2}, we notice a 4 dB SNR loss when the window size $K = 2N$, and a 7 dB SNR loss when the BEM window size $K = N$. Note that, both serial and block equalizers suffer from an early error floor for $K = N$, ZF-BLE exhibits an error floor at $BER = 3 \times 10^{-3}$, whereas ZF-SLE exhibits an error floor at $BER = 6 \times 10^{-3}$. Now, using $N_r = 4$ receive antennas, the performance of the ZF-SLE with $Q' = 8$ and $L' = 8$ comes much closer to the performance of the ZF-BLE. At a BER of 10^{-2}, the gap is now reduced to 2 dB for the case of a BEM with $K = N$ as well as for the case of a BEM with $K = 2N$, as shown in Figure 3.11. Similarly, for the case of $K = N$, both the ZF-BLE and the ZF-SLE exhibit an error floor. ZF-BLE exhibits an

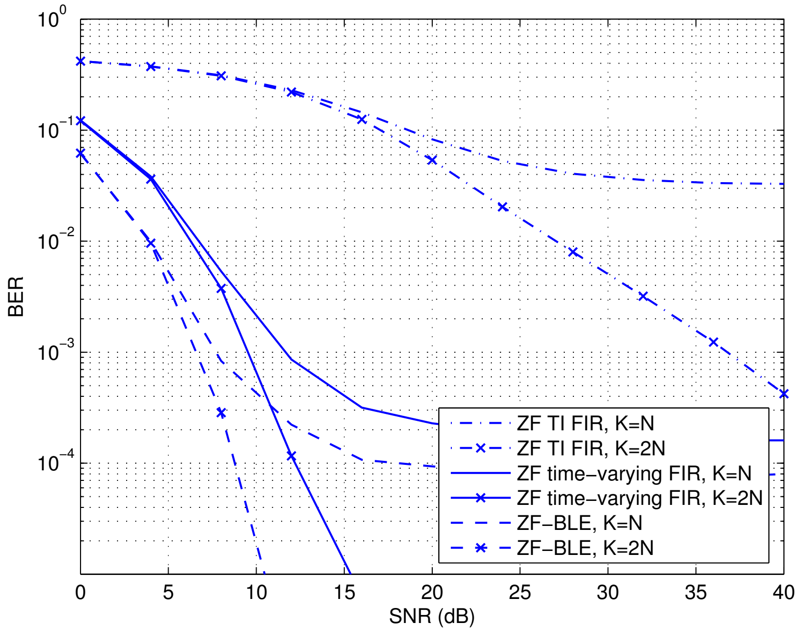

Figure 3.12: BER vs. SNR for ZF receivers ($N_r = 6$ receive antennas).

error floor at $BER = 4 \times 10^{-4}$, whereas the ZF-SLE exhibits an error floor at $BER = 7 \times 10^{-4}$.

In Figure 3.12, we use $N_r = 6$ receive antennas, which also allows us to equalize the channel using a TI FIR equalizer (see also [75]). We can see that the ZF time-varying FIR equalizer with $Q' = 4$ and $L' = 4$ significantly outperforms the ZF TI FIR equalizer with $Q' = 0$ and $L' = 20$. Note that for this case the design complexity of the ZF time-varying FIR equalizer is one fifth of the design complexity of the ZF TI FIR equalizer. On the other hand, the implementation complexity of the ZF time-varying FIR equalizer is less than a quarter of the implementation complexity of the ZF TI FIR equalizer. This leads us to conclude that incorporating time variation in the equalizer really pays off.

MMSE equalizers: In Figure 3.13, we use $N_r = 1$ receive antenna, and apply the MMSE-SLE with $Q' = 20$ and $L' = 20$. We can see that the performance loss of the MMSE-SLE compared to the MMSE-BLE is less than 1 dB at a BER of 10^{-2} for both BEM with $K = N$ and BEM with $K = 2N$. For this number of receive antennas, both the BLE and the SLE suffer from an error floor for the BEM with $K = N$ as well as for the BEM with $K = 2N$. For the BEM with

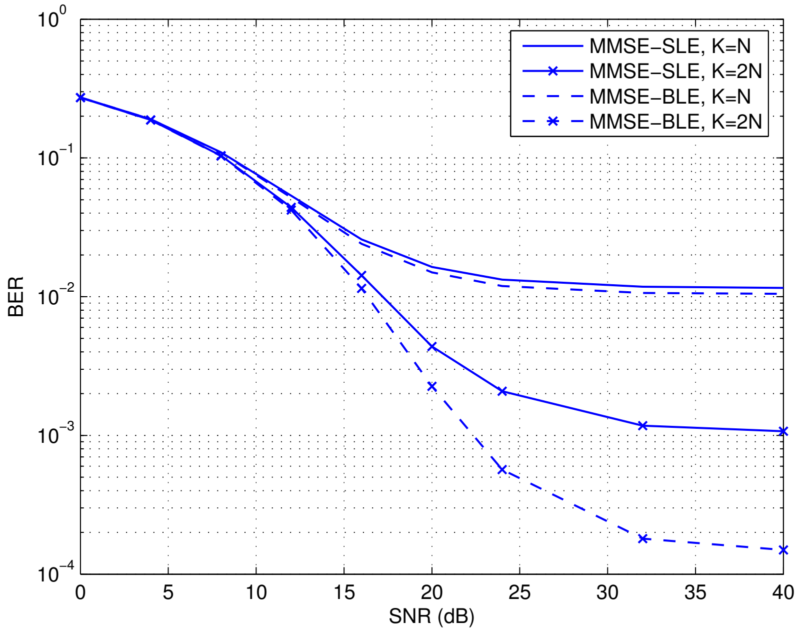

Figure 3.13: BER vs. SNR for MMSE receivers ($N_r = 1$ receive antenna).

$K = N$, the BLE and the SLE exhibit an error floor at $BER = 10^{-2}$. For the BEM with $K = 2N$, the MMSE-BLE exhibits an error floor at $BER = 2^{-4}$, while the MMSE-SLE exhibits an error floor at $BER = 10^{-3}$.

For $N_r = 2$ receive antennas, where $Q' = 12$ and $L' = 12$ is used, and $N_r = 4$ receive antennas, where $Q' = 8$ and $L' = 8$ is used, we observe that the performance of the MMSE-SLE almost coincides with that of the MMSE-BLE (for the BEM with $K = N$ as well as for the BEM with $K = 2N$). The results corresponding to $N_r = 2$ and $N_r = 4$ are shown in Figures 3.14 and 3.15, respectively. In all cases an error floor is observed for the case of a BEM with $K = N$. This again stresses the fact that using a BEM with $K = N$ exhibits a modeling error that dominates the BER performance for high SNR.

Complexity: To compute the BLE we require the number of floating point operations to be $\boldsymbol{\mathcal{O}}(N^3)$ flops, where $N^3 = 512,000,000$ for this channel setup. The implementation complexity associated with the BLE requires N^2 MA operations per receive antenna, where $N^2 = 640,000$. Note that, this complexity analysis does not change with the number of receive antennas. On the other hand, the complexity associated with computing and implementing the time-varying FIR equalizer does change with the number of receive antennas, because

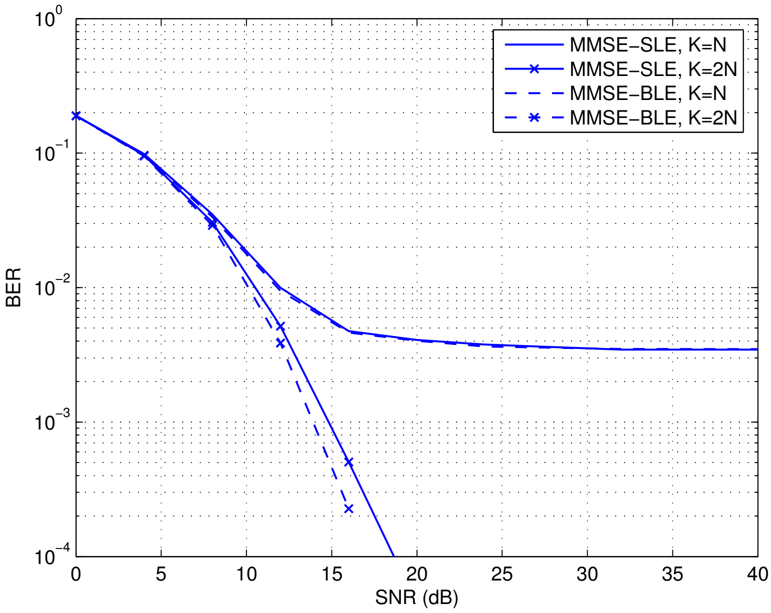

Figure 3.14: BER vs. SNR for MMSE receivers ($N_r = 2$ receive antennas).

Table 3.2: time-varying FIR equalizer Complexity table.

	ZF time-varying FIR			
N_r	Design*	% red	Run-Time†	% red
1	NA	NA	NA	NA
2	$216,000,000$	57.81	$352,800$	44.87
4	$3,796,416$	99.26	$64,800$	89.87
	MMSE time-varying FIR			
N_r	Design*	% red	Run-Time†	% red
1	$216,000,000$	57.81	$352,800$	44.87
2	$20,123,648$	96.07	$135,200$	78.88
4	$3,796,416$	99.26	$64,800$	89.87

* in flops (order of magnitude)
† in MA operations

we consider different values for Q' and L'. These complexities are shown in Table 3.2 for both the ZF and MMSE criterion.

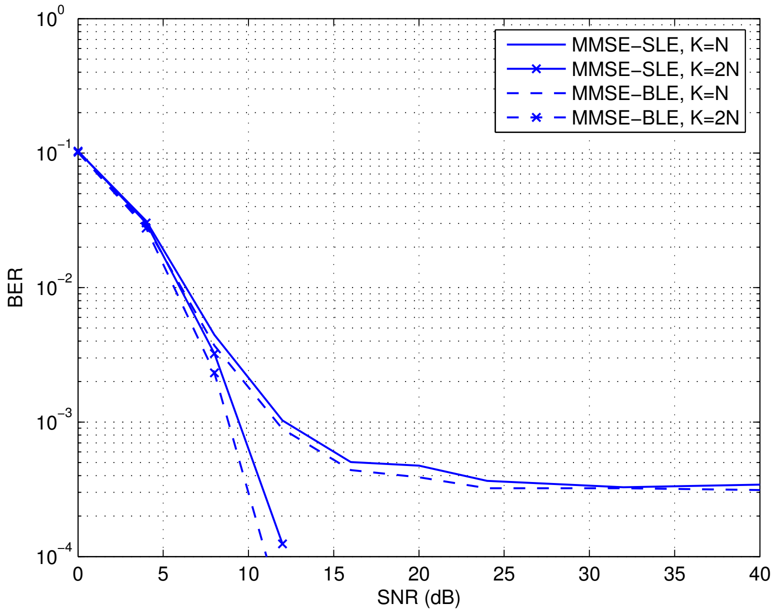

Figure 3.15: BER vs. SNR for MMSE receivers ($N_r = 4$ receive antennas).

3.8 Conclusions

In this chapter, we have investigated the problem of equalization for SC transmission over doubly selective channels. We proposed a BLE as well as a SLE implemented as a time-varying FIR filter. In our equalizer design, we consider the MMSE as well as the ZF solutions for both the BLE and the SLE. We used the BEM to approximate the doubly selective channel and to design the BLE as well as the SLE. Implementing the SLE using a time-varying FIR filter designed according to the BEM allowed us to turn a complicated time-varying 1-D deconvolution problem into an equivalent simpler TI 2-D deconvolution problem, containing only the BEM coefficients of both the doubly selective channel and the time-varying FIR filter. It is shown that a time-varying FIR equalizer generally requires at least two receive antennas for the ZF solution to exist (a ZF solution eliminates ISI completely when the underlying doubly selective channel perfectly follows the BEM channel model). In contrast to the BLE, the proposed SLE implemented by a time-varying FIR filter allows for a flexible tradeoff between complexity and performance. Moreover, through computer simulations we have shown that the performance of the proposed MMSE-SLE comes close to the performance of the MMSE-BLE, at a point where the design as well as the implementation complexity are much lower.

Chapter 4

Decision-Feedback Equalization of SC Transmission over Doubly Selective Channels

4.1 Introduction

IN Chapter 3, we treated the case of linear equalization of doubly selective channels considering the MMSE and ZF criterion. In this chapter we will focus on the case of decision feedback equalization (DFE) of doubly selective channels. We, similar to Chapter 3, consider two types of equalizers. First, we focus on block decision feedback equalizers (BDFE). Second, we propose a serial DFE (SDFE). Unlike linear equalizers which apply one feedforward filter, DFEs apply two filters; a feedforward filter and a feedback filter. For the SDFE, the feedforward and feedback filters are implemented by using time-varying FIR filters. The time-varying FIR filters are designed according to the BEM model.

DFEs usually give a better compromise between complexity and performance. Their complexity is similar to the complexity of linear equalizers, but they typically provide better performance. On the other hand, they are still less complex than the highly complex optimal maximum likelihood (ML) estimator, at the cost of only a slightly lower performance.

DFE has been previously proposed in literature for the case of frequency-selective channels, some based on block processing [95, 118] and others based on serial processing by means of finite impulse response (FIR) filters [5]. DFE for multiuser detection is proposed in [114] and DFE for multiuser CDMA is proposed in [35]. Block DFE is proposed in [48] in the presence of co-channel interference. However, these works consider a time-invariant frequency-selective channel.

In this chapter, we extend the idea of linear equalization to design DFEs, which are shown to give better performance and to be more robust against channel imperfections [118, 95]. The proposed SDFE consists of a time-varying FIR feedforward filter, a time-varying FIR feedback filter, and a decision device. We use the BEM to model the time-varying FIR feedforward and feedback filters. The beauty of using the BEM is that it allows us to turn a large design problem into a small design problem, containing only the BEM coefficients of the channel, and the BEM coefficients of the feedforward and feedback time-varying FIR filters. We also show that this approach extends the results obtained for the case of purely frequency-selective channels.

This chapter is organized as follows. The system model is described in Section 4.2. The block decision feedback equalizer (BDFE) is introduced in Section 4.3. The serial DFE (SDFE) is introduced in Section 4.4. Discussion and comparison are introduced in Section 4.5. In Section 4.6, we show some computer simulations. Finally, our conclusions are drawn in Section 4.7.

4.2 System Model

The system under consideration is depicted in Figure 4.1. We assume a single-input multiple-output (SIMO) system, where N_r receive antennas are used. The DFE consists of feedforward filters and a feedback filter. On each receive antenna a feedforward filter is applied. The feedforward is then assisted by means of a feedback filter that feeds back previously estimated symbols.

In this chapter, we consider the case of **ZP-based block transmission**. The CP-based case may be defined similarly. Define $\mathbf{x} = [x[0], \ldots, x[N-1]]^T$, and $\mathbf{y}^{(r)} = [y^{(r)}[0], \ldots, y^{(r)}[N-1]]^T$, the input-output relationship on the rth receive antenna can be written as

$$\mathbf{y}^{(r)} = \mathbf{H}^{(r)}\mathbf{T}_{zp}\mathbf{x} + \mathbf{v}^{(r)}, \tag{4.1}$$

where the $N \times (N+L)$ Toeplitz matrix $\mathbf{H}^{(r)}$ is given by

$$\mathbf{H}^{(r)} = \sum_{l=0}^{L} \sum_{q=-Q/2}^{Q/2} h_{q,l}^{(r)} \mathbf{D}_q \mathbf{Z}_l,$$

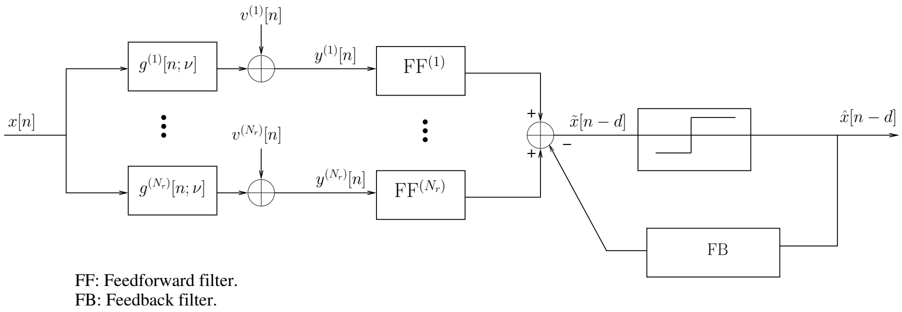

Figure 4.1: Block diagram of Decision Feedback Equalizer

with $\mathbf{D}_q = \text{diag}\{[1, e^{j2\pi q/K}, \ldots, e^{j2\pi q(N-1)/K}]^T\}$, and $\mathbf{Z}_l = [\mathbf{0}_{N\times(L-l)}, \mathbf{I}_N, \mathbf{0}_{N\times l}]$. $\mathbf{T}_{zp}$ is the zero-padding matrix defined as $\mathbf{T}_{zp} = [\mathbf{I}_N, \mathbf{0}_{N\times L}]^T$, and the additive noise $\mathbf{v}^{(r)}$ is similarly defined as $\mathbf{y}^{(r)}$.

Stacking the N_r received vectors as $\mathbf{y} = [\mathbf{y}^{(1)T}, \ldots, \mathbf{y}^{(N_r)T}]^T$, the input-output relationship (see also (3.35)) can be written as

$$\mathbf{y} = \bar{\mathbf{H}}\mathbf{x} + \mathbf{v}, \tag{4.2}$$

where $\bar{\mathbf{H}} = \mathbf{H}\mathbf{T}_{zp}$.

4.3 Block Decision-Feedback Equalization

In this section, we review BDFEs. We first focus on the minimum mean-square error BDFE (MMSE-BDFE) and then derive the zero-forcing BDFE (ZF-BDFE). The BDFE consists of a feedforward equalizer represented by the $N \times N$ matrix $\mathbf{W}^{(r)}$ on the rth receive antenna, the decision making device, and the feedback equalizer represented by the $N \times N$ matrix $\mathbf{B}$, as shown in Figure 4.2. Hence, a soft estimate of $\mathbf{x}$ is computed as

$$\begin{aligned}\tilde{\mathbf{x}}_* =& \sum_{r=1}^{N_r} \mathbf{W}^{(r)}\mathbf{y}^{(r)} - \mathbf{B}\hat{\mathbf{x}},\\ \hat{\mathbf{x}} =& Q\left(\tilde{\mathbf{x}}\right),\end{aligned} \tag{4.3}$$

where $Q\left(\cdot\right)$ is the quantizer used by the decision device.

4.3.1 MMSE-BDFE

The MMSE-BDFE is designed to minimize the error at the decision device. Define the error vector $\mathbf{e} = \tilde{\mathbf{x}} - \mathbf{x}$ (see Figure 4.2). Assuming past decisions are

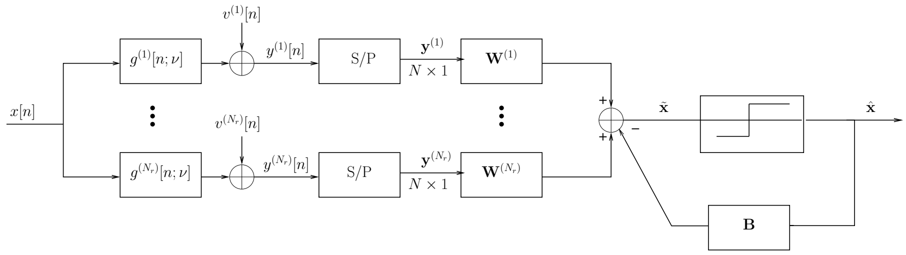

Figure 4.2: Block Decision Feedback Equalizer

correct ($\hat{\mathbf{x}} = \mathbf{x}$) we get

$$\mathbf{e} = \sum_{r=1}^{N_r} \mathbf{W}^{(r)} \left(\mathbf{H}^{(r)} \mathbf{T}_{zp} \mathbf{x} + \mathbf{v}^{(r)} \right) - (\mathbf{B} + \mathbf{I}_N)\, \mathbf{x}. \tag{4.4}$$

Defining $\mathbf{W} = [\mathbf{W}^{(1)}, \ldots, \mathbf{W}^{(N_r)}]$, (4.4) can be written as

$$\mathbf{e} = \mathbf{W}\bar{\mathbf{H}}\mathbf{x} + \mathbf{W}\mathbf{v} - (\mathbf{B} + \mathbf{I}_N)\, \mathbf{x}, \tag{4.5}$$

Define the MSE cost function $\mathcal{J} = \mathcal{E}\|\mathbf{e}\|^2$, the MMSE-BDFE is obtained by minimizing $\mathcal{J}$ subject to the constraint that $(\mathbf{B} + \mathbf{I}_N)$ is an upper triangular matrix. In a fashion similar to that of the BLE, we can write the MSE cost function $\mathcal{J}$ as [95]

$$\begin{aligned} \mathcal{J} &= \mathrm{tr}\{\mathbf{W}(\bar{\mathbf{H}}\mathbf{R}_x\bar{\mathbf{H}}^H + \mathbf{R}_v)\mathbf{W}^H + (\mathbf{B} + \mathbf{I}_N)\mathbf{R}_x(\mathbf{B}^H + \mathbf{I}_N)\} \\ &\quad - 2\mathrm{tr}\{\Re\{(\mathbf{B} + \mathbf{I}_N)\mathbf{R}_x\bar{\mathbf{H}}^H\mathbf{W}^H\}\}. \end{aligned} \tag{4.6}$$

The MMSE feedforward BDFE is then obtained by solving $\partial\mathcal{J}/\partial\mathbf{W}$ as

$$\mathbf{W}_{MMSE} = (\mathbf{B} + \mathbf{I}_N)\, \mathbf{R}_x\bar{\mathbf{H}}^H \left(\bar{\mathbf{H}}\mathbf{R}_x\bar{\mathbf{H}}^H + \mathbf{R}_v^{-1}\right)^{-1} \tag{4.7}$$

$$= (\mathbf{B} + \mathbf{I}_N) \left(\bar{\mathbf{H}}^H\mathbf{R}_v^{-1}\bar{\mathbf{H}} + \mathbf{R}_x^{-1}\right)^{-1} \bar{\mathbf{H}}^H\mathbf{R}_v^{-1}, \tag{4.8}$$

where (4.8) is obtained by applying the matrix inversion lemma in (4.7). Substituting (4.8) in (4.6), the MSE cost function reduces to

$$\mathcal{J} = \mathrm{tr}\{(\mathbf{B} + \mathbf{I}_N)\, \mathbf{R}_\perp^{-1} \left(\mathbf{B}^H + \mathbf{I}_N\right)\}, \tag{4.9}$$

where $\mathbf{R}_\perp$ is given by

$$\mathbf{R}_\perp = \left(\bar{\mathbf{H}}^H\mathbf{R}_v^{-1}\bar{\mathbf{H}} + \mathbf{R}_x^{-1}\right).$$

Hence, the feedback matrix filter of the BDFE is obtained by minimizing the MSE cost function $\mathcal{J}$ in (4.9) subject to $(\mathbf{B} + \mathbf{I}_N)$ being an upper triangular matrix.

Consider the Cholesky factorization of $\mathbf{R}_\perp$ as

$$\mathbf{R}_\perp = \mathbf{LDL}^H,$$

where $\mathbf{L}$ is a lower triangular matrix with unit diagonal, and $\mathbf{D}$ is a diagonal matrix. Hence, the MMSE feedback BDFE is obtained as

$$\mathbf{B}_{MMSE} = \mathbf{L}^H - \mathbf{I}_N. \tag{4.10}$$

Substituting (4.10) in (4.9) we obtain the MMSE cost function as

$$\mathcal{J} = \mathrm{tr}\{\mathbf{D}^{-1}\}. \tag{4.11}$$

To summarize the above discussion the feedforward and feedback BDFE are obtained as follows:

$$\begin{aligned}
\mathbf{R}_\perp &= \left(\bar{\mathbf{H}}^H \mathbf{R}_v^{-1} \bar{\mathbf{H}} + \mathbf{R}_x^{-1}\right) \\
&= \mathbf{LDL}^H \\
\mathbf{B}_{MMSE} &= \mathbf{L}^H - \mathbf{I}_N \\
\mathbf{W}_{MMSE} &= (\mathbf{B} + \mathbf{I}_N) \left(\bar{\mathbf{H}}^H \mathbf{R}_v^{-1} \bar{\mathbf{H}} + \mathbf{R}_x^{-1}\right)^{-1} \bar{\mathbf{H}}^H \mathbf{R}_v^{-1}.
\end{aligned}$$

4.3.2 ZF-BDFE

So far we have considered the MMSE-BDFE, however, the ZF BDFE is obtained by setting the source power to infinity as follows:

$$\begin{aligned}
\mathbf{R}_\perp &= \left(\bar{\mathbf{H}}^H \mathbf{R}_v^{-1} \bar{\mathbf{H}}\right) \\
&= \mathbf{LDL}^H \\
\mathbf{B}_{ZF} &= \mathbf{L}^H - \mathbf{I}_N \\
\mathbf{W}_{ZF} &= (\mathbf{B} + \mathbf{I}_N) \left(\bar{\mathbf{H}}^H \mathbf{R}_v^{-1} \bar{\mathbf{H}}\right)^{-1} \bar{\mathbf{H}}^H \mathbf{R}_v^{-1}.
\end{aligned}$$

The above approach is rather complex in particular for large N. In the next section, we will, therefore, develop a DFE equalizer with time-varying FIR feedforward filters and a time-varying FIR feedback filter. Doing this we lower the design and the equalization complexity at the cost of a slightly lower performance. This approach is referred to as serial DFE (SDFE).

4.4 Serial Decision-Feedback Equalization

In this section, we will apply a time-varying FIR feedforward filter $w^{(r)}[n;\nu]$ on the rth receive antenna and a time-varying FIR feedback filter $b[n;\nu]$, as

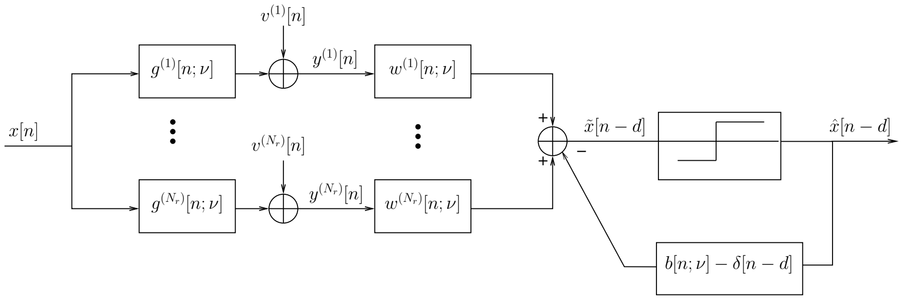

Figure 4.3: time-varying FIR Decision Feedback Equalizer

depicted in Figure 4.3. Hence, a soft estimate of $x[n-d]$ is computed as

$$\begin{aligned}\tilde{x}[n-d] =& \sum_{r=1}^{N_r} \sum_{\nu=-\infty}^{\infty} w^{(r)}[n;\nu] y^{(r)}[n-\nu] - \sum_{\nu=-\infty}^{\infty} b[n;\nu]\hat{x}[n-d-\nu], \\ \hat{x}[n-d] =& Q\left(\tilde{x}[n-d]\right), \end{aligned} \tag{4.12}$$

where d is some decision delay delay. Since the doubly selective channel $g^{(r)}[n;\nu]$ was modeled by the BEM, it is also convenient to design the time-varying FIR feedforward and feedback filters, $w^{(r)}[n;\nu]$ and $b[n;\nu]$, using the BEM. This will allow us to turn a large design problem into an equivalent small design problem, containing only the BEM coefficients of the doubly selective channel and the BEM coefficients of the time-varying FIR feedforward and feedback filters.

Using the BEM, we design the time-varying FIR feedforward filter $w^{(r)}[n;\nu]$ to have $L'+1$ taps, where the time-variation of each tap is modeled by $Q'+1$ complex exponential basis functions. Similarly we design the time-varying FIR feedback filter $b[n;\nu]$ to have L'' taps, where the time-variation of each tap is captured by $Q''+1$ complex exponential basis functions. Note that the time-varying FIR feedforward (feedback) equalizer is designed as in Figure 2.8 with L, Q, and $h_{q,l}^{(r)}$ replaced by L' $(L''-1)$, Q' (Q''), and $w_{q',l'}^{(r)}$ $(b_{q'',l''})$, respectively. Hence, we can write the time-varying FIR feedforward and feedback filters as

$$w^{(r)}[n;\nu] = \sum_{l'=0}^{L'} \delta[\nu - l'] \sum_{q'=-Q'/2}^{Q'/2} w_{q',l'}^{(r)} e^{j2\pi q' n/K}, \tag{4.13a}$$

$$b[n;\nu] = \sum_{l''=\Delta}^{L''+\Delta-1} \delta[\nu - l''] \sum_{q''=-Q''/2}^{Q''/2} b_{q'',l''} e^{j2\pi q'' n/K}, \tag{4.13b}$$

where Δ is chosen to be larger than the synchronization delay, i.e., $\Delta \geq d+1$, since we can only feedback the past decisions and not the future ones. Therefore, the soft estimate in (4.12) is obtained as

$$
\begin{aligned}
\tilde{x}[n-d] = & \sum_{q'=-Q'/2}^{Q'/2} \sum_{l'=0}^{L'} w_{q',l'}^{(r)} e^{j2\pi q' n/K} y^{(r)}[n-l'] \\
& - \sum_{q''=-Q''/2}^{Q''/2} \sum_{l''=\Delta}^{L''} b_{q'',l''} e^{j2\pi q'' n/K} \hat{x}[n-l'']. \qquad (4.14)
\end{aligned}
$$

Instead of continuing to work on the sample level, it is easier to switch to the block level at this point. On the block level, (4.14) corresponds to estimating $\mathbf{x}$ as in (4.3) but with $\mathbf{W}^{(r)}$ and $\mathbf{B}$ constrained to

$$
\mathbf{W}^{(r)} = \sum_{l'=0}^{L'} \sum_{q'=-Q'/2}^{Q'/2} w_{q',l'}^{(r)} \mathbf{D}_{q'} \bar{\mathbf{Z}}_{l'}, \qquad (4.15)
$$

$$
\mathbf{B} = \sum_{l''=\Delta}^{L''+\Delta-1} \sum_{q''=-Q''/2}^{Q''/2} b_{q'',l''} \mathbf{D}_{q''} \bar{\mathbf{Z}}_{l''}, \qquad (4.16)
$$

where $\bar{\mathbf{Z}}_{l'}$ is a lower diagonal Toeplitz matrix with the first column $[\mathbf{0}_{1\times l'}, 1, \mathbf{0}_{1\times(N-l'-1)}]^T$. This can be achieved by clearing out the feedforward and feedback filters after processing a block of M samples. Taking the decision delay d into account, we redefine the transmitted block to count for this decision as $\mathbf{x} = [\mathbf{x}_*^T, \mathbf{0}_{1\times d}]^T$, where $\mathbf{x}_* = [x[0], \ldots, x[M-1]]^T$ with $M = N - d$. A relation between $\mathbf{x}$ and $\mathbf{x}_*$ is obtained as

$$
\mathbf{x} = \bar{\mathbf{T}}_{zp} \mathbf{x}_*,
$$

where $\bar{\mathbf{T}}_{zp} = [\mathbf{I}_M, \mathbf{0}_{M\times d}]^T$.

Hence, we can write the estimated block of useful samples subject to the decision delay d as

$$
\begin{aligned}
\tilde{\mathbf{x}} = & \sum_{r=1}^{N_r} \sum_{q'=-Q'/2}^{Q'/2} \sum_{l'=0}^{L'} w_{q',l'}^{(r)} \mathbf{D}_{q'} \bar{\mathbf{Z}}_{l'} \sum_{q=-Q/2}^{Q/2} \sum_{l=0}^{L} h_{q,l}^{(r)} \mathbf{D}_q \bar{\mathbf{Z}}_l \mathbf{x} \\
& + \sum_{r=1}^{N_r} \sum_{q'=-Q'/2}^{Q'/2} \sum_{l'=0}^{L'} w_{q',l'}^{(r)} \mathbf{D}_{q'} \bar{\mathbf{Z}}_{l'} \mathbf{v}^{(r)} - \sum_{q''=-Q''/2}^{Q''/2} \sum_{l''=\Delta}^{L''+\Delta-1} b_{q'',l''} \mathbf{D}_{q''} \bar{\mathbf{Z}}_{l''} \hat{\mathbf{x}}.
\end{aligned}
\qquad (4.17)
$$

Let us define $p = q + q'$ and $k = l + l'$ (see Section 3.4, and using the property $\mathbf{Z}_{l'} \mathbf{D}_q = e^{-j2\pi q l'/K} \mathbf{D}_q \mathbf{Z}_{l'}$, (4.17) can be written as

$$
\tilde{\mathbf{x}} = \sum_{p=-(Q+Q')/2}^{(Q+Q')/2} \sum_{k=0}^{L+L'} f_{p,k} \mathbf{D}_p \bar{\mathbf{Z}}_k \mathbf{x} + \sum_{r=1}^{N_r} \sum_{q'=-Q'/2}^{Q'/2} \sum_{l'=0}^{L'} w_{q',l'}^{(r)} \mathbf{D}_{q'} \bar{\mathbf{Z}}_{l'} \mathbf{v}^{(r)}
$$

$$-\sum_{q''=-Q''/2}^{Q''/2}\sum_{l''=\Delta}^{L''+\Delta-1} b_{q'',l''}\mathbf{D}_{q''}\bar{\mathbf{Z}}_{l''}\hat{\mathbf{x}}, \tag{4.18}$$

where

$$f_{p,k}=\sum_{r=1}^{N_r}\sum_{q'=-Q'/2}^{Q'/2}\sum_{l'=0}^{L'} e^{-j2\pi(p-q')l'/K} w_{q',l'}^{(r)} h_{p-q',k-l'}^{(r)}. \tag{4.19}$$

We can further rewrite (4.18) as

$$\begin{aligned}\tilde{\mathbf{x}} &= (\mathbf{f}^T\otimes\mathbf{I}_N)\mathbf{A}\mathbf{x}+\sum_{r=1}^{N_r}(\mathbf{w}^{(r)T}\otimes\mathbf{I}_N)\mathbf{C}\mathbf{v}^{(r)}-(\tilde{\mathbf{b}}^T\otimes\mathbf{I}_N)\mathbf{A}\hat{\mathbf{x}}\\ &= (\mathbf{f}^T\otimes\mathbf{I}_N)\mathbf{A}\mathbf{x}+(\mathbf{w}^T\otimes\mathbf{I}_N)(\mathbf{I}_{N_r}\otimes\mathbf{C})\mathbf{v}-(\tilde{\mathbf{b}}^T\otimes\mathbf{I}_N)\mathbf{A}\hat{\mathbf{x}},\end{aligned} \tag{4.20}$$

where we have $\mathbf{f}=[f_{-Q/2-Q'/2,0},\ldots,f_{-Q/2-Q'/2,L+L'},\ldots,f_{Q/2+Q'/2,L+L'}]^T$, $\mathbf{w}^{(r)}=[w_{-Q'/2,0}^{(r)},\ldots,w_{-Q'/2,L'}^{(r)},\ldots,w_{Q'/2,L'}^{(r)}]^T$, $\mathbf{w}=[\mathbf{w}^{(1)T},\ldots,\mathbf{w}^{(N_r)T}]^T$, and the augmented vector $\tilde{\mathbf{b}}=[\mathbf{0}_{1\times(Q+Q'-Q'')(L+L'+1)/2},\mathbf{0}_{1\times\Delta},\mathbf{b}_{-Q''/2}^T,\mathbf{0}_{1\times u},\ldots,\mathbf{0}_{\Delta\times 1},\mathbf{b}_{Q''/2}^T,\mathbf{0}_{1\times u},\mathbf{0}_{1\times(Q+Q'-Q'')(L+L'+1)/2}]^T$, where $u=L+L'-L''-\Delta-1$ and $\mathbf{b}_{q''}=[b_{q'',\Delta},\cdots,b_{q'',L''+\Delta-1}]^T$, i.e. we construct $\tilde{\mathbf{b}}$ in a way to match $\mathbf{f}$ in dimension. Defining the matrices $\mathbf{A}$ and $\mathbf{C}$ as

$$\mathbf{A}=\begin{bmatrix}\mathbf{D}_{-Q/2-Q'/2}\bar{\mathbf{Z}}_0\\ \vdots\\ \mathbf{D}_{-Q/2-Q'/2}\bar{\mathbf{Z}}_{L+L'}\\ \vdots\\ \mathbf{D}_{Q/2+Q'/2}\bar{\mathbf{Z}}_{L+L'}\end{bmatrix},\quad \mathbf{C}=\begin{bmatrix}\mathbf{D}_{-Q'/2}\bar{\mathbf{Z}}_0\\ \vdots\\ \mathbf{D}_{-Q'/2}\bar{\mathbf{Z}}_{L'}\\ \vdots\\ \mathbf{D}_{Q'/2}\bar{\mathbf{Z}}_{L'}\end{bmatrix}.$$

The relationship between the feedforward filter coefficients and the $\mathbf{f}$ can be obtained similarly as in (3.22) as

$$\mathbf{f}^T=\mathbf{w}^T\boldsymbol{\mathcal{H}}. \tag{4.21}$$

4.4.1 MMSE-SDFE

Assuming past decisions are correct, the error at the decision device $\mathbf{e}$ considering only the useful symbols:

$$\mathbf{e}=\mathbf{R}_{zp}\tilde{\mathbf{x}}-\mathbf{x}_*,$$

where $\mathbf{R}_{zp}=[\mathbf{0}_{M\times d},\mathbf{I}_M]$. Hence, we can write the error vector as

$$\mathbf{e}=\mathbf{R}_{zp}(\mathbf{f}^T\otimes\mathbf{I}_N)\mathbf{A}\bar{\mathbf{T}}_{zp}\mathbf{x}_*+\mathbf{R}_{zp}(\mathbf{w}^T\otimes\mathbf{I}_N)(\mathbf{I}_{N_r}\otimes\mathbf{C})\mathbf{v}-\mathbf{R}_{zp}(\tilde{\mathbf{b}}^T\otimes\mathbf{I}_N)\mathbf{A}\bar{\mathbf{T}}_{zp}\mathbf{x}_*-\mathbf{x}_*. \tag{4.22}$$

Substitute for $\mathbf{x}_*$ as $\mathbf{x}_* = \mathbf{R}_{zp}(\mathbf{e}_d^T \otimes \mathbf{I}_N)\mathbf{A}\bar{\mathbf{T}}_{zp}\mathbf{x}_*$, where $\mathbf{e}_d$ is a $(Q+Q'+1)(L+L'+1)\times 1$ unit vector with the 1 in position $(Q+Q')(L+L'+1)/2+d+1$, (4.22) can be written as

$$\mathbf{e} = (\mathbf{w}^T\boldsymbol{\mathcal{H}}\otimes\mathbf{I}_M)\tilde{\mathbf{A}}\mathbf{x}_* + (\mathbf{w}^T\otimes\mathbf{I}_M)(\mathbf{I}_{N_r}\otimes\tilde{\mathbf{C}})\mathbf{v} - ((\tilde{\mathbf{b}}+\mathbf{e}_d)^T\otimes\mathbf{I}_M)\tilde{\mathbf{A}}\mathbf{x}_*. \quad (4.23)$$

The matrices $\tilde{\mathbf{A}}$ and $\tilde{\mathbf{C}}$ in (4.23) are $\tilde{\mathbf{A}} = (\mathbf{I}_{(Q+Q'+1)(L+L'+1)}\otimes\mathbf{R}_{zp})\mathbf{A}\bar{\mathbf{T}}_{zp}$ and $\tilde{\mathbf{C}} = (\mathbf{I}_{(Q'+1)(L'+1)}\otimes\mathbf{R}_{zp})\mathbf{C}$, respectively.

Now we can write the mean-square error $MSE = \mathcal{E}\{\mathbf{e}^H\mathbf{e}\}$ as

$$\begin{aligned} MSE =\ & \mathrm{tr}\{(\mathbf{w}^T\boldsymbol{\mathcal{H}}\otimes\mathbf{I}_M)\tilde{\mathbf{A}}\mathbf{R}_x\tilde{\mathbf{A}}^H(\boldsymbol{\mathcal{H}}^H\mathbf{w}^*\otimes\mathbf{I}_M)\} \\ & + \mathrm{tr}\{(\mathbf{w}^T\otimes\mathbf{I}_M)(\mathbf{I}_{N_r}\otimes\tilde{\mathbf{C}})\mathbf{R}_v(\mathbf{I}_{N_r}\otimes\tilde{\mathbf{C}}^H)(\mathbf{w}^*\otimes\mathbf{I}_M)\} \\ & + \mathrm{tr}\{((\tilde{\mathbf{b}}^T+\mathbf{e}_d^T)\otimes\mathbf{I}_M)\tilde{\mathbf{A}}\mathbf{R}_x\tilde{\mathbf{A}}^H((\tilde{\mathbf{b}}^*+\mathbf{e}_d)\otimes\mathbf{I}_M) \\ & - 2\Re\{\mathrm{tr}\{(\mathbf{w}^T\boldsymbol{\mathcal{H}}\otimes\mathbf{I}_M)\tilde{\mathbf{A}}\mathbf{R}_x\tilde{\mathbf{A}}^H((\tilde{\mathbf{b}}^*+\mathbf{e}_d)\otimes\mathbf{I}_M)\}\} \end{aligned} \quad (4.24)$$

with $\mathbf{R}_x$ is defined here as $\mathbf{R}_x = \mathcal{E}\{\mathbf{x}_*\mathbf{x}_*\}$.

Using the properties introduced in (3.26) and (3.27), we can write (4.24) as

$$\begin{aligned} MSE =\ & \mathbf{w}^T\left(\boldsymbol{\mathcal{H}}\mathbf{R}_{\tilde{A}}\boldsymbol{\mathcal{H}}^H+\mathbf{R}_{\tilde{C}}\right)\mathbf{w}^* + (\tilde{\mathbf{b}}^T+\mathbf{e}_d^T)\mathbf{R}_{\tilde{A}}(\tilde{\mathbf{b}}^*+\mathbf{e}_d) \\ & - 2\Re\{\mathbf{w}^T\boldsymbol{\mathcal{H}}\mathbf{R}_{\tilde{A}}(\tilde{\mathbf{b}}^*+\mathbf{e}_d)\}, \end{aligned} \quad (4.25)$$

where $\mathbf{R}_{\tilde{A}} = \mathrm{subtr}\{\tilde{\mathbf{A}}\mathbf{R}_x\tilde{\mathbf{A}}^H\}$, and $\mathbf{R}_{\tilde{C}} = \mathrm{subtr}\{(\mathbf{I}_{N_r}\otimes\tilde{\mathbf{C}})\mathbf{R}_v(\mathbf{I}_{N_r}\otimes\tilde{\mathbf{C}}^H)\}$.

By solving $\partial MSE/\partial\mathbf{w} = \mathbf{0}$, we then obtain the MMSE feedforward time-varying FIR filter coefficients as

$$\mathbf{w}_{MMSE}^T = (\tilde{\mathbf{b}}^T+\mathbf{e}_d^T)\left(\boldsymbol{\mathcal{H}}^H\mathbf{R}_{\tilde{C}}^{-1}\boldsymbol{\mathcal{H}}+\mathbf{R}_{\tilde{A}}^{-1}\right)^{-1}\boldsymbol{\mathcal{H}}^H\mathbf{R}_{\tilde{C}}^{-1}, \quad (4.26)$$

Substituting (4.26) in (4.25) we obtain the following expression for the MSE:

$$MSE = (\tilde{\mathbf{b}}^T+\mathbf{e}_d^T)\mathbf{R}_\perp(\tilde{\mathbf{b}}^*+\mathbf{e}_d), \quad (4.27)$$

where

$$\begin{aligned} \mathbf{R}_\perp &= \mathbf{R}_{\tilde{A}} - \mathbf{R}_{\tilde{A}}\boldsymbol{\mathcal{H}}^H\left(\boldsymbol{\mathcal{H}}\mathbf{R}_{\tilde{A}}\boldsymbol{\mathcal{H}}^H+\mathbf{R}_{\tilde{C}}\right)^{-1}\boldsymbol{\mathcal{H}}\mathbf{R}_{\tilde{A}} \\ &= \left(\mathbf{R}_{\tilde{A}}^{-1}+\boldsymbol{\mathcal{H}}^H\mathbf{R}_{\tilde{C}}^{-1}\boldsymbol{\mathcal{H}}\right)^{-1}. \end{aligned} \quad (4.28)$$

The last line in (4.28) is obtained by applying the matrix inversion lemma (see page 41). By defining the selection matrix $\mathbf{P}_\Delta$ as

$$\mathbf{P}_\Delta = \left[\begin{array}{c|ccc|c} & \mathbf{I}_{Q''/2}\otimes\mathbf{P} & \mathbf{0} & \mathbf{0} & \\ \mathbf{0}_{k\times v} & \mathbf{0} & \bar{\mathbf{P}} & \mathbf{0} & \mathbf{0}_{k\times v} \\ & \mathbf{0} & \mathbf{0} & \mathbf{I}_{Q''/2}\otimes\mathbf{P} & \end{array}\right] \quad (4.29)$$

where $k = Q''L'' + 1$, $v = (Q + Q' - Q'')(L + L' + 1)/2$, $\mathbf{P} = [\mathbf{0}_{L''\times\Delta}, \mathbf{I}_{L''}, \mathbf{0}_{L''\times(L+L'+1-\Delta)}]$ and

$$\bar{\mathbf{P}} = \begin{bmatrix} \mathbf{0}_{1\times d} & 1 & \mathbf{0}_{1\times(L+L'-d)} \\ \mathbf{0}_{L''\times\Delta} & \mathbf{I}_{L''} & \mathbf{0}_{L''\times(L+L'-L''-\Delta+1)} \end{bmatrix},$$

We can write (4.27) as

$$MSE = \underbrace{[\mathbf{b}_{-Q''/2}^T, \cdots, \mathbf{b}_{-1}^T,\ 1,\ \mathbf{b}_0^T, \cdots, \mathbf{b}_{Q''/2}^T]}_{\mathbf{b}^T} \mathbf{R}_\Delta \mathbf{b}^*, \tag{4.30}$$

where $\mathbf{R}_\Delta = \mathbf{P}_\Delta \mathbf{R}_\perp^T \mathbf{P}_\Delta^T$. The formula in (4.30) is a quadratic form that is minimized by choosing the time-varying FIR feedback filter coefficients as

$$\mathbf{b}_{MMSE} = \frac{\mathbf{R}_\Delta^{-1}\mathbf{e}_x}{\mathbf{e}_x^T \mathbf{R}_\Delta^{-1}\mathbf{e}_x} \tag{4.31}$$

where $\mathbf{e}_x$ is a $Q''L'' + 1$ unit vector, with the 1 in position $(Q''L''/2 + 1)$. By substituting (4.31) in (4.26) we can solve for the time-varying FIR feedforward equalizer coefficients.

To summarize the MMSE feedforward and feedback time-varying FIR DFE filters' coefficients are obtained as follows:

$$\mathbf{R}_\perp = \left(\mathbf{R}_{\tilde{A}}^{-1} + \boldsymbol{\mathcal{H}}^H \mathbf{R}_{\tilde{C}}^{-1} \boldsymbol{\mathcal{H}}\right)^{-1} \tag{4.32}$$

$$\mathbf{R}_\Delta = \mathbf{P}_\Delta \mathbf{R}_\perp^T \mathbf{P}_\Delta^T \tag{4.33}$$

$$\mathbf{b}_{MMSE}^T = \frac{\mathbf{R}_\Delta^{-1}\mathbf{e}_x}{\mathbf{e}_x^T \mathbf{R}_\Delta^{-1}\mathbf{e}_x} \tag{4.34}$$

$$\mathbf{w}_{MMSE}^T = (\tilde{\mathbf{b}}^T + \mathbf{e}_d^T)\left(\boldsymbol{\mathcal{H}}^H \mathbf{R}_{\tilde{C}}^{-1} \boldsymbol{\mathcal{H}} + \mathbf{R}_{\tilde{A}}^{-1}\right)^{-1} \boldsymbol{\mathcal{H}}^H \mathbf{R}_{\tilde{C}}^{-1}, \tag{4.35}$$

4.4.2 ZF-SDFE

The ZF-SDFE is then obtained by setting the input source power to infinity resulting into the following:

$$\mathbf{R}_\perp = \left(\boldsymbol{\mathcal{H}}^H \mathbf{R}_{\tilde{C}}^{-1} \boldsymbol{\mathcal{H}}\right)^{-1} \tag{4.36}$$

$$\mathbf{R}_\Delta = \mathbf{P}_\Delta \mathbf{R}_\perp^T \mathbf{P}_\Delta^T \tag{4.37}$$

$$\mathbf{b}_{ZF}^T = \frac{\mathbf{R}_\Delta^{-1}\mathbf{e}_x}{\mathbf{e}_x^T \mathbf{R}_\Delta^{-1}\mathbf{e}_x} \tag{4.38}$$

$$\mathbf{w}_{ZF}^T = (\mathbf{b}^T \mathbf{P}_\Delta + \mathbf{e}_d^T)\left(\boldsymbol{\mathcal{H}}^H \mathbf{R}_{\tilde{C}}^{-1} \boldsymbol{\mathcal{H}}\right)^{-1} \boldsymbol{\mathcal{H}}^H \mathbf{R}_{\tilde{C}}^{-1} \tag{4.39}$$

For white noise and a white source with covariance matrices $\mathbf{R}_v = \sigma_n^2\mathbf{I}$ and $\mathbf{R}_s = \sigma_s^2\mathbf{I}$ respectively, and $M \gg L$ it is easy to show that $\mathbf{R}_{\tilde{A}}$ and $\mathbf{R}_{\tilde{C}}$ can be approximated as

$$\mathbf{R}_{\tilde{A}} \approx \sigma_s^2 M\mathbf{I}_{(Q+Q'+1)(L+L'+1)}$$

$$\mathbf{R}_{\tilde{C}} \approx \sigma_v^2 M\mathbf{I}_{N_r(Q'+1)(L'+1)}$$

The solution for the feedforward time-varying FIR filter coefficients (4.26) and the feedback time-varying FIR filter coefficients (4.31), unifies and extends results obtained for the case of purely frequency-selective channels [5]. For the case of no feedback, we end up with the MMSE-SLE obtained in Chapter 3.

4.5 Discussion and Comparison

4.5.1 Existence of the ZF Solution

In deriving the DFEs we assumed that the past decisions are correct (see (4.4) and (4.22)). Under this assumption, we can view the DFEs (block and serial) as linear equalizers. Thus, a ZF solution for the case of BDFE is obtained if the following is satisfied:

$$[\mathbf{W} \;\; -\mathbf{B}] \begin{bmatrix} \bar{\mathbf{H}} \\ \mathbf{I}_N \end{bmatrix} = \mathbf{I}_N,$$

under the constraint that $\mathbf{B}$ is a lower triangular matrix. This can always be satisfied.

Similarly, for the case of serial decision feedback equalization, a ZF solution exists if the following is satisfied (see (4.20)):

$$[\mathbf{w}^T \;\; -\mathbf{b}^T] \underbrace{\begin{bmatrix} \boldsymbol{\mathcal{H}} \\ \mathbf{P}_\Delta \end{bmatrix}}_{\mathbf{G}} = \mathbf{e}_d^T,$$

which is satisfied if the $N_r(Q'+1)(L'+1)+(Q''+1)L''+1 \times (Q+Q'+1)(L+L'+1)$ matrix $\mathbf{G}$ is of full column rank. It appears from this condition that, unlike the ZF existence condition for the case of SLE, a ZF-SDFE can exist for the case of SISO systems ($N_r = 1$).

4.5.2 Complexity Comparison

In comparing the two approaches, BDFE and SDFE, we consider two types of complexity: design complexity and implementation complexity.

The *design complexity* is the complexity associated with computing the equalizer (feedforward and feedback) coefficients. To design the BDFE, we need a matrix inversion of size $N \times N$ to compute the feedforward matrix $\mathbf{W}$, and a Cholesky factorization of an $N \times N$ matrix to compute the feedback matrix $\mathbf{B}$. Both require about $\mathcal{O}(N^3)$ flops. On the other hand, to design the SDFE, we need to compute the inverse of an $A \times A$ matrix to obtain the feedforward filter coefficients, where $A = (Q+Q'+1)(L+L'+1)$, and we need to compute the inverse of a $(Q''+1)L''+1 \times (Q''+1)L''+1$ matrix to obtain the feedback filter coefficients. So, provided that A and $(Q''+1)L''+1$ are smaller than M, the design complexity of the SDFE is less than the design complexity of the BDFE. In practice, the SDFE parameters Q', L', Q'' and L'' generally satisfy $A < N$ and $(Q''+1)L''+1 < N$.

The *implementation complexity* is the complexity associated with estimating a block of N samples. For the BDFE, to estimate a block of N samples, we require N^2 multiply-add (MA) operations per receive antenna for the feedforward part, and $(N-1)N/2$ MA operations for the feedback part. To estimate the same block using the SDFE we require $N(Q'+1)(L'+1)$ MA operations per receive antenna for the feedforward part and $N(Q''+1)L''$ MA operations for the feedback part. So, provided that $(Q'+1)(L'+1)$ is smaller than the block size N, and $(Q''+1)L''$ is smaller than $(N-1)/2$, the implementation complexity of the SDFE is lower than the implementation complexity of the BDFE. In practice, the SDFE parameters Q', L', Q'' and L'' generally satisfy $(Q'+1)(L'+1) < N$ and $(Q''+1)L'' < (N-1)/2$.

For the case of TI channels there is no need to design the feedforward and feedback filters as time-varying FIRs, instead they can be designed as TI FIRs with $Q' = 0$ and $Q'' = 0$. For this case we can easily show that our approach unifies and extends the FIR DFEs proposed for the case of TI channels (e.g. [5]).

4.6 Simulations

In the simulations, we consider a SISO as well as a SIMO system. The channel is assumed to be doubly selective and is approximated with the BEM. The BEM coefficients are used to design the DFE equlaizers block and serial. The designed equalizers are then used to equalize the real Jakes' time-varying channel. For the simulations we consider the following channel setup:

- transmitted block size $N = 800$,
- the BEM resolution $K = N$, and $K = 2N$,
- symbol period $T = 25\mu sec$,

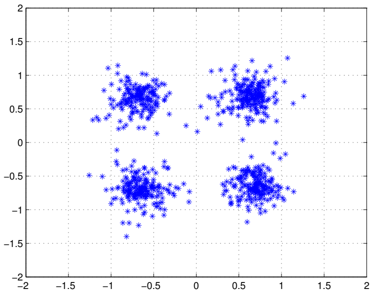

(a) MMSE-SLE for QPSK $K = 2N$, and $N_r = 1$.

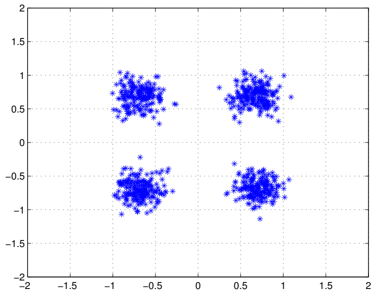

(b) MMSE-SDFE for QPSK $K = 2N$, and $N_r = 1$.

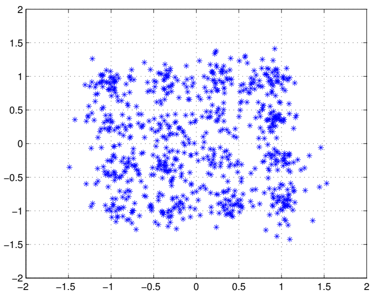

(c) MMSE-SLE for 16QAM $K = 2N$, and $N_r = 1$.

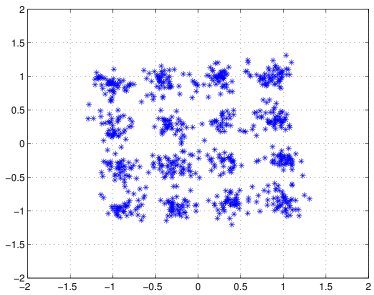

(d) MMSE-SDFE for 16QAM $K = 2N$, and $N_r = 1$.

Figure 4.4: After equalization using MMSE-SLE and MMSE-SDFE for $K = 2N$ and $N_r = 1$ for QPSK and 16QAM constellations at $SNR = 30$dB.

- maximum delay spread $\tau_{\max} = 75\mu sec$,
- maximum Doppler spread $f_{\max} = 100Hz$,
- number of basis functions $Q = 2\lceil f_{\max}KT \rceil$, which is then obtained as $Q = 4$ for $K = N$, and $Q = 8$ for $K = 2N$,
- channel order $L = \lceil \tau_{\max}/T \rceil = 3$.

For the SDFE, the feedforward and feedback time-varying FIRs are as listed in Table 4.1 (see 3.1 and the reasoning for obtaining these parameters as explained

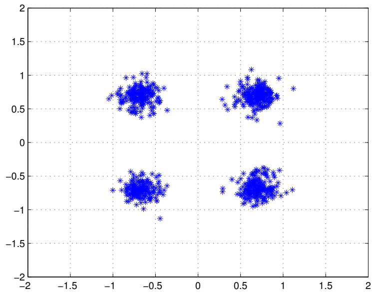

(a) MMSE-SLE for QPSK $K = 2N$, and $N_r = 2$.

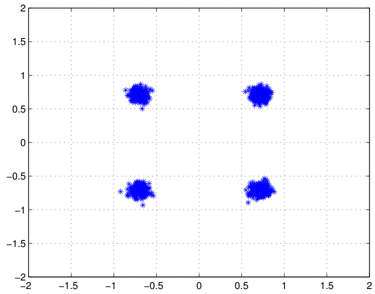

(b) MMSE-SDFE for QPSK $K = 2N$, and $N_r = 2$.

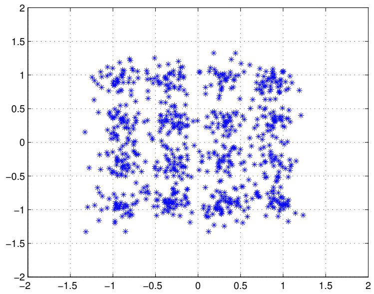

(c) MMSE-SLE for 16QAM $K = 2N$, and $N_r = 2$.

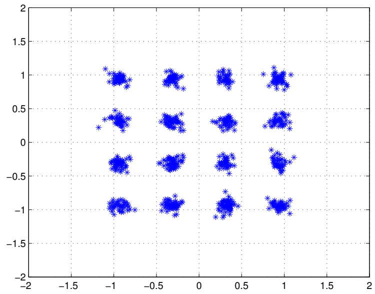

(d) DFE-SDFE for 16QAM $K = 2N$, and $N_r = 2$.

Figure 4.5: After equalization using MMSE-SLE and MMSE-SDFE for $K = 2N$ and $N_r = 2$ for QPSK and 16QAM constellations at $SNR = 30$dB.

Table 4.1: Filter coefficients for different receive antennas

	Feedforward Filter		**Feedback Filter**	
N_r	Q'	L'	Q''	L''
1	20	20	Q	3
2	12	12	Q	3
4	8	8	Q	3

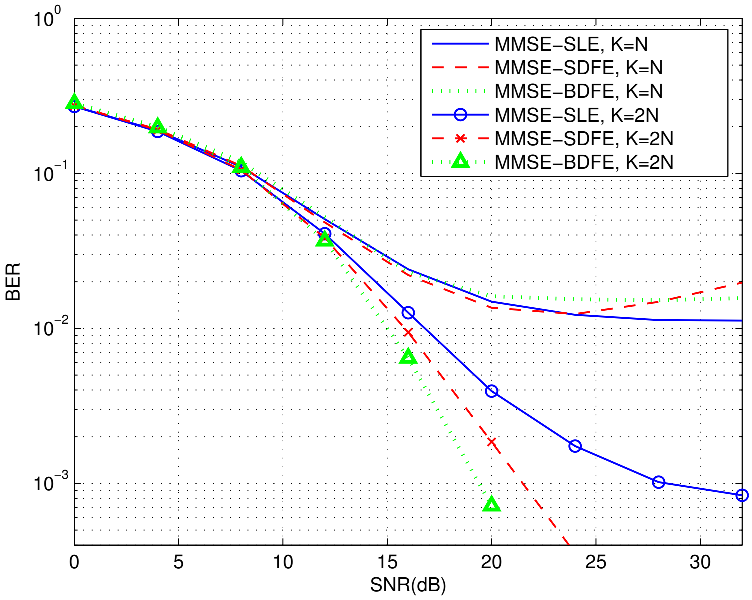

Figure 4.6: BER vs. SNR for $Nr = 1$

in Section 3.7) for the different number of receive antennas. For all simulations, we consider the decision delay $d = \lfloor \frac{L+L'}{2} \rfloor + 1$ and $\Delta = d + 1$.

We first examine the MMSE-SDFE along with the MMSE-SLE proposed in Chapter 3 for different constellations. In particular QPSK and 16QAM transmission. We consider the case of a single receive antenna as well as the case of two receive antennas. We also consider the BEM resolution $K = 2N$. The operating signal-to-noise ration value is $SNR = 30dB$. These results are shown in Figures 4.4 for one receive antenna and 4.5 for two receive antennas. As is clear from these figures, the MMSE-SDFE is more successful than the MMSE-SLE in recovering the transmitted signal.

From now on we examine the performance of the proposed MMSE-BDFE, MMSE-SDFE along with the MMSE-SLE in terms of the BER vs. SNR considering only QPSK transmission.

As shown in Figure 4.6 (SISO $N_r = 1$), the SNR loss for the SDFE compared to BDFE is less than $1dB$ at $BER = 10^{-2}$ for $K = 2N$. On the other hand, the proposed SDFE outperforms the SLE, and the latter suffers from an early error floor. However, for the case of $K = N$ the proposed equalizers all suffer from an early error floor due to large BEM modeling error. As for a complexity comparison, to compute the BDFE, we require $\mathcal{O}(N^3)$ flops, where

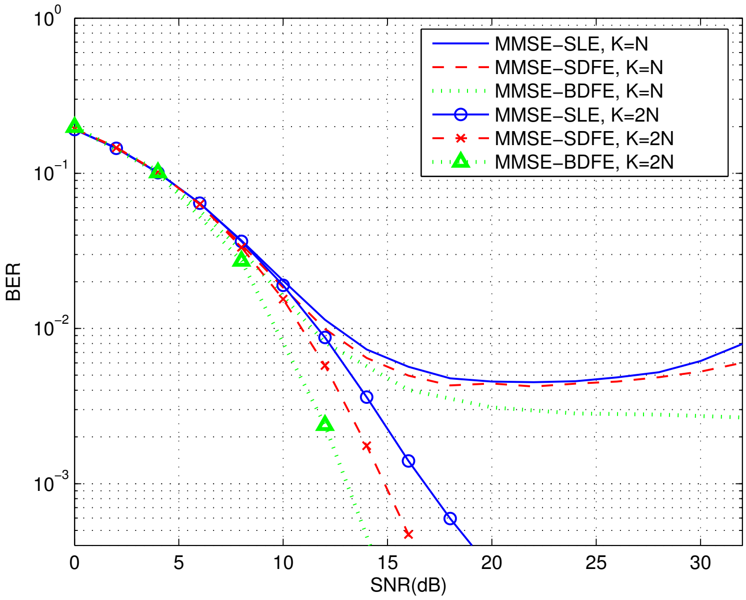

Figure 4.7: BER vs. SNR for $Nr = 2$

$N^3 = 512,000,000$ for this channel setup. On the other hand, to compute the SDFE we require $\mathcal{O}(A^3)$ flops, where $A^3 = 216,000,000$ for $K = N$ and $A^3 = 337,153,536$ for $K = 2N$ for this channel setup. Hence, the design complexity of the SDFE is clearly much lower than the design complexity of the BDFE ($\sim 60\%$ reduction in complexity for the case of $K = N$ and $\sim 34\%$ reduction in complexity for $K = 2N$). A similar observation can be drawn for the implementation complexity, where the BDFE requires $N^2+(N-1)N/2 = 959,600$ MA operations for this channel setup. On the other hand, the SDFE requires $M(Q'+1)(L'+1) + M(Q''+1)L'' = 363,432$ MA operations for this channel setup for $K = N$, and $372,996$ MA operations for $K = 2N$, which also shows around 60% reduction in implementation complexity.

In Figure 4.7 (SIMO $N_r = 2$), we see that the performance of the proposed SDFE almost coincides with that of the BDFE, whilst it significantly outperforms the SLE for $K = 2N$. On the other hand, the proposed equalizers suffer from an error floor for the case of $K = N$, due to the large BEM modeling error. In terms of complexity for this channel setup, the design complexity of the BDFE does not change from the previous example, whereas, to compute the SDFE we require $\mathcal{O}(A^3)$ MA operations, where $A^3 = 24137569$ for $K = N$ and $A^3 = 37,933,056$ for $K = 2N$. This means that the SDFE achieves a 96% reduction in complexity compared to the BDFE for $K = N$ and a 92.5%

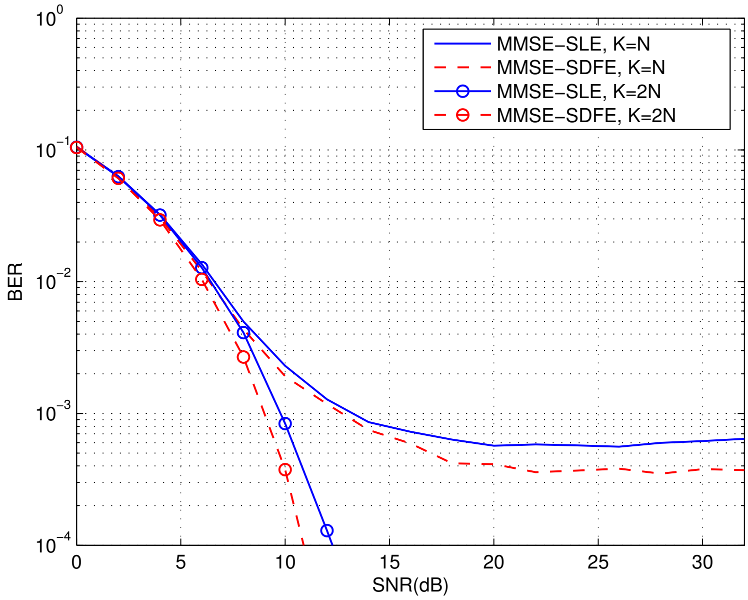

Figure 4.8: BER vs. SNR for $Nr = 4$

reduction in complexity for $K = 2N$. The implementation complexity, on the other hand, requires $954, 806$ MA operations for the BDFE, whereas it requires $146, 648$ MA operations per receive antenna for the SDFE for $K = N$ and $156, 212$ MA operations per receive antenna for $K = 2N$. This means that the SDFE now achieves a reduction of approximately 84% in implementation complexity over the BDFE.

In Figure 4.8 we show only the performance of the MMSE-SDFE and the MMSE-SLE for the case of $N_r = 4$ receive antennas. Similar observations can be easily drawn for this case in terms of performance and complexity.

4.7 Conclusion

In this chapter, we extend the linear equalization techniques proposed in Chapter 3 to decision-feedback. We discuss in this chapter a block DFE as well as a serial DFE. The SDFE consists of feedforward filters and a feedback filter and a decision device. As we approximate the channel by using the BEM, we also design the feedforward and feedback filters by the BEM resulting into what we denote as SDFE, where the feedforward and feedback filters are implemented using time-varying FIR filters.

We show that the implementation as well as the design complexity of the proposed SDFE are much lower than the design and implementation complexity of the BDFE. By properly choosing the feedforward and feedback filters' coefficients we can closely approach the performance of the BDFE. Finally, we also show that the SDFE outperforms the SLE.

Chapter 5

Pilot Symbol Assisted Modulation Techniques

5.1 Introduction

IN Chapters 3 and 4, linear and decision feedback equalizers have been developed for single carrier transmission over doubly selective channels. In these chapters, the time-varying channel was modeled using the basis expansion model (BEM). The BEM coefficients are then used to design the equalizer (linear or decision feedback). So far, it was assumed that the BEM coefficients are perfectly known at the receiver, and they were obtained by a least squares (LS) fitting of the noiseless real channel. This is, however, far from realistic. A more realistic approach is to either use training symbols to estimate and/or directly equalize the channel or obtain the channel estimate and/or directly equalize the channel blindly. In this chapter we will focus on pilot symbol assisted modulation (PSAM)-based techniques for channel estimation and direct equalization of rapidly time-varying channels. Blind and semi-blind techniques will be treated in the next chapter.

PSAM techniques rely on time multiplexing data symbols and known pilot symbols at known positions, which the receiver utilizes to either estimate the channel or obtain the equalizer coefficients directly. In this chapter, we first derive the optimal minimum mean-square error (MMSE) interpolation filter based channel estimation technique. Then we derive the conventional BEM channel estimation technique (based on LS fitting). It has been shown that the modeling error (between the true channel and the BEM channel model) is quite large for the case when the BEM period equals the time window (see Section 2.6). This case corresponds to a critical sampling of the Doppler spectrum.

Reducing this modeling error can be achieved by setting the BEM period equal to a multiple of the time window. In other words, we can reduce the modeling error by oversampling the Doppler spectrum. In [78] the authors treated the first case ignoring the modeling error. However, when an oversampling of the Doppler spectrum is used, the BEM based PSAM channel estimation is sensitive to noise. Here, we show that robust PSAM based channel estimation can be obtained by combining the optimal MMSE interpolation based channel estimation with the BEM considering an oversampling rate greater than one (an oversampling rate equal to 2 appears to be sufficient).

In addition, we show that the channel estimation step can be skipped and obtain the equalizer coefficients directly based on the pilot symbols. This is referred to as PSAM-based direct equalization.

This chapter is organized as follows. In Section 5.2, we first derive the PSAM MMSE channel estimation and then the BEM channel estimation is introduced. In Section 5.3, we introduce PSAM-based direct equalization. Our simulations for both approaches are shown in Section 5.4. Finally, our conclusions are drawn in Section 5.5.

5.2 PSAM Channel Estimation

In this section we assume a single-input single-output (SISO) system, but the results can be easily extended to a single-input multiple-output (SIMO) system or a multiple-input multiple-output (MIMO) system. Focusing on a baseband-equivalent description, when transmitting a symbol sequence $x[n]$ at rate $1/T$, the received signal $y[n]$ can be written as

$$y[n] = \sum_{k=-\infty}^{\infty} x[k]g[n; n-k] + v[n].$$

Using the optimal training procedure proposed in [78], the doubly selective channel of order L can be viewed as L flat fading channels on the part of the received sequence that corresponds to training. The data/training multiplexing is shown in Figure 5.1, where the training part consists of a training symbol surrounded by L zeros on each side. Assuming we use P such training clusters where the pilot symbols are located at positions $n_0, \ldots, n_{P-1}$, the input-output relation on the pilot positions can be written as

$$y[n_{p,l}] = g[n_{p,l}; l]x[n_p] + v[n_{p,l}],$$

where $n_{p,l} = n_p + l$ for $l = 0, \ldots, L$.

In this section, we first derive the optimal minimum mean-square error (MMSE) PSAM-based channel estimation, which leads to the development of the optimal

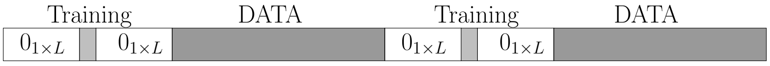

Figure 5.1: Optimal training for doubly selective channels

interpolation filter. However, since the BEM coefficients of the TV channels are needed to design the equalizers (linear and decision feedback), the PSAM-based estimation of the BEM coefficients is also discussed and combined with PSAM-based MMSE channel estimation to enhance the LS fitting of the true channel and the estimated one.

MMSE Channel Estimation

A noisy estimate of the channel at the pth pilot is easily obtained by

$$\hat{g}[n_{p,l}; l] = \frac{y[n_{p,l}]}{x[n_p]} = g[n_{p,l}; l] + \tilde{v}[n_{p,l}], \text{ for } p = 0, \ldots, P-1. \tag{5.1}$$

where $\tilde{v}[n_{p,l}] = v[n_{p,l}]/x[n_p]$. Define $\hat{\mathbf{g}}_{t,l} = [\hat{g}[n_{0,l}; l], \ldots, \hat{g}[n_{P-1,l}; l]]^T$, which is a vector containing the noisy estimates of the channel on the pilot positions. From these noisy estimates we have to reconstruct the channel response for all $n \in \{0, \ldots, N-1\}$. In other words, we need to design a $P \times N$ interpolation matrix $\mathbf{W}$ such that

$$\hat{\mathbf{g}}_l = \mathbf{W}^H \hat{\mathbf{g}}_{t,l}, \tag{5.2}$$

where $\hat{\mathbf{g}}_l = [\hat{g}[0; l], \ldots, \hat{g}[N-1; l]]^T$, with $\hat{g}[n; l]$ an estimate of the lth tap of the true channel at time index n. The mean square-error (MSE) criterion can be written as

$$\begin{aligned} \mathcal{J} &= \frac{1}{N} \sum_{n=0}^{N-1} \mathcal{E}\{|\hat{g}[n; l] - g[n; l]|^2\} \\ &= \frac{1}{N} \mathcal{E}\{\|\mathbf{W}^H \hat{\mathbf{g}}_{t,l} - \mathbf{g}_l\|^2\}, \end{aligned} \tag{5.3}$$

where $\mathbf{g}_l = [g[0; l], \ldots, g[N-1; l]]^T$ is the channel state information at the lth tap.

The MMSE interpolation matrix $\mathbf{W}$ is then obtained by solving

$$\min_{\mathbf{W}} \mathcal{J}$$

The solution of this problem is obtained as follows [30]

$$\mathbf{W} = (\mathbf{R}_p + \mathbf{R}_{\tilde{v}})^{-1} \mathbf{R}_h \tag{5.4}$$

where $\mathbf{R}_p$ is the channel correlation matrix on the pilots given by

$$\mathbf{R}_p = \begin{bmatrix} r_h[0] & \cdots & r_h[n_{P-1}-n_0] \\ r_h[n_1] & \cdots & r_h[n_{P-1}-n_1] \\ \vdots & \ddots & \vdots \\ r_h[n_{P-1}] & \cdots & r_h[0] \end{bmatrix},$$

and $\mathbf{R}_h$ is given by

$$\mathbf{R}_h = \begin{bmatrix} r_h[n_0] & \cdots & r_h[N-n_0-1] \\ r_h[n_1] & \cdots & r_h[N-n_1-1] \\ \vdots & \ddots & \vdots \\ r_h[n_{P-1}] & \cdots & r_h[N-n_{P-1}-1] \end{bmatrix},$$

with $r_h[k] = \mathcal{E}\{g[n;l]g^*[n-|k|;l]\}$ which is independent of the tap index l assuming that the channel taps are independent identically distributed (i.i.d) random variables. $\mathbf{R}_{\tilde{v}}$ is the channel estimate error at the pilot positions covariance matrix. Both $\mathbf{R}_p$ and $\mathbf{R}_h$ are assumed to be known[1]. Note that we used the assumption that the channel is wide sense stationary (WSS). Assuming i.i.d input symbols $x[n]$, and the training is of Kronecker delta form (i.e. $x[n_p] = 1\ \forall p = 0, \ldots, P-1$), and white noise with normalized power β, then $\mathbf{R}_{\tilde{v}} = \beta \mathbf{I}_P$.

5.2.1 BEM Channel Estimation

As discussed earlier in this chapter, for our equalizer design we require the channel BEM coefficients. Therefore, we use the BEM to approximate the time-varying channel $g[n;\nu]$ over a window of size N samples. In this BEM the lth tap time-varying channel $g[n;l]$ is expressed as a superposition of complex exponential basis functions with frequencies on a discrete DFT grid (see Chapter 2). In other words, the lth tap time-varying channel $g[n;l]$ is modeled for $n \in \{0, \cdots, N-1\}$ by a BEM as:

$$h[n;l] = \sum_{q=-Q/2}^{Q/2} h_{q,l} e^{j2\pi qn/K}, \tag{5.5}$$

where Q is the number of basis functions, and K is the BEM period. Q and K should be chosen such that $Q/(2KT)$ is larger than the maximum Doppler frequency, i.e. $Q/(2KT) \geq f_{\max}$. h_q is the coefficient of the qth basis function of the channel, which is kept invariant over a period of NT seconds, but may change from block to block.

[1]In this thesis we assume the realistic time-varying channel follows Jakes' model. Therefore, we only require the knowledge of the system maximum Doppler shift $f_{\max}$ and the sampling time to obtain these matrices.

Define $\mathbf{h}_l = [h_{-Q/2,l}, \ldots, h_{Q/2,l}]^T$ as the vector containing the BEM coefficients of the lth tap of the channel. In the ideal case, where the TV channel $\mathbf{g}_l$ is perfectly known at the receiver, the channel BEM coefficients can be obtained by solving the following LS problem:

$$\min_{\mathbf{h}_l} \|\mathbf{g}_l - \boldsymbol{\mathcal{L}}\mathbf{h}_l\|^2, \tag{5.6}$$

where

$$\boldsymbol{\mathcal{L}} = \begin{bmatrix} 1 & \ldots & 1 \\ e^{-j2\pi\frac{Q}{2}\frac{1}{K}} & \ldots & e^{j2\pi\frac{Q}{2}\frac{1}{K}} \\ \vdots & & \vdots \\ e^{-j2\pi\frac{Q}{2}\frac{N-1}{K}} & \ldots & e^{j2\pi\frac{Q}{2}\frac{N-1}{K}} \end{bmatrix}.$$

The solution of (5.6) is given by

$$\mathbf{h}_l = \boldsymbol{\mathcal{L}}^{\dagger}\mathbf{g}_l.$$

In practice, only a few pilot symbols are available for channel estimation. Assuming the noisy estimates are obtained as in (5.1), then the channel BEM coefficients can be obtained by solving the following LS problem:

$$\min_{\mathbf{h}_l} \|\hat{\mathbf{g}}_{t,l} - \tilde{\boldsymbol{\mathcal{L}}}_l\mathbf{h}_l\|^2, \tag{5.7}$$

where

$$\tilde{\boldsymbol{\mathcal{L}}}_l = \begin{bmatrix} e^{-j2\pi\frac{Q}{2}\frac{n_{0,l}}{K}} & \ldots & e^{j2\pi\frac{Q}{2}\frac{n_{0,l}}{K}} \\ \vdots & & \vdots \\ e^{-j2\pi\frac{Q}{2}\frac{n_{P-1,l}}{K}} & \ldots & e^{j2\pi\frac{Q}{2}\frac{n_{P-1,l}}{K}} \end{bmatrix}.$$

The solution of (5.7) is obtained by

$$\mathbf{h}_l = \tilde{\boldsymbol{\mathcal{L}}}_l^{\dagger}\hat{\mathbf{g}}_t \tag{5.8}$$

It has been shown in [78], that when we critically sample the Doppler spectrum ($K = N$) and ignore the modeling error, the optimal training strategy consists of inserting equipowered, equispaced pilot symbols. However, critical sampling of the Doppler spectrum results in an error floor due to the large modeling error. On the other hand, oversampling the Doppler spectrum ($K = rN$, with integer $r > 1$) reduces the modeling error when the ideal case is considered [65, 10], i.e. when (5.6) is applied. However, this channel estimate is sensitive to noise when PSAM channel estimation is used.

A robust channel estimate can then be obtained by combining the optimal MMSE interpolation based channel estimate obtained in (5.2) with the BEM channel estimate obtained in (5.6) as follows:

- First, obtain the channel estimate $\hat{\mathbf{g}}_l$ as in (5.2).
- Second, obtain the LS solution of the following problem:

$$\min_{\mathbf{h}_l} \|\hat{\mathbf{g}}_l - \boldsymbol{\mathcal{L}}\mathbf{h}_l\|^2, \tag{5.9}$$

The solution of (5.9) can be obtained as

$$\mathbf{h}_l = \boldsymbol{\mathcal{L}}^\dagger \hat{\mathbf{g}}_l, \tag{5.10}$$

or equivalently in one step as

$$\mathbf{h}_l = \boldsymbol{\mathcal{L}}^\dagger \mathbf{W}^H \hat{\mathbf{g}}_{t,l}. \tag{5.11}$$

Even though this applies to critical sampling as well as to the oversampling case, little gain is obtained when combining the MMSE interpolation based channel estimate with the critically sampled BEM ($K = N$), as will be clear in Section 5.4.

5.3 PSAM Direct Equalization

In this section we propose a PSAM-based direct equalization of doubly selective channels, where the time-varying FIR equalizer coefficients are obtained directly without passing through the channel estimation step. For this purpose, we derive a new input-output relationship that is equivalent to the input-output relationship derived in Chapter 3. Starting from (3.13), the estimate of $x[n]$ for $n \in \{0, \ldots, N-1\}$ after applying the time-varying FIR equalizer $w^{(r)}[n;\nu]$ at the rth receive antenna sequence $y^{(r)}[n]$ can be obtained as

$$\hat{x}[n-d] = \sum_{r=1}^{N_r} \sum_{\nu=-\infty}^{\infty} w^{(r)}[n;\nu] y^{(r)}[n-\nu]. \tag{5.12}$$

We design each time-varying FIR equalizer $w^{(r)}[n;\nu]$ for $n \in \{0, 1, \ldots, N-1\}$ to have $L'+1$ taps, where the time-variation of each tap is modeled by $Q'+1$ complex exponential basis functions with frequencies on the same DFT grid as for the channel

$$w^{(r)}[n;\nu] = \sum_{l'=0}^{L'} \delta[\nu - l'] \sum_{q'=-Q'/2}^{Q'/2} w_{q',l'}^{(r)} e^{j2\pi q' n/K}, \tag{5.13}$$

Substituting (5.13) in (5.12) we obtain

$$\hat{x}[n-d] = \sum_{l'=0}^{L'} \sum_{q'=-Q'/2}^{Q'/2} e^{j2\pi q' n/K} w_{q',l'}^{(r)} y^{(r)}[n-l']. \tag{5.14}$$

On the block level formulation, (5.14) can be written as

$$\begin{aligned}\hat{\mathbf{x}}_*^T &= \sum_{r=1}^{N_r} \mathbf{w}^{(r)T}\boldsymbol{\mathcal{Y}}^{(r)} \\ &= \mathbf{w}^T\boldsymbol{\mathcal{Y}}, \end{aligned} \tag{5.15}$$

where $\mathbf{w} = [\mathbf{w}^{(1)T}, \ldots, \mathbf{w}^{(N_r)T}]^T$, and $\boldsymbol{\mathcal{Y}} = [\boldsymbol{\mathcal{Y}}^{(1)T}, \ldots, \boldsymbol{\mathcal{Y}}^{(N_r)T}]^T$, with $\boldsymbol{\mathcal{Y}}^{(r)}$ is a $(Q'+1)(L'+1) \times (N+L')$ matrix given by $\boldsymbol{\mathcal{Y}}^{(r)} = [\mathbf{y}^{(r)}_{-Q'/2,0}, \ldots, \mathbf{y}^{(r)}_{-Q'/2,L'}, \ldots, \mathbf{y}^{(r)}_{Q'/2,L'}]^T$ with the q' frequency-shifted and l' time-shifted received sequence related to the rth receive antenna given by

$$\mathbf{y}^{(r)}_{q',l'} = \mathbf{D}_{q'}\mathbf{Z}_{l'}\mathbf{y}^{(r)}.$$

with $\mathbf{Z}_{l'}$ and $\mathbf{D}_{q'}$ as defined in Section 3.4.

Assume that we have P pilot symbols as training collected as before in the vector $\mathbf{x}_t$. We define $\boldsymbol{\mathcal{Y}}_t$ as the collection of columns of $\boldsymbol{\mathcal{Y}}$ that corresponds to the training symbol positions subject to some decision delay. Define $[\boldsymbol{\mathcal{Y}}]_i$ as the ith column of the matrix $\boldsymbol{\mathcal{Y}}$, and define $\boldsymbol{\mathcal{Y}}_t = [[\boldsymbol{\mathcal{Y}}]_{d+n_0}, \ldots, [\boldsymbol{\mathcal{Y}}]_{d+n_{P-1}}]$. We therefore require to find the time-varying FIR coefficients $\mathbf{w}$ such that the following cost function is minimized

$$\mathcal{J}(\mathbf{w}) = \|\mathbf{w}^T\boldsymbol{\mathcal{Y}}_t - \mathbf{x}_t^T\|^2.$$

Solving for $\mathbf{w}$ using LS, we arrive at

$$\mathbf{w} = \left(\boldsymbol{\mathcal{Y}}_t^*\boldsymbol{\mathcal{Y}}_t^T\right)^{-1}\boldsymbol{\mathcal{Y}}_t^*\mathbf{x}_t. \tag{5.16}$$

The LS solution in (5.16) is exactly obtained in the noiseless case if $P \geq N_r(Q'+1)(L'+1)$, providing that $N_r(Q'+1)(L'+1) \geq (Q+Q'+1)(L+L'+1)$ (see Section 3.6).

5.4 Simulation Results

In this section, we evaluate the performance of the proposed PSAM-based channel estimation and direct equalization techniques. We consider a rapidly time-varying channel simulated according to Jakes' model with $f_{\max} = 100\ Hz$, and sampling time $T = 25\mu sec$. the channel order is considered as $L = 3$. The channel autocorrelation function is given by $r_h[k] = \sigma_h^2 J_0(2\pi f_{\max}kT)$, where J_0 is the zero-th order Bessel function and $\sigma_h^2 = 1$ denotes the variance of the channel. We consider a window size of $N = 800$ symbols. For the BEM, we consider the critically sampled Doppler spectrum $K = N$, as well as the

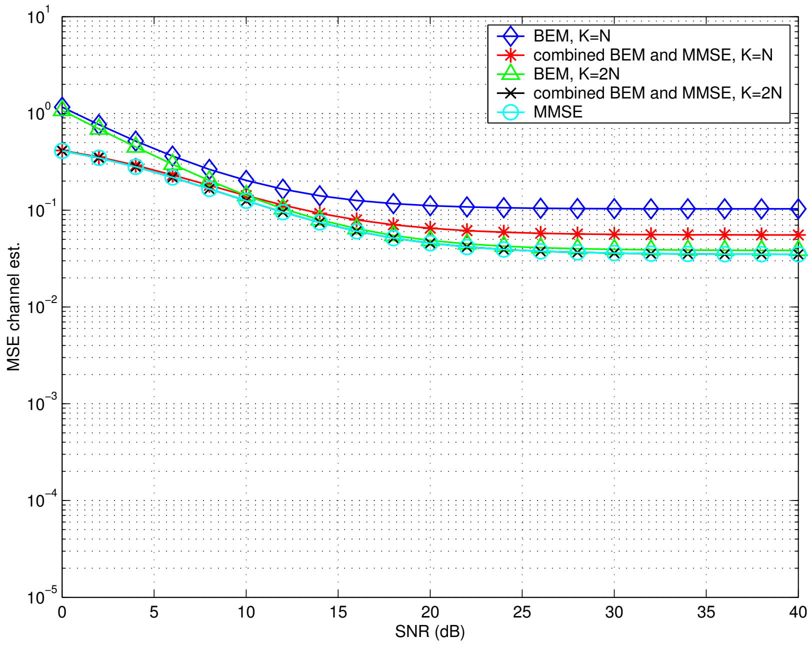

Figure 5.2: MSE vs. SNR for $P = 5$, $M = 160$

oversampled Doppler spectrum with oversampling rate 2 (i.e. $K = 2N$). The number of basis functions is, therefore, chosen to be $Q = 4$ for the critical sampling case, and $Q = 8$ for the oversampling case.

PSAM-Based Channel Estimation: We use PSAM to estimate the channel. We consider equipowered and equispaced pilot symbols with M the spacing between the pilots. The number of pilots is then computed as $P = \lfloor N/M \rfloor + 1$. Since we adhere to the optimal training [78], the optimal training consists of P-clusters, and each cluster consists of a training symbol and L surrounding zeros on each side as explained in Figure 5.1. This means that the training overhead is $\frac{P(2L+1)}{N-d}\%$.

First, we consider the normalized channel MSE versus SNR. We evaluate the performance of the different estimation techniques, in particular, BEM with $K = N$, combined BEM and MMSE with $K = N$, BEM with $K = 2N$, combined BEM and MMSE with $K = 2N$, and the MMSE channel estimate. We consider the case when the spacing between pilot symbols is 160 which corresponds to $P = 5$ pilot symbols dedicated for channel estimation. This choice is well suited for the case of $K = N$, where the number of BEM coefficients to be estimated is $Q + 1 = 5$. As shown in Figure 5.2, all the MSE channel estimates suffer from an early error floor. However, combining the critically sampled

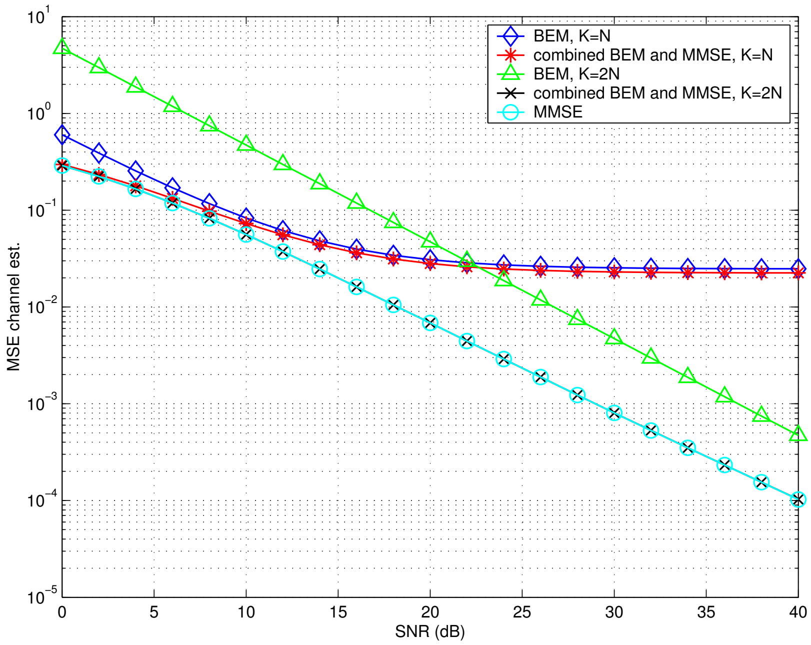

Figure 5.3: MSE vs. SNR for $P = 9$, $M = 95$

BEM with the MMSE results in a slightly better performance. We further consider the case when the spacing between the pilot symbols is $M = 95$ which corresponds to $P = 9$ pilot symbols dedicated for channel estimation. This case is well suited for the case when $K = 2N$. As shown in Figure 5.3, the performance of BEM with $K = N$ suffers from an early error floor, which means that increasing the number of pilot symbols does not enhance the channel estimation technique. Whilst for the case when $K = 2N$, the MSE curves do not suffer from an early error floor. However, the oversampled BEM channel estimate is sensitive to noise. A significant improvement is obtained when the combined BEM and MMSE method is used, where a gain of 9 dB at $MSE = 10^{-2}$ is obtained over the conventional BEM method, when the oversampling rate is 2. Note also that the performance of the combined BEM and MMSE method when $K = 2N$ coincides with the performance of the MMSE only.

Second, the estimated channel BEM coefficients are used to design a time-varying FIR equalizer. We consider here a single-input multiple-output (SIMO) system with $N_r = 2$ receive antennas. We use MMSE-SLE as well as MMSE-SDFE. For the case of MMSE-SLE, the SLE equalizer is designed to have order $L' = 12$ and number of time-varying basis functions $Q' = 12$. For the case of MMSE-SDFE, the time-varying FIR feedforward filter is designed to have order $L' = 12$ and number of time-varying basis functions $Q' = 12$, and

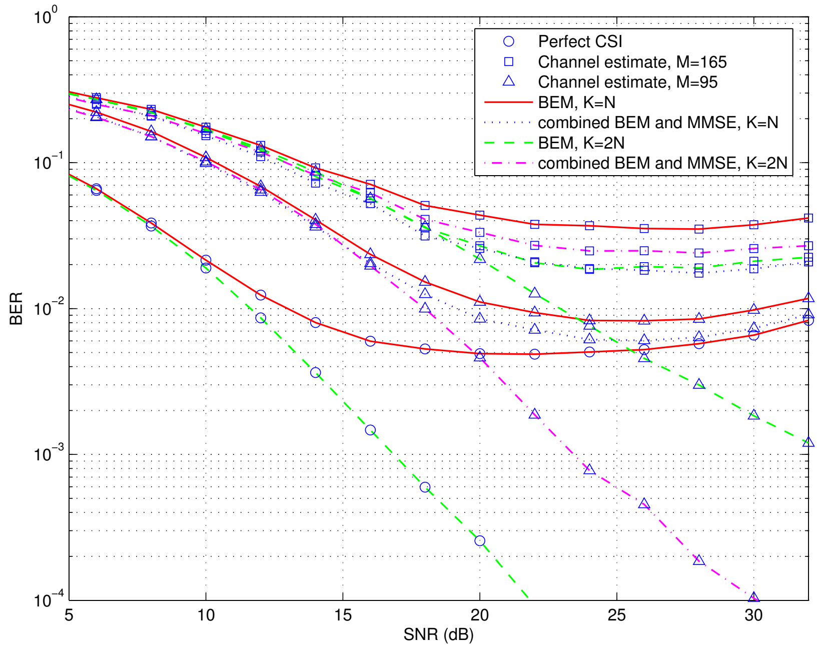

Figure 5.4: BER vs. SNR using the MMSE-SLE.

the time-varying FIR feedback filter to have order $L'' = L$ and $Q'' = Q$. The SLE coefficients as well as the SDFE coefficients are computed as explained in Section 3.4 for the MMSE-SLE, and in Section 4.4 for the MMSE-SDFE. The BEM resolution of the time-varying FIR equalizer matches that of the channel. QPSK signaling is assumed. We define the SNR as $SNR = \sigma_h^2(L+1)E_s/\sigma_n^2$, where E_s is the QPSK symbol power. As shown in Figure 5.4 for the case of MMSE time-varying FIR SLE, the BER curve experiences an error floor when $M = 165$ for the different scenarios. For the case of $M = 95$, we experience an SNR loss of 11.5 dB for the case of $K = 2N$ compared to the case when perfect channel state information (CSI) is known at $BER = 10^{-2}$, while the SNR loss is reduced to 6 dB for the case of combined BEM and MMSE when $K = 2N$. For $K = N$, both cases (BEM and combined BEM and MMSE) suffer from an error floor. Similar observations can be made for the case of MMSE time-varying FIR DFE shown in Figure 5.5.

Finally, we measure the MSE of the channel estimation techniques as a function of the maximum Doppler frequency. We design the system to have a maximum target Doppler frequency of $f_{\max} = 100\ Hz$. We then examine the performance of the channel estimation techniques for different maximum Doppler frequencies at a fixed signal to noise ratio $SNR = 25\ dB$. The results are shown in Figure 5.6 for the case when $P = 5$ pilot symbols are used for channel estimation, and

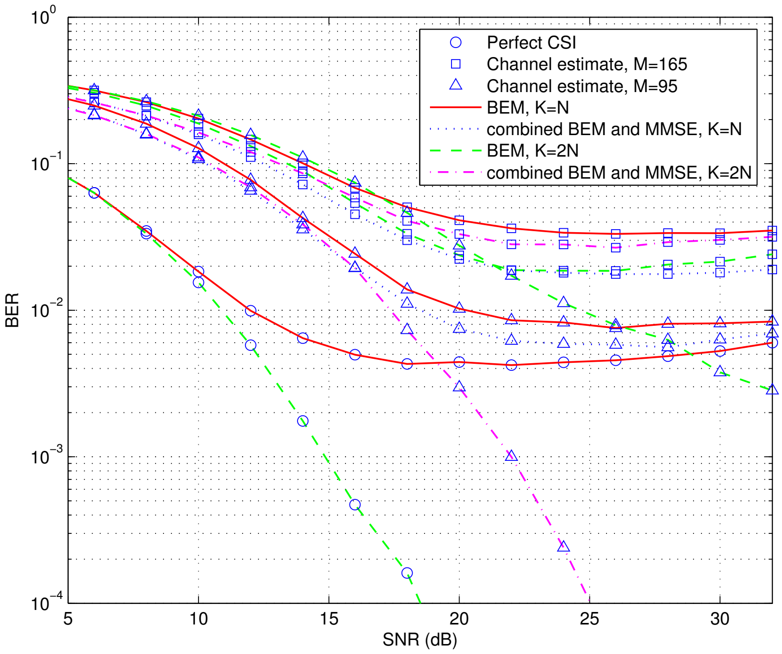

Figure 5.5: BER vs. SNR using the MMSE-SDFE.

Figure 5.7 when $P = 9$ pilot symbols are used. For either case, the channel estimation techniques maintain a low MSE channel estimate as long as the channel maximum Doppler frequency is less than the target maximum Doppler frequency.

PSAM Direct Equalization: We use here the same channel setup. For this setup, where for the ZF solution to exist the training overhead is measured to be 50%, i.e. inserting a pilot symbol every second symbol. The simulation results are shown in Figure 5.8 for window size $K = N$ as well as for window size $K = 2N$. In PSAM direct equalization the SNR loss is about 9dB for $K = N$ compared to perfect CSI at $BER = 10^{-2}$. For the case of window size $K = 2N$ the equalizer fails. At high SNRs the PSAM direct equalization for $K = N$ outperforms the case when the perfect channel state information based equalizer for $K = N$. This is due to the fact that the direct equalizer compensate for the noise as well as the modeling error. Due to this modeling error the equalizer based on perfect channel state information suffers from an error floor.

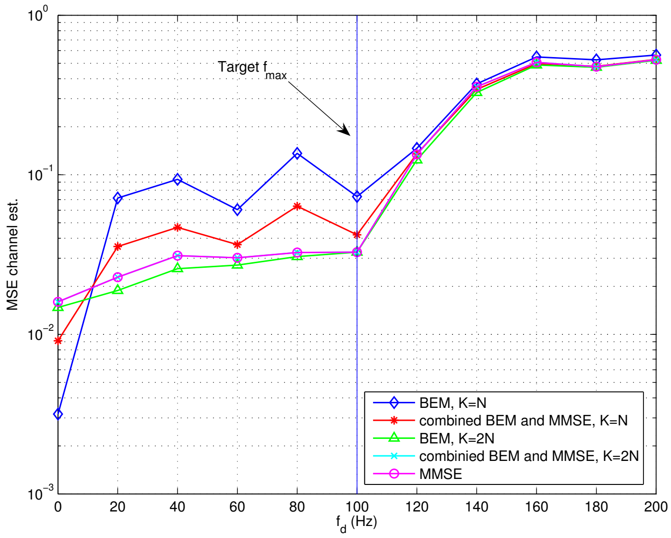

Figure 5.6: MSE vs. $f_{\max}$ for $P = 5$, $M = 160$, and $SNR = 25\ dB$

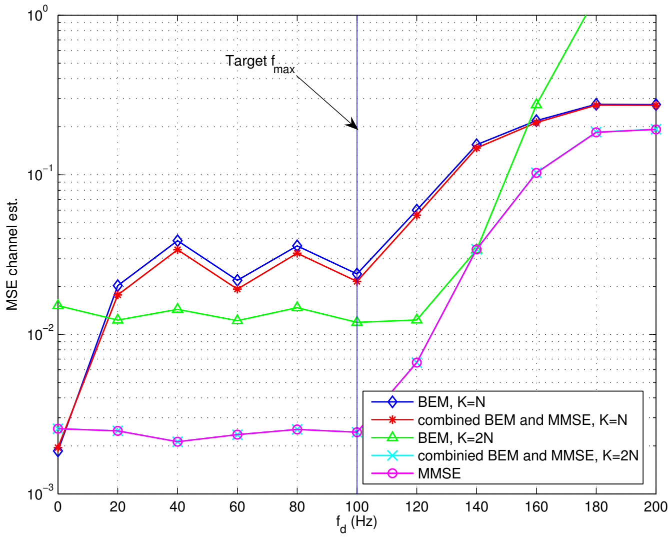

Figure 5.7: MSE vs. $f_{\max}$ for $P = 9$, $M = 95$, and $SNR = 25\ dB$

5.5 Conclusions

In this chapter, we propose a channel parameter estimation technique for rapidly time-varying channels derived from an interpolation based MMSE es-

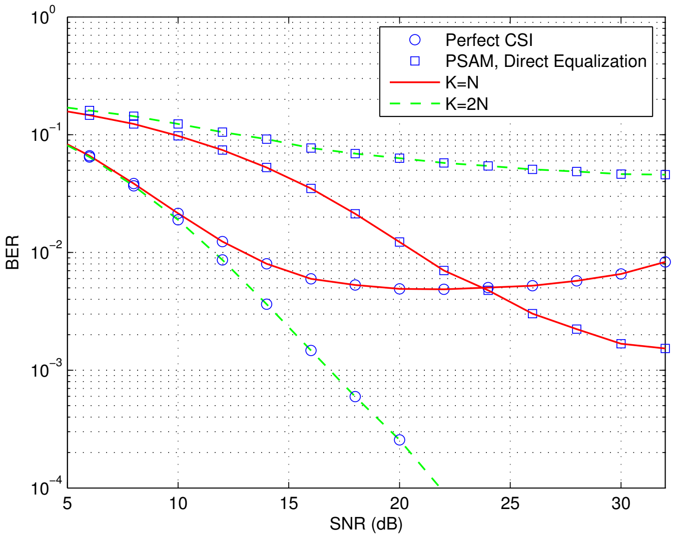

Figure 5.8: BER vs SNR for PSAM-based direct equalization.

timation scheme. We use the BEM to approximate the time-varying channel. Using the BEM, we only require to estimate the time-invariant coefficients. We rely on PSAM to estimate the channel. We consider the case when the Doppler spectrum is critically sampled ($K = N$) and when it is oversampled (K is a multiple of the window size N). While in the first case, the estimation scheme suffers from an early error floor due to the large modeling error, the estimation is sensitive to noise in the oversampled case. It has been shown through computer simulations that combining the MMSE interpolation based channel estimate with the oversampled BEM significantly improves the channel estimation. We also show that the channel estimation step can be skipped to perform direct equalization based on PSAM.

Chapter 6

Blind and Semi-Blind Techniques

6.1 Introduction

IN Chapter 5, we discussed PSAM techniques for channel estimation and direct equalization. The idea there is to insert known pilot symbols at known positions, which the receiver then utilizes to estimate and/or equalize the channel. The training overhead imposed on the system can be completely eliminated by using blind techniques. Due to the poor performance of blind techniques and their high implementation complexity, better performance and reduced complexity semi-blind techniques can be obtained. Semi-blind techniques are obtained by combining training-based and blind techniques. In this chapter we focus on blind and semi-blind techniques for channel estimation and direct equalization.

For our blind techniques we focus on deterministic approaches. For TI channels, a least-squares based deterministic method is discussed in [120]. Deterministic mutually referenced equalization is proposed in [87, 47]. For doubly selective channels, deterministic blind identification/equalization techniques are proposed in [46, 75], where for a ZF FIR solution to exist, the number of sub-channels (receive antennas) is required to be greater than the number of basis functions used for BEM channel modeling. However, for our approaches we show that the ZF solution exists for only two sub-channels (receive antennas). Subspace based methods are also proposed for channel identification/equalization for TI channels [82, 1, 2, 115, 101, 45].

In [105, 106] blind techniques based on linear prediction are proposed for doubly selective channels, where second-order statistics of the data are used. However, these techniques also require the number of receive antennas to be greater than the number of basis functions of the BEM channel.

This chapter is organized as follows. Blind and semi-blind channel estimation techniques are presented in Section 6.2. In Section 6.3, we present blind and semi-blind direct equalization. In Section 6.4 we show some simulation results of the proposed techniques. Finally, we summarize in Section 6.5.

6.2 Channel estimation

In this section we focus on the problem of channel estimation. We first discuss a deterministic blind channel estimation. In blind methods the channel is estimated up to a scalar ambiguity and computed from the singular value decomposition (eigenvalue decomposition) of a large matrix. To resolve the scalar ambiguity, blind techniques combined with training based techniques are favorable resulting into semi-blind techniques.

6.2.1 Blind Channel Estimation

In this section we discuss deterministic subspace based blind channel estimation [68]. It operates on time- and frequency-shifted versions of the received sequence. Assume that $Q'+1$ frequency shifts and $L'+1$ time shifts of the received sequence related to the rth receive antenna are stored in an $(Q'+1)(L'+1) \times (N+L')$ matrix (see Section 5.3) $\boldsymbol{\mathcal{Y}}^{(r)} = [\mathbf{y}^{(r)}_{-Q'/2,0}, \ldots, \mathbf{y}^{(r)}_{-Q'/2,L'}, \ldots, \mathbf{y}^{(r)}_{Q'/2,L'}]^T$ with the q'th frequency-shifted and l'th time-shifted received sequence related to the rth receive antenna given by

$$\mathbf{y}^{(r)}_{q',l'} = \mathbf{D}_{q'}\mathbf{Z}_{l'}\mathbf{y}^{(r)}.$$

A relationship between $\boldsymbol{\mathcal{Y}}^{(r)}$ and the transmitted sequence can be obtained by substituting (3.5) in $\boldsymbol{\mathcal{Y}}^{(r)}$ resulting into:

$$\boldsymbol{\mathcal{Y}}^{(r)} = \boldsymbol{\mathcal{H}}^{(r)}\boldsymbol{\mathcal{X}} + \boldsymbol{\mathcal{V}}^{(r)} \tag{6.1}$$

where $\boldsymbol{\mathcal{X}} = [\mathbf{x}_{-(Q'+Q)/2,0}, \ldots, \mathbf{x}_{-(Q'+Q)/2,(L+L'+1)}, \ldots, \mathbf{x}_{(Q'+Q)/2,(L+L'+1)}]^T$, where $\mathbf{x}_{p,k}$ is obtained as

$$\mathbf{x}_{p,k} = \mathbf{D}_p\tilde{\mathbf{Z}}_k\mathbf{x}.$$

The noise matrix $\boldsymbol{\mathcal{V}}^{(r)}$ is similarly defined as $\boldsymbol{\mathcal{Y}}^{(r)}$.

Stacking the N_r resulting matrices $\boldsymbol{\mathcal{Y}} = [\boldsymbol{\mathcal{Y}}^{(1)T}, \ldots, \boldsymbol{\mathcal{Y}}^{(N_r)T}]^T$, we obtain:

$$\boldsymbol{\mathcal{Y}} = \boldsymbol{\mathcal{H}}\boldsymbol{\mathcal{X}} + \boldsymbol{\mathcal{V}}, \tag{6.2}$$

where $\boldsymbol{\mathcal{H}} = [\boldsymbol{\mathcal{H}}^{(1)T}, \ldots, \boldsymbol{\mathcal{H}}^{(N_r)T}]^T$ and $\boldsymbol{\mathcal{V}} = [\boldsymbol{\mathcal{V}}^{(1)T}, \ldots, \boldsymbol{\mathcal{V}}^{(N_r)T}]^T$.

Let us assume the following:

A1) $\boldsymbol{\mathcal{H}}$ has full column rank $(Q+Q'+1)(L+L'+1)$ (see Section 3.6).

A2) $\boldsymbol{\mathcal{X}}$ has full row rank $(Q+Q'+1)(L+L'+1)$.

A3) $N \geq N_r(Q'+1)(L'+1)$.

Under these assumptions, the matrix $\boldsymbol{\mathcal{Y}}$ has $I = N_r(Q'+1)(L'+1) - (Q+Q'+1)(L+L'+1)$ zero singular values in the noiseless case. Suppose that $\mathbf{u}_1, \ldots, \mathbf{u}_I$ are the I left singular vectors corresponding to the I zero singular values. Then we can write

$$\mathbf{u}_i^H \boldsymbol{\mathcal{H}} = \mathbf{0}_{1\times(Q+Q'+1)(L+L'+1)}, \ \forall i \in \{1, \ldots, I\}. \tag{6.3}$$

Define $\mathbf{u}_i = [\mathbf{u}_i^{(1)T}, \ldots, \mathbf{u}_i^{(N_r)T}]^T$, and define $\mathbf{u}_i^{(r)} = [\mathbf{u}_{i,-Q'/2}^{(r)T}, \ldots, \mathbf{u}_{i,Q'/2}^{(r)T}]^T$ with $\mathbf{u}_{i,q'}^{(r)} = [u_{i,q',0}^{(r)}, \ldots, u_{i,q',L'}^{(r)}]^T$, (6.3) can be equivalently written as

$$\boldsymbol{\mathcal{U}}_i^H \mathbf{h} = \mathbf{0}_{1\times(Q+Q'+1)(L+L'+1)}, \ \forall i \in \{1, \ldots, I\}, \tag{6.4}$$

where $\mathbf{h} = [\mathbf{h}^{(1)T}, \ldots, \mathbf{h}^{(N_r)T}]^T$ with $\mathbf{h}^{(r)} = [\mathbf{h}_{-Q/2}^{(r)T}, \ldots, \mathbf{h}_{Q/2}^{(r)T}]^T$ where $\mathbf{h}_q^{(r)} = [h_{q,0}^{(r)}, \ldots, h_{q,L}^{(r)}]^T$. In (6.4), $\boldsymbol{\mathcal{U}}_i = [\boldsymbol{\mathcal{U}}_i^{(1)^T}, \ldots, \boldsymbol{\mathcal{U}}_i^{(N_r)T}]^T$, where $\boldsymbol{\mathcal{U}}_i^{(r)}$ is defined as

$$\boldsymbol{\mathcal{U}}_i^{(r)} = \begin{bmatrix} \boldsymbol{\Omega}_1^{-Q/2} \boldsymbol{\mathcal{U}}_{i,-Q'/2}^{(r)} \boldsymbol{\Omega}_2^{Q/2} & \ldots & \boldsymbol{\Omega}_1^{-Q/2} \boldsymbol{\mathcal{U}}_{i,Q'/2}^{(r)} \boldsymbol{\Omega}_2^{Q/2} & & \mathbf{0} \\ & \ddots & & \ddots & \\ \mathbf{0} & & \boldsymbol{\Omega}_1^{Q/2} \boldsymbol{\mathcal{U}}_{i,-Q'/2}^{(r)} \boldsymbol{\Omega}_2^{-Q/2} & \ldots & \boldsymbol{\Omega}_1^{Q/2} \boldsymbol{\mathcal{U}}_{i,Q'/2}^{(r)} \boldsymbol{\Omega}_2^{-Q/2} \end{bmatrix},$$

with $\boldsymbol{\mathcal{U}}_{i,q'}^{(r)}$ an $(L+1)\times(L'+L+1)$ Toeplitz matrix given by:

$$\boldsymbol{\mathcal{U}}_{i,q'}^{(r)} = \begin{bmatrix} u_{i,q',0}^{(r)} & \ldots & u_{i,q',L'}^{(r)} & & 0 \\ & \ddots & & \ddots & \\ 0 & & u_{i,q',0}^{(r)} & \ldots & u_{i,q',L'}^{(r)} \end{bmatrix},$$

and $\boldsymbol{\Omega}_1 = \text{diag}\{[1, \ldots, e^{j2\pi L/K}]^T\}$ and $\boldsymbol{\Omega}_2 = \text{diag}\{[1, \ldots, e^{j2\pi L'/K}]^T\}$.

Stacking the I left singular vectors we obtain

$$\boldsymbol{\mathcal{U}}^H \mathbf{h} = \mathbf{0}_{I(Q+Q'+1)(L+L'+1)\times 1},$$

where $\boldsymbol{\mathcal{U}} = [\boldsymbol{\mathcal{U}}_1, \ldots, \boldsymbol{\mathcal{U}}_I]$, from which $\mathbf{h}$ can be computed up to a scalar ambiguity. In the presence of noise, we compute the I left singular vectors of

$\boldsymbol{\mathcal{Y}}$ corresponding to the I smallest singular values. We denote these vectors as $\hat{\mathbf{u}}_1, \ldots, \hat{\mathbf{u}}_I$, and obtain the corresponding $\hat{\boldsymbol{\mathcal{U}}}$ in a similar fashion as we computed $\boldsymbol{\mathcal{U}}$. The channel estimate is then obtained as

$$\min_{\mathbf{h}} \|\hat{\boldsymbol{\mathcal{U}}}^H \mathbf{h}\|^2.$$

The solution is obtained by the singular vector of $\hat{\boldsymbol{\mathcal{U}}}$ corresponding to the smallest singular value.

6.2.2 Semi-Blind Channel Estimation

In blind methods, the channel is estimated up to a scalar multiplication. To resolve the scalar ambiguity, training symbols are used along with the blind technique resulting into the so-called semi-blind technique. In semi-blind techniques, the channel estimate is obtained by minimizing a cost function consisting of two parts. The first part corresponds to the training, and the second part corresponds to blind estimation.

First, let us consider the channel estimate that relies on known symbols. To facilitate channel estimation, we write the input-output relationship as

$$\mathbf{y}^T = \mathbf{h}^T(\mathbf{I}_{N_r} \otimes \boldsymbol{\mathcal{X}}_{sb}) + \mathbf{v}^T, \tag{6.5}$$

where $\mathbf{y} = [\mathbf{y}^{(1)T}, \ldots, \mathbf{y}^{(N_r)T}]^T$, $\mathbf{v} = [\mathbf{v}^{(1)T}, \ldots, \mathbf{v}^{(N_r)T}]^T$, and the $(Q'+1)(L'+1) \times N$ matrix $\boldsymbol{\mathcal{X}}_{sb} = [\mathbf{x}^T_{-Q/2,0}, \ldots, \mathbf{x}^T_{Q/2,L}]$ with the qth frequency-shift and lth time-shift of the transmitted sequence $\mathbf{x}_{q,l}$ given by

$$\mathbf{x}_{q,l} = \mathbf{D}_q \mathbf{Z}_l \mathbf{x}.$$

Let us assume that N_t symbols are used for training, and the remaining symbols are data symbols. Collecting the received symbols that correspond to training in one vector $\mathbf{y}_t$, and the training symbols in a matrix $\boldsymbol{\mathcal{X}}_{sb,t}$. We can write the received sequence corresponding to training as

$$\mathbf{y}_t^T = \mathbf{h}^T(\mathbf{I}_{N_r} \otimes \boldsymbol{\mathcal{X}}_{sb,t}) + \mathbf{v}_t.$$

A LS channel estimate $\hat{\mathbf{h}}_{tr}$ is then computed based on the training symbols as

$$\hat{\mathbf{h}}_{tr} = \left(\mathbf{I}_{N_r} \otimes \boldsymbol{\mathcal{X}}^T_{sb,t}\right)^\dagger \mathbf{y}_t.$$

To avoid the under-determined case it is required that the number of training symbols is $N_t \geq N_r(Q+1)(L+1)$[1]. This training overhead can be greatly

[1] Actually to have non overlapping data and training the optimal training strategy consists of $N_r(Q+1)$ clusters of $2L+1$ training symbols. Each cluster consists of a training symbol and L surrounding zeros on each side [78]. Therefore, the training overhead is actually $N_r(Q+1)(2L+1)$, and the non overlapping part is $N_t = N_r(Q+1)(L+1)$

reduced by combining the training with a blind estimation technique resulting in a semi-blind technique.

The semi-blind channel estimate can be obtained by using the following cost function:

$$\hat{\mathbf{h}}_{sb} = \arg\min_{\mathbf{h}} \left\{ \alpha \mathbf{h}^T \hat{\boldsymbol{\mathcal{U}}}^* \hat{\boldsymbol{\mathcal{U}}}^T \mathbf{h}^* + \|\mathbf{y}_t^T - \mathbf{h}^T (\mathbf{I}_{N_r} \otimes \boldsymbol{\mathcal{X}}_{sb,t})\|^2 \right\} \tag{6.6}$$

where $\alpha > 0$ is a weighting factor. If α is large, then the blind method is emphasized, whereas the LS training based is emphasized for small α. In (6.6) the first part corresponds to blind estimation while the second part corresponds to training.

The solution for the semi-blind channel estimation is then obtained as

$$\hat{\mathbf{h}}_{sb} = \left(\alpha \hat{\boldsymbol{\mathcal{U}}} \hat{\boldsymbol{\mathcal{U}}}^H + \mathbf{I}_{N_r} \otimes (\boldsymbol{\mathcal{X}}_{sb,t} \boldsymbol{\mathcal{X}}_{sb,t}^H)^T \right)^{-1} (\mathbf{I}_{N_r} \otimes \boldsymbol{\mathcal{X}}_{sb,t}^H)^T \mathbf{y}_t. \tag{6.7}$$

6.3 Direct Equalization

In direct equalization the equalizer coefficients are obtained directly without passing through the channel estimation stage. There are many techniques that can be applied to obtain directly the equalizer coefficients for the case of frequency-selective channels. These techniques range from stochastic to deterministic. However, due to the fact that we assume the BEM channel model, and the fact that the channel BEM coefficients may change from block to block, stochastic techniques cannot be applied. In this section we will rely on deterministic direct equalization techniques. We first discuss a deterministic blind direct equalization that relies on the so-called mutually referenced equalization (MRE). MRE is successfully applied to the case of TI channels [87, 47]. In MRE the idea is to tune a number of equalizers, where the outputs of these tuned equalizers are used to train the other equalizers in a mutual fashion. For the case of time-varying channels, the same idea can be applied, but taking into account the time- and frequency-shifts of the received signal. A semi-blind algorithm is then obtained by combining the training based LS method and the blind MRE method.

6.3.1 Blind Direct Equalization

The idea of blind direct equalization depends on tuning various equalizers associated with reconstructing the transmitted signal subject to a time- and frequency shift. Define $\mathbf{w}_{p,k}^T$ as the time-varying FIR equalizer that reconstructs the pth frequency-shifted and kth time-shifted (delayed) version of the received sequence in the noiseless case as:

$$\mathbf{w}_{p,k}^T \boldsymbol{\mathcal{Y}} = \mathbf{x}^T \tilde{\mathbf{Z}}_k^T \mathbf{D}_p. \tag{6.8}$$

where $\mathbf{x} = [x[-L-L'], \ldots, x[N-1]]^T$. In order to have mutually referenced equalizers training each other for frequency-shifts $p \in \{-(Q+Q')/2, \ldots, (Q+Q')/2\}$ and time-shifts (delays) $k \in \{0, \ldots, L+L'\}$, we set $\mathbf{x} = [\mathbf{0}_{1\times(L+L')}, \mathbf{x}_*^T, \mathbf{0}_{1\times(L+L')}]^T$, with $\mathbf{x}_*$ a data vector of length $M = N-L-L'$.

Define $\boldsymbol{\mathcal{Y}}_{p,k} = \boldsymbol{\mathcal{Y}}\mathbf{D}_{-p}\breve{\mathbf{Z}}_k$, with $\breve{\mathbf{Z}}_k = [\mathbf{0}_{M\times k}, \mathbf{I}_M, \mathbf{0}_{M\times(L+L'-k)}]^T$. Hence, we can write (6.8) as:

$$\mathbf{w}_{p,k}^T \boldsymbol{\mathcal{Y}}_{p,k} = \mathbf{x}_*^T. \tag{6.9}$$

In order that (6.8) is satisfied in the noiseless case (i.e. a ZF solution exists) we require that:

A1) the matrix $\boldsymbol{\mathcal{H}}$ is of full column rank $(Q+Q'+1)(L+L'+1)$ (see Chapter 3).

A2) the inequality $N_r(Q'+1)(L'+1) \geq (Q+Q'+1)(L+L'+1)$ is satisfied, which requires at least two receive antennas.

A3) the data length $M > (Q+Q'+1)(L+L'+1)$

A4) the input $x[n]$ is persistently exciting of order at least $(Q+Q'+1)(L+L'+1)$, i.e. rank $\boldsymbol{\mathcal{X}}$ equals $(Q+Q'+1)(L+L'+1)$ [47].

Taking the 0th frequency-shift and the 0th time-shift equalizer $\mathbf{w}_{0,0}$ as a reference equalizer and collecting the different equalizer coefficients in one vector $\mathbf{w} = [\mathbf{w}_{0,0}^T, \mathbf{w}_{-(Q+Q')/2,0}^T, \ldots, \ldots, \mathbf{w}_{-1,L+L'}^T, \mathbf{w}_{0,1}^T, \ldots, \mathbf{w}_{(Q+Q')/2,L+L'}^T]^T$, we arrive at the following:

$$\mathbf{w}^T \breve{\boldsymbol{\mathcal{Y}}} = \mathbf{0}_{1\times M(Q+Q'+1)(L+L'+1)}, \tag{6.10}$$

where

$$\breve{\boldsymbol{\mathcal{Y}}} = \begin{bmatrix} \boldsymbol{\mathcal{Y}}_{0,0} & \boldsymbol{\mathcal{Y}}_{0,0} & \cdots & \boldsymbol{\mathcal{Y}}_{0,0} \\ -\boldsymbol{\mathcal{Y}}_{-(Q+Q')/2,0} & \mathbf{0} & & \mathbf{0} \\ \mathbf{0} & -\boldsymbol{\mathcal{Y}}_{-(Q+Q')/2,1} & & \\ \vdots & & \ddots & \vdots \\ \mathbf{0} & \cdots & \mathbf{0} & -\boldsymbol{\mathcal{Y}}_{(Q+Q')/2,L+L'} \end{bmatrix}.$$

Note that in the noiseless case, it can be proven that the rank of $\breve{\boldsymbol{\mathcal{Y}}}$ is $(Q+Q'+1)^2(L+L'+1)^2-1$.

The different $\mathbf{w}_{p,k}$'s are linearly independent and cannot be obtained from each other. The different equalizers can be used as rows of a $(Q+Q'+1)(L+L'+1) \times N_r(Q'+1)(L'+1)$ matrix $\boldsymbol{\mathcal{W}}$. Based on the ZF conditions we obtain the following relation:

$$\boldsymbol{\mathcal{W}}\boldsymbol{\mathcal{H}} = \alpha \mathbf{I}_{(Q+Q'+1)(L+L'+1)}, \tag{6.11}$$

where α is some scale ambiguity satisfying:

$$\mathbf{w}_{0,0}^T \boldsymbol{\mathcal{Y}}_{0,0} = \mathbf{w}_{p,k}^T \boldsymbol{\mathcal{Y}}_{p,k} = \alpha \mathbf{x}_*^T, \ \forall p,k \ p \neq 0, \ k \neq 0. \tag{6.12}$$

We can solve (6.10) either by using LS or by subspace methods [47]. For the LS solution we constrain the first entry of $\mathbf{w}$ to 1 and solve for the normalized $\bar{\mathbf{w}}$ as:

$$\bar{\mathbf{w}}_{LS}^T = \left(\bar{\check{\boldsymbol{\mathcal{Y}}}}^H \bar{\check{\boldsymbol{\mathcal{Y}}}} \right)^{-1} \bar{\check{\boldsymbol{\mathcal{Y}}}}^H \bar{\mathbf{y}},$$

where $\bar{\check{\boldsymbol{\mathcal{Y}}}}$ is the matrix obtained after removing the first row of $\check{\boldsymbol{\mathcal{Y}}}$ and $\bar{\mathbf{y}}$ is this row multiplied by -1. The subspace approach is obtained by setting $\|\mathbf{w}\|^2 = 1$ and taking $\mathbf{w}$ as the left singular vector corresponding to the minimum singular value of $\check{\boldsymbol{\mathcal{Y}}}$.

Note that, if channel estimation is required, then using (6.11) the channel can be estimated subject to some scalar ambiguity.

6.3.2 Semi-Blind Direct Equalization

The MRE blind algorithm estimates the transmitted signal up to a scalar ambiguity α (see (6.12)). In addition, the blind MRE is very complex. These two difficulties with the blind MRE can be resolved by combining training with the blind MRE method resulting into so-called semi-blind direct equalization. The proposed semi-blind approach consists of a combination of the training-based least-squares (LS) method [87] and the blind MRE method [44, 47], both well-known for frequency-selective channels, but here applied to doubly selective channels. The basic idea is that we consider different SLEs that detect different time- and frequency-shifted versions of the transmitted sequence (blind MRE part discussed earlier in this chapter). While during training periods, the training symbols are used to train all equalizers, during data transmission periods, each equalizer output is used to train the other equalizers.

Starting from (6.9), we assume that N_t symbols in $\mathbf{x}_*$ are training symbols and the remaining $N_d = M - N_t$ symbols in $\mathbf{x}_*$ are data symbols. Let us then collect the training symbols of $\mathbf{x}_*$ in $\mathbf{x}_{*,t}$ and the data symbols of $\mathbf{x}_*$ in $\mathbf{x}_{*,d}$. Let us further collect the corresponding columns of $\boldsymbol{\mathcal{Y}}_{p,k}$ in $\boldsymbol{\mathcal{Y}}_{p,k,t}$ and $\boldsymbol{\mathcal{Y}}_{p,k,d}$, respectively. Splitting (6.9) into its training part and data part and stacking the results for $p \in \{-(Q+Q')/2, \ldots, (Q+Q')/2\}$ and $k \in \{0, \ldots, L+L'\}$ we arrive at the following:

$$\mathbf{w}^T [\underline{\boldsymbol{\mathcal{Y}}}_t, \underline{\boldsymbol{\mathcal{Y}}}_d] = [\mathbf{x}_{*,t}^T \underline{\mathbf{I}}_{N_t}, \mathbf{x}_{*,d}^T \underline{\mathbf{I}}_{N_t}],$$

where $\underline{\boldsymbol{\mathcal{Y}}}_t$ and $\underline{\boldsymbol{\mathcal{Y}}}_d$ are defined as

$$\underline{\boldsymbol{\mathcal{Y}}}_t = \begin{bmatrix} \boldsymbol{\mathcal{Y}}_{-(Q+Q')/2,0,t} & & & & \\ & \ddots & & & \\ & & \boldsymbol{\mathcal{Y}}_{-(Q+Q')/2,L+L',t} & & \\ & & & \ddots & \\ & & & & \boldsymbol{\mathcal{Y}}_{(Q+Q')/2,L+L',t} \end{bmatrix},$$

$$\underline{\boldsymbol{\mathcal{Y}}}_d = \begin{bmatrix} \boldsymbol{\mathcal{Y}}_{-(Q+Q')/2,0,d} & & & & \\ & \ddots & & & \\ & & \boldsymbol{\mathcal{Y}}_{-(Q+Q')/2,L+L',d} & & \\ & & & \ddots & \\ & & & & \boldsymbol{\mathcal{Y}}_{(Q+Q')/2,L+L',d} \end{bmatrix}$$

and

$$\underline{\mathbf{I}}_{N_t} = \mathbf{1}_{1\times R} \otimes \mathbf{I}_{N_t},$$
$$\underline{\mathbf{I}}_{N_d} = \mathbf{1}_{1\times R} \otimes \mathbf{I}_{N_d}.$$

where $R = (Q + Q' + 1)(L + L' + 1)$.

In the noisy case, we then have to solve

$$\min_{\mathbf{w},\mathbf{x}_{*,d}} \{\|\mathbf{w}^T[\underline{\boldsymbol{\mathcal{Y}}}_t, \underline{\boldsymbol{\mathcal{Y}}}_d] - [\mathbf{x}_{*,t}^T \underline{\mathbf{I}}_{N_t}, \mathbf{x}_{*,d}^T \underline{\mathbf{I}}_{N_d}]\|^2\}. \tag{6.13}$$

The solution for $\mathbf{x}_{*,d}$ is given by

$$\hat{\mathbf{x}}_{*,d}^T = \mathbf{w}^T \underline{\boldsymbol{\mathcal{Y}}}_d R^{-1} \underline{\mathbf{I}}_{N_d}^T. \tag{6.14}$$

Substituting (6.14) into (6.13), we obtain

$$\min_{\underline{\mathbf{w}}} \{\|\underline{\mathbf{w}}^T[\underline{\boldsymbol{\mathcal{Y}}}_t, \underline{\boldsymbol{\mathcal{Z}}}_d] - [\mathbf{x}_{*,t}^T \underline{\mathbf{I}}_{N_t}, \mathbf{0}_{1\times N_d R}]\|^2\}, \tag{6.15}$$

where $\underline{\boldsymbol{\mathcal{Z}}}_d$ is given by:

$$\underline{\boldsymbol{\mathcal{Z}}}_d = R^{-1} \begin{bmatrix} (R-1)\boldsymbol{\mathcal{Y}}_{-(Q+Q')/2,0,d} & \cdots & -\boldsymbol{\mathcal{Y}}_{-(Q+Q')/2,0,d} \\ \vdots & \ddots & \vdots \\ -\boldsymbol{\mathcal{Y}}_{(Q+Q')/2,L+L',d} & \cdots & (R-1)\boldsymbol{\mathcal{Y}}_{(Q+Q')/2,L+L',d} \end{bmatrix} \tag{6.16}$$

In this equation, the left and right part respectively correspond to the training-based LS method [87] and the blind MRE method [44, 47], applied to doubly selective channels. So far in our analysis we considered all possible time- and frequency-shits which exhibits similar complexity to the blind technique. Due to the existence of the training part, we can limit the number of time- and frequency-shifts resulting in a much lower complexity semi-blind technique. Therefore, we can redo the above analysis for time-shifts $k \in \{0, \ldots, K_1\}$ for $K_1 \leq (L + L')$ and frequency-shifts $p \in \{-K_2, \ldots, K_2\}$ for $K_2 \leq (Q + Q')/2$. In other words, by the aid of training the number of tuned equalizers can be greatly reduced resulting in a much lower complexity than the blind techniques. In contrast, for blind techniques, when a ZF solution is to be found, we require to tune the equalizers corresponding to all possible time- and frequency-shifts.

6.4 Simulation Results

In this section we show some numerical results for the techniques proposed in this chapter. We investigate the performance of blind and semi-blind techniques for channel estimation as well as for direct equalization.

Channel Estimation

For the case of channel estimation we consider the following channel setup:

- A SIMO system with $N_r = 2$ receive antennas.
- The channel is doubly selective according to Jakes' model with order $L = 3$ and maximum Doppler frequency $f_{max} = 100\ Hz$.
- The channel is approximated using the BEM over a period of $N = 800$ symbols, and sampling time $T = 25\ \mu sec$.
- The number of time-varying basis functions are $Q = 2,\ 4$ for a BEM resolution $K = N$, and $K = 2N$ respectively.

We consider the case when the approximated BEM channel is the true channel, and the case when the Jakes' channel is the true channel. The number of frequency-shifts considered here is $Q' = 12$ and the number of frequency-shifts is $L' = 12$.

Blind channel estimation:
For the case of channel estimation, we first plot the realization of one of the taps of the true channel and its estimate as a function of time at $SNR = 16\ dB$. For this case, we consider the BEM resolution $K = N$. The complex scalar ambiguity is resolved by means of LS fitting the estimated channel with the true channel.

Considering the BEM channel as the true channel, the mismatch between the BEM channel and its estimate is shown in Figure 6.1. Considering the Jakes'

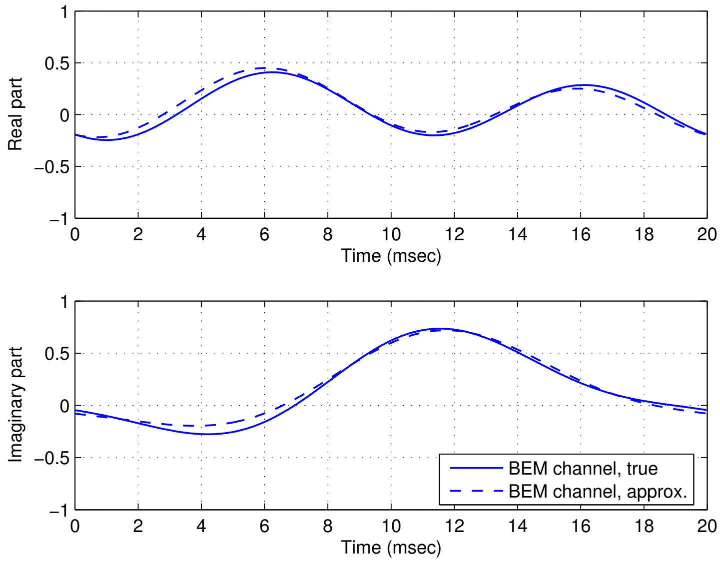

Figure 6.1: Mismatch between the true BEM channel and its estimate for $SNR = 16\ dB$ using blind channel estimation.

channel as the true channel, the mismatch between the true channel and its estimate is shown in Figure 6.2. Assuming the true channel obeys the BEM, we see that the mismatch is considerably smaller for this channel setup. However, the mismatch is clearly larger when the true channel obeys Jakes' model.

We also consider the MSE of the channel estimate versus SNR. We consider the case where the true channel obeys the BEM as well as the case where the true channel obeys Jakes' model. When the true channel obeys the BEM, the MSE channel is computed as

$$MSE = \frac{1}{N_{ch}N_rN(L+1)}\sum_{i=1}^{N_{ch}}\sum_{r=1}^{N_r}\sum_{n=0}^{N-1}\sum_{\nu=0}^{L}|\hat{h}^{(r)}[n;\nu] - h^{(r)}[n;\nu]|^2$$

The MSE channel estimate is computed as

$$MSE = \frac{1}{N_{ch}N_rN(L+1)}\sum_{i=1}^{N_{ch}}\sum_{r=1}^{N_r}\sum_{n=0}^{N-1}\sum_{\nu=0}^{L}|\hat{h}^{(r)}[n;\nu] - g^{(r)}[n;\nu]|^2$$

when the true channel obeys Jakes' model. N_{ch} is the number of channel realizations.

As shown in Figure 6.3, the MSE is a monotonically decreasing function in SNR when the true channel obeys the BEM and $K = N$, whereas the MSE

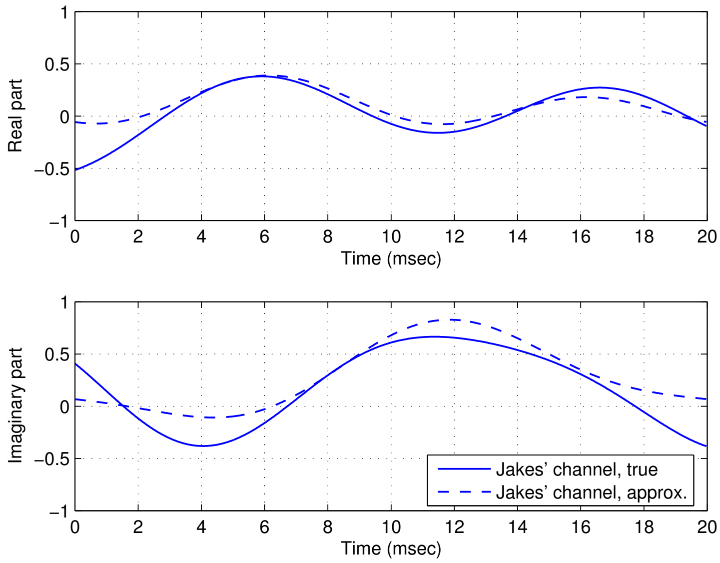

Figure 6.2: Mismatch between the true Jakes' channel and its estimate for $SNR = 16\ dB$ using blind channel estimation.

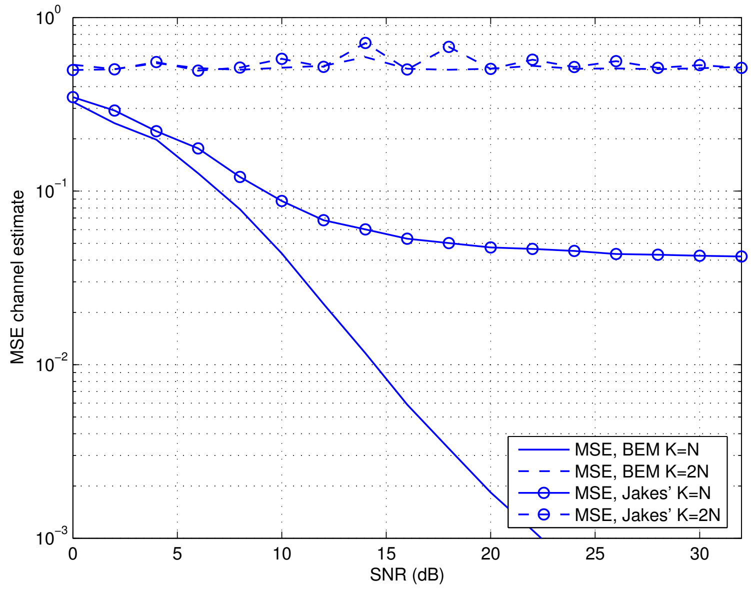

Figure 6.3: MSE vs. SNR for the blind channel estimation technique.

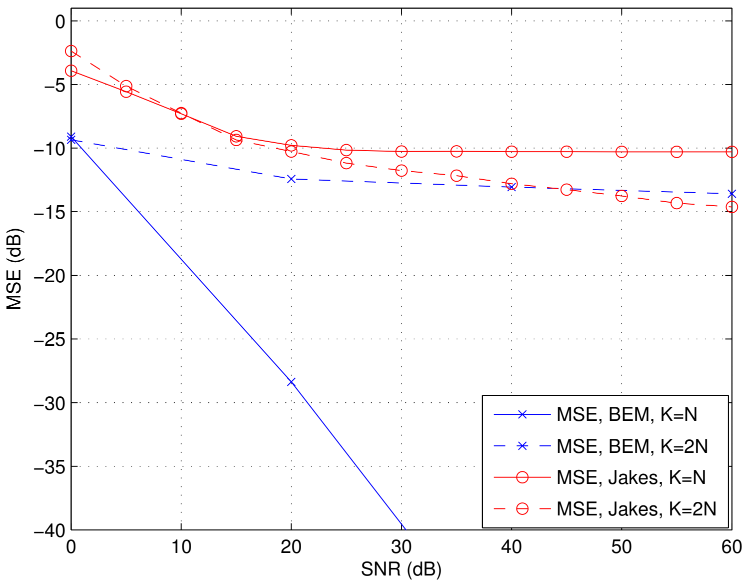

Figure 6.4: MSE vs. SNR for the semi-blind channel estimation technique.

channel estimate suffers from an error floor at $MSE = 4 \times 10^{-2}$ when the true channel obeys Jakes' model and the BEM resolution is taken as $K = N$. For $K = 2N$, the blind technique fails to estimate the channel for either channel models.

Semi-Blind channel estimation:
For this case we use the same channel setup used before. We consider the true channel to obey the BEM and the Jakes' model. The training part consists of two training clusters of $L + 1$ training symbols each. The first one is placed at the beginning of the transmitted block and the other one is placed in the middle of the transmitted block.

First, we consider the MSE channel estimate versus SNR for a a fixed $\alpha = 0.1$. We consider the case when the approximated BEM channel as the true channel as well as the channel follows Jakes model. In both cases we consider the BEM resolution $K = N$ as well as $K = 2N$. The simulation results are shown in Figure 6.4. For the case when the true channel follows the BEM, the MSE channel estimate decreases with increasing the SNR when $K = N$, while it suffers from an early error floor for $K = 2N$. When the true channel follows Jakes' model, the MSE channel suffers from an error floor for $K = N$, whereas it shows a slight improvement for $K = 2N$ specially for $SNR \geq 15\ dB$.

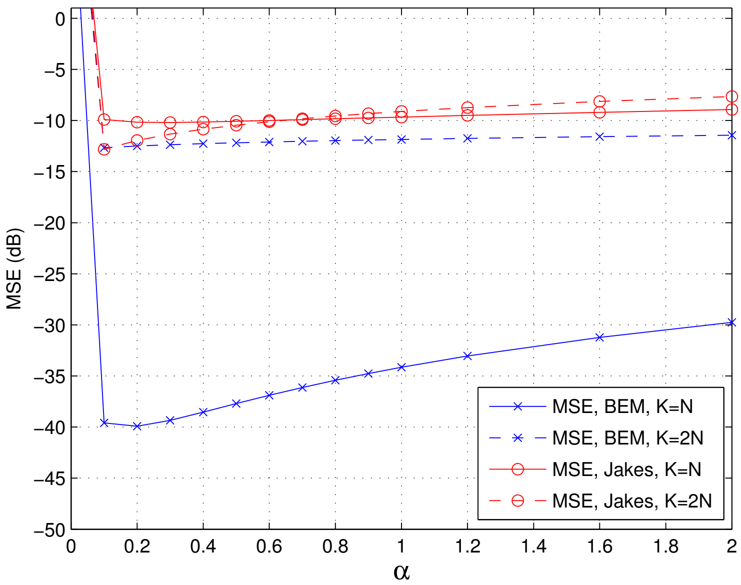

Figure 6.5: MSE vs. α for the semi-blind channel estimation technique at $SNR = 30\ dB$.

Second, the MSE channel estimate is plotted versus *alpha* for a fixed value of $SNR = 30\ dB$. The simulation results are shown in figure 6.5. For all cases (BEM channel with $K = N$, BEM channel with $K = 2N$, Jakes' channel, with $K = N$, and Jakes' channel with $K = 2N$) it is found that the MMSE channel estimate is obtained for $\alpha = 0.1$.

Direct Equalization

Blind direct equalization:
For the case of blind equalization and for feasibility and complexity reasons we consider the following channel setup:

- A SIMO system with $N_r = 2$ receive antennas.
- The channel is doubly selective according to Jakes' model with order $L = 1$ and maximum Doppler frequency $f_{max} = 100\ Hz$.
- The equalizer order $L' = 3$ and number of time-varying basis functions $Q' = 2$.

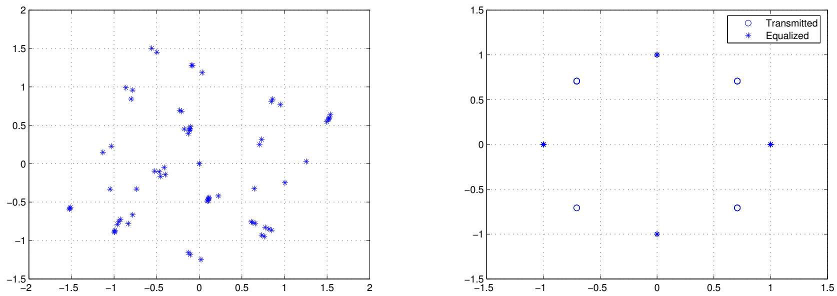

(a) Before equalization (b) After equalization

Figure 6.6: Received and equalized symbols.

- The channel is approximated using the BEM over a period of $N = 37$, and $M = 32$ symbols, and sampling time $T = 25$ μsec, and hence the number of time-varying basis functions $Q = 2$.
- The BEM resolution $K = N$.

For this channel setup we can easily prove that the ZF solution exists in the noiseless case. However, in the noisy case, in order to obtain good results we require a large Q' and L' which entails a high complexity that makes it very difficult to obtain the SVD of $\breve{\boldsymbol{\mathcal{Y}}}$. Therefore, we restrict ourselves to the noiseless case.

As shown in Figure 6.6, the blind technique retrieves the transmitted symbols subject to a complex scalar ambiguity. This scalar ambiguity can be resolved by combining the training based technique with the blind technique.

Semi-blind direct equalization:
For the semi-blind technique we consider a SIMO system with $N_r = 4$ receive antennas. We assume a doubly selective channel with Doppler spread of $f_{\max} = 100$ and order $L = 3$. We use QPSK signaling. We assume the data sequence and the additive noises are mutually uncorrelated and white.

We consider a time-window of $NT = 200T$. As already mentioned, when $NT \leq 1/(2f_{\max})$, which is the case here, an accurate channel model can be obtained by taking $Q = 2$. We use pilot symbol assisted modulation (PSAM) [30] in this work and insert a pilot symbol after every three data symbols. We consider three SLE designs: ideal design where perfect channel state information is assumed to be known at the receiver (see Chapter 3), the direct training-based design where the equalizer coefficients are obtained directly based on PSAM

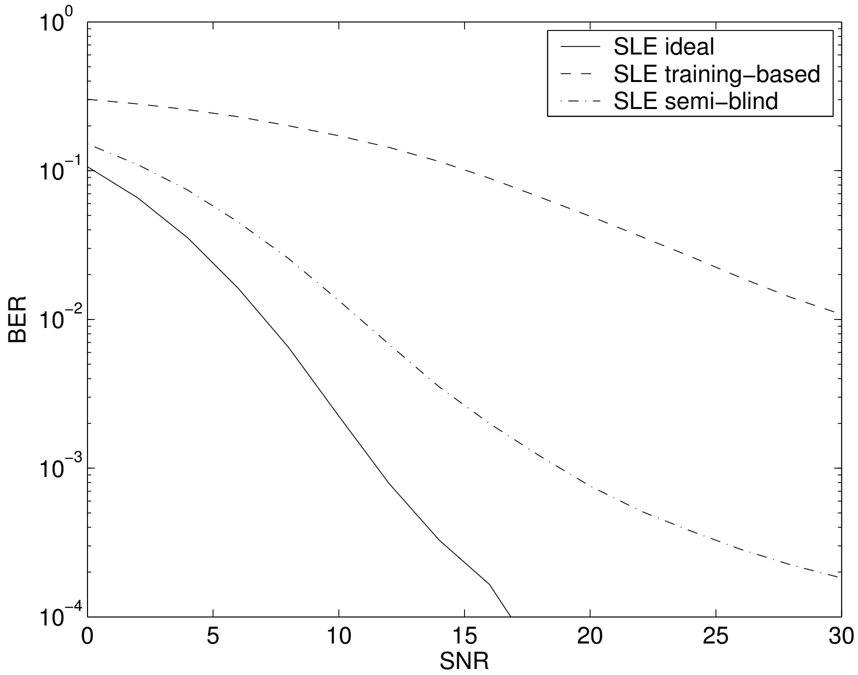

Figure 6.7: Comparison of different SLE designs for doubly selective channels.

(see Chapter 5), and the direct semi-blind design proposed in this chapter. For all designs, we assume $Q' = 2$, $L' = 3$, and $d = (L + L')/2 = 3$.For the direct semi-blind design we take $K_1 = L$ and $K_2 = Q/2$, i.e. we consider the time-shifts $k \in \{0, \ldots, L\}$, and frequency-shifts $p \in \{-Q/2, \ldots, Q/2\}$. For the ideal design, we first fit a BEM to the true doubly selective channel over the time window of $NT = 200T$, and use the obtained BEM coefficients to design the BEM coefficients of the SLE as in (3.29b). From Figure 6.7, we can observe that the direct semi-blind design clearly outperforms the direct training-based design, and is not too far from the performance of the ideal design.

6.5 Conclusions

In this chapter we have discussed blind and semi-blind techniques for channel estimation and direct equalization. The semi-blind techniques are combinations of the blind and training-based techniques which enables us to to resolve the scalar ambiguity of the blind techniques. For the channel estimation part we show through computer simulations that the blind and semi-blind techniques perform well when the true channel obeys the BEM channel, and noticeably when the BEM resolution equals the window size. For BEM resolutions larger than the window size the different algorithms fail to identify and/or directly equalize the doubly selective channel.

Part II

OFDM Transmission over Time- and Frequency-Selective Fading Channels

In this part we investigate OFDM transmission over doubly selective channels as well as over TI channels with receiver analog front-end impairment. Similar to the case of SC transmission, conventional time- or frequency-domain equalization techniques are not adequate to cope with the problems introduced by the underlying challenging mobile wireless communication channel. In OFDM transmission, time-varying channels induce intercarrier interference, i.e. the energy of a particular subcarrier is leaked to neighboring subcarriers. Time-domain and/or frequency-domain equalization techniques are called for to cope with this problem of ICI.

In Chapter 7, a brief overview of OFDM transmission is studied. The system model and ICI analysis are also covered.

In Chapter 8, we propose time-domain and frequency-domain per-tone equalization techniques. In addition to the time-variation of the channel, we assume the CP length is shorter than the channel impulse response, which in turn introduces inter-block interference (IBI). In some applications that use OFDM as the transmission technique such as digital video broadcasting (DVB), such long delay multipath channels are indeed encountered. Using a CP of length equal to the channel order results in a significant decrease in throughput. In such applications one way to increase the transmission throughput is by using a shorter CP length at the cost of compensating for the results by means of equalization. This material has been published in [15, 17, 16, 14, 10]

OFDM is not only sensitive to channel time-variation, but equally well to the receiver/transmitter analog front-end impairments. In Chapter 9, we study OFDM transmission over time-invariant channels (in this case), but with receiver analog front-end impairments, mainly the so-called IQ imbalance and carrier frequency-offset. While IQ imbalance results in mirroring effect, CFO results in ICI. Frequency-domain techniques for joint channel equalization, IQ imbalance and CFO compensation are investigated. In a similar manner to the time-varying case, the time-domain equalizer is modeled using the BEM. This results in combining adjacent subcarriers to mitigate ICI introduced due to the CFO. This material has been submitted as [22, 21].

Chapter 7

OFDM Background

ORTHOGONAL Frequency Division Multiplexing (OFDM) is a multicarrier transmission technique, where the information symbols are transmitted on multiple subcarriers [33, 116]. By means of the DFT, IDFT, and transmit redundancy (through the use of cyclic prefix (CP)) [25] the orthogonality between subcarriers is preserved. Hence, OFDM divides the available system bandwidth W into orthogonal parallel overlapping multiple frequency bins as shown in Figure 7.1(a). The orthogonality between the different subcarriers is preserved even after propagating through the channel if the following conditions are satisfied:

C1) The channel coherence time is much larger than the OFDM symbol period (the channel is not time-selective).

C2) The transmit redundancy (CP length) is greater than or equal to the channel maximum delay spread.

Under C1) and C2), and by choosing the number of subcarriers sufficiently large such that the subcarrier spacing is narrow compared to the coherence bandwidth of the channel, each subcarrier experiences frequency-flat fading. This results in a low complexity one-tap frequency-domain equalizer (FEQ) for each subcarrier. Due to this simple implementation and robustness against frequency-selective propagation, OFDM has been adopted for digital audio and video broadcasting [37] and chosen by the IEEE 802.11 standard [54] as well as by the HIPERLAN-2 standard [52] for wireless LAN (WLAN).

In the case of OFDM transmission over doubly selective channels, the channel time-variation over an OFDM symbol period destroys the orthogonality between subcarriers and hence induces intercarrier interference (ICI) [57, 8, 31,

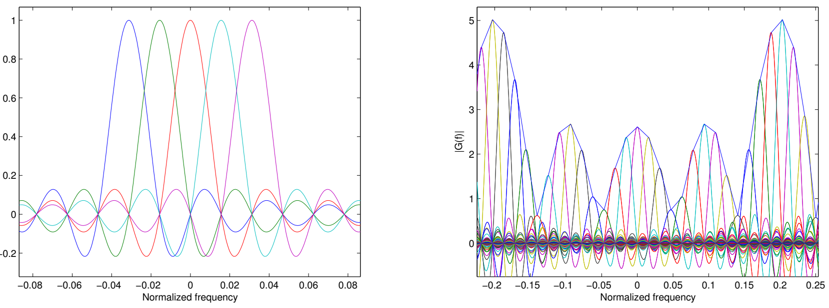

(a) Orthogonal subcarriers

(b) With channel response

Figure 7.1: Spectrum associated with OFDM signal over TI channels.

28]. As shown in Figure 7.2(a), the subcarriers are no longer orthogonal, and as a result ICI arises as shown in Figure 7.2(b).

As far as the bit error rate (BER) is concerned ICI results in an error floor limiting the performance of the system even for high signal-to-noise ratios. ICI is a measure of the amount of energy on a specific subcarrier leaked from neighboring subcarriers. This energy leakage is proportional to the channel time-variation (Doppler spread). The larger the Doppler spread, the wider the ICI span (see Figure 7.2(b)) and the higher the BER error floor [71, 29, 28]. ICI analysis will be discussed later in this chapter.

The channel time-variation is not the source of ICI. ICI arises for OFDM transmission over TI channels due to the carrier frequency offset (CFO). This ICI is similar to the ICI introduced due to channel time-variation. In this chapter, the ICI arises due to CFO only will also be analyzed. Note that, for time-varying channels, the channel time variation resulted from user's mobility and that resulted from CFO are inseparable, and therefore, the channel maximum frequency shift is then computed as $\max\{\Delta f, f_{\max}\}$, where Δf is the CFO.

In the presence of ICI, the simple one-tap FEQ is not adequate to restore orthogonality between subcarriers. More sophisticated/robust equalization techniques are then required to restore orthogonality between subcarriers and so to reduce/eliminate ICI. In this part of the thesis we are targeting time- and frequency-domain equalization techniques.

This chapter is organized as follows. In Section 7.1 a brief description of the system models is given. ICI analysis is discussed in Section 7.2. Finally, our conclusions are drawn in Section 7.3.

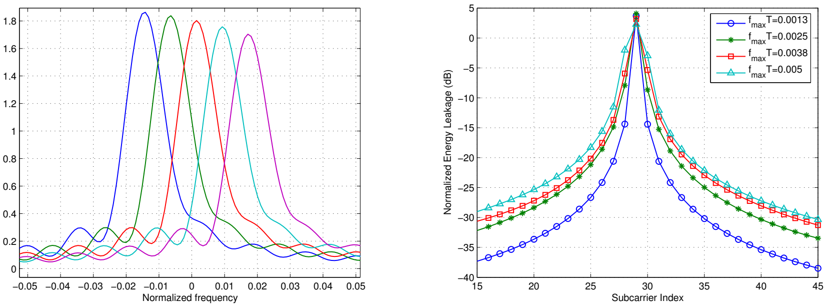

(a) No longer orthogonal subcarriers

(b) Normalized power leakage from subcarrier $k = 30$ to neighboring subcarriers

Figure 7.2: Effect of channel time-variation on the OFDM spectrum.

7.1 System Model

We assume a single-input multiple-output (SIMO) OFDM system with N_r receive antennas as shown in Figure 7.3. The results can be easily extended to multiple-input multiple-output (MIMO) systems. At the transmitter, the conventional OFDM modulation is applied, i.e., the incoming bit sequence is parsed into blocks of N frequency-domain QAM symbols. Each block is then transformed into a time-domain sequence using an N-point IDFT. A cyclic prefix (CP) of length ν is inserted at the head of each block. The time-domain blocks are then serially transmitted over a multipath fading channel. The channel is assumed to be time-varying. Focusing only on the baseband-equivalent description, the received signal $y^{(r)}(t)$ at the rth receive antenna at time t, is given by:

$$y^{(r)}(t) = \sum_{n=-\infty}^{\infty} g^{(r)}(t; t - nT)x[n] + v^{(r)}(t).$$

Assuming $S_k[i]$ is the QAM symbol transmitted on the kth subcarrier ($k \in \{0, \cdots, N-1\}$, N is the total number of subcarriers in the OFDM block) of the ith OFDM block, $x[n]$ can be written as:

$$x[n] = \frac{1}{\sqrt{N}} \sum_{k=0}^{N-1} S_k[i] e^{j2\pi(m-\nu)k/N}, \tag{7.1}$$

where $i = \lfloor n/(N+\nu) \rfloor$ and $m = n - i(N+\nu)$. Note that this description includes the transmission of a CP of length ν.

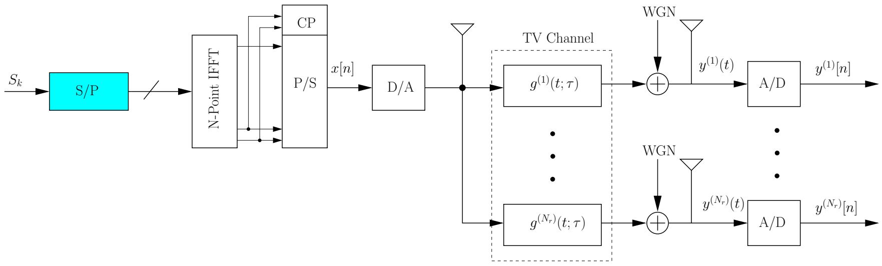

Figure 7.3: OFDM system diagram

Sampling each receive antenna at the symbol period T, the received sample sequence at the rth receive antenna $y^{(r)}[n] = y^{(r)}(nT)$, can be written as:

$$y^{(r)}[n] = \sum_{\theta=-\infty}^{\infty} g^{(r)}[n;\theta]x[n-\theta] + v^{(r)}[n], \tag{7.2}$$

where $v^{(r)}[n] = v^{(r)}(nT)$ and $g^{(r)}[n;\theta] = g^{(r)}(nT;\theta T)$.

7.2 Inter-carrier Interference Analysis

Due to the time-variation of the channel, orthogonality between subcarriers is destroyed, and hence ICI is introduced. ICI is the amount of energy on a specific subcarrier leaked from neighboring subcarriers. This energy leakage is proportional to the channel Doppler spread. In this section, we will give a brief analysis of the ICI introduced by the time-varying channel and CFO. This analysis will help us to understand the mechanism of ICI, and hence to develop an ICI suppression technique.

7.2.1 Time-Varying Channels

Assuming the channel delay spread is bounded by τ_{max}, (7.2) can be written as:

$$y^{(r)}[n] = \sum_{l=0}^{L} g^{(r)}[n;l]x[n-l] + v^{(r)}[n], \tag{7.3}$$

where $L = \lfloor \tau_{max}/T \rfloor$ is the channel order.

Defining $Y_k^{(r)}[i]$, as the frequency response of the received sequence at the rth receive antenna after removing the CP at the kth subcarrier in the ith OFDM block:

$$Y_k^{(r)}[i] = \frac{1}{\sqrt{N}} \sum_{m=0}^{N-1} y^{(r)}[n] e^{-j2\pi km/N}. \tag{7.4}$$

Substituting (7.1) and (7.3) in (7.4) we obtain:

$$\begin{aligned} Y_k^{(r)}[i] &= \sum_{k'=0}^{N-1} S_{k'}[i] \sum_{l=0}^{L} G_{l,k'-k}^{(r)}[i] e^{-j2\pi lk'/N} + V_k^{(r)}[i] \\ &= S_k[i] \sum_{l=0}^{L} G_{l,0}^{(r)}[i] e^{-j2\pi lk/N} + \sum_{\substack{k'=0 \\ k' \neq k}}^{N-1} S_{k'}[i] \sum_{l=0}^{L} G_{l,k'-k}^{(r)}[i] e^{-j2\pi lk'/N} + V_k^{(r)}[i], \end{aligned} \tag{7.5}$$

where $G_{l,k}^{(r)}[i]$ is given by:

$$G_{l,k}^{(r)}[i] = \frac{1}{N} \sum_{m=0}^{N-1} g^{(r)}[n;l] e^{-j2\pi mk/N}, \tag{7.6}$$

and $V_k^{(r)}[i]$ is the frequency response of the noise at subcarrier k in the ith OFDM block. In (7.5), $S_{k'}[i] \sum_{l=0}^{L} G_{l,k'-k}^{(r)}[i] e^{-j2\pi lk'/N}$ represents the amount of interference induced by subcarrier k' on subcarrier k when $k' \neq k$. In matrix form representation, (7.5) can be written as:

$$\begin{bmatrix} Y_0^{(r)}[i] \\ Y_1^{(r)}[i] \\ \vdots \\ Y_{N-1}^{(r)}[i] \end{bmatrix} = \sum_{l=0}^{L} \underbrace{\begin{bmatrix} G_{l,0}^{(r)}[i] & G_{l,-1}^{(r)}[i] & \ldots, & G_{l,-N+1}^{(r)}[i] \\ G_{l,-1}^{(r)}[i] & G_{l,0}^{(r)}[i] & \ldots, & G_{l,-N+2}^{(r)}[i] \\ \vdots & & & \vdots \\ G_{l,N-1}^{(r)}[i] & G_{l,N-2}^{(r)}[i] & \ldots, & G_{l,0}^{(r)}[i] \end{bmatrix}}_{\boldsymbol{\mathcal{G}}_l^{(r)}[i]} \mathbf{D}_l \begin{bmatrix} S_0[i] \\ S_1[i] \\ \vdots \\ S_{N-1}[i] \end{bmatrix} + \begin{bmatrix} V_0^{(r)}[i] \\ V_1^{(r)}[i] \\ \vdots \\ V_{N-1}^{(r)}[i] \end{bmatrix}, \tag{7.7}$$

where $\mathbf{D}_l = \text{diag}\{[1, e^{j2\pi l/N}, \ldots, e^{j2\pi l(N-1)/N}]^T\}$.

Note that, when the channel is time-invariant for at least one OFDM block (i.e. $g^{(r)}[n;l] = g_l^{(r)}[i]$, $\forall n \in \{i(N+\nu)+\nu, \ldots, (i+1)(N+\nu)-1\}$), (7.5) can be written as:

$$Y_k^{(r)}[i] = S_k[i] G_k^{(r)}[i] + V_k^{(r)}[i], \tag{7.8}$$

where $G_k^{(r)}[i]$ is the frequency response of the channel at the kth subcarrier in the ith OFDM block characterizing the link between the transmitter and the rth receive antenna. For this case, we see that no ICI is present and orthogonality between subcarriers is preserved.

We use the BEM to approximate the doubly selective channel $g^{(r)}[n;\theta]$ for $n \in \{i(N+\nu)+\nu, \ldots, (i+1)(N+\nu)-1\}$ as:

$$h^{(r)}[n;\theta] = \sum_{l=0}^{L} \delta[\theta - l] \sum_{q=-Q/2}^{Q/2} h_{q,l}^{(r)}[i] e^{j2\pi qn/K}, \tag{7.9}$$

where $h_{q,l}^{(r)}[i]$ is the coefficient of the lth tap and qth basis function of the channel between the transmitter and rth receive antenna in the ith OFDM block, which is kept invariant over a period of NT. Q is the number of time-varying basis functions. K determines the BEM frequency-resolution, and is assumed to be larger than or equal to the number of subcarriers, i.e., $K \geq N$. The parameter Q should be selected such that $Q/(2KT) \geq f_{max}$.

Considering $h^{(r)}[n;\theta]$ as an approximation for $g^{(r)}[n;\theta]$, an approximation of (7.6) can be obtained as follows:

$$H_{l,k}^{(r)}[i] = \frac{1}{N} \sum_{q=-Q/2}^{Q/2} \tilde{h}_{q,l}^{(r)}[i] \sum_{m=0}^{N-1} e^{-j2\pi m(k/N - q/K)}, \tag{7.10}$$

where $\tilde{h}_{q,l}^{(r)}[i] = h_{q,l}^{(r)}[i] e^{j2\pi q(i(N+\nu)+\nu)/K}$. We will assume that K is an integer multiple of the block size N, i.e., $K = PN$, where P is an integer greater than or equal to 1. Then, $H_l^{(t)}[i]$ can be written as:

$$H_{l,k}^{(r)}[i] = \sum_{q=-Q/2}^{Q/2} \tilde{h}_{q,l}^{(r)}[i] \frac{e^{-j\pi\phi}}{e^{-j\pi\phi/N}} \left. \frac{\text{sinc}(\phi)}{\text{sinc}(\phi/N)} \right|_{\phi = k - q/P} \tag{7.11}$$

where $\text{sinc}(\phi) = \sin(\pi\phi)/\pi\phi$.

Note that for $P = 1$, the ICI support is limited to Q neighboring subcarriers. This will be more clear by replacing $G_{l,k}^{(r)}[i]$ by $H_{l,k}^{(r)}[i]$ in $\boldsymbol{\mathcal{G}}_l^{(r)}[i]$ in (7.7). Doing this, $\boldsymbol{\mathcal{G}}_l^{(r)}[i]$ becomes a structured banded matrix with bandwidth equal to $Q+1$ (i.e. exactly $Q/2$ interfering subcarriers on each side). For $P > 1$, the ICI support comes from all subcarriers but the main part is still related to the Q neighboring subcarriers (see Figure 7.4). For this reason, conventional frequency-domain equalization techniques combine a number of neighboring subcarriers to remove the ICI. However, this approach can be generalized as discussed in the forthcoming chapters, where we develop novel time-domain and frequency-domain per-tone ICI mitigation techniques.

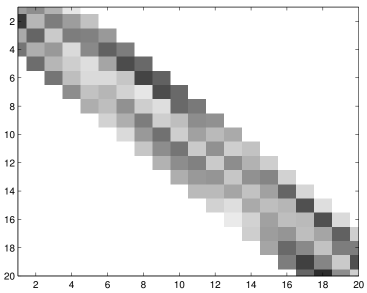

(a) BEM approximation ICI matrix $K = N$

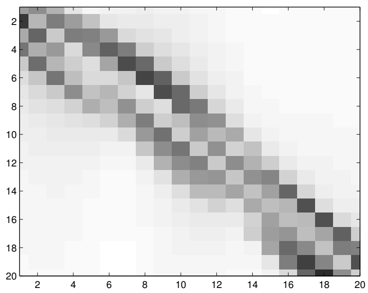

(b) BEM approximation ICI matrix $K = 2N$

Figure 7.4: Visualizing the ICI matrix using the BEM for $K = N$ and $K = 2N$

7.2.2 CFO

For OFDM transmission over TI channels with CFO Δf, the received sequence at the rth receive antenna $r^{(r)}[n]$ can be written as

$$r^{(r)}[n] = e^{j2\pi\epsilon n/N} y^{(r)}[n], \tag{7.12}$$

where $\epsilon = \Delta f T$, and $y^{(r)}[n]$ is

$$y^{(r)}[n] = \sum_{l=0}^{L} x[n-l] g_l^{(r)} + v^{(r)}[n].$$

Taking the DFT of the received sequence $r^{(r)}[n]$, the frequency response at subcarrier k in the ith OFDM symbol can be written as

$$\begin{aligned} R_k^{(r)}[i] &= \sum_{m=0}^{N-1} r^{(r)}[n] e^{-j2\pi mk/N} \\ &= \sum_{m=0}^{N-1} \frac{1}{N} \sum_{k'=0}^{N-1} Y_{k'}^{(r)}[i] e^{j2\pi mk'/N} e^{j2\pi i(N+\nu)\epsilon/N} e^{j2\pi\epsilon m/N} \\ &= \sum_{k'=0}^{N-1} G_{k'}^{(r)}[i] S_{k'}[i] e^{j2\pi i(N+\nu)\epsilon/N} \sum_{m=0}^{N-1} e^{-j2\pi m(k-k'+\epsilon)/N} + \tilde{V}_k^{(r)}[i] \\ &= e^{j2\pi i(N+\nu)\epsilon/N} \sum_{k'=0}^{N-1} G_{k'}^{(r)}[i] S_{k'}[i] \frac{\operatorname{sinc}(\pi(k-k'+\epsilon))}{\operatorname{sinc}(\pi(k-k'+\epsilon)/N)} + \tilde{V}_k^{(r)}[i] \end{aligned} \tag{7.13}$$

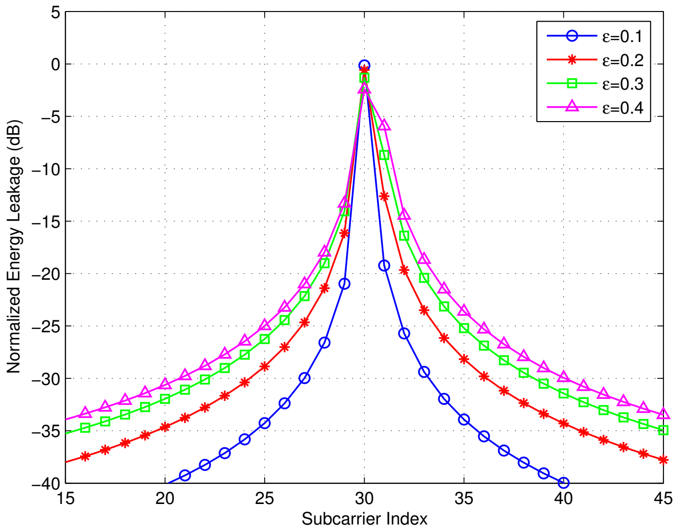

Figure 7.5: Normalized power leakage on subcarrier $k = 30$ due to CFO

where $\tilde{V}_k[i]$ is some noise related term at subcarrier k at the rth receive antenna. From (7.13) the ICI on subcarrier k is given by:

$$I_k = e^{j2\pi i(N+\nu)\epsilon/N} \sum_{\substack{k'=0 \\ k'\neq k}}^{N-1} G_{k'}^{(r)}[i] S_{k'}[i] \frac{\mathrm{sinc}(\pi(k-k'+\epsilon))}{\mathrm{sinc}(\pi(k-k'+\epsilon)/N)}. \tag{7.14}$$

The ICI power $\mathcal{E}\{|I_k|^2\}$ is given by:

$$\mathcal{E}\{|I_k|^2\} = \sigma_s^2 \sigma_h^2 \sum_{\substack{k'=0 \\ k'\neq k}}^{N-1} \frac{\mathrm{sinc}^2(\pi(k-k'+\epsilon))}{\mathrm{sinc}^2(\pi(k-k'+\epsilon)/N)}.$$

the normalized power leakage due to CFO is plotted in Figure 7.5. Notice the similarity with Figure 7.2(b).

7.3 Conclusions

In this chapter, we briefly discussed the OFDM transmission technique. We mainly discuss OFDM transmission over doubly selective channels and over TI channels with CFO. Due to the fact that the channel is time-varying the subcarriers are no longer orthogonal which means that the energy of each subcarrier leaks to neighboring subcarriers inducing ICI. The larger the Doppler spread, the more severe the ICI and the wider the ICI span will be. This motivates us to develop new equalization (ICI mitigation) techniques that restore orthogonality between subcarriers. In addition to the channel time-variation, CFO results in ICI. The ICI due to CFO has similar characteristics to that resulting from time-varying channels. This allows to develop similar equalization techniques that combine neighboring subcarrier to mitigate ICI on a particular subcarrier. In the following chapter we develop time- and frequency-domain equalizers that tackle the problem of ICI.

Chapter 8

Equalization of OFDM Transmission over Doubly Selective Channels

8.1 Introduction

AS mentioned in Chapter 7, the channel time variation destroys orthogonality between subcarriers in OFDM transmission. Therefore, equalization techniques are called for to compensate for the doubly selective channel effects. In this chapter, we propose time-domain and frequency-domain equalization techniques. In addition to the time-variation of the channel, we assume that the CP length is shorter than the channel impulse response length, which in turn introduces inter-block interference (IBI). In some applications that use OFDM as the transmission technique such as digital video broadcasting (DVB), such long delay multipath channels are indeed encountered. Using a CP of length equal to the channel order, results into a significant decrease in throughput. In such applications one way to increase the transmission throughput is to use a shorter CP length at the cost of compensating for the results by means of equalization. The purpose of the time-domain equalizer (TEQ), implemented by a time-varying FIR filter, is two-fold:

1. shorten the channel to fit within the CP length, and hence to eliminate the IBI.

2. eliminate the channel time-variation to eliminate/reduce ICI.

In other words, the TEQ is aimed at restoring orthogonality between subcarriers by converting the doubly selective channel into a purely frequency-selective channel of order less than or equal to the CP length.

Channel memory shortening to reduce the complexity of the Viterbi decoder was suggested in [41, 85]. **Time-domain** approaches have been proposed for channel shortening/equalization in the context of digital subscriber lines (DSL). In this context, a time-invariant finite impulse response (TI FIR) filter is applied to the time-domain received samples for OFDM transmission over frequency-selective channels whose delay spread is larger than the CP length [32, 6, 121, 112]. The purpose of this time-domain equalizer (TEQ) is thus to shorten the channel delay-spread to fit within the CP length. Similarly, in this chapter we apply a time-varying FIR TEQ to convert the doubly selective channel whose delay-spread is larger than the CP into a purely frequency-selective target impulse response (TIR) with a delay spread that fits within the CP. By doing this, we restore orthogonality between subcarriers (eliminate IBI and ICI). As we approximate the channel using the BEM, we design the time-varying FIR TEQ according to the BEM (similar to the SC case discussed in Part I of this thesis). An additional one-tap frequency-domain equalizer corresponding to the TIR is then used to estimate the QAM transmitted symbols. To design the TEQ, non-triviality constraints are required. In this chapter we only focus on the unit energy and unit norm constraints, which have shown to yield superior performance in the DSL context, ant this will be of no exception in the context of OFDM over doubly selective channels.

Along with the time-domain approach we propose a **frequency-domain equalizer** to mitigate the problem of ICI/IBI. While the TEQ optimizes the performance on all subcarriers in a joint fashion, a frequency-domain equalizer that optimizes the performance on each subcarrier separately can be obtained by transferring the TEQ operations to the frequency-domain, resulting in the so-called frequency-domain per-tone equalizer (PTEQ). The idea of obtaining the PTEQ from the TEQ was first proposed by [110] for DSL systems.

Different approaches for reducing ICI for OFDM over doubly selective channels have already been proposed, including frequency-domain equalization and/or time-domain windowing. In [31, 57] the authors propose matched-filter, least-squares (LS) and minimum mean-square error (MMSE) receivers incorporating all subcarriers. Receivers considering the dominant adjacent subcarriers have been presented in [28, 29]. For multiple-input multiple-output (MIMO) OFDM over doubly selective channels, a frequency-domain ICI mitigation technique is proposed in [94]. A time-domain windowing (linear pre-processing) approach to restrict ICI support in conjunction with iterative MMSE estimation is presented in [90]. ICI self-cancellation schemes are proposed in [126, 8]. There, redundancy is added to enable self-cancellation, which implies a substantial reduction in bandwidth efficiency. To avoid this rate loss, partial response encoding in conjunction with maximum-likelihood sequence detection to mitigate

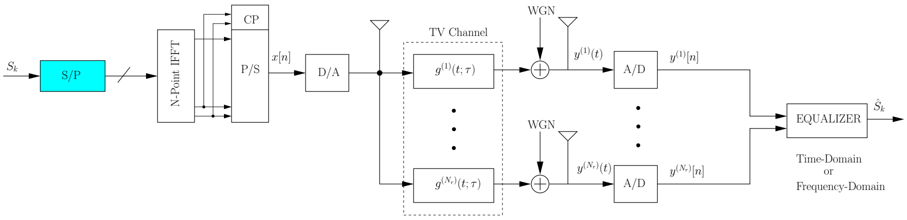

Figure 8.1: System Model.

ICI in OFDM systems is studied in [125]. *However, all of the above mentioned works, assume the channel delay spread fits within the CP, and hence, no IBI is present.* Moreover, in these works, the time-varying channel matrix (or an estimated version of it) is required to design the equalizer. This in return, requires a large number of parameters to be identified or tracked.

It is worth mentioning at this point the differences between the TEQ proposed in this chapter and the time-varying FIR equalizer proposed in Chapter 3. In particular this chapter deals with

1. Time-varying shortening (and not equalization) in the time-domain. Although these two principles are related (as in the time-invariant case), many additional issues pop up, such as the choice of the target impulse response and the different constraints one can take to solve the shortening problem.

2. The translation and generalization of this time-domain shortener to the frequency-domain, which results in a novel frequency-domain equalization structure.

This chapter is organized as follows. The proposed TEQ is presented in Section 8.2. The frequency-domain PTEQ is presented in Section 8.3. In Section 8.5, we show through computer simulations the performance of the proposed equalizers. An efficient implementation of the PTEQ is discussed in Section 8.4. Finally, our conclusions are drawn in Section 8.6.

8.2 Time-Domain Equalization

In this section, we introduce time-domain equalization (TEQ) for OFDM systems over doubly selective channels. We assume a SIMO system as shown in Figure 8.1. We assume the most general case, where the time-varying channel delay spread is larger than the CP. The TEQ is implemented by a time-varying FIR filter, i.e., at the rth receive antenna, we apply a time-varying FIR TEQ

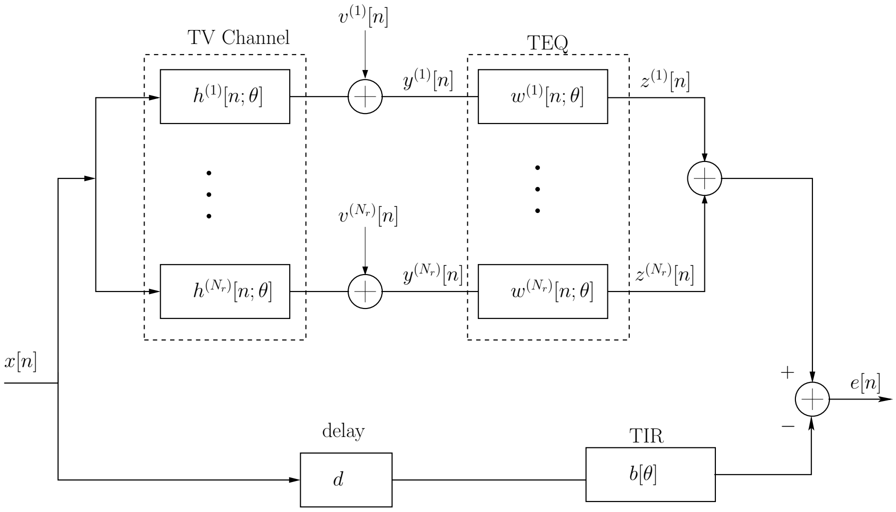

Figure 8.2: TEQ equivalent figure.

denoted by $w^{(r)}[n;\theta]$. The purpose of the TEQ is to convert the doubly selective channel into a frequency-selective channel with a delay spread that fits within the CP. i.e. to convert the doubly selective channel of order $L > \nu$ and $f_{\max} \neq 0$ into a target impulse response (TIR) $b[\theta]$ that is purely frequency-selective with order $L'' \leq \nu$ and $f_{\max} = 0$. The purpose of the time-varying FIR TEQ is thus to mitigate both IBI and ICI. As shown in Figure 8.2, we require to design a time-varying FIR TEQ and TIR such that the difference term $e[n]$ is minimized in the mean square error sense, subject to some decision delay d.

The output of the time-varying FIR TEQ at the rth receive antenna subject to some decision delay d, can be written as

$$z^{(r)}[n-d] = \sum_{\theta=-\infty}^{\infty} w^{(r)}[n;\theta] y^{(r)}[n-\theta]. \tag{8.1}$$

Since we approximate the doubly selective channel using the BEM, it is convenient to also model the time-varying FIR TEQ using the BEM. In other words, we design the time-varying FIR TEQ $w^{(r)}[n;\theta]$ to have $L'+1$ taps, where the time variation of each tap is modeled by $Q'+1$ time-varying complex exponential basis functions. Hence, we can write the time-varying FIR TEQ $w^{(r)}[n;\theta]$ for $n \in \{i(N+\nu)+\nu, \cdots, (i+1)(N+\nu)-1\}$ as

$$w^{(r)}[n;\theta] = \sum_{l'=0}^{L'} \delta[\theta - l'] \sum_{q'=-Q'/2}^{Q'/2} w_{q',l'}^{(r)}[i] e^{j2\pi q' n/K}. \tag{8.2}$$

Substituting (8.2) in (8.1) we obtain:

$$
\begin{aligned}
z^{(r)}[n-d] &= \sum_{l'=0}^{L'} \sum_{q'=-Q'/2}^{Q'/2} w_{q',l'}^{(r)}[i] e^{j2\pi q' n/K} y^{(r)}[n-l'] \\
&= \sum_{l'=0}^{L'} \sum_{q'=-Q'/2}^{Q'/2} \sum_{l=0}^{L} \sum_{q=-Q/2}^{Q/2} w_{q',l'}^{(r)}[i] h_{q,l}^{(r)}[i] e^{j2\pi q' n/K} e^{j2\pi q n/K} x[n-l-l'] \\
&+ \sum_{l'=0}^{L'} \sum_{q'=-Q'/2}^{Q'/2} w_{q',l'}^{(r)}[i] e^{j2\pi q' n/K} v^{(r)}[n-l']. \qquad (8.3)
\end{aligned}
$$

It is more convenient at this point to switch to a block level formulation. Defining $\mathbf{z}^{(r)}[i] = [z^{(r)}[i(N+\nu)+\nu-d], \cdots, z^{(r)}[(i+1)(N+\nu)-d-1]]^T$, $\mathbf{x}[i] = [x[i(N+\nu)+\nu-L-L'], \cdots, x[(i+1)(N+\nu)-1]]^T$ and $\mathbf{v}^{(r)}[i] = [v^{(r)}[i(N+\nu)-L'], \cdots, v^{(r)}[(i+1)(N+\nu)-1]]^T$, then (8.3) on a block level can be formulated as

$$
\begin{aligned}
\mathbf{z}^{(r)}[i] &= \sum_{l'=0}^{L'} \sum_{q'=-Q'/2}^{Q'/2} \sum_{l=0}^{L} \sum_{q=-Q/2}^{Q/2} w_{q',l'}^{(r)}[i] h_{q,l}^{(r)}[i] \mathbf{D}_{q'}[i] \mathbf{Z}_{l'} \tilde{\mathbf{D}}_q[i] \tilde{\mathbf{Z}}_l \mathbf{x}[i] \\
&+ \sum_{l'=0}^{L'} \sum_{q'=-Q'/2}^{Q'/2} w_{q',l'}^{(r)} \mathbf{D}_{q'}[i] \mathbf{Z}_{l'} \mathbf{v}[i], \qquad (8.4)
\end{aligned}
$$

where the diagonal matrix $\mathbf{D}_{q'}[i] = \mathrm{diag}\{[e^{j2\pi q'(i(N+\nu)+\nu)/K}, \ldots, e^{j2\pi q'((i+1)(N+\nu)-1)/K}]^T\}$ (note the difference between this definition and the definition in Section 3.4), $\mathbf{Z}_{l'} = [\mathbf{0}_{N\times(L'-l')}, \mathbf{I}_N, \mathbf{0}_{N\times l'}]$, $\tilde{\mathbf{D}}_q[i] = \mathrm{diag}\{[e^{j2\pi q(i(N+\nu)+\nu-L')/K}, \ldots, e^{j2\pi q((i+1)(N+\nu)-1)/K}]^T\}$, and finally the matrix $\tilde{\mathbf{Z}}_l = [\mathbf{0}_{(N+L')\times(L-l)}, \mathbf{I}_{N+L'}, \mathbf{0}_{(N+L')\times l}]$. Using the property $\mathbf{Z}_{l'}\tilde{\mathbf{D}}_q[i] = e^{j2\pi q(L'-l')/K}\mathbf{D}_q[i]\mathbf{Z}_{l'}$, and defining $p = q+q'$ and $k = l+l'$, we can write (8.4) as

$$
\begin{aligned}
\mathbf{z}[i] &= \sum_{p=-(Q+Q')/2}^{(Q+Q')/2} \sum_{k=0}^{L+L'} f_{p,k}[i] \mathbf{D}_p[i] \bar{\mathbf{Z}}_k \mathbf{x}[i] \\
&+ \sum_{r=1}^{N_r} \sum_{l'=0}^{L'} \sum_{q'=-Q'/2}^{Q'/2} w_{q',l'}^{(r)}[i] \mathbf{D}_{q'}[i] \mathbf{Z}_{l'} \mathbf{v}[i], \qquad (8.5)
\end{aligned}
$$

where $\mathbf{z}[i] = \sum_{r=1}^{N_r} \mathbf{z}^{(r)}[i]$, $\bar{\mathbf{Z}}_k = [\mathbf{0}_{N\times(L+L'-k)}, \mathbf{I}_N, \mathbf{0}_{N\times k}]$, and $f_{p,k}[i]$ can be written as

$$
f_{p,k}[i] = \sum_{r=1}^{N_r} \sum_{q'=-Q'/2}^{Q'/2} \sum_{l'=0}^{L'} e^{j2\pi(p-q')l'/K} w_{q',l'}^{(r)}[i] h_{p-q',k-l'}^{(r)}[i]. \qquad (8.6)
$$

Defining $\mathbf{f}[i] = [f_{-(Q+Q')/2,0}[i], \cdots, f_{(Q+Q')/2,L+L'}[i]]^T$, we can further write (8.5) as

$$\begin{aligned}\mathbf{z}[i] &= (\mathbf{f}^T[i] \otimes \mathbf{I}_N)\mathbf{A}[i]\mathbf{x}[i] + \sum_{r=1}^{N_r}(\mathbf{w}^{(r)T}[i] \otimes \mathbf{I}_N)\mathbf{B}[i]\mathbf{v}^{(r)}[i] \\ &= (\mathbf{f}^T[i] \otimes \mathbf{I}_N)\mathbf{A}[i]\mathbf{x}[i] + (\mathbf{w}^T[i] \otimes \mathbf{I}_N)(\mathbf{I}_{N_r} \otimes \mathbf{B}[i])\mathbf{v}[i], \end{aligned} \tag{8.7}$$

where $\mathbf{w}^{(r)}[i] = [w^{(r)}_{-Q'/2,0}[i], \cdots, w^{(r)}_{Q'/2,L'}[i]]^T$, $\mathbf{w}[i] = [\mathbf{w}^{(1)T}[i], \cdots, \mathbf{w}^{(N_r)T}[i]]^T$, $\mathbf{v}[i] = [\mathbf{v}^{(1)T}[i], \cdots, \mathbf{v}^{(N_r)T}[i]]^T$, and $\mathbf{A}[i]$ and $\mathbf{B}[i]$ are given by

$$\mathbf{A}[i] = \begin{bmatrix} \mathbf{D}_{-(Q+Q')/2}[i]\bar{\mathbf{Z}}_0 \\ \vdots \\ \mathbf{D}_{-(Q+Q')/2}[i]\bar{\mathbf{Z}}_{L+L'} \\ \vdots \\ \mathbf{D}_{(Q+Q')/2}[i]\bar{\mathbf{Z}}_{L+L'} \end{bmatrix}, \quad \mathbf{B}[i] = \begin{bmatrix} \mathbf{D}_{-Q'/2}[i]\mathbf{Z}_0 \\ \vdots \\ \mathbf{D}_{-Q'/2}[i]\mathbf{Z}_{L'} \\ \vdots \\ \mathbf{D}_{Q'/2}[i]\mathbf{Z}_{L'} \end{bmatrix},$$

Note that the term in $f_{p,k}[i]$ corresponding to the rth receive antenna is related to a 2-dimensional convolution of the BEM coefficients of the doubly selective channel for the rth receive antenna and the BEM coefficients of the time-varying FIR TEQ for the rth receive antenna. This allows us to derive a linear relationship between $\mathbf{f}[i]$ and $\mathbf{w}[i]$. We first define the $(L'+1) \times (L'+L+1)$ Toeplitz matrix

$$\mathcal{T}_{l,L'+1}(h^{(r)}_{q,l}[i]) = \begin{bmatrix} h^{(r)}_{q,0}[i] & \dots & h^{(r)}_{q,L}[i] & & 0 \\ & \ddots & & \ddots & \\ 0 & & h^{(r)}_{q,0}[i] & \dots & h^{(r)}_{q,L}[i] \end{bmatrix}.$$

We define $\boldsymbol{\mathcal{H}}^{(r)}_q[i] = \mathbf{\Omega}_q \mathcal{T}_{l,L'+1}(h^{(r)}_{q,l}[i])$, where $\mathbf{\Omega}_q = \text{diag}\{[e^{j2\pi qL'/K}, \dots, 1]^T\}$, and consequently introduce the $(Q'+1)(L'+1) \times (Q+Q'+1)(L+L'+1)$ block Toeplitz matrix

$$\mathcal{T}_{q,Q'+1}(\boldsymbol{\mathcal{H}}^{(r)}_q[i]) = \begin{bmatrix} \boldsymbol{\mathcal{H}}^{(r)}_{-Q/2}[i] & \dots & \boldsymbol{\mathcal{H}}^{(r)}_{Q/2}[i] & & \mathbf{0} \\ & \ddots & & \ddots & \\ \mathbf{0} & & \boldsymbol{\mathcal{H}}^{(r)}_{-Q/2}[i] & \dots & \boldsymbol{\mathcal{H}}^{(r)}_{Q/2}[i] \end{bmatrix}.$$

Introducing $\boldsymbol{\mathcal{H}}^{(r)}[i] = \mathcal{T}_{q,Q'+1}(\boldsymbol{\mathcal{H}}^{(r)}_q[i])$ and $\boldsymbol{\mathcal{H}}[i] = [\boldsymbol{\mathcal{H}}^{(1)T}[i], \dots, \boldsymbol{\mathcal{H}}^{(N_r)T}[i]]^T$, we can finally derive from (8.6) that:

$$\mathbf{f}^T[i] = \mathbf{w}^T[i]\boldsymbol{\mathcal{H}}[i]. \tag{8.8}$$

As already mentioned, the purpose of the TEQ is to convert the doubly selective channel into a frequency-selective equivalent channel with order less than or equal the CP. To this aim, we define the so called target-impulse response (TIR) denoted by $b[\theta]$ and of order $L'' \leq \nu$, which can be modeled for $n \in \{i(N+\nu)+\nu, \ldots, (i+1)(N+\nu)-1\}$ as

$$b[\theta] = \sum_{l''=0}^{L''} \delta[\theta - l'']b_{l''}[i].$$

As shown in Figure 8.2, we will now design a TEQ $\mathbf{w}[i]$, a TIR $\mathbf{b}[i] = [b_0[i], \ldots, b_{L''}[i]]^T$ and a synchronization delay d such that the difference between the outputs of the upper branch and the lower branch is minimized. Defining $\mathbf{e}[i] = [e[i(N+\nu)], \ldots, e[i(N+\nu)+N-1]]^T$, we can express $\mathbf{e}[i]$ as

$$\begin{aligned}\mathbf{e}[i] &= (\mathbf{f}^T[i] \otimes \mathbf{I}_N)\mathbf{A}[i]\mathbf{x}[i] + (\mathbf{w}^T[i] \otimes \mathbf{I}_N)(\mathbf{I}_{N_r} \otimes \mathbf{B}[i])\mathbf{v}[i] - \sum_{l''=0}^{L''} b_{l''}[i]\bar{\mathbf{Z}}_{l''}\mathbf{x}[i] \\ &= (\mathbf{f}^T[i] \otimes \mathbf{I}_N)\mathbf{A}[i]\mathbf{x}[i] + (\mathbf{w}^T[i] \otimes \mathbf{I}_N)(\mathbf{I}_{N_r} \otimes \mathbf{B}[i])\mathbf{v}[i] - (\tilde{\mathbf{b}}[i] \otimes \mathbf{I}_N)\mathbf{A}[i]\mathbf{x}[i]\end{aligned} \tag{8.9}$$

where the augmented vector $\tilde{\mathbf{b}}[i]$ can be written as $\tilde{\mathbf{b}}[i] = \mathbf{C}\mathbf{b}[i]$ with the selection matrix $\mathbf{C}$ given by

$$\mathbf{C} = \left[\begin{array}{c} \mathbf{0}_{((Q+Q')(L+L'+1)/2+d)\times(L''+1)} \\ \hline \mathbf{I}_{L''+1} \\ \hline \mathbf{0}_{((Q+Q')(L+L'+1)/2-L''-d-1)\times(L''+1)} \end{array}\right].$$

Hence, we can write the following cost function

$$\begin{aligned}\mathcal{J}[i] &= \mathcal{E}\left\{\mathbf{e}^H[i]\mathbf{e}[i]\right\} \\ &= \operatorname{tr}\left\{(\mathbf{f}^T[i] \otimes \mathbf{I}_N)\mathbf{A}[i]\mathbf{R}_x\mathbf{A}^H[i](\mathbf{f}^*[i] \otimes \mathbf{I}_N)\right\} \\ &+ \operatorname{tr}\left\{(\mathbf{w}^T[i] \otimes \mathbf{I}_N)(\mathbf{I}_{N_r} \otimes \mathbf{B}[i])\mathbf{R}_v(\mathbf{I}_{N_r} \otimes \mathbf{B}^H[i])(\mathbf{w}^*[i] \otimes \mathbf{I}_N)\right\} \\ &+ \operatorname{tr}\left\{(\tilde{\mathbf{b}}^T[i] \otimes \mathbf{I}_N)\mathbf{A}[i]\mathbf{R}_x\mathbf{A}^H[i](\tilde{\mathbf{b}}^*[i] \otimes \mathbf{I}_N)\right\} \\ &- 2\operatorname{tr}\left\{\Re\{(\mathbf{f}^T[i] \otimes \mathbf{I}_N)\mathbf{A}[i]\mathbf{R}_x\mathbf{A}^H[i](\tilde{\mathbf{b}}^*[i] \otimes \mathbf{I}_N)\}\right\}\end{aligned} \tag{8.10}$$

Let us now introduce the following properties

$$\begin{aligned}\operatorname{tr}\{(\mathbf{x}^T \otimes \mathbf{I}_N)\mathbf{X}(\mathbf{x}^* \otimes \mathbf{I}_N)\} &= \mathbf{x}^T \operatorname{subtr}\{\mathbf{X}\}\mathbf{x}^* \\ \operatorname{tr}\{(\mathbf{x}^T \otimes \mathbf{I}_N)\mathbf{V}(\mathbf{y}^* \otimes \mathbf{I}_N)\} &= \mathbf{x}^T \operatorname{subtr}\{\mathbf{V}\}\mathbf{y}^*,\end{aligned}$$

where $\operatorname{subtr}\{\cdot\}$ splits the matrix up into $N \times N$ sub-matrices and replaces each sub-matrix by its trace. Note that $\mathbf{X}$ is a square matrix while $\mathbf{V}$ is not necessarily square. Hence, $\operatorname{subtr}\{\cdot\}$ reduces the row and column dimension by a factor N. Hence, the cost function in (8.10) reduces to

$$\mathcal{J}[i] = \mathbf{w}^T[i]\left(\boldsymbol{\mathcal{H}}[i]\mathbf{R}_{\tilde{A}}[i]\boldsymbol{\mathcal{H}}^H[i] + \mathbf{R}_{\tilde{B}}[i]\right)\mathbf{w}^*[i] + \tilde{\mathbf{b}}^T[i]\mathbf{R}_{\tilde{A}}[i]\tilde{\mathbf{b}}^*[i]$$

$$- 2\Re\{\mathbf{w}^T[i]\boldsymbol{\mathcal{H}}[i]\mathbf{R}_{\tilde{A}}[i]\tilde{\mathbf{b}}^*[i]\}, \tag{8.11}$$

where $\mathbf{R}_{\tilde{A}}[i] = \text{subtr}\{\mathbf{A}[i]\mathbf{R}_x\mathbf{A}^H[i]\}$, and $\mathbf{R}_{\tilde{B}}[i] = \text{subtr}\left\{(\mathbf{I}_{N_r} \otimes \mathbf{B}[i])\mathbf{R}_v(\mathbf{I}_{N_r} \otimes \mathbf{B}^H[i])\right\}$. This cost function is now to be optimized w.r.t $\mathbf{w}[i]$ and $\mathbf{b}[i]$. In order to avoid the trivial solution (zero vector $\mathbf{w}[i]$ and zero vector $\mathbf{b}[i]$), non-triviality constraints have to be added. e.g., a unit tap constraint, $b_0[i] = 1$; a unit-norm constraint, $\|\mathbf{b}[i]\|^2 = 1$ or $\|\mathbf{w}[i]\|^2 = 1$; or a unit-energy constraint, $\mathbf{b}^H[i]\mathbf{R}_{\tilde{A}}[i]\mathbf{b}[i] = 1$ or $\mathbf{w}^H[i]\mathbf{R}_{\tilde{B}}[i]\mathbf{w}[i] = 1$. More details about these constraints for TI channels can be found in [4] and [6] for the unit-tap and unit-norm constraints, and in [121] for the unit-energy constraint. An extensive study of the different constraints and their application for DMT-based systems are given in [122, 111]. A TEQ for the MIMO case is proposed in [3].

In this chapter we only consider the unit norm constraint (UNC) on the TIR and the unit energy constraint (UEC) on the TIR for their superior performance compared to the other constraint (this is proven to be the case in DMT systems, and is found to be of no exception here).

Unit norm constraint on TIR

In this case we have the following optimization problem

$$\min_{\mathbf{w}[i],\mathbf{b}[i]} \mathcal{J}[i] \text{ such that } \|\mathbf{b}[i]\|^2 = 1.$$

The solution to this problem is given by

$$\begin{aligned}\mathbf{w}^T[i] &= \tilde{\mathbf{b}}^T[i]\left(\boldsymbol{\mathcal{H}}^H[i]\mathbf{R}_{\tilde{B}}^{-1}[i]\boldsymbol{\mathcal{H}}[i] + \mathbf{R}_{\tilde{A}}^{-1}[i]\right)^{-1}\boldsymbol{\mathcal{H}}^H[i]\mathbf{R}_{\tilde{B}}^{-1}[i],\\ \mathbf{b}[i] &= \text{eig}_{\min}(\mathbf{R}^{\perp}[i]),\end{aligned}$$

where $\mathbf{R}^{\perp}[i]$ is given by

$$\mathbf{R}^{\perp}[i] = \mathbf{C}^T\left(\boldsymbol{\mathcal{H}}^H[i]\mathbf{R}_{\tilde{B}}^{-1}[i]\boldsymbol{\mathcal{H}}[i] + \mathbf{R}_{\tilde{A}}^{-1}[i]\right)^{-1}\mathbf{C}$$

Unit energy constraint on TIR

In this case we have the following optimization problem:

$$\min_{\mathbf{w}[i],\mathbf{b}[i]} \mathcal{J}[i] \text{ such that } \tilde{\mathbf{b}}^H[i]\mathbf{R}_{\tilde{A}}[i]\tilde{\mathbf{b}}[i] = 1.$$

The solution to this optimization problem is given by

$$\begin{aligned}\mathbf{w}^T[i] &= \tilde{\mathbf{b}}^T[i]\left(\boldsymbol{\mathcal{H}}^H[i]\mathbf{R}_{\tilde{B}}^{-1}[i]\boldsymbol{\mathcal{H}}[i] + \mathbf{R}_{\tilde{A}}^{-1}[i]\right)^{-1}\boldsymbol{\mathcal{H}}^H[i]\mathbf{R}_{\tilde{B}}^{-1}[i],\\ \mathbf{b}[i] &= \text{eig}_{\max}(\tilde{\mathbf{R}}^{\perp}[i]),\end{aligned}$$

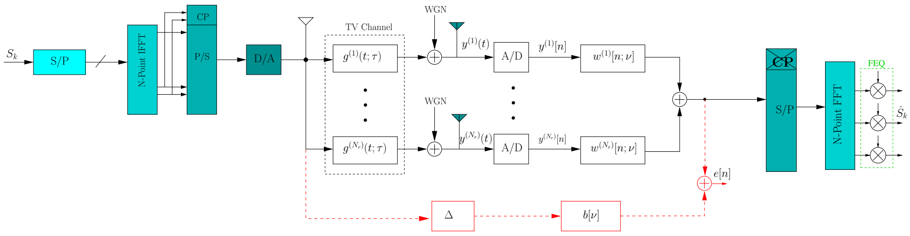

Figure 8.3: TEQ.

where $\tilde{\mathbf{R}}^{\perp}[i]$ is given by

$$\tilde{\mathbf{R}}^{\perp}[i] = \mathbf{C}^T \left(\boldsymbol{\mathcal{H}}^H[i] \mathbf{R}_{\tilde{B}}^{-1}[i] \boldsymbol{\mathcal{H}}[i] + \mathbf{R}_{\tilde{A}}^{-1}[i] \right)^{-1} \boldsymbol{\mathcal{H}}^H \mathbf{R}_{\tilde{B}}^{-1}[i] \boldsymbol{\mathcal{H}} \mathbf{R}_{\tilde{A}}[i] \mathbf{C}.$$

Note that $\text{eig}_{\min}(\mathbf{A})$ ($\text{eig}_{\max}(\mathbf{A})$) is the eigenvector corresponding to the minimum (maximum) eigenvalue of the matrix $\mathbf{A}$.

In conjunction with the designed TEQ, a one-tap FEQ applied to the filtered received sequence in the frequency-domain is still necessary to fully recover the transmitted QAM symbols. Define $\hat{S}_k[i]$ as the estimate of the transmitted QAM symbol on the kth subcarrier of the ith OFDM symbol. This estimate is then obtained by applying a 1-tap FEQ to the TEQ output after the DFT-demodulation as shown in Figure 8.3 as

$$\hat{S}_k[i] = \frac{1}{d_k[i]} \mathcal{F}^{(k)} \sum_{r=1}^{N_r} \sum_{q'=-Q'/2}^{Q'/2} \mathbf{D}_{q'}[i] \mathbf{W}_{q'}^{(r)}[i] \mathbf{y}^{(r)}[i], \tag{8.12}$$

where $\mathcal{F}^{(k)}$ is the $(k+1)$st row of the FFT matrix $\boldsymbol{\mathcal{F}}$, $\mathbf{W}_{q'}^{(r)}[i]$ is an $N \times (N + L')$ Toeplitz matrix, with first column $[w_{q',L'}^{(r)}[i], \mathbf{0}_{1\times(N-1)}]^T$ and first row $[w_{q',L'}^{(r)}[i], \ldots, w_{q',0}^{(r)}[i], \mathbf{0}_{1\times(N-1)}]$, $d_k[i]$ is the frequency response of the TIR on the kth subcarrier of the ith OFDM block ($1/d_k[i]$ represents the 1-tap FEQ), and $\mathbf{y}^{(r)}[i] = [y^{(r)}[i(N+\nu)+\nu-L'], \ldots, y^{(r)}[(i+1)(N+\nu)-1]]^T$.

The existence of a perfect shortening TEQ (a TEQ that completely eliminates IBI/ICI in the noiseless case) requires that $\boldsymbol{\mathcal{H}}$ is of full column rank. A necessary condition for $\boldsymbol{\mathcal{H}}$ to have full column rank is that $Nr(Q'+1)(L'+1) \geq (Q+Q'+1)(L+L'+1)$. It is clear that we need at least two receive antennas, i.e. $N_r \geq 2$ and this can be fulfilled for sufficiently large Q' and L'. This justifies our assumption of SIMO systems. Conditions like column reducedness and irreducibility can be deduced from the MIMO time-invariant FIR case. These are discussed in more details in Chapter 3 (see also [20]).

8.3 Frequency-Domain Per-Tone Equalization

In Section 8.2, a time-domain equalizer is proposed to combat the effect of the propagation channel. The purpose of the proposed TEQ is to convert the doubly selective channel into a purely frequency-selective channel of order that fits within the CP length. The proposed TEQ optimizes the performance on all subcarriers in a joint fashion. An optimal frequency-domain per-tone equalizer (PTEQ) can then be obtained by transferring the TEQ operations to the frequency-domain. Hence, the estimate of the transmitted QAM symbol on the kth subcarrier in the ith OFDM block is then obtained as

$$\hat{S}_k[i] = \sum_{r=1}^{N_r} \sum_{q'=-Q'/2}^{Q'/2} \mathcal{F}^{(k)} \mathbf{D}_{q'}[i] \mathbf{Y}^{(r)}[i] \mathbf{w}_{q'}^{(r)}[i] / d_k[i] \tag{8.13a}$$

$$= \sum_{r=1}^{N_r} \sum_{q'=-Q'/2}^{Q'/2} \mathcal{F}^{(k)} \underbrace{\mathbf{D}_{q'}[i] \mathbf{Y}^{(r)}[i] \hat{\mathbf{D}}_{q'}^{*}}_{\tilde{\mathbf{Y}}_{q'}^{(r)}[i]} \underbrace{\hat{\mathbf{D}}_{q'} \mathbf{w}_{q'}^{(r)}[i] / d_k[i]}_{\tilde{\mathbf{w}}_{q'}^{(r,k)}[i]} \tag{8.13b}$$

where $\mathbf{Y}^{(r)}[i]$ is an $N \times (L'+1)$ Toeplitz matrix, with first column $[y^{(r)}[i(N+\nu)+\nu], \ldots, y^{(r)}[(i+1)(N+\nu)-1]]^T$ and first row $[y^{(r)}[i(N+\nu)+\nu], \ldots, y^{(r)}[i(N+\nu)+\nu-L']]$, $\mathbf{w}_{q'}^{(r)}[i] = [w_{q',0}^{(r)}[i], \ldots, w_{q',L'}^{(r)}[i]]^T$, and $\hat{\mathbf{D}}_{q'} = \text{diag}\{[1, \ldots, e^{j2\pi q' L'/K}]^T\}$. Note that the right multiplication of $\mathbf{Y}^{(r)}[i]$ with the diagonal matrix $\hat{\mathbf{D}}_{q'}$ in (8.13b) is done here to restore the Toeplitz structure in $\mathbf{Y}_{q'}^{(r)}[i] = \mathbf{D}_{q'} \mathbf{Y}^{(r)}[i]$, which will simplify the analysis and implementation, as will become clear later. From (8.13b), we can see that each subcarrier has its own $(L'+1)$-tap FEQ. This allows us to optimize the equalizer coefficients $\tilde{\mathbf{w}}_{q'}^{(r,k)}[i]$ for each subcarrier k separately, without taking into account the specific relation that existed originally between $\tilde{\mathbf{w}}_{q'}^{(r,k)}[i]$, $\mathbf{w}_{q'}^{(r,k)}[i]$, and $d_k[i]$.

Defining $\tilde{\mathbf{Y}}^{(r)}[i] = \left[\tilde{\mathbf{Y}}_{-Q'/2}^{(r)}[i], \ldots, \tilde{\mathbf{Y}}_{Q'/2}^{(r)}[i]\right]$ and $\tilde{\mathbf{w}}^{(r,k)}[i] = \left[\tilde{\mathbf{w}}_{-Q'/2}^{(r,k)T}[i], \ldots, \tilde{\mathbf{w}}_{Q'/2}^{(r,k)T}[i]\right]^T$, (8.13b) reduces to:

$$\hat{S}_k[i] = \sum_{r=1}^{N_r} \mathcal{F}^{(k)} \tilde{\mathbf{Y}}^{(r)}[i] \tilde{\mathbf{w}}^{(r,k)}[i]. \tag{8.14}$$

Transferring the TEQ operation to the frequency-domain by interchanging the TEQ with the DFT in (8.14), we obtain:

$$\hat{S}_k[i] = \sum_{r=1}^{N_r} \tilde{\mathbf{w}}^{(r,k)T}[i] \mathbf{F}^{(k)}[i] \mathbf{y}^{(r)}[i], \tag{8.15}$$

where $\mathbf{F}^{(k)}[i] = \left(\mathbf{I}_{Q'+1} \otimes \tilde{\boldsymbol{\mathcal{F}}}^{(k)}\right) \left[\tilde{\mathbf{D}}_{-Q'/2}^{T}[i], \ldots, \tilde{\mathbf{D}}_{Q'/2}^{T}[i]\right]^T$, and $\tilde{\boldsymbol{\mathcal{F}}}^{(k)}$ is given by:

$$\tilde{\boldsymbol{\mathcal{F}}}^{(k)} = \begin{bmatrix} 0 & \cdots & 0 & \boxed{\mathcal{F}^{(k)}} \\ \vdots & 0 & \boxed{\mathcal{F}^{(k)}} & 0 \\ 0 & \iddots & \iddots & 0 & \vdots \\ \boxed{\mathcal{F}^{(k)}} & 0 & \cdots & 0 \end{bmatrix},$$

which corresponds to a sliding DFT operation, which can be implemented more cheaply as a sliding FFT.

To compute (8.15), we require $(Q'+1)$ sliding FFTs per receive antenna. Each sliding FFT is applied to a modulated version of the sequence received on a particular antenna. The q'th sliding FFT on the rth receive antenna is shown in Figure 8.4. To estimate the transmitted QAM symbol on the kth subcarrier we then have to combine the outputs of the $N_r(Q'+1)$ PTEQs corresponding to the kth subcarrier. This results in a complexity of $(Q'+1)(L'+1)$ multiply-add (MA) operations per receive antenna per subcarrier, i.e., $N_rN(Q'+1)(L'+1)$ MA operations for a block of N symbols. In Section 8.4, we show how we can further reduce the complexity of the proposed PTEQ by replacing the $Q'+1$ sliding FFTs by only a few sliding FFTs, the number of which is entirely independent of Q' but rather depends on the BEM frequency resolution K. The removed sliding FFTs are compensated for by combining the PTEQ outputs of neighboring subcarriers on the remaining sliding FFTs.

In the following, we will show how the PTEQ coefficients can be computed in order to minimize the mean square error (MSE). Defining $\tilde{\mathbf{w}}^{(k)}[i] = [\tilde{\mathbf{w}}^{(1,k)T}[i], \ldots, \tilde{\mathbf{w}}^{(N_r,k)T}[i]]^T$ and $\mathbf{y}[i] = [\mathbf{y}^{(1)T}[i], \ldots, \mathbf{y}^{(N_r)T}[i]]^T$, (8.15) can be written as

$$\hat{S}_k[i] = \tilde{\mathbf{w}}_k^T[i] \left(\mathbf{I}_{N_r} \otimes \mathbf{F}^{(k)}[i]\right) \mathbf{y}[i]. \tag{8.16}$$

At this point we may introduce a model for the received sequence on the rth receive antenna $\mathbf{y}^{(r)}[i]$ as

$$\mathbf{y}^{(r)}[i] = \underbrace{\sum_{q=-Q/2}^{Q/2} \tilde{\mathbf{D}}_q[i] \left[\boldsymbol{O}_1, \mathbf{H}_q^{(r)}[i], \boldsymbol{O}_2\right] (\mathbf{I}_3 \otimes \mathbf{P}) \left(\mathbf{I}_3 \otimes \boldsymbol{\mathcal{F}}^H\right)}_{\mathbf{G}^{(r)}[i]} \underbrace{\begin{bmatrix} \mathbf{s}[i-1] \\ \mathbf{s}[i] \\ \mathbf{s}[i+1] \end{bmatrix}}_{\tilde{\mathbf{s}}} + \mathbf{v}^{(r)}[i], \tag{8.17}$$

where $\boldsymbol{O}_1 = \mathbf{0}_{(N+L')\times(N+2\nu-L-L')}$, $\boldsymbol{O}_2 = \mathbf{0}_{(N+L')\times(N+\nu-d)}$, $\mathbf{H}_q^{(r)}[i]$ is an $(N+L')\times(N+L'+L)$ Toeplitz matrix with first column $[h_{q,L}^{(r)}[i], \mathbf{0}_{1\times(N+L'-1)}]^T$ and first row $[h_{q,L}^{(r)}[i], \ldots, h_{q,0}^{(r)}[i], \mathbf{0}_{1\times(N+L'-L-1)}]$, and $\mathbf{P}$ is the CP insertion matrix given by:

$$\mathbf{P} = \begin{bmatrix} \mathbf{0}_{\nu\times(N-\nu)} & \mathbf{I}_\nu \\ \multicolumn{2}{c}{\mathbf{I}_N} \end{bmatrix}.$$

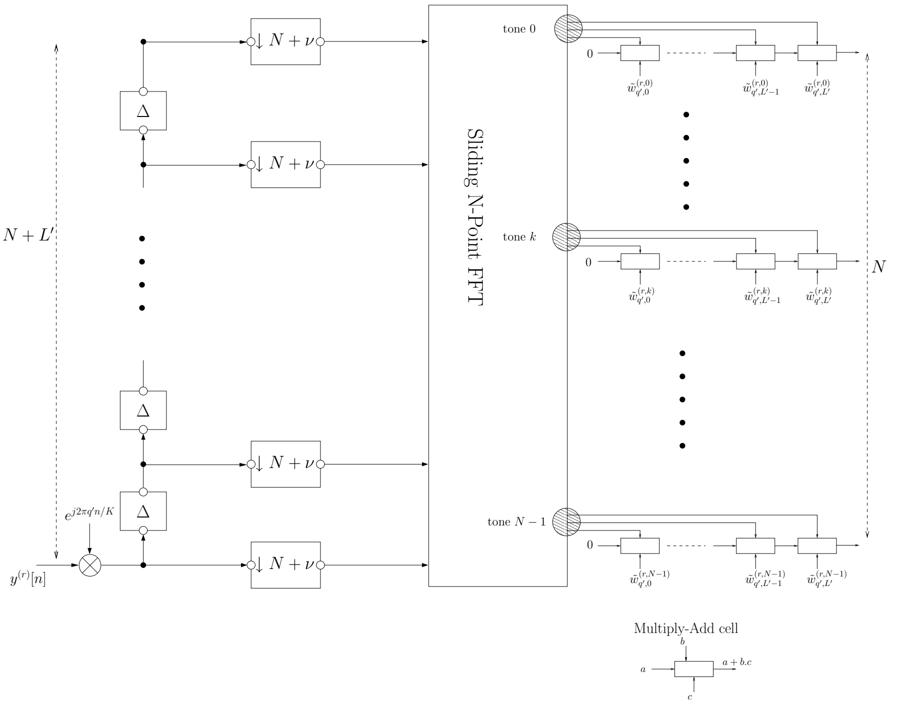

Figure 8.4: Sliding FFT of the q'th modulated version of the received sequence $y^{(r)}[n]$.

To obtain the PTEQ coefficients for the kth subcarrier, we define the following mean-square error (MSE) cost function:

$$\mathcal{J}[i] = \mathcal{E}\left\{ \left\| S_k[i] - \tilde{\mathbf{w}}^{(k)T}[i] \left(\mathbf{I}_{N_r} \otimes \mathbf{F}^{(k)}[i] \right) \mathbf{y}[i] \right\|^2 \right\}$$

Hence, the MMSE PTEQ coefficients for the kth subcarrier are given by:

$$\tilde{\mathbf{w}}^{(k)}_{MMSE}[i] = \arg \min_{\tilde{\mathbf{w}}^{(k)}[i]} \mathcal{J}[i] \tag{8.18}$$

The solution of (8.18) is obtained by solving $\partial \mathcal{J}[i]/\partial \tilde{\mathbf{w}}^{(k)}[i] = \mathbf{0}$, which reduces to:

$$\begin{aligned} \tilde{\mathbf{w}}^{(k)T}_{MMSE}[i] = &\left(\left(\mathbf{I}_{N_r} \otimes \mathbf{F}^{(k)}[i] \right) \left(\mathbf{G}[i] \mathbf{R}_{\tilde{s}} \mathbf{G}^H[i] + \mathbf{R}_v \right) \left(\mathbf{I}_{N_r} \otimes \mathbf{F}^{(k)H}[i] \right) \right)^{-1} \\ &\times \left(\mathbf{I}_{N_r} \otimes \mathbf{F}^{(k)}[i] \right) \mathbf{G}[i] \mathbf{R}_{\tilde{s}} \mathbf{e}^{(k)}, \end{aligned} \tag{8.19}$$

where $\mathbf{G}[i] = [\mathbf{G}^{(1)T}[i], \ldots, \mathbf{G}^{(N_r)T}[i]]^T$ and $\mathbf{e}^{(k)}$ is the unit vector with a 1 in the $N + k$th position.

Note that, in contrast to the time-domain approach, where the BEM resolution of the channel model and the BEM resolution of the time-varying FIR TEQ are assumed to be the same, the BEM resolution of the channel model and the BEM resolution of the PTEQ can be different.

8.4 Efficient Implementation of the PTEQ

In Section 8.3, we have shown that to implement the proposed PTEQ, we basically require $(Q'+1)$ sliding FFTs. In this section, we show how we can reduce the complexity of the proposed PTEQ by further exploiting the special structure of $\tilde{\mathbf{Y}}_{q'}^{(r)}[i]$ (see (8.13b)). Our complexity reduction will proceed in two steps:

Step 1:

In general, the BEM frequency resolution K is greater than or equal to the DFT size N. We will assume that K is an integer multiple of the FFT size, i.e., $K = PN$, where P is an integer greater than or equal to 1 ($P \in \mathbb{Z}^+$). We start by defining $\mathbb{Q} = \{-Q'/2, \ldots, Q'/2\}$, and $\mathbb{Q}_p = \{q \in \mathbb{Q} \mid q \mod P = p\}$. Based on these definitions, (8.13b) and (8.14) can be written as

$$\hat{S}_k[i] = \sum_{r=1}^{N_r}\sum_{p=0}^{P-1}\sum_{q_p\in\mathbb{Q}_p} \mathcal{F}^{(k-l_p)} \underbrace{\mathbf{D}_p[i]\mathbf{Y}^{(r)}[i]\hat{\mathbf{D}}_p^*}_{\tilde{\mathbf{Y}}_p^{(r)}[i]} \underbrace{\hat{\mathbf{D}}_p\mathbf{w}_{p,l_p}^{(r,k)}[i]/d_k[i]}_{\bar{\mathbf{w}}_{p,l_p}^{(r,k)}[i]} \tag{8.20a}$$

$$= \sum_{r=1}^{N_r}\sum_{p=0}^{P-1}\sum_{q_p\in\mathbb{Q}_p} \mathcal{F}^{(k-l_p)}\tilde{\mathbf{Y}}_p^{(r)}[i]\bar{\mathbf{w}}_{p,l_p}^{(r,k)}[i], \tag{8.20b}$$

where $l_p = \frac{q_p - p}{P}$, and $\mathbf{w}_{p,l_p}^{(r,k)}[i] = \mathbf{w}_{q_p}^{(r,k)}[i]$. Note that (8.20b) splits the $Q'+1$ different terms of (8.14) into P different groups, with the pth group containing $|\mathbb{Q}_p|$ terms, where $|\mathbb{Q}_p|$ denotes the cardinality of the set $\mathbb{Q}_p$ for $p = 0, \ldots, P-1$. Transferring the TEQ operation to the frequency-domain, we obtain:

$$\hat{S}_k[i] = \sum_{r=1}^{N_r}\sum_{p=0}^{P-1}\sum_{q_p\in\mathbb{Q}_p} \bar{\mathbf{w}}_{p,l_p}^{(r,k)T}[i]\tilde{\boldsymbol{\mathcal{F}}}^{(k-l_p)} \underbrace{\tilde{\mathbf{D}}_p[i]\mathbf{y}^{(r)}[i]}_{\tilde{\mathbf{y}}_p^{(r)}[i]} \tag{8.21}$$

Note that $\tilde{\mathbf{y}}_p^{(r)}[i] = [\tilde{y}_p^{(r)}[i(N+\nu)+\nu-L'], \ldots, \tilde{y}_p^{(r)}[(i+1)(N+\nu)-1]]^T$, with $\tilde{y}_p^{(r)}[n] = e^{j2\pi pn/K}y^{(r)}[n]$ is the pth modulated version of the received sequence.

Defining $\bar{\mathbf{w}}_p^{(r,k)}[i] = [\ldots, \bar{\mathbf{w}}_{p,-1}^{(r,k)T}[i], \bar{\mathbf{w}}_{p,0}^{(r,k)T}[i], \bar{\mathbf{w}}_{p,1}^{(r,k)T}[i], \ldots]^T$, (8.21) can now be written as

$$\hat{S}_k[i] = \sum_{r=1}^{N_r} \sum_{p=0}^{P-1} \bar{\mathbf{w}}_p^{(r,k)T}[i] \tilde{\mathbf{F}}_p^{(k)} \tilde{\mathbf{y}}_p^{(r)}[i] \tag{8.22}$$

where $\tilde{\mathbf{F}}_p^{(k)} = [\ldots, \tilde{\boldsymbol{\mathcal{F}}}^{(k-1)T}, \tilde{\boldsymbol{\mathcal{F}}}^{(k)T}, \tilde{\boldsymbol{\mathcal{F}}}^{(k+1)T}, \ldots]^T$. Let us now define $\tilde{\mathbf{F}}^{(k)} = \text{diag}\left\{\tilde{\mathbf{F}}_0^{(k)T}, \ldots, \tilde{\mathbf{F}}_{P-1}^{(k)T}\right\}$, $\tilde{\mathbf{y}}^{(r)}[i] = [\tilde{\mathbf{y}}_0^{(r)T}[i], \ldots, \tilde{\mathbf{y}}_{P-1}^{(r)T}[i]]^T$ and $\tilde{\mathbf{y}}[i] = [\tilde{\mathbf{y}}^{(1)T}[i], \ldots, \tilde{\mathbf{y}}^{(N_r)T}[i]]^T$. Further defining $\bar{\mathbf{w}}^{(r,k)}[i] = [\bar{\mathbf{w}}_0^{(r,k)T}[i], \ldots, \bar{\mathbf{w}}_{P-1}^{(r,k)T}[i]]^T$ and $\bar{\mathbf{w}}^{(k)}[i] = [\bar{\mathbf{w}}^{(1,k)T}[i], \ldots, \bar{\mathbf{w}}^{(N_r,k)T}[i]]^T$, (8.22) can finally be written as

$$\hat{S}_k[i] = \bar{\mathbf{w}}^{(k)T}[i](\mathbf{I}_{N_r} \otimes \tilde{\mathbf{F}}^{(k)})\tilde{\mathbf{y}}[i] \tag{8.23}$$

To implement (8.22), we require P sliding FFTs per receive antenna rather than $Q'+1$ sliding FFTs per receive antenna as in Section 8.3 (in practice and in our simulations $P \ll Q'+1$, typically $P=1$ or $P=2$). Each sliding FFT is applied to a modulated version of the received sequence. This reduction in the number of sliding FFTs per receive antenna is compensated for by combining $|\mathbb{Q}_p|$ neighboring subcarriers on the pth sliding FFT. Notice here that apart from the reduction in the number of sliding FFTs, the implementation complexity remains the same as in Section 8.3, i.e., $N_r N(Q'+1)(L'+1)$ MA operations for a block of N symbols.

Similar to (8.18), we can construct the MSE cost function as

$$\mathcal{J}[i] = \mathcal{E}\left\{\left\|S_k[i] - \bar{\mathbf{w}}^{(k)T}[i]\left(\mathbf{I}_{N_r} \otimes \tilde{\mathbf{F}}^{(k)}\right)\tilde{\mathbf{y}}[i]\right\|^2\right\} \tag{8.24}$$

The solution of (8.24) is:

$$\begin{aligned}\bar{\mathbf{w}}_{MMSE}^{(k)T}[i] = &\left(\left(\mathbf{I}_{N_r} \otimes \tilde{\mathbf{F}}^{(k)}[i]\right)\left(\mathbf{G}[i]\mathbf{R}_{\tilde{s}}\mathbf{G}^H[i] + \mathbf{R}_v\right)\left(\mathbf{I}_{N_r} \otimes \tilde{\mathbf{F}}^{(k)H}[i]\right)\right)^{-1} \\ &\times \left(\mathbf{I}_{N_r} \otimes \tilde{\mathbf{F}}^{(k)}[i]\right)\mathbf{G}[i]\mathbf{R}_{\tilde{s}}\mathbf{e}^{(k)},\end{aligned} \tag{8.25}$$

which is equivalent to the one obtained in (8.19).

Step 2:

We can further simplify the computational complexity associated with the proposed PTEQ by replacing each sliding FFT by only one full FFT and L' difference terms that are common to all subcarriers similar to the procedure in [42]. To explain this, we will consider only one sliding FFT. Let us consider the kth subcarrier of the pth sliding FFT, i.e., $\tilde{\boldsymbol{\mathcal{F}}}^{(k)}\tilde{\mathbf{y}}_p^{(r)}[i]$. Define $\tilde{Y}_p^{(r,k)} = \mathcal{F}^{(k)}[\tilde{y}_p^{(r)}[i(N+\nu)+\nu], \ldots, \tilde{y}_p^{(r)}[(i+1)(N+\nu)-1]]^T$ as the frequency response on the kth subcarrier of the pth modulated version of the received sequence on the rth receive antenna. It can then be shown that:

$$\tilde{\boldsymbol{\mathcal{F}}}^{(k)}\tilde{\mathbf{y}}_p^{(r)}[i] = \mathbf{T}^{(k)} \begin{bmatrix} \tilde{Y}_p^{(r,k)} \\ \Delta\tilde{\mathbf{y}}_p^{(r)}[i] \end{bmatrix} \begin{matrix} \updownarrow 1 \times 1 \\ \updownarrow L' \times 1 \end{matrix} , \tag{8.26}$$

where $\mathbf{T}^{(k)}$ is an $(L'+1)\times(L'+1)$ lower triangular Toeplitz matrix given by:

$$\mathbf{T}^{(k)} = \begin{bmatrix} 1 & 0 & \cdots & 0 \\ \beta^k & \ddots & \ddots & \vdots \\ \vdots & \ddots & \ddots & 0 \\ \beta^{kL'} & \cdots & \beta^k & 1 \end{bmatrix}, \tag{8.27}$$

with $\beta = e^{-j2\pi/N}$. The difference terms $\Delta\tilde{\mathbf{y}}_p^{(r)}[i]$ are given by:

$$\Delta\tilde{\mathbf{y}}_p^{(r)}[i] = \begin{bmatrix} \tilde{y}_p^{(r)}[i(N+\nu)+\nu-1] - \tilde{y}_p^{(r)}[(i+1)(N+\nu)-1] \\ \vdots \\ \tilde{y}_p^{(r)}[i(N+\nu)+\nu-L'] - \tilde{y}_p^{(r)}[(i+1)(N+\nu)-L'-1] \end{bmatrix}.$$

In a similar fashion, we can obtain an expression for the neighboring subcarriers on the same sliding FFT by replacing the subcarrier index. The symbol estimate (8.23) can then be written as follows. We first define $\mathbf{u}_{p,l_p}^{(r,k)T}[i] = \bar{\mathbf{w}}_{p,l_p}^{(r,k)T}[i]\mathbf{T}^{(k+l_p)}$ and also define the following $|\mathbb{Q}_p|(L'+1)\times(|\mathbb{Q}_p|+L')$ selection matrix:

$$\mathbf{S}_p = \tilde{\mathbf{I}} \otimes \begin{bmatrix} 1 \\ \mathbf{0}_{L'\times 1} \end{bmatrix} + \begin{bmatrix} \mathbf{0}_{1\times(|\mathbb{Q}_p|+L')} \\ \tilde{\tilde{\mathbf{I}}} \end{bmatrix} \otimes \mathbf{1}_{|\mathbb{Q}_p|},$$

where $\tilde{\mathbf{I}}$ contains the first $|\mathbb{Q}_p|$ rows of the matrix $\mathbf{I}_{|\mathbb{Q}_p|+L'}$, and $\tilde{\tilde{\mathbf{I}}}$ contains the last L' rows of the matrix $\mathbf{I}_{|\mathbb{Q}_p|+L'}$. Introducing $\mathbf{u}_p^{(r,k)T}[i] = [\ldots, \mathbf{u}_{p,-1}^{(r,k)T}[i], \mathbf{u}_{p,0}^{(r,k)T}[i], \mathbf{u}_{p,1}^{(r,k)T}[i], \ldots]^T$ and $\mathbf{v}_p^{(r,k)T}[i] = \mathbf{u}_p^{(r,k)T}[i]\mathbf{S}_p$, (8.23) can then be written as

$$\hat{S}_k[i] = \sum_{r=1}^{N_r}\sum_{p=0}^{P-1} \mathbf{v}_p^{(r,k)T}[i] \left[\begin{array}{c} \vdots \\ \tilde{Y}_p^{(r,k-1)}[i] \\ \tilde{Y}_p^{(r,k)}[i] \\ \tilde{Y}_p^{(r,k+1)}[i] \\ \vdots \\ \hline \Delta\tilde{\mathbf{y}}_p^{(r)}[i] \end{array}\right] \begin{matrix} \\ \\ \updownarrow |\mathbb{Q}_p| \times 1 \\ \\ \\ \updownarrow L' \times 1 \end{matrix}$$

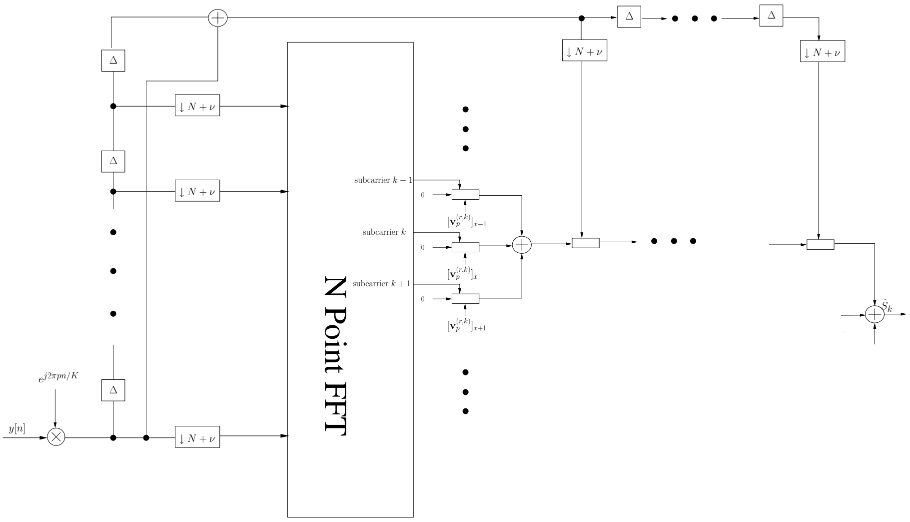

Figure 8.5: Low complexity PTEQ on the pth branch.

$$= \sum_{r=1}^{N_r} \sum_{p=0}^{P-1} \mathbf{v}_p^{(r,k)T}[i] \underbrace{\left[\begin{array}{ccc} \vdots & \vdots & \\ \mathbf{0}_{1\times L'} & \mathcal{F}^{(k-1)} & \\ \mathbf{0}_{1\times L'} & \mathcal{F}^{(k)} & \\ \mathbf{0}_{1\times L'} & \mathcal{F}^{(k+1)} & \\ \vdots & \vdots & \\ \hline \bar{\mathbf{I}}_{L'} & \mathbf{0}_{L'\times(N-L')} & -\bar{\mathbf{I}}_{L'} \end{array} \right]}_{\tilde{\mathbf{F}}_p^{(k)}} \tilde{\mathbf{y}}_p^{(r)}[i], \tag{8.28}$$

where $\bar{\mathbf{I}}_{L'}$ is the anti-diagonal identity matrix of size $L' \times L'$. Defining $\mathbf{v}^{(r,k)}[i] = [\mathbf{v}_0^{(r,k)T}[i], \ldots, \mathbf{v}_{P-1}^{(r,k)T}[i]]^T$, $\mathbf{v}^{(k)}[i] = [\mathbf{v}^{(1,k)T}[i], \ldots, \mathbf{v}^{(N_r,k)T}[i]]^T$ and $\tilde{\mathbf{F}} = \mathrm{diag}\{\tilde{\mathbf{F}}_0^T, \ldots, \tilde{\mathbf{F}}_P^T\}$, (8.28) can finally be written as

$$\hat{S}_k = \mathbf{v}^{(k)T}[i](\mathbf{I}_{N_r} \otimes \tilde{\mathbf{F}}^{(k)})\tilde{\mathbf{y}}[i]. \tag{8.29}$$

Note that, due to the fact that the difference terms are common to all subcarriers in a particular sliding FFT, the implementation complexity is $P(L'+1)+Q'+1$ MA operations per receive antenna per subcarrier, compared to $(Q'+1)(L'+1)$ per receive antenna per subcarrier in Section 8.3. In Figure 8.5, we show how (8.29) can be realized for the pth sliding FFT on the rth receive antenna. Note that replacing the sliding FFT with one full DFT and L' difference terms in Section 8.3, will not reduce the implementation complexity. This is due to the fact that we only consider a single subcarrier output for each

Table 8.1: Implementation Complexity Comparison

	MA/tone/rx	FFT/rx
TEQ	$(Q'+1)(L'+1)+1$	1
PTEQ (Figure 8.4)	$(Q'+1)(L'+1)$	$(Q'+1)$ sliding FFTs
PTEQ (Figure 8.5)	$P(L'+1)+Q'+1$	P FFTs

sliding FFT to estimate a particular symbol. The implementation complexity of the TEQ and the different configurations of the PTEQ is summarized in Table 8.1[1].

On the other hand, the design complexity of the PTEQ is higher than the design complexity of the TEQ. We can easily show that the design of the TEQ requires $\mathcal{O}\big((Q+Q'+1)^3(L+L'+1)^3\big)$ multiply-add (MA) operations, while it requires $\mathcal{O}\left((Q'+1)(L'+1)N\right)$ MA operations per subcarrier to design the PTEQs. The design complexity of the TEQ is mainly due to a matrix inversion of size $(Q+Q'+1)(L+L'+1)\times(Q+Q'+1)(L+L'+1)$. The complexity associated with computing the max (min) eigenvector of an $(L''+1)\times(L''+1)$ matrix, which requires $\mathcal{O}\left((L''+1)^2\right)$ MA operations [49], is negligible compared to the above matrix inversion.

Unifying Framework

We finally note that our approach unifies and extends many existing frequency-domain approaches, for the case of TI as well as time-varying channels as follows:

1. TI Channels ($Q=0$, and hence $Q'=0$):
   a) $\nu \geq L$, and $L'=0$: the proposed PTEQ corresponds to the 1-tap MMSE FEQ as in [116].
   b) $\nu < L$, and $L' \neq 0$: the proposed PTEQ corresponds to the per-tone equalizer proposed in [110] for DMT-based transmission (e.g., for DSL modems).
2. time-varying Channels ($Q' \neq 0$):
   a) $\nu \geq L$, $L'=0$, and $P=1$: the proposed PTEQ corresponds to the FEQ proposed in [29].
   b) $\nu \geq L$, $L'=0$, and $P \geq 1$: the proposed PTEQ corresponds to the FEQ proposed in [10].

[1] These figures do not take into account the BEM channel coefficients estimation/computation.

8.5 Simulations

In this section, we show some simulation results for the proposed IBI/ICI mitigation techniques. We consider a SISO system as well as a SIMO system with $N_r = 2$ receive antennas. The channel is assumed to be doubly selective of order $L = 6$ with a maximum Doppler frequency of $f_{\max} = 100Hz$ (corresponds to a speed of $120Km/hr$ on the GSM band of $900MHz$). The channel taps are simulated as i.i.d., correlated in time with a correlation function according to Jakes' model $\mathcal{E}\{g^{(r)}[n_1; l_1]g^{(r')*}[n_2; l_2]\} = \sigma_h^2 J_0(2\pi f_{\max} T(n_1 - n_2))\delta[l_1 - l_2]\delta[r - r']$, where J_0 is the zeroth-order Bessel function of the first kind and σ_h^2 denotes the variance of the channel. We consider an OFDM transmission with $N = 128$ subcarriers, and QPSK signaling. The sampling time is $T = 50\mu sec$ which corresponds to a data rate of $40kbps$, which is suitable for applications like mobile multimedia. The normalized Doppler frequency is then obtained as $f_{\max}T = 0.005$. We define the SNR as $SNR = \sigma_h^2(L + 1)E_s/\sigma_n^2$, where E_s is the QPSK symbol power. The decision delay d is always chosen as $d = \lfloor (L + L')/2 \rfloor + 1$.

We use a BEM to approximate the channel. We assume that the BEM coefficients are known at the receiver (obtained through an LS fit of the true channel in the noiseless case). The BEM coefficients of the approximated channel are used to design the time-domain and the frequency-domain per-tone equalizers. These equalizers, however, are used to equalize the true channel (Jakes' model). The BEM resolution is determined by $K = PN$ with P is chosen as $P = 1, 2$. The number of time-varying basis functions of the channel is chosen such that $Q/(2KT) \geq f_{\max}$ is satisfied, which results into $Q = 2$ for $P = 1$, and $Q = 4$ for $P = 2$.

• First, we consider a SISO system, where the channel impulse response fits within the CP, i.e., $\nu = L$. Hence, the total OFDM symbol duration is 6.7 *msec*. We measure the performance in terms of the BER vs. SNR. We consider a TEQ with $Q' = 14$, $L' = 14$ and $P = 2$. We consider the unit energy constraint (UEC), and the unit norm constraint (UNC). For the PTEQ, we use different scenarios. More specifically, we consider a PTEQ resulting from:

- a purely time-selective TEQ with $Q' = 10$ and $L' = 0$, and $P = 1$ as in [15].
- a purely time-selective TEQ with $Q' = 10$ and $L' = 0$, and $P = 2$ as in [15].
- a doubly selective TEQ with $Q' = 10$ and $L' = 6$, and $P = 1$.
- a doubly selective TEQ with $Q' = 10$ and $L' = 6$, and $P = 2$.

As a benchmark, we consider the case of OFDM transmission over purely

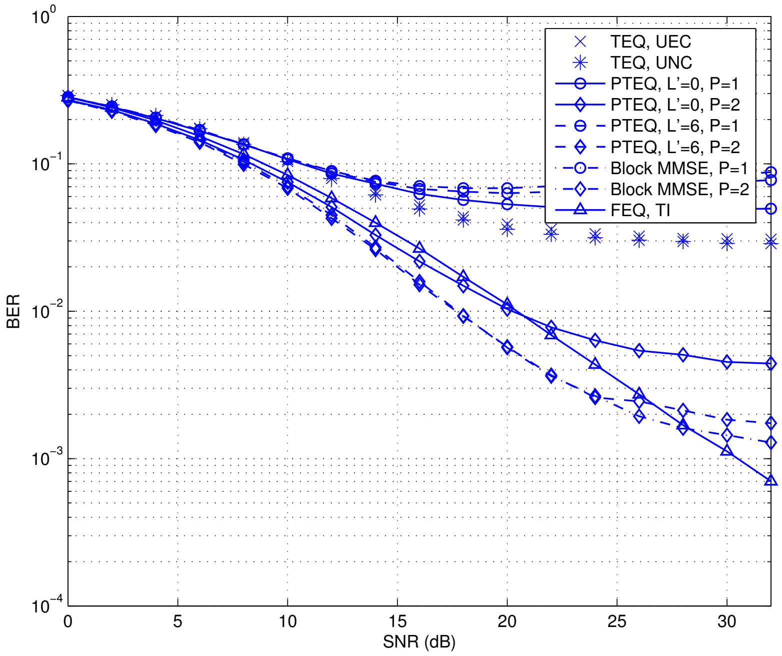

Figure 8.6: BER vs. SNR for TEQ and PTEQ, $N_r = 1$ receive antenna.

frequency-selective (TI) channels where the equalizer is the conventional 1-tap MMSE FEQ, as well as OFDM transmission over doubly selective (time-varying) channels with a block MMSE equalizer. The block MMSE equalizer for OFDM used here is similar to the block MMSE proposed in [20] designed for single carrier (SC) transmission with CP. As shown in Figure 8.6, the performance of the TEQ suffers from an early error floor for both UEC and UNC. The PTEQ exhibits a similar performance when $P = 1$ for both $L' = 0$ and $L' = 6$. However, the performance of the PTEQ is significantly improved when $P = 2$. For $P = 2$ with $L' = 0$, we see that the PTEQ slightly outperforms the 1-tap MMSE equalizer for OFDM over TI channels for low SNR ($SNR \leq 20\,dB$), and it experiences a 3 dB loss in SNR compared to the block MMSE for OFDM over time-varying channels. On the other hand, when $P = 2$ with $L' = 6$, the PTEQ outperforms the conventional 1-tap MMSE FEQ of OFDM over TI channels, with an SNR gain of 2 dB at $BER = 10^{-2}$, and coincides with the performance of the block MMSE equalizer for OFDM over time-varying channels.

• Second, we consider a SIMO system with $N_r = 2$ receive antennas. We consider the case where the cyclic prefix ν is shorter than the channel order, ν is chosen to be $\nu = 3$. The OFDM symbol duration is then 6.55 $msec$. We

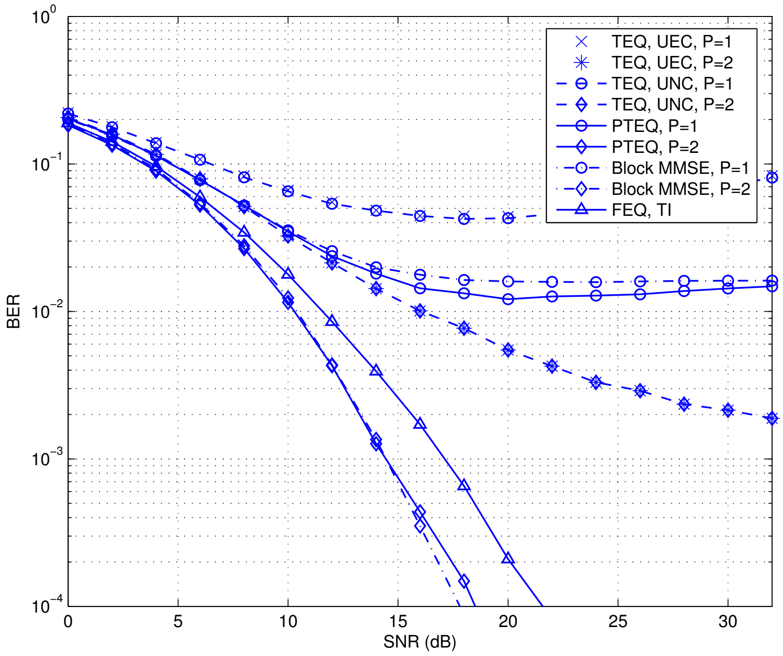

Figure 8.7: BER vs. SNR for TEQ and PTEQ, $N_r = 2$ receive antennas.

consider a TEQ with $Q' = 8$ and $L' = 8$. A PTEQ is then obtained by transferring this TEQ to the frequency-domain. We consider the case when $P = 1$ and $P = 2$. As shown in Figure 8.7, both the TEQ and the PTEQ suffer from an early error floor when $P = 1$, where the former exhibits an error floor at $BER = 4 \times 10^{-2}$ and $SNR = 20\ dB$ and the latter exhibits an error floor at $BER = 10^{-2}$ and $SNR = 20\ dB$. The performance is significantly improved when $P = 2$ for both the TEQ and the PTEQ. The PTEQ significantly outperforms the TEQ, where we can see a 6 dB gain in SNR for the PTEQ over the TEQ at $BER = 10^{-2}$. The TEQ experiences a 4 dB loss in SNR compared to the 1-tap MMSE FEQ for OFDM over TI channels, and 6 dB loss in SNR compared to the PTEQ which coincides with the block MMSE for OFDM over time-varying channels.

• Third, we examine the effect of the decision delay d on the BER performance for the TEQ considering the UEC and UNC, and the PTEQ. We consider again the cases $P = 1$ and $P = 2$ for a SIMO system with $N_r = 2$ receive antennas and the same equalizer parameters as before. We examine the performance at $SNR = 15\ dB$. As shown in Figure 8.8, the performance of the PTEQ approach is a much smoother function of the synchronization delay than the performance

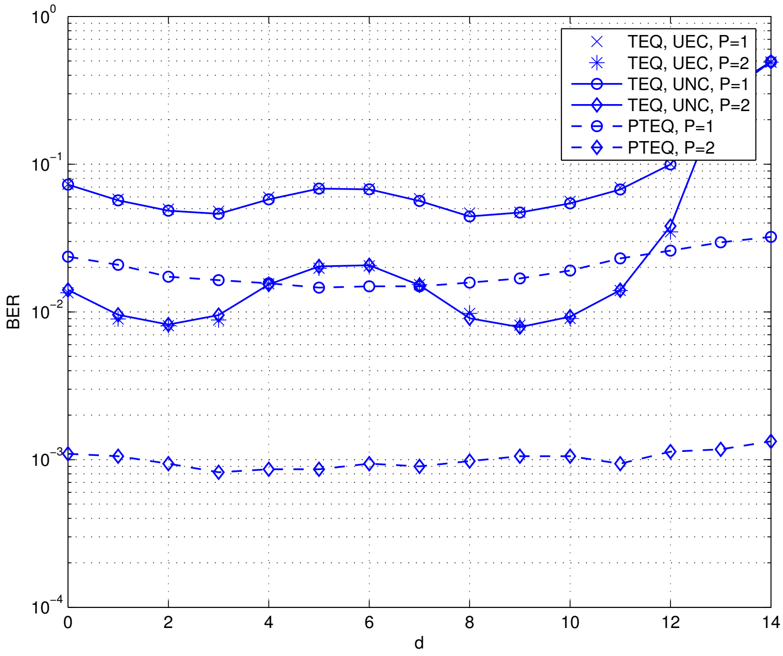

Figure 8.8: BER vs. decision delay d for TEQ and PTEQ, $N_r = 2$ receive antennas at $SNR = 15\ dB$.

of the TEQ approach. Hence, for the PTEQ approach the synchronization delay setting is less critical than for the TEQ approach.

• In our setup so far we use the BEM coefficients (i.e., the approximated channel) to design the PTEQ. Here, we consider the performance of the PTEQ when the true channel is used for equalizer designs as well as for the evaluation. The channel is assumed to be a doubly selective channel with maximum Doppler frequency $f_{\max} = 100\ Hz$, and sampling time $T = 50\ \mu sec$. The channel order is assumed to be $L = 6$. We consider a SISO system as well as a SIMO system with $N_r = 2$ receive antennas. For both cases we consider an OFDM transmission with $N = 128$ subcarriers and a cyclic prefix of length $\nu = 3$. We examine the performance of the PTEQ for $P = 1$ and $P = 2$. For the SISO system, the equalizer parameters are chosen as $Q' = 4$ and $L' = 10$ for $P = 1$ and $Q' = 8$ and $L' = 10$ for $P = 2$. For the SIMO system, the equalizer parameters are chosen as $Q' = 2$ and $L' = 8$ for $P = 1$ and $Q' = 4$ and $L' = 8$ for $P = 2$. Note that, in order to keep the same subcarrier span, the Q' for $P = 2$ is chosen to be twice as large as the Q' for $P = 1$. As shown in Figure 8.9, the PTEQ with $P = 2$ outperforms the PTEQ with $P = 1$ for the same

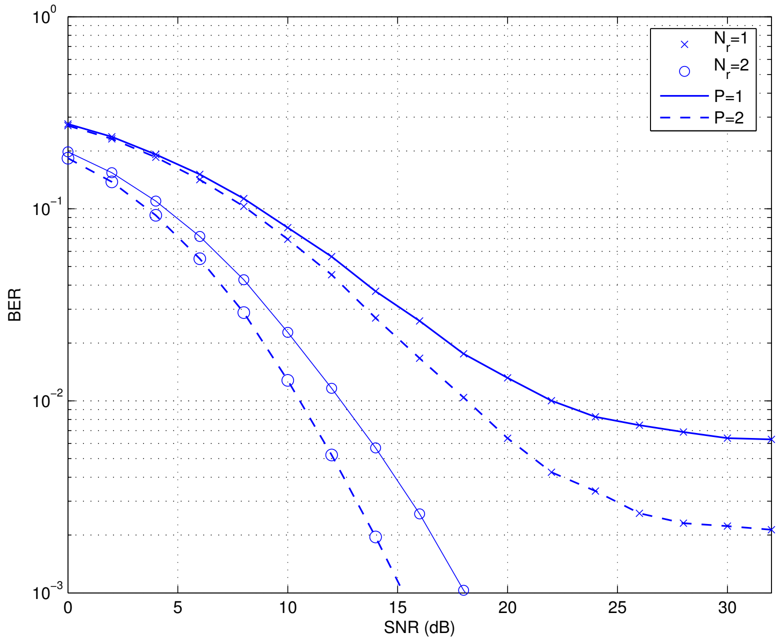

Figure 8.9: BER vs. SNR for the PTEQ, when the true channel is used to design the equalizer.

subcarrier span. For the SISO case, an SNR gain of 4 dB is obtained for the PTEQ with $P = 2$ over the PTEQ with $P = 1$ at $BER = 10^{-2}$. Similarly, an SNR gain of 2 dB is obtained for the PTEQ with $P = 2$ over the PTEQ with $P = 1$ at $BER = 10^{-2}$ for the SIMO case.

- Referring to **Example** 1.1 we consider the following set up:

  - We consider OFDM transmission over time-invariant (TI) as well as time-varying channels.
  - The channel is considered to be Rayleigh fading.
  - The channel taps adhere with the Nokia 6 tap model.
  - For the time-varying case we consider a Doppler frequency $f_{\max} = 300\ Hz$. The TI channel corresponds to zero Doppler frequency.
  - We consider uncoded transmission.

In the simulations we consider the 2k (2048 subcarriers are used) and 8k (8192 subcarriers are used) modes. We consider two types of equalizers:

1. Time-invariant (TI) equalizer:
   - The channel is TI, and hence a 1-tap frequency-domain equalizer is used.
   - The channel is time-varying: In this case we consider the channel to be time-varying and approximated by a TI one, and accordingly we use a 1-tap frequency-domain equalizer. The maximum Doppler shift is $f_{\max} = 300\ Hz$. For this case, the channel time average is used to design the equalizer. This corresponds to taking a basis expansion model fit for the channel of order zero.
2. Time-varying frequency-domain per-tone equalizer (PTEQ). The frequency-domain PTEQ combines neighboring subcarriers to estimate the transmitted symbol on a specific subcarrier. The span of neighboring subcarriers is determined by Q'. for complexity reasons, the BEM resolution K is taken as $K = N$, i.e. no oversampling is considered.

2k mode
The results concerning the 2k mode are shown in Figure 8.10. From this figure we draw the following conclusions/observations:

- For the case of time-varying channels, using a TI 1-tap frequency-domain equalizer results into an error floor at $BER = 4 \times 10^{-3}$.
- An SNR loss of 2dB at $BER = 10^{-2}$ is observed compared to the TI case with zero Doppler shift.
- The Doppler effect can be compensated for by using a PTEQ with ICI span $Q' = 4$. An SNR gain of 3dB at $BER = 10^{-2}$ is observed compared to the case of the TI 1-tap frequency-domain equalizer for the time-varying channel of Doppler spread $f_{\max} = 300\ Hz$.

8k mode
The results considering the 8k mode are shown in Figure 8.11. From this figure we can draw the following conclusions:

- The Doppler effect is more severe than that for the 2k mode. Assuming a TI channel results into a much earlier error floor compared to the 2k mode. The error floor is observed now at $BER = 5 \times 10^{2}$.
- The Doppler effect can be corrected by using a PTEQ with $Q' = 4$. The performance of the equalizer almost coincides with that of the TI case with zero Doppler shift.

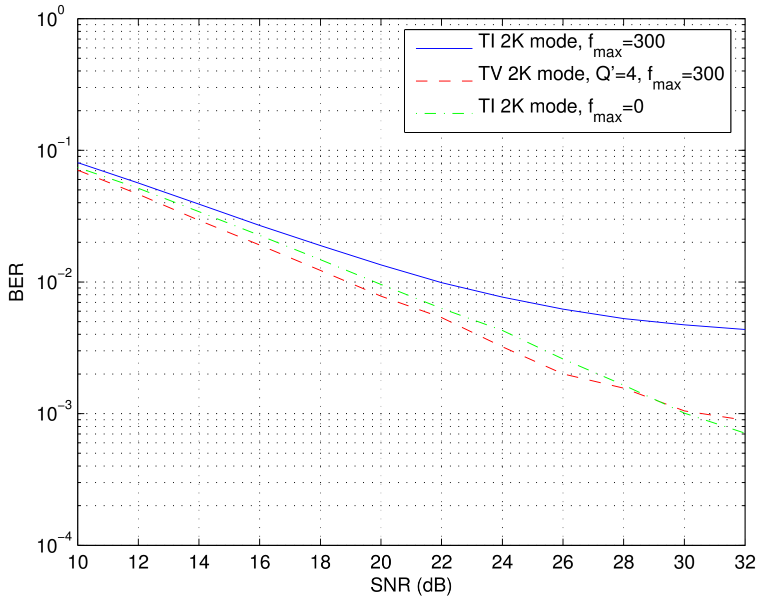

Figure 8.10: BER vs SNR for DVB-H 2k mode

- Increasing the equalizer order from $Q' = 4$ to $Q' = 6$, slightly enhances the performance especially at high SNR values.

8.6 Conclusions

In this chapter, we have proposed time-domain (TEQ) and a frequency-domain per-tone equalizer (PTEQ) for OFDM over doubly selective channels. We have considered the most general case where the channel delay spread is larger than the CP. The time-varying channel is approximated using the BEM. The TEQ is implemented as a time-varying FIR filter. We use a BEM to model the time-varying FIR TEQ. The PTEQ is then obtained by transferring the TEQ operation to the frequency-domain. Comparing the TEQ to the PTEQ we arrive at the following conclusions[2]:

- While the TEQ optimizes the performance on all subcarriers in a joint

[2]Note that some of these conclusions are analogous to the results obtained for the time-invariant case.

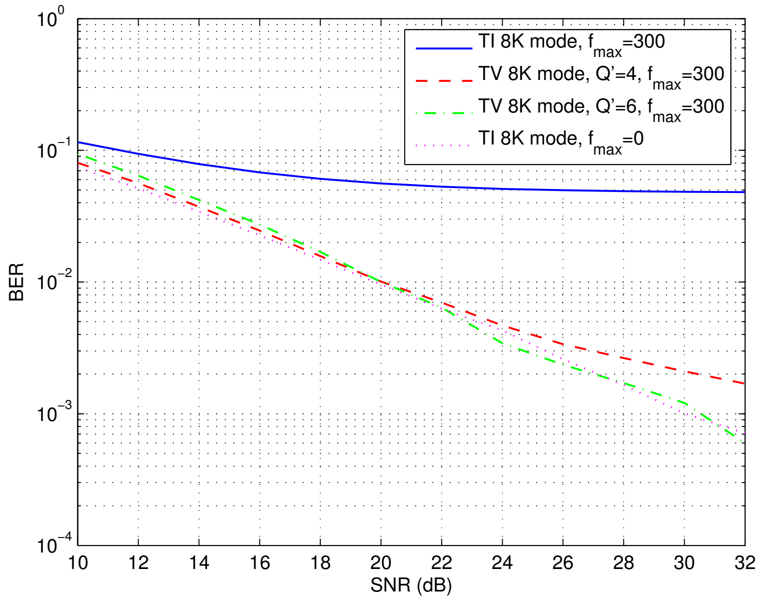

Figure 8.11: BER vs SNR for DVB-H 8k mode

fashion, the PTEQ optimizes the performance on each subcarrier separately, leading to improved performance.

- The design complexity of the PTEQ is higher than the design complexity of the TEQ.
- The implementation complexity of the PTEQ is comparable to the implementation complexity of the TEQ (apart from the fact that the PTEQ may require additional FFTs).

From the simulations we arrive at the following conclusions:

- The PTEQ always outperforms the TEQ.
- The PTEQ is less sensitive to the choice of the decision delay.
- A key parameter in the performance of the TEQ and PTEQ is the BEM frequency resolution. We show that a BEM resolution equal to twice the DFT resolution (the DFT size) is enough to get an acceptable performance.
- The PTEQ outperforms the conventional 1-tap FEQ for OFDM over TI channels.

- The PTEQ approaches the performance of the block MMSE equalizer for OFDM over doubly selective channels.
- Oversampling the received sequence while keeping the same ICI span gives an additional performance improvement.

Chapter 9

IQ Compensation for OFDM in the Presence of IBI and Carrier Frequency-Offset

9.1 Introduction

OFDM has been adopted for several applications like digital audio and video broadcasting [37] and chosen by the IEEE 802.11 standard [54] as well as by the HIPERLAN-2 standard [52] for wireless LAN (WLAN) transmission. This is due to its robustness against multipath fading and its relatively simple implementation. These properties are valid given that the channel is time-invariant and the OFDM receiver does not suffer from analog front-end impairments, and moreover, the CP length is larger than the channel impulse response length. In the previous chapter we tackled the problem of OFDM transmission over time-varying channels assuming ideal transmitter/receiver conditions. In this chapter we tackle the problem of OFDM transmission over TI channels for the case of a non-ideal receiver. We assume that the OFDM receiver suffers from analog front-end impairments, in particular the amplitude and phase imbalance (IQ imbalance) and carrier frequency-offset (CFO). Moreover, we assume that the CP length is shorter than the channel impulse response length. Extending this work to time-varying channels is rather straightforward, yet it significantly complicates the analysis. Note that CFO and the channel time-variation induce ICI almost in the same manner. This motivates us to apply here a similar analysis as in the previous chapter in order to mitigate ICI and in addition to compensate for the IQ imbalance.

The presence of IQ imbalance and CFO and the fact that the channel impulse response length may be larger than the CP length cause a severe degradation in performance of OFDM systems. This motivates us to search for alternative equalization techniques that are robust against these imperfections.

Different approaches have been proposed to overcome the analog front-end problems for OFDM transmission. In [81] a training based-technique for CFO estimation is proposed assuming perfect IQ balance. A maximum likelihood (ML) CFO estimation is proposed in [123], also assuming perfect IQ balance. The IQ imbalance only problem is treated in [103, 74, 98] assuming zero CFO. Joint compensation of IQ imbalance and CFO is treated in [104, 43]. In [104] it is assumed that the CFO is corrected based on perfect knowledge of the IQ imbalance parameters, and that the IQ imbalance parameters can be estimated correctly in the presence of CFO. The assumption here is valid for small CFO and small IQ imbalance parameters. In [43], nulled subcarriers are used to estimate the CFO by maximizing the energy on the designated subcarrier and its image and it is done by invoking an exhaustive search algorithm. *However, in the above mentioned works, the cyclic prefix (CP) is consistently assumed to be longer than or equal to the channel impulse response length.*

In this chapter we consider the case where the CP is shorter than the channel impulse response length, and furthermore IQ imbalance and CFO are present. We devise a frequency-domain per-tone equalization technique to combat the channel effect as well as the imperfection of the analog front-end. We first treat the case of IQ imbalance and zero CFO, and then extend the analysis to the case of IQ imbalance and non-zero CFO. The per-tone equalizer is obtained by transferring a time-domain equalizer (TEQ) to the frequency-domain. The purpose of the TEQ is to shorten the channel to fit within the CP and eliminate the effect of the IQ imbalance. The proposed PTEQ is first designed assuming perfect knowledge of the channel as well as the IQ imbalance parameters and the CFO or assuming they can be accurately estimated. This is, however, far from practical, since the channel estimate in the presence of IQ imbalance and/or CFO is typically not sufficiently accurate. To avoid the intermediate stage of parameters estimation, a training-based RLS-type initialization scheme is proposed for such per-tone equalization.

Note that here under the assumption that the IQ parameters and the channel impulse response are perfectly known at the receiver, then IQ compensation can be easily done in time-domain. However, in practice this assumption is far from true. In our analysis we are aiming at developing a PTEQ assuming perfect knowledge of the IQ parameters and the channel impulse response which paves the way for developing the RLS-based direct equalizer. On the other hand, when CFO is present, knowing the IQ parameters and CFO and the channel impulse response does not lead to a simple time-domain equalizer. We, therefore, develop a frequency-domain PTEQ assuming perfect knowledge of the different system parameters and then again develop a training-based RLS direct equalizer.

This chapter is organized as follows. In Section 9.2, we introduce the system model. The per-tone equalizer for the IQ only case is introduced in Section 9.3. In Section 9.4, the per-tone equalizer is extended to the case of IQ imbalance and CFO. Simulation results are introduced in Section 9.5. Finally, our conclusions are drawn in Section 9.6.

9.2 System Model

We consider OFDM transmission over time-invariant frequency-selective channels. We assume a single-input single-output (SISO) system, but the results can be easily extended to single-input multiple-output (SIMO) or multiple-input multiple-output (MIMO) systems. At the transmitter the information-bearing symbols are parsed into blocks of N frequency-domain QAM symbols. Each block is then transformed to the time-domain by an inverse discrete Fourier transform (IDFT). A cyclic prefix (CP) of length ν is added to the head of each block. The time domain blocks are then serially transmitted over the channel. In the ideal case where neither IQ imbalance nor CFO are present, the discrete time-domain baseband equivalent description of the received signal at time index n is given by:

$$y[n] = \sum_{l=0}^{L} h_l x[n-l] + v[n],$$

where h_l is the lth tap of the multipath fading channel, $v[n]$ is the baseband equivalent noise, and $x[n]$ is the discrete time-domain sequence transmitted at a rate of $1/T$ symbols per second. The channel is assumed to be time-invariant for a burst of OFDM symbols and may change independently from burst to burst. Assuming $S_k[i]$ is the QAM symbol transmitted on the kth subcarrier of the ith OFDM block, $x[n]$ can be written as

$$x[n] = \frac{1}{\sqrt{N}} \sum_{k=0}^{N-1} S_k[i] e^{j2\pi(m-\nu)k/N},$$

where $i = \lfloor n/(N+\nu) \rfloor$ and $m = n - i(N+\nu)$. Note that this description includes the transmission of a CP of length ν.

In this chapter we focus on OFDM transmission over TI channels with receiver front-end impairments. The front-end impairments we discuss in this chapter are IQ imbalance and CFO. The equivalent system model under consideration is depicted in Figure 9.1.

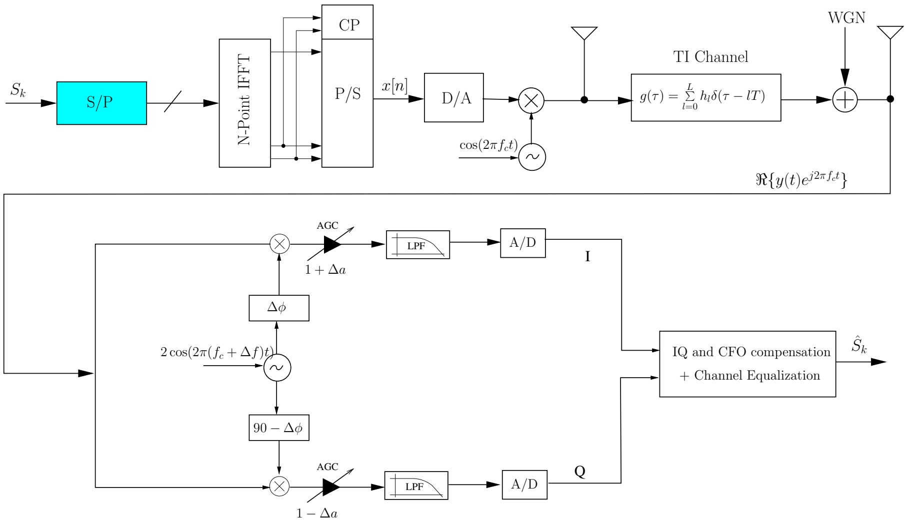

Figure 9.1: Block diagram of OFDM transmission over TI channel with Rx front-end impairments.

9.3 Equalization in the Presence of IQ Imbalance

In this section we tackle the problem of channel equalization for OFDM in the presence of IQ imbalance and IBI. In this section we assume zero CFO. The equalization problem in conjunction with IQ imbalance and CFO will be treated in Section 9.4. IQ imbalance is characterized by two parameters: the amplitude imbalance Δa and the phase mismatch $\Delta\phi$. The discrete-time baseband received sequence in the presence of IQ imbalance at time index n can be written as

$$r[n] = \gamma y[n] + \delta y^*[n] \tag{9.1}$$

where the parameters γ and δ are given by [109]

$$\begin{aligned} \gamma &= \cos(\Delta\phi) + \jmath \Delta a \sin(\Delta\phi) \\ \delta &= \Delta a \cos(\Delta\phi) - \jmath \sin(\Delta\phi) \end{aligned}$$

We further consider that the CP length is smaller than the channel order, which means that interlock interference (IBI) is present. To eliminate such IBI, time-domain filtering may be used to shorten the channel such that it fits within the CP. It is well-known that the presence of IQ imbalance results in the reception on subcarrier k of a mixture of the symbol transmitted on subcarrier k and the symbol transmitted on the mirror subcarrier $N - k$ (referred to as the image

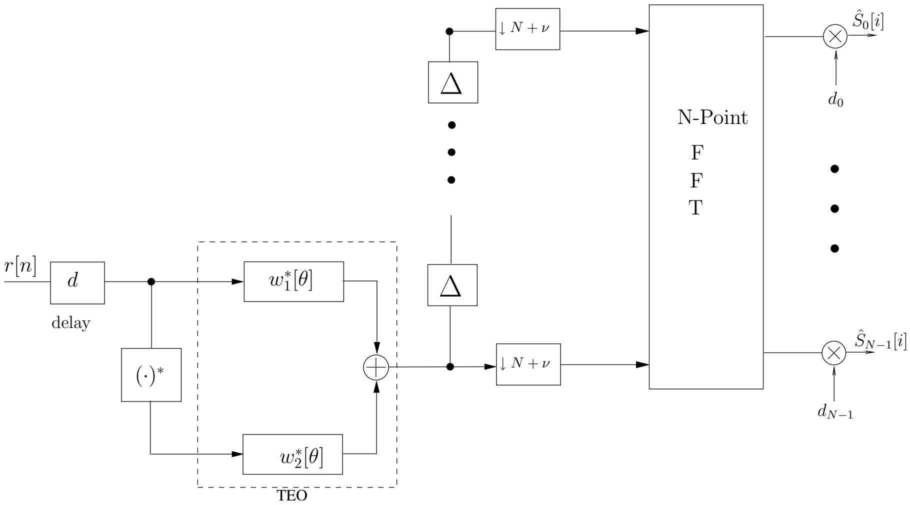

Figure 9.2: Time-domain equalizer block diagram.

signal). For this reason the conventional time-domain shortening where one time-domain equalizer (TEQ) is applied to the received signal is not sufficient. However, it will be shown that two TEQs can be used, where one is applied to the received signal and the other is applied to the conjugated version of the received sequence, as shown in Figure 9.2. The second TEQ is necessary here to compensate for the image symbol, as will become clear later.

The output of the TEQs subject to some decision delay d can be written as

$$z[n] = \sum_{l'=0}^{L'} w_{1,l'}^* r[n+d-l'] + \sum_{l'=0}^{L'} w_{2,l'}^* r^*[n+d-l'] \tag{9.2}$$

On a block level formulation, (9.2) can be written as

$$\mathbf{z}[i] = \mathbf{W}_1^H \mathbf{r}[i] + \mathbf{W}_2^H \mathbf{r}^*[i], \tag{9.3}$$

where $\mathbf{z}[i] = [z[i(N+\nu)+\nu, \ldots, z[(i+1)(N+\nu)-1]]^T$, $\mathbf{r}[i] = [r[i(N+\nu)+\nu+d-L'], \ldots, r[(i+1)(N+\nu)+d-1]]^T$, and $\mathbf{W}_p$ (for $p=1,2$) is an $(N+L')\times N$ Toeplitz matrix with first column $[w_{p,L'}, \ldots, w_{p,0}, \mathbf{0}_{1\times(N-1)}]^T$ and first row $[w_{p,L'}, \mathbf{0}_{1\times(N-1)}]$.

In conjunction with the time-domain filtering, a one-tap FEQ is applied to the received sequence in the frequency-domain to recover the transmitted QAM symbols. Define $\hat{S}_k[i]$ as the estimate of the transmitted QAM symbol on the kth subcarrier of the ith OFDM symbol. This estimate is then obtained as

$$\hat{S}_k[i] = \frac{1}{d_k}\left(\mathcal{F}^{(k)}\mathbf{W}_1^H \mathbf{r}[i] + \mathcal{F}^{(k)}\mathbf{W}_2^H \mathbf{r}^*[i]\right), \tag{9.4}$$

where d_k is the 1-tap FEQ operating on the kth subcarrier, and $\mathcal{F}^{(k)}$ is the $(k+1)$st row of the DFT matrix $\boldsymbol{\mathcal{F}}$.

Transferring the TEQ operation to the frequency domain we obtain

$$\hat{S}_k[i] = \tilde{\mathbf{w}}_1^{(k)H} \tilde{\boldsymbol{\mathcal{F}}}^{(k)} \mathbf{r}[i] + \tilde{\mathbf{w}}_2^{(k)H} \tilde{\boldsymbol{\mathcal{F}}}^{(k)} \mathbf{r}^*[i], \tag{9.5}$$

where $\tilde{\mathbf{w}}_p^{(k)} = [w_{p,1}, \ldots, w_{p,L'}]^T / d_k$, and $\tilde{\boldsymbol{\mathcal{F}}}^{(k)}$ is given by:

$$\tilde{\boldsymbol{\mathcal{F}}}^{(k)} = \begin{bmatrix} 0 & \cdots & 0 & \boxed{\mathcal{F}^{(k)}} \\ \vdots & 0 & \boxed{\mathcal{F}^{(k)}} & 0 \\ 0 & \iddots & \iddots \; 0 & \vdots \\ \boxed{\mathcal{F}^{(k)}} & & 0 \; \cdots & 0 \end{bmatrix}.$$

Note that the above matrix corresponds to performing a sliding DFT on the received sequence, which corresponds to performing $L'+1$ DFTs. The implementation of (9.5) can be significantly reduced by replacing the sliding DFT with one FFT and the remaining FFTs are compensated for by L' difference terms as explained in the following properties:

$$\tilde{\boldsymbol{\mathcal{F}}}^{(k)} \mathbf{r}[i] = \mathbf{T}^{(k)} \begin{bmatrix} R^{(k)}[i] \\ \Delta \mathbf{r}[i] \end{bmatrix} \begin{matrix} \updownarrow 1 \ \times 1 \\ \updownarrow L' \times 1 \end{matrix} , \tag{9.6a}$$

and

$$\tilde{\boldsymbol{\mathcal{F}}}^{(k)} \mathbf{r}^*[i] = \mathbf{T}^{(k)} \begin{bmatrix} R^{(N-k)*}[i] \\ \Delta \mathbf{r}^*[i] \end{bmatrix} \begin{matrix} \updownarrow 1 \ \times 1 \\ \updownarrow L' \times 1 \end{matrix} , \tag{9.6b}$$

where $R^{(k)}[i] = \mathcal{F}^{(k)}[r[i(N+\nu)+\nu+d], \ldots, r[(i+1)(N+\nu)+d-1]]^T$, $\mathbf{T}^{(k)}$ is an $(L'+1) \times (L'+1)$ lower triangular Toeplitz matrix given by:

$$\mathbf{T}^{(k)} = \begin{bmatrix} 1 & 0 & \cdots & 0 \\ \beta^k & \ddots & \ddots & \vdots \\ \vdots & \ddots & \ddots & 0 \\ \beta^{kL'} & \cdots & \beta^k & 1 \end{bmatrix}, \tag{9.7}$$

with $\beta = e^{-j2\pi/N}$. The difference terms $\Delta \mathbf{r}[i]$ are given by:

$$\Delta \mathbf{r}[i] = \begin{bmatrix} r[i(N+\nu)+\nu+d-1] - r[(i+1)(N+\nu)+d-1] \\ \vdots \\ r[i(N+\nu)+\nu+d-L'] - r[(i+1)(N+\nu)+d-L'-1] \end{bmatrix}.$$

By defining $\mathbf{v}_1^{(k)H} = \tilde{\mathbf{w}}_1^{(k)H} \mathbf{T}^{(k)}$, and $\mathbf{v}_2^{(k)H} = \tilde{\mathbf{w}}_2^{(k)H} \mathbf{T}^{(k)}$, formula (9.5) can be written as

$$\hat{S}_k[i] = \mathbf{v}_1^{(k)H} \begin{bmatrix} R^{(k)}[i] \\ \Delta \mathbf{r}[i] \end{bmatrix} + \mathbf{v}_2^{(k)H} \begin{bmatrix} R^{(N-k)*}[i] \\ \Delta \mathbf{r}^*[i] \end{bmatrix}. \tag{9.8}$$

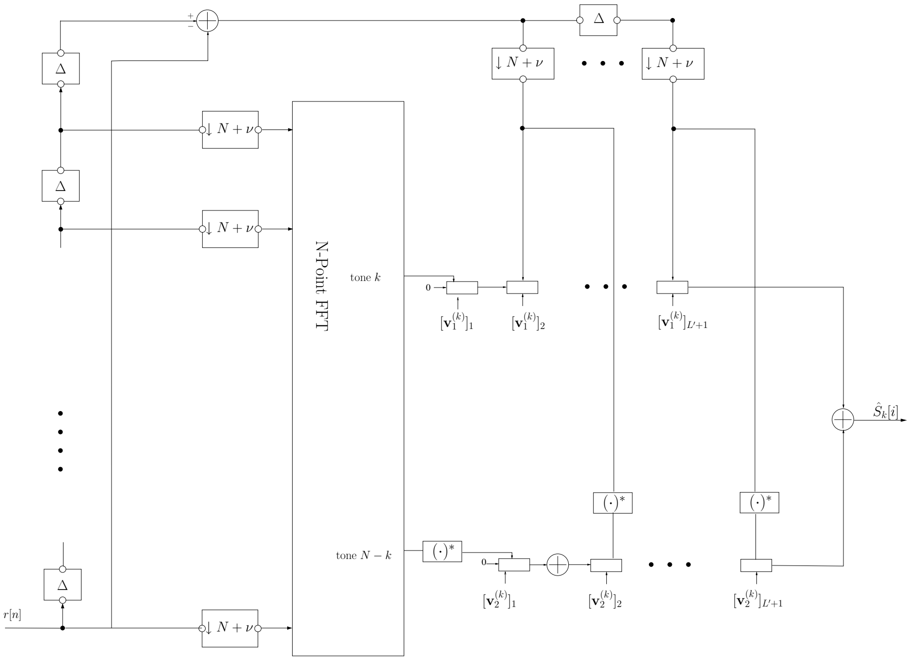

Figure 9.3: PTEQ for OFDM with IQ imbalance.

Note that due to the IQ imbalance the quantity $R^{(k)}[i]$ contains information about $S_k[i]$ as well as $S_{N-k}[i]$ for $k \in \{1, \ldots, N/2-1\}$. The same holds for the quantity $R^{(N-k)}[i]$. A proper equalizer should then consider the estimation of the transmitted QAM symbol on the kth subcarrier and the transmitted QAM symbol on the $(N-k)$th subcarrier in a joint fashion.

Hence, we can write the estimate of the transmitted QAM symbol on the $(N-k)$th subcarrier as

$$\hat{S}_{N-k}[i] = \mathbf{v}_1^{(N-k)H} \begin{bmatrix} R^{(N-k)}[i] \\ \Delta\mathbf{r}[i] \end{bmatrix} + \mathbf{v}_2^{(N-k)H} \begin{bmatrix} R^{(k)*}[i] \\ \Delta\mathbf{r}^*[i] \end{bmatrix}. \tag{9.9}$$

Combining (9.8) and (9.9) we arrive at

$$\underbrace{\begin{bmatrix} \hat{S}_k[i] \\ \hat{S}^*_{N-k}[i] \end{bmatrix}}_{\tilde{\mathbf{s}}_k[i]} = \underbrace{\begin{bmatrix} \mathbf{v}_1^{(k)H} & \mathbf{v}_2^{(k)H} \\ \mathbf{v}_2^{(N-k)T} & \mathbf{v}_1^{(N-k)T} \end{bmatrix}}_{\mathbf{V}_k^H} \underbrace{\begin{bmatrix} R^{(k)}[i] \\ \Delta\mathbf{r}[i] \\ R^{(N-k)*}[i] \\ \Delta\mathbf{r}^*[i] \end{bmatrix}}_{\tilde{\mathbf{r}}_k[i]} \tag{9.10}$$

The implementation of (9.10) is shown in Figure 9.3. The relation between

$\tilde{\mathbf{r}}_k[i]$ (defined in (9.10)) and the received sequence can be drawn as

$$\tilde{\mathbf{r}}_k[i] = \underbrace{\begin{bmatrix} \mathbf{F}^{(k)} & \mathbf{0} \\ \mathbf{0} & \mathbf{F}^{(N-k)*} \end{bmatrix}}_{\tilde{\mathbf{F}}_k} \begin{bmatrix} \mathbf{r}[i] \\ \mathbf{r}^*[i] \end{bmatrix} \tag{9.11}$$

where $\mathbf{F}^{(k)}$ is given by:

$$\mathbf{F}^{(k)} = \left[\begin{array}{ccc} \mathbf{0}_{1\times L'} & & \mathcal{F}^{(k)} \\ \hline \bar{\mathbf{I}}_{L'} & \mathbf{0}_{L'\times(N-L')} & -\bar{\mathbf{I}}_{L'} \end{array} \right]$$

with $\bar{\mathbf{I}}_{L'}$ the anti-diagonal identity matrix of size $L' \times L'$.

At this point we may introduce a model for the received sequence $\mathbf{r}[i]$. Define $\mathbf{y}[i] = [y[i(N+\nu)+\nu+d-L'], \ldots, y[(i+1)(N+\nu)+d-1]]^T$, $\mathbf{y}[i]$ can be written as

$$\mathbf{y}[i] = \underbrace{[\boldsymbol{O}_1, \mathbf{H}, \boldsymbol{O}_2]}_{\tilde{\mathbf{H}}} (\mathbf{I}_3 \otimes \mathbf{P}) \left(\mathbf{I}_3 \otimes \boldsymbol{\mathcal{F}}^H\right) \begin{bmatrix} \mathbf{s}[i-1] \\ \mathbf{s}[i] \\ \mathbf{s}[i+1] \end{bmatrix} + \mathbf{v}[i], \tag{9.12}$$

where $\boldsymbol{O}_1 = \mathbf{0}_{(N+L')\times(N+2\nu+d-L-L')}$, $\boldsymbol{O}_2 = \mathbf{0}_{(N+L')\times(N+\nu-d)}$, $\mathbf{H}$ is an $(N+L')\times(N+L'+L)$ Toeplitz matrix with first column $[h_L, \mathbf{0}_{1\times(N+L'-1)}]^T$ and first row $[h_L, \ldots, h_0, \mathbf{0}_{1\times(N+L'-L-1)}]$, and $\mathbf{P}$ is the CP insertion matrix given by:

$$\mathbf{P} = \begin{bmatrix} \mathbf{0}_{\nu\times(N-\nu)} & \mathbf{I}_\nu \\ \multicolumn{2}{c}{\mathbf{I}_N} \end{bmatrix},$$

and the transmitted vector of QAM symbols transmitted on the ith OFDM block $\mathbf{s}[i] = [S_0[i], \ldots, S_{N-1}[i]]^T$. Hence, we can write the received sequence and its conjugate as

$$\begin{bmatrix} \mathbf{r}[i] \\ \mathbf{r}^*[i] \end{bmatrix} = \underbrace{\begin{bmatrix} \gamma\tilde{\mathbf{H}}(\mathbf{I}_3\otimes\mathbf{P})\left(\mathbf{I}_3\otimes\boldsymbol{\mathcal{F}}^H\right) & \delta\tilde{\mathbf{H}}^*(\mathbf{I}_3\otimes\mathbf{P})\left(\mathbf{I}_3\otimes\boldsymbol{\mathcal{F}}^H\right) \\ \delta^*\tilde{\mathbf{H}}(\mathbf{I}_3\otimes\mathbf{P})\left(\mathbf{I}_3\otimes\boldsymbol{\mathcal{F}}^H\right) & \gamma^*\tilde{\mathbf{H}}^*(\mathbf{I}_3\otimes\mathbf{P})\left(\mathbf{I}_3\otimes\boldsymbol{\mathcal{F}}^H\right) \end{bmatrix}}_{\mathbf{G}}$$

$$\times \begin{bmatrix} \mathbf{s}[i-1] \\ \mathbf{s}[i] \\ \mathbf{s}[i+1] \\ \mathbf{Z}_1\mathbf{s}^*[i-1] \\ \mathbf{Z}_1\mathbf{s}^*[i] \\ \mathbf{Z}_1\mathbf{s}^*[i+1] \end{bmatrix} + \tilde{\mathbf{v}}[i], \tag{9.13}$$

where $\mathbf{Z}_1$ is an $N \times N$ matrix defined as

$$\mathbf{Z}_1 = \begin{bmatrix} 1 & 0 & \cdots & 0 \\ 0 & & & \\ \vdots & & \bar{\mathbf{I}}_{N-1} & \\ 0 & & & \end{bmatrix},$$

To obtain the PTEQ coefficients for the k and $N-k$ subcarriers (i.e. solve for $\mathbf{V}_k$), we define the following mean-square error (MSE) cost function:

$$\mathcal{J} = \mathcal{E}\left\{ \left\| \tilde{\mathbf{s}}_k - \mathbf{V}_k^H \tilde{\mathbf{r}}_k \right\|^2 \right\}.$$

The minimum MSE (MMSE) solution can be then obtained as

$$\mathbf{V}_k = \arg\min_{\mathbf{V}_k} \mathcal{J}. \tag{9.14}$$

The solution of (9.14) is obtained by solving $\partial\mathcal{J}/\partial\mathbf{V}_k = \mathbf{0}$ and equals:

$$\mathbf{V}_k = \left(\tilde{\mathbf{F}}_k \left(\mathbf{G}\mathbf{R}_s\mathbf{G}^H + \mathbf{R}_{\tilde{v}} \right) \tilde{\mathbf{F}}_k^H \right)^{-1} \tilde{\mathbf{F}}_k \mathbf{G}\mathbf{R}_s [\mathbf{e}_{3N+k+1}\mathbf{e}_{4N+k+1}]. \tag{9.15}$$

where $\mathbf{R}_s$ and $\mathbf{R}_{\tilde{v}}$ are the transmitted symbols covariance matrix, and the noise covariance matrix respectively, and $\mathbf{e}_{k'}$ is a $6N$ long unity vector with a 1 in the k'th position.

For the case of OFDM transmission over TI channel with a CP length that is larger than the channel impulse response length, we can consider a TEQ of order $L' = 0$ and the decision delay that does not have to be different from zero (i.e. $d = 0$). The estimate of $\tilde{\mathbf{s}}_k[i]$ in (9.10) becomes as follows (see also [98])

$$\tilde{\mathbf{s}}_k[i] = \mathbf{V}_k^H \tilde{\mathbf{r}}_k[i] \tag{9.16}$$

with

$$\mathbf{V}_k = \begin{bmatrix} V_1^{(k)} & V_2^{(N-k)*} \\ V_2^{(k)} & V_1(N-k)* \end{bmatrix}$$

and

$$\tilde{\mathbf{r}}_k[i] = \begin{bmatrix} R^{(k)}[i] \\ R^{(N-k)*}[i] \end{bmatrix}$$

For this case the received symbol at the k subcarrier in the ith OFDM block $R^{(k)}[i]$ can be written as

$$R^{(k)}[i] = \gamma H_k S_k[i] + \delta H_{N-k}^* S_{N-k}^*[i] + \tilde{\Xi}_k[i], \tag{9.17}$$

where H_k is the channel frequency response at the kth subcarrier and $\tilde{\Xi}_k[i]$ is the noise on the kth subcarrier in the ith OFDM block. Hence, we can write (9.16) as

$$\tilde{\mathbf{s}}_k[i] = \begin{bmatrix} V_1^{(k)} & V_2^{(N-k)*} \\ V_2^{(k)} & V_1^{(N-k)*} \end{bmatrix} \begin{bmatrix} \gamma H_k & \delta H_{N-k} \\ \delta^* H_k^* & \gamma^* H_{N-k}^* \end{bmatrix} \begin{bmatrix} S_k[i] \\ S_{N-k}^*[i] \end{bmatrix} + \begin{bmatrix} \tilde{\Xi}_k[i] \\ \tilde{\Xi}_{N-k}^*[i] \end{bmatrix} \tag{9.18}$$

In the noiseless case perfect symbol estimation (i.e. zero-forcing (ZF) equalization) is possible as long as the channel does not experience deep fades on subcarrier k and subcarrier $N-k$ simultaneously. Note that with only one TEQ, the ZF solution does not exist. While, the MMSE solution always exists. However, it can be easily shown that the MMSE solution with one TEQ has a very poor performance.

Equation (9.15) requires that the channel and the IQ imbalance parameters are known at the receiver. If the IQ imbalance parameters are known then probably it is better to do a time-domain IQ-compensation based on (9.1) [103], and then a per-tone equalization, which leads to a much simpler solution. In practice, since it is hard to obtain the IQ and the channel impulse response sufficiently accurate, we look for direct initialization schemes, which indeed skip the estimation stage. The previous analysis was however essential to define a proper equalizer structure. In the following we discuss a training-based recursive least squares (RLS) initialization scheme for direct equalization.

RLS Initialization

In our discussion so far in developing our PTEQ, we have assumed that the channel and the IQ imbalance parameters are known at the receiver. In this subsection, we will derive a training-based RLS algorithm for direct equalizer design without passing through the intermediate stage of channel and IQ imbalance parameters estimation. Assume that I OFDM symbols are dedicated for training, the optimal $\mathbf{V}_k$ for the kth subcarrier can be computed as

$$\min_{\mathbf{V}_k} \mathcal{J}(\mathbf{V}_k) = \min_{\mathbf{V}_k} \sum_{i=0}^{K-1} \left\| \tilde{\mathbf{s}}_k[i] - \mathbf{V}_k^H \tilde{\mathbf{r}}_k[i] \right\|^2 \tag{9.19}$$

The problem in (9.19) can be solved recursively. The RLS algorithm for finding the PTEQ coefficients is listed in Algorithm 9.1.

9.4 Equalization in the Presence of IQ and CFO

In Section 9.3 we tackled the problem of per-tone equalization for OFDM in the presence of IQ imbalance and zero CFO. In this section, we assume that the receiver analog front-end suffers from CFO due to drift in the local oscillator. Due to the CFO, the orthogonality between subcarriers is destroyed. In addition we again assume that the analog front-end suffers from an IQ imbalance and the CP length is smaller than the channel impulse response length. Assuming that the local oscillator exhibits a CFO of $\epsilon = \Delta f T$, the base-band equivalent received sequence at time index n is given by [104, 119]:

$$r[n] = \gamma e^{j2\pi\epsilon n/N} y[n] + \delta e^{-j2\pi\epsilon n/N} y^*[n]. \tag{9.20}$$

Algorithm 9.1 RLS Direct Equalization

for $k \in \{1, \ldots, N/2-1\}$ **do**
  initialize $\mathbf{R}_{\tilde{r}}^{k}[-1] = \kappa^{-1}\mathbf{I}$
  initialize $\mathbf{V}_k[-1] = \mathbf{0}_{2(L'+1)\times 2}$
end for
for $i = 0$ to I **do**
  for $k \in \{1, \ldots, N/2-1\}$ **do**
    $\mathbf{R}_{\tilde{r}}^{k^{-1}}[i] \leftarrow \mathbf{R}_{\tilde{r}}^{k^{-1}}[i-1] - \frac{\mathbf{R}_{\tilde{r}}^{k^{-1}}[i-1]\tilde{\mathbf{r}}_k[i]\tilde{\mathbf{r}}_k^H[i]\mathbf{R}_{\tilde{r}}^{k^{-1}}[i-1]}{1+\tilde{\mathbf{r}}_k^H[i]\mathbf{R}_{\tilde{r}}^{k^{-1}}[i-1]\tilde{\mathbf{r}}_k[i]}$
    $\mathbf{e}[i] = \tilde{\mathbf{s}}_k[i] - \mathbf{V}_k^H[i-1]\tilde{\mathbf{r}}_k[i]$
    $\mathbf{V}_k[i] \leftarrow \mathbf{V}_k[i-1] + \frac{\mathbf{R}_{\tilde{r}}^{k^{-1}}[i-1]\tilde{\mathbf{r}}_k[i]}{1+\tilde{\mathbf{r}}_k^H[i]\mathbf{R}_{\tilde{r}}^{k^{-1}}[i-1]\tilde{\mathbf{r}}_k[i]}\mathbf{e}[i]^H$
  end for
end for

where κ is a small positive constant.

On a block level formulation, (9.20) can be written as

$$\mathbf{r}[i] = \gamma\alpha_i\mathbf{D}_\epsilon\mathbf{y}[i] + \delta\alpha_i^*\mathbf{D}_\epsilon^*\mathbf{y}^*[i], \tag{9.21}$$

where $\alpha_i = e^{j2\pi(i(N+\nu)+\nu+d-L')\epsilon/N}$, and $\mathbf{D}_\epsilon = \text{diag}\{[1, \cdots, e^{j2\pi(N+L'-1)\epsilon/N}]^T\}$.

Similar to the case of IQ imbalance only, we start from the time-domain equalization. In the time-domain we apply two TEQs; one is applied to the received sequence and the other one is applied to a conjugated version of the received sequence. Similar to (9.3), the output of the TEQs in the ith OFDM block can be written as

$$\mathbf{z}[i] = \mathbf{W}_1^H[i]\mathbf{r}[i] + \mathbf{W}_2^H[i]\mathbf{r}^*[i]. \tag{9.22}$$

Note that unlike (9.3), the TEQs are time varying. The time variance here stems from the fact that the presence of CFO also imposes time-variations on the system, and hence, the TEQs may change from block to block.

The purpose of the TEQs is to eliminate IBI and ICI and to compensate for the IQ imbalance and CFO. In other words, to restore the orthogonality between subcarriers that was destroyed by IBI/ICI and compensate for the mirroring effect induced by the IQ imbalance. Hence, the TEQ is required to shorten the channel into a target impulse response which length fits within the CP and to eliminate ICI (eliminate the time-variations imposed on the system due to CFO). Designing and optimizing the performance of the TEQ is beyond the scope of this chapter. In this section, we are targeting frequency-domain per-tone equalizers, which are obtained by transferring the TEQ operation to the frequency-domain, as will become clear later.

It was shown in Chapter 8 that modeling the TEQ using the basis expansion model (BEM) is an efficient way to tackle the problem of IBI/ICI for OFDM transmission over doubly selective channels. Using the BEM to model the TEQs, $\mathbf{W}_1[i]$ and $\mathbf{W}_2[i]$ can be written as

$$\mathbf{W}_p[i] = \sum_{q=-Q/2}^{Q/2} \mathbf{W}_{p,q}[i]\tilde{\mathbf{D}}_q^*, \qquad \text{for } p = 1, 2, \tag{9.23}$$

where $\tilde{\mathbf{D}}_q = \text{diag}\{[1, \cdots, e^{j2\pi q(N-1)/N}]^T\}$, and $\mathbf{W}_{p,q}[i]$ is an $(N + L') \times N$ Toeplitz matrix with first column $[w_{p,q,L'}[i], \ldots, w_{p,q,0}[i], \mathbf{0}_{1\times(N-1)}]^T$ and first row $[w_{p,q,L'}[i], \mathbf{0}_{1\times(N-1)}]$. In conjunction with the time-domain filtering, a 1-tap FEQ is applied in the frequency-domain to recover the transmitted QAM symbols. Hence, an estimate of the QAM symbol transmitted on the kth subcarrier in the ith OFDM block can be written as

$$\begin{aligned}\hat{S}_k[i] &= \frac{1}{d_k}\left(\mathcal{F}^{(k)} \sum_{q=-Q/2}^{Q/2} \tilde{\mathbf{D}}_q \mathbf{W}_{1,q}^H[i]\mathbf{r}[i] + \mathcal{F}^{(k)} \sum_{q=-Q/2}^{Q/2} \tilde{\mathbf{D}}_q \mathbf{W}_{2,q}^H[i]\mathbf{r}^*[i]\right) \\ &= \frac{1}{d_k}\left(\sum_{q=-Q/2}^{Q/2} \mathcal{F}^{(k-q)}\mathbf{W}_{1,q}^H[i]\mathbf{r}[i] + \sum_{q=-Q/2}^{Q/2} \mathcal{F}^{(k-q)}\mathbf{W}_{2,q}^H[i]\mathbf{r}^*[i]\right) \end{aligned} \tag{9.24}$$

A PTEQ is then obtained by transferring the TEQ operation to the frequency-domain. Doing so we obtain the estimate of the transmitted QAM symbol at the kth subcarrier in the ith OFDM symbol as

$$\hat{S}_k[i] = \sum_{q=-Q/2}^{Q/2} \tilde{\mathbf{w}}_{1,q}^{(k)H}[i]\tilde{\boldsymbol{\mathcal{F}}}^{(k-q)}\mathbf{r}[i] + \sum_{q=-Q/2}^{Q/2} \tilde{\mathbf{w}}_{2,q}^{(k)H}[i]\tilde{\boldsymbol{\mathcal{F}}}^{(k-q)}\mathbf{r}^*[i] \tag{9.25}$$

where $\tilde{\mathbf{w}}_{p,q}^{(k)}[i] = [w_{p,q,0}^{(k)}[i], \ldots, w_{p,q,L'}^{(k)}[i]]^T/d_k$ for $p = 1, 2$. Using the properties introduced in (9.6a) and (9.6b) and defining $\mathbf{v}_{1,q}^{(k)H}[i] = \tilde{\mathbf{w}}_{1,q}^{(k)H}[i]\mathbf{T}^{(k-q)}$ and $\mathbf{v}_{2,q}^{(k)H}[i] = \tilde{\mathbf{w}}_{2,q}^{(k)H}[i]\mathbf{T}^{(k-q)}$, (9.25) can now be written as

$$\hat{S}_k[i] = \sum_{q=-Q/2}^{Q/2} \mathbf{v}_{1,q}^{(k)H}[i] \begin{bmatrix} R^{(k-q)}[i] \\ \Delta\mathbf{r}[i] \end{bmatrix} + \sum_{q=-Q/2}^{Q/2} \mathbf{v}_{2,q}^{(k)H}[i] \begin{bmatrix} R^{(N-k+q)*}[i] \\ \Delta\mathbf{r}^*[i] \end{bmatrix} \tag{9.26}$$

Define $\mathbf{v}_1^{(k)}[i] = [\mathbf{v}_{1,-Q/2}^{(k)T}[i], \ldots, \mathbf{v}_{1,Q/2}^{(k)T}[i]]^T$ and $\mathbf{v}_2^{(k)}[i] = [\mathbf{v}_{2,-Q/2}^{(k)T}[i], \ldots, \mathbf{v}_{2,Q/2}^{(k)T}[i]]^T$. Define the selection matrix $\mathbf{J}$ as

$$\mathbf{J} = \begin{bmatrix} \mathbf{I}_{Q+1} \otimes \tilde{\mathbf{I}}_{L'+1} \\ \mathbf{0}_{L'\times(Q+1)(L'+1)} \end{bmatrix} + \begin{bmatrix} \mathbf{0}_{(Q+1)\times(Q+1)(L'+1)} \\ \mathbf{1}_{Q+1}^T \otimes \tilde{\tilde{\mathbf{I}}}_{L'+1} \end{bmatrix},$$

where $\tilde{\mathbf{I}}_{L'+1}$ is the first row of the matrix $\mathbf{I}_{L'+1}$ and $\tilde{\tilde{\mathbf{I}}}_{L'+1}$ is the matrix consisting of the last L' rows of the matrix $\mathbf{I}_{L'+1}$. Finally, define $\mathbf{u}_1^{(k)}[i] = \mathbf{J}\mathbf{v}_1^{(k)}[i]$ and $\mathbf{u}_2^{(k)}[i] = \mathbf{J}\mathbf{v}_2^{(k)}[i]$, formula (9.26) can now be written as

$$\hat{S}_k[i] = \mathbf{u}_1^{(k)H}[i] \begin{bmatrix} R^{(k+Q/2)}[i] \\ \vdots \\ R^{(k-Q/2)}[i] \\ \Delta\mathbf{r}[i] \end{bmatrix} + \mathbf{u}_2^{(k)H}[i] \begin{bmatrix} R^{(N-k-Q/2)*}[i] \\ \vdots \\ R^{(N-k+Q/2)*}[i] \\ \Delta\mathbf{r}^*[i] \end{bmatrix} \tag{9.27}$$

Due to the IQ imbalance the mirroring effect arises, and hence a proper equalizer takes into account this effect by estimating the transmitted symbol on subcarrier k and its mirror subcarrier $N-k$ in a joint fashion. Writing a similar equation for the estimated symbol on the $(N-k)$th subcarrier and combining it with (9.27) we arrive at

$$\underbrace{\begin{bmatrix} \hat{S}_k[i] \\ \hat{S}^*_{N-k}[i] \end{bmatrix}}_{\tilde{\mathbf{s}}_k[i]} = \underbrace{\begin{bmatrix} \mathbf{u}_1^{(k)H}[i] & \mathbf{u}_2^{(k)H}[i] \\ \mathbf{u}_2^{(N-k)T}[i] & \mathbf{u}_1^{(N-k)T}[i] \end{bmatrix}}_{\mathbf{U}_k^H[i]} \underbrace{\begin{bmatrix} R^{(k+Q/2)}[i] \\ \vdots \\ R^{(k-Q/2)}[i] \\ \Delta\mathbf{r}[i] \\ R^{(N-k-Q/2)*}[i] \\ \vdots \\ R^{(N-k+Q/2)*}[i] \\ \Delta\mathbf{r}^*[i] \end{bmatrix}}_{\tilde{\mathbf{r}}_k[i]}. \tag{9.28}$$

From (9.28) the estimate of the QAM transmitted symbols can be obtained by applying a time-varying PTEQ that varies from block to block. However, the implementation/computation of the time-varying PTEQ $\mathbf{U}_k^H[i]$ can be significantly reduced by splitting the PTEQ into two parts: a time-invariant part that is fixed as long as the channel is stationary and a time-varying part that can be compensated for by means of a complex rotation applied to all subcarriers in the same OFDM block, as will become clear later on.

Note that $\tilde{\mathbf{r}}_k[i]$ defined in (9.28) can now be written as

$$\tilde{\mathbf{r}}_k[i] = \underbrace{\begin{bmatrix} \mathbf{F}^{(k)} & \mathbf{0} \\ \mathbf{0} & \mathbf{F}^{(N-k)*} \end{bmatrix}}_{\tilde{\mathbf{F}}_k} \begin{bmatrix} \mathbf{r}[i] \\ \mathbf{r}^*[i] \end{bmatrix} \tag{9.29}$$

where $\mathbf{F}^{(k)}$ is given by:

$$\mathbf{F}^{(k)} = \left[\begin{array}{ccc} \mathbf{0}_{1\times L'} & & \mathcal{F}^{(k+Q/2)} \\ & \vdots & \\ \mathbf{0}_{1\times L'} & & \mathcal{F}^{(k-Q/2)} \\ \hline \bar{\mathbf{I}}_{L'} & \mathbf{0}_{L'\times(N-L')} & -\bar{\mathbf{I}}_{L'} \end{array}\right]$$

We can also write the received sequence and its conjugate as

$$\begin{bmatrix}\mathbf{r}[i]\\ \mathbf{r}^*[i]\end{bmatrix} = \underbrace{\begin{bmatrix}\gamma\mathbf{D}_\epsilon\tilde{\mathbf{H}}\left(\mathbf{I}_3\otimes\mathbf{P}\right)\left(\mathbf{I}_3\otimes\boldsymbol{\mathcal{F}}^H\right) & \delta\mathbf{D}_\epsilon^*\tilde{\mathbf{H}}^*\left(\mathbf{I}_3\otimes\mathbf{P}\right)\left(\mathbf{I}_3\otimes\boldsymbol{\mathcal{F}}^H\right)\\ \delta^*\mathbf{D}_\epsilon\tilde{\mathbf{H}}\left(\mathbf{I}_3\otimes\mathbf{P}\right)\left(\mathbf{I}_3\otimes\boldsymbol{\mathcal{F}}^H\right) & \gamma^*\mathbf{D}_\epsilon^*\tilde{\mathbf{H}}^*\left(\mathbf{I}_3\otimes\mathbf{P}\right)\left(\mathbf{I}_3\otimes\boldsymbol{\mathcal{F}}^H\right)\end{bmatrix}}_{\mathbf{G}}$$

$$\times \underbrace{\begin{bmatrix}\alpha_i\mathbf{I}_{3N} & \mathbf{0}_{3N\times 3N}\\ \mathbf{0}_{3N\times 3N} & \alpha_i^*\mathbf{I}_{3N}\end{bmatrix}}_{\boldsymbol{\Lambda}[i]}\begin{bmatrix}\mathbf{s}[i-1]\\ \mathbf{s}[i]\\ \mathbf{s}[i+1]\\ \mathbf{Z}_1\mathbf{s}^*[i-1]\\ \mathbf{Z}_1\mathbf{s}^*[i]\\ \mathbf{Z}_1\mathbf{s}^*[i+1]\end{bmatrix} + \tilde{\mathbf{v}}[i], \tag{9.30}$$

To solve for $\mathbf{U}_k[i]$, we define the following MMSE cost function:

$$\mathcal{J}(\mathbf{U}_k[i]) = \mathcal{E}\left\{\|\tilde{\mathbf{s}}_k[i] - \mathbf{U}_k^H[i]\tilde{\mathbf{r}}_k[i]\|^2\right\}.$$

Hence, the MMSE solution of $\mathbf{U}_k[i]$ can be obtained by setting $\partial\mathcal{J}(\mathbf{U}_k[i])/\partial\mathbf{U}_k[i] = \mathbf{0}$, and equals:

$$\mathbf{U}_k[i] = \left(\tilde{\mathbf{F}}_k\left(\mathbf{G}\boldsymbol{\Lambda}[i]\mathbf{R}_s\boldsymbol{\Lambda}^H[i]\mathbf{G}^H + \mathbf{R}_{\tilde{v}}\right)\tilde{\mathbf{F}}_k^H\right)^{-1}\tilde{\mathbf{F}}_k\mathbf{G}\boldsymbol{\Lambda}[i]\mathbf{R}_s[\mathbf{e}_k\mathbf{e}_k]. \tag{9.31}$$

For a white source $\mathbf{R}_s = \sigma_s^2\mathbf{I}$, formula (9.31) can be written as

$$\begin{aligned}\mathbf{U}_k[i] &= \left(\tilde{\mathbf{F}}_k\left(\mathbf{G}\mathbf{G}^H + \sigma_s^{-2}\mathbf{R}_{\tilde{v}}\right)\tilde{\mathbf{F}}_k^H\right)^{-1}\tilde{\mathbf{F}}_k\mathbf{G}\boldsymbol{\Lambda}[i][\mathbf{e}_{N+k+1}\mathbf{e}_{4N+k+1}]\\ &= \underbrace{\left(\tilde{\mathbf{F}}_k\left(\mathbf{G}\mathbf{G}^H + \sigma_s^{-2}\mathbf{R}_{\tilde{v}}\right)\tilde{\mathbf{F}}_k^H\right)^{-1}\tilde{\mathbf{F}}_k\mathbf{G}[\mathbf{e}_{N+k+1}\mathbf{e}_{4N+k+1}]}_{\mathbf{Q}_k}\underbrace{\begin{bmatrix}\alpha_i & 0\\ 0 & \alpha_i^*\end{bmatrix}}_{\tilde{\boldsymbol{\Lambda}}[i]}\end{aligned} \tag{9.32}$$

The MMSE PTEQ obtained in (9.32) for the case of a white input source consists of two parts. A time-invariant part denoted by $\mathbf{Q}_k$ and a time-varying part captured by the complex rotation matrix $\tilde{\boldsymbol{\Lambda}}[i]$. The time-invariant part is fixed as long as the channel, the IQ imbalance parameters and the CFO are fixed. The complex rotation, on the other hand, changes from block to block. Note that, the complex rotation within the same OFDM block is fixed over all subcarriers. Exploiting this structure we can significantly reduce the computational complexity by computing the time-invariant part of the PTEQ and compensating for the time-variations by means of the complex rotation afterwards. On the implementation level, the PTEQ is explained in Figure 9.4. The implementation complexity associated with estimating a block of N symbols is $(N-2)((Q+L')+5)$ MA operations [1].

[1]Note here due to the IQ imbalance the symbols transmitted on the 0th and the $N/2$th subcarriers are not estimated.

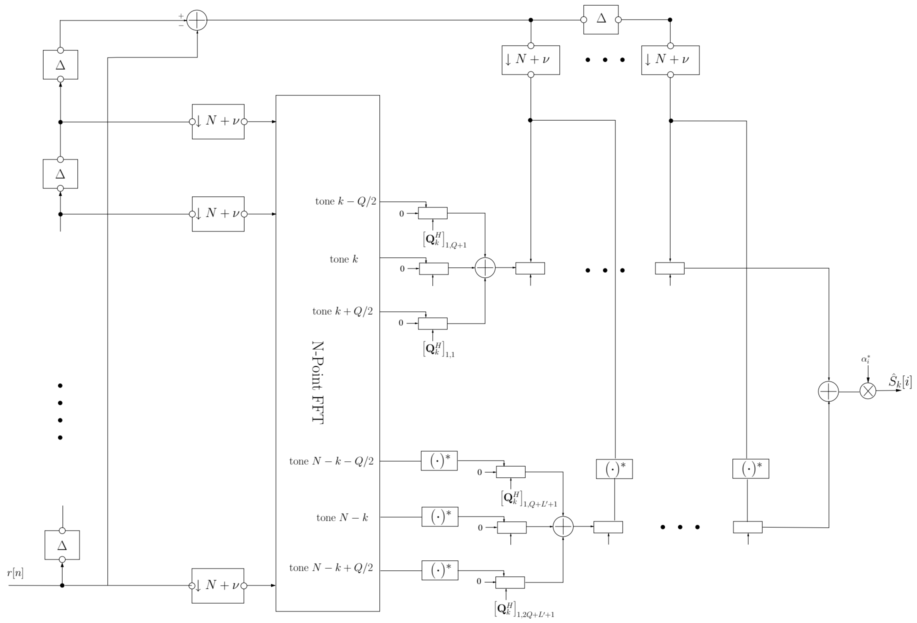

Figure 9.4: PTEQ for OFDM with IQ imbalance and CFO.

Contrary to the IQ imbalance only case, knowing the IQ imbalance parameters and CFO, will not help in developing time-domain separate compensation of CFO and IQ imbalance. Only joint algorithms are possible.

A Note on Time-Varying Channels with IQ Imbalance

So far we have treated the case of OFDM transmission over TI channels with IQ imbalance in the absence as well as in the presence of CFO. As mentioned earlier, in the presence of CFO (viewed as a source of time-variation and hence as a source of ICI) the PTEQ is split into two parts; a time-invariant part that can be incorporated in the equalizer and a time-varying part than can be compensated for by means of a time-varying complex rotation. For time-varying channels, the channel time variation caused by the Doppler effect (user's mobility) and that caused by CFO are inseparable. Therefore, the problems of OFDM transmission over time-varying channel with IQ imbalance in the presence of CFO or in the absence of CFO are equal. Hence, for the case of a BEM resolution of $K = N$, the PTEQ equalizer is similar to the one developed in Figure 9.4 except for the fact that the PTEQ is time-varying and can not be split into time-invariant and time-varying parts. For a BEM resolution of $K = rN$ with r integer $r > 1$ (when a better BEM fit is sought) the PTEQ structure is slightly different than that proposed in Figure 9.4. In addition to taking into account the modulation on the pth branch, a $-p$th modulated version is also required. This is still under further investigation.

RLS Initialization

In order to obtain the PTEQ (9.32), the channel as well as the IQ parameters and the CFO must be known/estimated. In this section, we devise a training-based RLS direct equalization/estimation of the time-invariant part of the PTEQ assuming that only the CFO is known at the receiver. In a similar fashion to the RLS algorithm devised in Section 9.3, assuming that I OFDM symbols are available for training, the optimal $\mathbf{Q}_k$ for the kth subcarrier can be computed as

$$\min_{\mathbf{Q}_k} \mathcal{J}(\mathbf{Q}_k) = \min_{\mathbf{Q}_k} \sum_{i=0}^{I-1} \left\| \tilde{\mathbf{\Lambda}}[i]\tilde{\mathbf{s}}_k[i] - \mathbf{Q}_k^H \tilde{\mathbf{r}}_k[i] \right\|^2 \tag{9.33}$$

The RLS algorithm to compute the time-invariant part of the PTEQ is listed in Algorithm 9.2.

Algorithm 9.2 RLS Direct Equalization with CFO

for $k \in \{1, \ldots, N/2-1\}$ **do**
  initialize $\mathbf{R}_{\tilde{r}}^{k}[-1] = \kappa^{-1}\mathbf{I}$
  initialize $\mathbf{Q}_k[-1] = \mathbf{0}_{2(L'+1)(Q+1)\times 2}$
end for
for $i = 0$ to $I-1$ **do**
  for $k \in \{1, \ldots, N/2-1\}$ **do**
    $\mathbf{R}_{\tilde{r}}^{k^{-1}}[i] \leftarrow \mathbf{R}_{\tilde{r}}^{k^{-1}}[i-1] - \frac{\mathbf{R}_{\tilde{r}}^{k^{-1}}[i-1]\tilde{\mathbf{r}}_k[i]\tilde{\mathbf{r}}_k^H[i]\mathbf{R}_{\tilde{r}}^{k^{-1}}[i-1]}{1+\tilde{\mathbf{r}}_k^H[i]\mathbf{R}_{\tilde{r}}^{k^{-1}}[i-1]\tilde{\mathbf{r}}_k[i]}$
    $\mathbf{e}[i] = \tilde{\mathbf{s}}_k[i] - \mathbf{Q}_k^H[i-1]\tilde{\mathbf{r}}_k[i]$
    $\mathbf{Q}_k[i] \leftarrow \mathbf{Q}_k[i-1] + \frac{\mathbf{R}_{\tilde{r}}^{k^{-1}}[i-1]\tilde{\mathbf{r}}_k[i]}{1+\tilde{\mathbf{r}}_k^H[i]\mathbf{R}_{\tilde{r}}^{k^{-1}}[i-1]\tilde{\mathbf{r}}_k[i]}\mathbf{e}[i]^H$
  end for
end for
$\mathbf{Q}_k = \mathbf{Q}_k[I-1]$

9.5 Simulations

In this section we present some of the simulation results of the proposed equalization technique for OFDM transmission over time-invariant channels. We consider an OFDM system with $N = 64$ subcarriers. The time-invariant channel is of order $L = 6$. The channel taps are simulated as i.i.d complex Gaussian

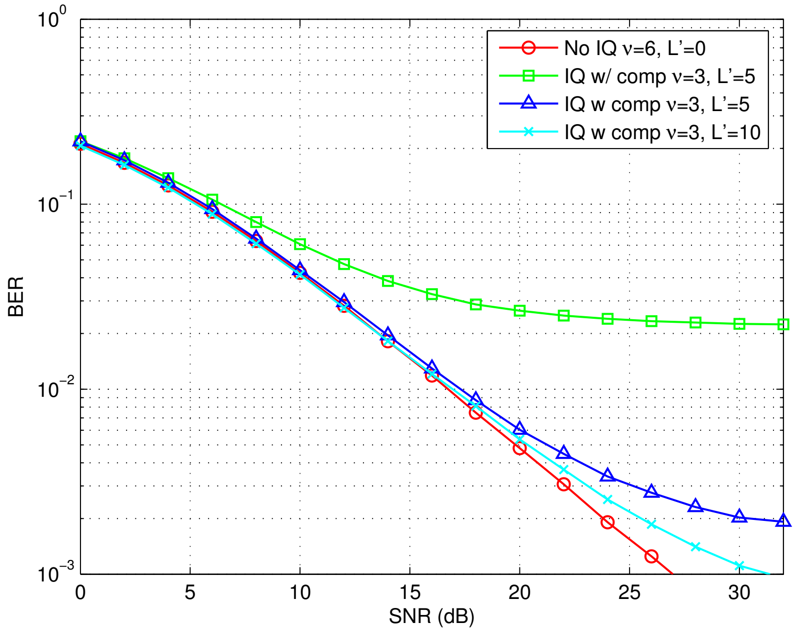

Figure 9.5: IQ compensation

random variables. The channel is kept fixed over a burst of transmission, and may change from burst to burst independently. The analog front-end of the OFDM receiver suffers from IQ imbalance and CFO.

First, we consider the case of IQ imbalance only (i.e. zero CFO). We consider an OFDM receiver with IQ phase imbalance $\Delta\phi = 10^o$ and IQ amplitude imbalance $\Delta a = 0.1$. We focus on the frequency-domain PTEQ obtained by transferring a TEQ operation to the frequency-domain.

In the first setup we assume that the channel and the IQ imbalance parameters (Δa and $\Delta\phi$) are known at the receiver. In Figure 9.5 we consider the following different scenarios:

- No IQ imbalance, no IBI ($\nu = L$), and $L' = 0$. This case corresponds to an ideal OFDM transmission over TI channels with perfect analog front-end. This case will serve as a benchmark for our equalizer.
- IQ imbalance and IBI with $\nu = 3$ are present. To evaluate the effect of the IQ imbalance on the system performance we design an equalizer that takes into account the IBI but not the IQ imbalance (no IQ compensation). A PTEQ of order $L' = 5$ is considered.

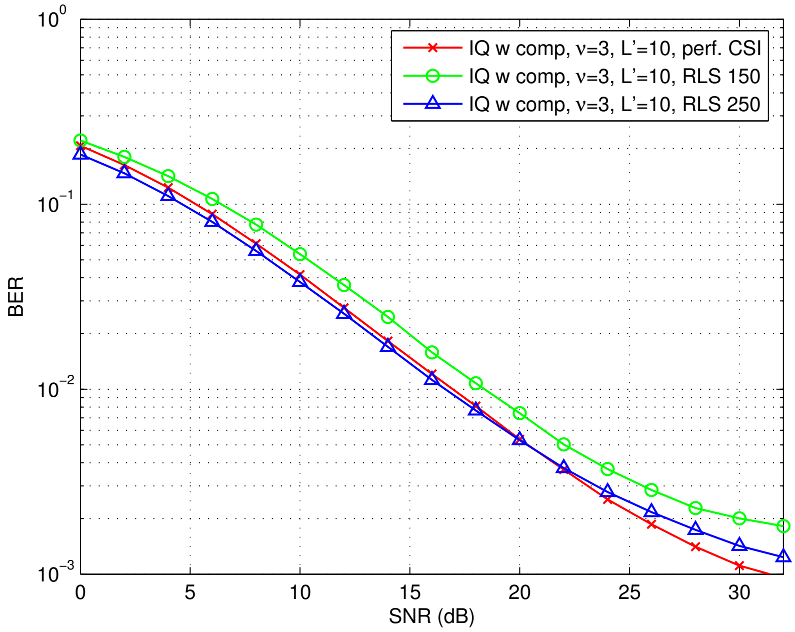

Figure 9.6: IQ RLS direct Equalization

- IQ imbalance and IBI with $\nu = 3$ are present. We design an equalizer that takes into account IBI and compensates for the IQ imbalance. The filter order is chosen to be $L' = 5$.

- This case is similar to the previous one, but the PTEQ order is chosen to be $L' = 10$.

As shown in Figure 9.5 the IQ imbalance degrades the performance significantly, where the BER curve suffers from an early error floor at $BER = 9 \times 10^{-1}$. IQ compensation enhances the performance significantly. A PTEQ with IQ compensation allows to approach the performance of the ideal OFDM system. For a PTEQ of order $L' = 5$, the BER error floor has been significantly reduced to 9×10^{-2}. For $L' = 10$ the performance is slightly improved and the error floor is reduced to 1×10^{-3}.

In the second setup, we assume that the channel and the IQ imbalance parameters are unknown at the receiver. In this case the training-based RLS type direct equalization listed as Algorithm 9.1 is considered. We consider an RLS scheme with $I = 150$ and $I = 250$ OFDM symbols available for training/initialization. We compare the obtained results with the case of perfect

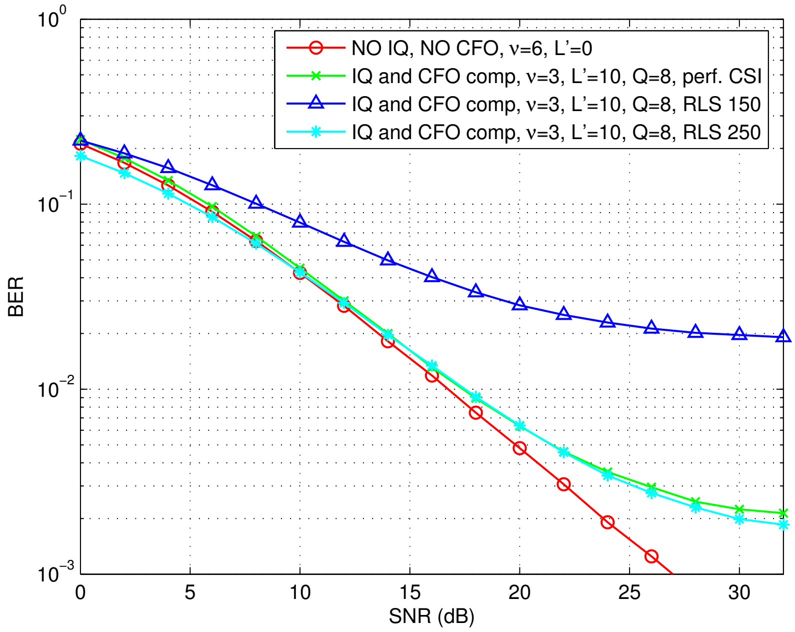

Figure 9.7: IQ and CFO direct Equalization

knowledge of the channel and the IQ parameters. As shown in Figure 9.6, the RLS scheme with $I = 150$ experiences a 1 dB loss in SNR compared to the perfect knowledge case, while the performance of the RLS scheme with $I = 250$ coincides with the perfect knowledge case.

Second, we consider that the OFDM receiver suffers from an IQ imbalance and CFO. The IQ imbalance parameters are assumed to be equal to the ones used before, i.e. IQ phase imbalance $\Delta\phi = 10^o$ and IQ amplitude imbalance $\Delta a = 0.1$. The CFO is assumed to be $\epsilon = 0.2$ (we consider the non-integer part of the CFO), since the integer part of the CFO results into a cyclic shift and does not contribute to the ICI. Again we focus on the frequency-domain PTEQ obtained by transferring the TEQ operation to the frequency-domain. The PTEQ is designed according to the BEM of order $L' = 10$ and the number of basis functions is $Q = 8$. The number of basis functions reflects the span of the ICI that is considered in the equalization process (which is in this case 4 neighboring subcarriers on each side).

In the first setup, we consider that the channel, the IQ imbalance parameters and the CFO are known at the receiver. As shown in Figure 9.7, the proposed PTEQ approaches the performance of ideal OFDM transmission over TI channels for low SNR values, and suffers from an error floor at $BER = 2 \times 10^{-3}$. This error floor results from the fact that there is residual ICI not compensated for. However, the error floor in this case is not that severe.

In the second setup, only the CFO is assumed to be known at the receiver. The training-based RLS type direct equalization listed as 9.2 is invoked to obtain the time-invariant part of the PTEQ. For the RLS algorithm we consider that $I = 150$ and $I = 250$ OFDM symbols are available for training. As shown in Figure 9.7, the RLS based direct equalization suffers from an error floor at $BER = 9 \times 10^{-1}$ for $I = 150$, while the performance coincides with the performance when perfect knowledge is assumed for $I = 250$. A slight enhancement is obtained for the RLS with $I = 250$ over the case when perfect knowledge of the system parameters is assumed. This is due to the fact that for the case of perfect knowledge we approximate the noise covariance matrix as $\mathbf{R}_{\breve{v}} = \sigma_n^2 \mathbf{I}$, which is not exact even under the assumption of white noise due to the IQ imbalance. The RLS algorithm appears to utilize the exact noise covariance matrix.

9.6 Conclusions

In this chapter we have proposed a frequency-domain PTEQ for OFDM transmission over time-invariant channels with imperfect analog front-end receivers. The CP length is assumed to be smaller than the channel order, which means that IBI is also present. We have shown that analog front-end imperfections degrade the performance significantly, and therefore equalization and analog front-end imperfection compensation are crucial. For the case of IQ imbalance only we devised a PTEQ to compensate for the channel and IQ imbalance under the assumption of knowing the channel and the IQ imbalance parameters. A more realistic scenario is either to estimate these parameters or to obtain the equalizer coefficients directly. In this sense we have developed a training-based RLS initialization scheme. For the case of IQ imbalance and CFO, the resulting PTEQ is time-varying. However, it was shown that if CFO is known the time-varying equalizer can be split into two parts assuming the input data source is white. A time-invariant part, and a time-varying part captured by means of complex rotation. In all cases a training-based RLS scheme can be used to design the time-invariant part of the PTEQ.

Chapter 10

Conclusions and Future Research

In this chapter we highlight the main conclusions in Section 10.1, and directions for further research in Section 10.2.

10.1 Conclusions

The goal of this thesis was to develop reliable transmission techniques over time- and frequency-selective channels. The thesis was divided into two parts, the first part was concerned with reliable SC transmission over doubly selective channels, and the second part was concerned with OFDM transmission over time- and frequency-selective channels as well as joint channel equalization analog front-end compensation for OFDM transmission over TI channels.

An overview study of the mobile wireless channel was presented in **Chapter 2**. It was shown that the mobile wireless channel is generally characterized as doubly selective in time and in frequency due to multipath propagation and user's mobility. Multipath propagation was shown to result in frequency-selectivity which in turn was shown to introduce ISI in time-domain. While user's mobility was shown to introduce time-variation which in turn was shown to induce ICI in the frequency-domain. Multipath propagation results from reflection, diffraction, and scattering of the radiated electromagnetic waves of buildings and other objects that lie in the vicinity of the transmitter and/or receiver. In this chapter, the main channel parameters of the underlying wireless channel were studied mainly under the WSSUS assumption. The basis expansion channel model and its relationship to the well known Jakes' channel model was also introduced.

Part I of this thesis investigated single carrier transmission over doubly selective channels. Future generations wireless systems are required to provide high data rates to high mobility users. For such scenarios, conventional time-invariant equalization schemes or adaptive schemes that are suitable for slowly time-varying channels are inadequate to cope with the mobile wireless channel, since the channel may vary significantly from sample to sample. In this part we presented channel equalization and estimation schemes as follows.

In **Chapter 3** we focused on the problem of linear equalization for SC transmission over doubly selective channels. We mainly derived the zero forcing (ZF) and minimum mean square-error (MMSE) equalizers. In this chapter we focused on two categories of linear equalizers, block linear equalizers (BLEs), and serial linear equalizers (SLEs). While the first type equalized a block of received samples, the second type operated on a sample by sample basis. However, the design and implementation of the SLEs was done on a block level basis. Implementing the SLE using time-varying FIR filters modeled using a BEM was shown to turn a complicated 1-D time-varying deconvolution problem into a simpler TI 2-D deconvolution problem. It was also shown that the SLEs can approach the performance of the BLES by judiciously choosing the equalizer's parameters but keeping the complexity of designing and implementing the SLEs much lower. In addition to this, we showed that using the BEM window size $K = 2N$ is sufficient to eliminate the modeling error and consequently the resulting error floor in BER performance. As far as the ZF solution was concerned, it was shown that a ZF solution for the SLE existed for sufficiently large Q' and L' when at least 2 receive antennas are used. State of the art equalizers, required at least $Q + 1$ receive antennas for the ZF solution to exist. It was also shown the the proposed equalization techniques unify and extend many existing techniques for TI as will as for time-selective frequency flat channels.

In **Chapter 4** we investigated decision feedback equalization of doubly selective channels. Similar to Chapter 3, two types of equalizers were considered, block decision feedback equalizers (BDFEs) and serial decision feedback equalizers (SDFEs). In general decision feedback equalizers (DFEs) consist of feedforward and feedback equalizers. SDFEs were designed to consist of feedforward and feedback filters. The feedforward and feedback filters were implemented using time-varying FIR filters modeled using the BEM. By this way, it was shown that a complicated 1-D time-varying deconvolution problem can be turned into a simpler TI 2-D deconvolution problem. It was also shown that judiciously choosing the feedforward and feedback filter coefficients, the performance of the BDFE can be approached. Using a BEM window of size $K = 2N$ was shown to be enough to eliminate the BER error floor.

In **Chapters 3 and 4** the equalizers (linear or decision feedback) were designed given that perfect channel state information was available at the receiver. Therefore, the channel BEM coefficients were then obtained by LS fitting of the true channel. In **Chapter 5** we investigated the problem of channel estimation and direct equalization based on pilot symbol assisted modulation (PSAM) techniques. PSAM-based channel estimation techniques were shown to suffer from an error floor for BEM window size $K = N$, and to be sensitive to system noise for $K = 2N$. Error floor and noise sensitivity were shown to be greatly eliminated by combining the MMSE Wiener solution and the LS technique. In contrast to PSAM channel estimation, PSAM direct equalization performed better for $K = N$ than for $K = 2N$.

Using pure pilot symbols for channel estimation and/or direct equalization can be actually either skipped resulting in blind techniques or combined with blind techniques resulting in semi-blind techniques as discussed in **Chapter 6**. In this chapter we showed that blind and semi-blind techniques can be applied to the case of doubly selective channels. These results obtained there showed to extend results obtained for the case of TI channels.

Part II of this thesis investigated OFDM transmission over doubly selective channels and OFDM over TI channels with analog front-end impairments at the receiver side. Similar to the case of SC transmission, conventional time- or frequency-domain equalization techniques were not adequate to cope with the problems introduced due to the challenging problem of the underlying mobile wireless communication channel. In OFDM transmission, time-varying channels were shown to induce ICI, i.e. the energy of a particular subcarrier is leaked to neighboring subcarriers. Time-domain and/or frequency-domain equalization techniques were designed to cope with the problem of ICI.

In **Chapter 7**, a brief overview of OFDM transmission was given. System model and ICI analysis were also covered.

In **Chapter 8**, we proposed a time-domain and frequency-domain per-tone equalization techniques. In addition to the time-variation of the channel, the CP length was assumed to be shorter than the channel impulse response, which in turn showed to introduce inter-block interference (IBI). Non triviality constraints were necessary to design the time-domain equalizers. While TEQs optimized the performance on all subcarriers in a joint fashion, an optimal per-tone equalizer was obtained through transferring the TEQ operation to the frequency-domain resulting in per-tone equalizers (PTEQ). It was shown that PTEQs combine adjacent subcarriers to estimate the QAM symbol transmitted on a particular subcarrier. The error floor due to the channel modeling error and residual ICI were shown to be greatly reduced by using a BEM window size greater than the block length. A BEM window size of length $K = PN$, with $P \in \mathbb{Z}^+$ was shown to correspond to frequency-oversampling in the frequency-domain with the oversampling rate equal to P. An oversampling rate of $P = 2$ was shown to improve the performance significantly and to be sufficient to overcome the channel modeling error and ICI problem.

Chapter 9 investigated the problem of OFDM transmission over TI channels with receiver analog front-end impairments. Mainly, IQ imbalance and CFO were considered. It was shown that IQ imbalance results in a mirroring effect while CFO induces ICI. Joint frequency-domain channel equalization and digital compensation schemes were considered. For the case of CFO, it was shown that combining adjacent subcarriers to a particular subcarrier and its mirror is effective to recover the transmitted symbol on that particular subcarrier. It was also shown that, the time-varying equalizer can be split into two parts, a TI part and a time-varying part captured by means of a complex rotation. A training-based RLS direct equalization was shown to be able to obtain the PTEQ coefficients given that CFO is known.

10.2 Further Research

This thesis is just a first step in developing reliable communications over time- and frequency-selective channels. The following are interesting directions for further research.

Exploiting the time-varying Channel Diversity

In spite of the fact that time- and frequency-selective channels introduce ISI in time-domain and ICI in frequency-domain, they provide multipath diversity as well as Doppler diversity. Exploiting the time- and frequency diversity of the doubly selective channel can be achieved by linearly pre-coding the transmitted signal. Maximum diversity is then guaranteed when the optimal maximum likelihood decoder is invoked at the receiver, which showed to be very complex. The potential time-diversity of a time-varying frequency-flat fading channel[1] is shown in Figure 10.1. In this figure, the diversity order is measured by the slope of the BER curve. The higher the slope the higher the diversity order. As it is clear from this figure, the diversity order is proportional to the normalized Doppler spread $f_{\max}T$.

In this thesis we proposed an alternative equalization techniques based on time-varying FIR filters for SC as well as for OFDM transmission. The proposed equalization schemes were based on approximating the doubly selective channel and designing the time-varying FIR using the BEM. The proposed equalization scheme is for uncoded transmission. Applying these schemes to linearly pre-coded transmissions will not be able to exploit the diversity offered by the doubly selective channel. Alternative to ML schemes, low complexity joint

[1] Also corresponds to the matched filter bound for OFDM transmission over doubly selective channels

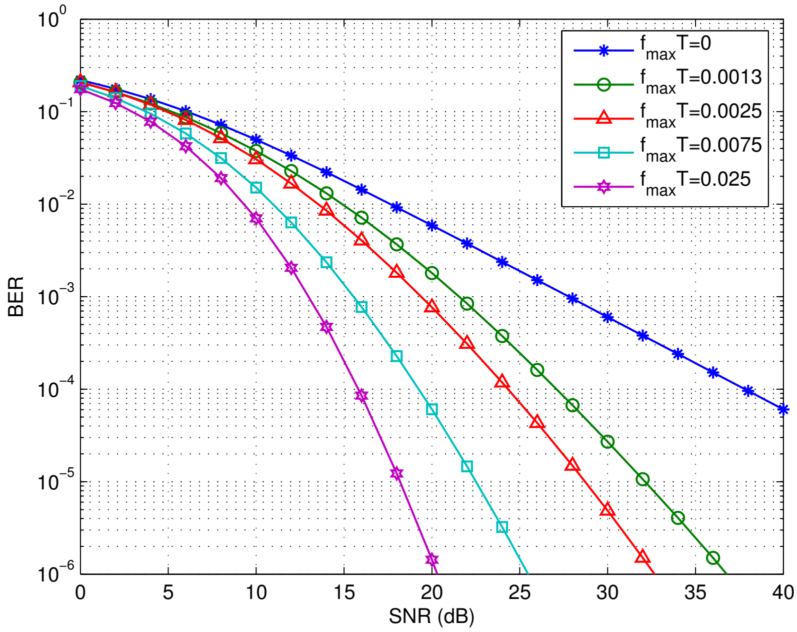

Figure 10.1: Diversity of time-varying flat fading channels

equalization and decoding schemes are an interesting direction for further research.

Channel Estimation and Tracking

Channel estimation and tracking are of crucial importance in system performance for both SC and OFDM transmission over doubly selective channels. Optimal channel estimation schemes (PSAM based, blind and semi-blind techniques) are interesting directions for further investigation especially for OFDM transmission. Part I of this thesis investigated channel estimation for SC transmission. Little, however, is known about optimal training design for doubly selective channel estimation. For the case of TI channels, a pilot-based optimal training design for OFDM transmission was investigated in [83] for SISO systems, and in [108, 11, 9, 70] for MIMO systems. The extension to doubly selective channels requires further investigation.

Multiuser Detection

Multiuser detection for transmission over doubly selective channels is another open issue. Multiuser detection based on CDMA or MC-CDMA implemented using OFDM are strong candidates for future wireless systems. For TI channels this problem was extensively studied for example in [61, 127, 113]. Extending the results to doubly selective channels is not straightforward and requires extensive investigations.

Digital Compensation for MIMO OFDM with Transmitter and Receiver Analog Front-End Imperfection

MIMO systems promise a huge increase in data rates over conventional SISO systems [55, 100, 7]. MIMO systems can be either used for spatial multiplexing (SM) based transmission schemes or space time coding (STC) based transmission schemes. Broadband MIMO OFDM is a strong candidate for future WLAN systems [96] (SM or STC). In Chapter 9 we assume SISO OFDM transmission over TI channels. We show there that OFDM is sensitive to analog front-end impairments, and thus joint channel equalization and analog front-end impairments compensation is necessary. Studying the effect of IQ imbalance and CFO on MIMO OFDM is timely and of great importance considering SM MIMO OFDM and STC MIMO OFDM. Early work is this area considering only IQ imbalance is studied in [99].

Bibliography

[1] K. Abed-Meraim, P. Loubaton, and E. Moulines. A Subspace Algorithm for Certain Blind Identification Problems. *IEEE Trans. Inform. Theory*, 43(2):499–511, March 1997.

[2] K. Abed-Meraim, W. Qiu, and Y. Hua. Blind system Identification. *Proc. IEEE*, 85(8):1310–1322, August 1997.

[3] N. Al-Dhahir. FIR Channel-Shortening Equalizers for MIMO ISI Channels. *IEEE Trans. Commun.*, 49(3):213–218, February 2001.

[4] N. Al-Dhahir and J. Cioffi. Efficiently Computed Reduced-Parameter Input-Aided MMSE Equalizers for ML Detection: A Unified Approach. *IEEE Trans. Inform. Theory*, 42(3):903–915, May 1996.

[5] N. Al-Dhahir and J. M. Cioffi. MMSE Decision-Feedback Equalizers: Finite Length Results. *IEEE Trans. Inform. Theory*, 41(4):961–975, July 1995.

[6] N. Al-Dhahir and J. M. Cioffi. Optimum Finite-Length Equalization for Multicarrier Transceivers. *IEEE Trans. Commun.*, 44(1):56–64, January 1996.

[7] S. A. Alamouti. A Simple Transmit Diversity Technique for Wireless Communication. *IEEE J. Select. Areas Commun.*, 16(8):1451–1458, October 1998.

[8] J. Armstrong. Analysis of New and Existing Methods of Reducing Intercarrier Interference Due to Carrier Frequency Offset in OFDM. *IEEE Trans. Commun.*, 47(3):365–369, March 1999.

[9] I. Barhumi, G. Leus, and M. Moonen. Optimal Training Sequences for Channel Estimation in MIMO OFDM Systems in Mobile Wireless Channels. In *International Zürich Seminar on Broadband Communications, Transmission, Access, and Networking, (IZS02)*, pages 44–1–44–6, Zürich, Switzerland, February, 18-21 2002.

[10] I. Barhumi, G. Leus, and M. Moonen. Frequency-Domain Equalization for OFDM over Doubly Selective Channels. In *Sixth Baiona Workshop on Signal Processing in Communications*, pages 103–107, Baiona, Spain, September 8-10 2003.

[11] I. Barhumi, G. Leus, and M. Moonen. Optimal Training Design for MIMO OFDM Systems in Mobile Wireless Channels. *IEEE Trans. Signal Processing*, 51(6):1615–1624, June 2003.

[12] I. Barhumi, G. Leus, and M. Moonen. Time-Varying FIR Decision Feedback Equalization of Doubly Selective Channels. In *IEEE Global Communications Conference*, volume 4, pages 2263–2268, San Francisco, CA USA, December, 1-5 2003.

[13] I. Barhumi, G. Leus, and M. Moonen. Time-Varying FIR Equalization of Doubly Selective Channels. In *IEEE Int. Conf. on Communications*, volume 5, pages 3246–3250, Anchorage, Alaska USA, May, 11-15 2003.

[14] I. Barhumi, G. Leus, and M. Moonen. Per-Tone Equalization for OFDM over Doubly Selective Channels. In *IEEE Int. Conf. on Communications*, Paris, France, June 2004.

[15] I. Barhumi, G. Leus, and M. Moonen. Time-Domain and Frequency-Domain Per-Tone Equalization for OFDM over Doubly Selective Channels. *Signal Processing*, 84/11:2055–2066, 2004. Special Section Signal Processing in Communications.

[16] I. Barhumi, G. Leus, and M. Moonen. Time-Domain Channel Shortening and Equalization of OFDM over Doubly Selective Channels. In *IEEE Int. Conf. on Acoustics, Speech, and Signal Processing*, Montreal, Canada, May 2004.

[17] I. Barhumi, G. Leus, and M. Moonen. Equalization for OFDM over Doubly Selective Channels. *IEEE Trans. Signal Processing*, February 2005. (accepted).

[18] I. Barhumi, G. Leus, and M. Moonen. Estimation and Direct Equalization of Doubly Selective Channels. *EURASIP Journal on Applied Signal Processing*, 2005. Submitted to Special issue on Reliable Communications over Rapidly Time-Varying Channels.

[19] I. Barhumi, G. Leus, and M. Moonen. MMSE Estimation of Basis Expansion Models for Rapidly Time-Varying Channels. In *EUSIPCO*, Antalya, Turkey, September 4-8 2005. Accepted.

[20] I. Barhumi, G. Leus, and M. Moonen. Time-Varying FIR Equalization of Doubly Selective Channels. *IEEE Trans. Wireless Commun.*, 4(1):202–214, January 2005.

[21] I. Barhumi and M. Moonen. IQ Compensation for OFDM in the Presence of IBI and Carrier Frequency-Offset. *IEEE Trans. Signal Processing*, May 2005. (submitted).

[22] I. Barhumi and M. Moonen. IQ Compensation for OFDM in the Presence of IBI and Carrier Frequency-Offset. In *IEEE Int. Conf. on Communications*, Istanbul, Turkey, 11-15 June 2006. (to be submitted).

[23] C. Belfiore and J. Park Jr. Decision Feedback Equalization. *Proc. IEEE*, 67(8):1143–1156, August 1979.

[24] P. A. Bello. Characterization of Randomly Time-Variant Linear Channels. *IEEE Trans. Commun. Sys.*, CS-11(4):360–393, December 1963.

[25] J.A.C. Bingham. Multicarrier Modulation for Data Transmission: an Idea Whose Time has Come. *IEEE Commun. Mag.*, 28(5):5–14, May 1990.

[26] D. K. Borah and B. D. Hart. A Robust Receiver Structure for Time-Varying Frequency-Flat, Rayleigh Fading Channels. *IEEE Trans. Commun.*, 47(3):360–364, March 1999.

[27] D. K. Borah and B. D. Hart. Receiver Structure for Time-Varying Frequency-Selective Fading Channels. *IEEE J. Select. Areas Commun.*, 17(11):1863–1875, November 1999.

[28] X. Cai and G. B. Giannakis. Low-Complexity ICI Suppression for OFDM over Time- and Frequency-Selective Rayleigh Fading Channels. In *Proc. of 36th Asilomar Conf. on Signals, Systems, and Computers*, pages 1822–1826, Pacific Grove, CA, November 2002.

[29] X. Cai and G. B. Giannakis. Bounding Performance and Suppressing Inter-Carrier Interference in Wireless Mobile OFDM. *IEEE Trans. Commun.*, 51(12):2047 – 2056, December 2003.

[30] J. K. Cavers. An Analysis of Pilot Symbol Assisted Modulation for Rayleigh Fading Channels [Mobile Radio]. *IEEE Trans. Veh. Technol.*, 40(4):686–693, November 1991.

[31] Y.-S. Choi, P. J. Voltz, and F. A. Cassara. On Channel Estimation and Detection for Multicarrier Signals in Fast and Selective Rayleigh Fading Channels. *IEEE Trans. Commun.*, 49(8):1375–1387, August 2001.

[32] J. S. Chow and J. M. Cioffi. A Discrete Multitone Transceiver System for HDSL Applications. *IEEE J. Select. Areas Commun.*, 9(6):895–907, August 1991.

[33] Jr. L. Cimini. Analysis and Simulation of a Digital Mobile Channel Using Orthogonal Frequency Division Multiplexing. *IEEE Trans. Commun.*, 33(7):665–675, July 1985.

[34] M. V. Clark. Adaptive Frequency-Domain Equalization and Diversity Combining for Broadband Wireless Communications. *IEEE J. Select. Areas Commun.*, 16(8):1385–1395, October 1998.

[35] A. Duel-Hallen. Decorrelating Decision-Feedback Multiuser Detectors for Synchronous Code-division Multiple-Access Channel. *IEEE Trans. Commun.*, 41(2):285–290, February 1993.

[36] A. E. El-Mahdy. Adaptive Channel Estimation and Equalization for Rapidly Mobile Communication Channels. *IEEE Trans. Commun.*, 52(7):1126–1135, July 2004.

[37] ETSI Digital Video Broadcasting (DVB); Framing Structure, Channel Coding and Modulation for Digital Terrestrial Television, August 2001.

[38] T. Ericson. Structure of Optimum Receiving Filters in Data Transmission Systems. *IEEE Trans. Inform. Theory*, IT-17(5):352–353, May 1971.

[39] E. Eweda. Comparisons of RLS, LMS, and Sign Algorithms for Tracking Randomly Time-Varying Channels. *IEEE Trans. Signal Processing*, 42(11):2937–2944, November 1994.

[40] D. Falconer and L. Ljung. Application of Fast Kalman Estimation to Adaptive Equalization. *IEEE Trans. Commun.*, 26(10):1439–1446, October 1988.

[41] D. D. Falconer and F. R. Magee. Adaptive Channel Memory Truncation for Maximum Likelihood Sequence Estimation. *Bell Syst. Tech. J.*, 52(11):1541–1562, November 1973.

[42] B. Farhang-Boroujeny and S. Gazor. Generalized Sliding FFT and its Application to Implementation of Block LMS Adaptive Filters. *IEEE Trans. Signal Processing*, 42(3):532–538, March 1994.

[43] S. Fouladifard and H. Shafiee. Frequency Offset Estimation in OFDM Systems in Presence of IQ Imbalance. In *ICCS*, Singapore, November 2002.

[44] D. Gesbert, P. Duhamel, and S. Mayrargue. On-Line Blind Multichannel Equalization Based on Mutually Referenced Filters. *IEEE Trans. Signal Processing*, 45(9):237–2317, September 1997.

[45] G. B. Giannakis, Y. Hua, P. Stoica, and L. Tong, editors. *Signal Processing Advances in Wireless & Mobile Communications: Trends in Single and Multi-User Systems.* Prentice-Hall, Inc., 2001.

[46] G. B. Giannakis and C. Tepedelenlioğlu. Basis Expansion Models and Diversity Techniques for Blind Identification and Equalization of Time-Varying Channels. *Proc. IEEE*, 86(10):1969–1986, October 1998.

[47] G. B. Giannakis and C. Tepedelenlioğlu. Direct Blind Equalization of Multiple FIR Channels: A Deterministic Approach. *IEEE Trans. Signal Processing*, 47(1):62–74, January 1999.

[48] A. Ginesi, G. M. Vitetta, and D. D. Falconer. Block Channel Equalization in the Presence of a Cochannel Interferent Signal. *IEEE J. Select. Areas Commun.*, 17(11):1853–1862, November 1999.

[49] G.H. Golub and C.F. Van Loan. *Matrix Computations*. Johns Hopkins University Press, third edition, 1996.

[50] E. Hänsler. Some Properties of Transmission Systems with Minimum Means Square Error. *IEEE Trans. Commun.*, COM-19(8):576–579, August 1971.

[51] L. Hanzo. Bandwidth-Efficient Wireless Multimedia Communications. *Proc. IEEE*, 86(7):1342–1382, July 1998.

[52] ETSI Broadband Radio Access Networks (BRAN); HIPERLAN Type 2 Technical Specification; Physical Layer, August 1999.

[53] W. Honcharenko, J. P. Kruys, D. Y. Lee, and N. J. Shah. Broadband Wireless Access. *IEEE Commun. Mag.*, 35(1):20–26, January 1997.

[54] IEEE 802.11 Local and Metropolitan Area Networks: Wireless LAN Medium Acess Control (MAC) and Physical (PHY) Specifications., 1999.

[55] M. Gans J. Foschini. On the Limit of Wireless Communications in a Fading Environment when Using Multiple Antennas. *Wireless Personal Communications*, 6(3):311–335, March 1998.

[56] W. C. Jakes, editor. *Microwave Mobile Communications*. Wiley, 1974.

[57] W. G. Jeon, K. H. Chang, and Y. S. Cho. An Equalization Technique for Orthogonal Frequency Division Multiplexing Systems in Time-Variant Multipath Channels. *IEEE Trans. Commun.*, 47(1):27–32, January 1999.

[58] G. Forney Jr. Maximum Likelihood Sequence Estimation of Digital Sequences in the Presence of Intersymbol Interference. *IEEE Trans. Inform. Theory*, IT-18(5):363–378, May 1972.

[59] T. Kailath. Measurements on Time-Variant Communications Channels. *IRE Trans. Information Theory*, 8(5):229–236, September 1962.

[60] T. Kailath, A. H. Sayed, and B. Hassibi. *Linear Estimation*. Prentice-Hall, Englewood Cliffs, NJ, 2000.

[61] A. Klein and P. Baier. Linear Unbiased Data Estimation in Mobile Radio System Applying CDMA. *IEEE J. Select. Areas Commun.*, 11:1058–1066, September 1993.

[62] A. Klein, G. K. Kaleh, and P. W. Baier. Zero Forcing and Minimum Mean-Square Error Equalization For Multiuser Detection in Code-Division Multiple-Access Channels. *IEEE Trans. Veh. Technol.*, 45(2):276–287, May 1996.

[63] R. Lawrence and H. Kaufman. The Kalman Filter for the Equalization of a Digital Communications Channel. *IEEE Trans. Commun.*, 19(6):1137–1141, December 1971.

[64] T. Lee and D. Cunningham. Kalman Filter Equalization for QPSK Communications. *IEEE Trans. Commun.*, 24(3):361–364, mar 1976.

[65] G. Leus, I. Barhumi, and M. Moonen. Low-Complexity Serial Equalization of Doubly Selective Channels. In *Sixth Baiona Workshop on Signal Processing in Communications*, pages 69–74, Baiona, Spain, September8-10 2003.

[66] G. Leus, I. Barhumi, and M. Moonen. MMSE Time-Varying FIR Equalization of Doubly Selective Channels. In *IEEE Int. Conf. on Acoustics, Speech, and Signal Processing*, volume 4, pages IV–485–8, Hong Kong, April 6-10 2003.

[67] G. Leus, I. Barhumi, O. Rousseaux, and M. Moonen. Direct Semi-Blind Design of Serial Linear Equalizers for Doubly Selective Channels. In *IEEE Int. Conf. on Communications*, Paris, France, June 19-24 2004.

[68] G. Leus and M. Moonen. Deterministic Subspace Based Blind Channel Estimation for Doubly Selective Channels. In *IEEE Workshop on Signal Processing Advances in Wireless Communications*, pages 210–214, Rome, Italy, June 15-18 2003.

[69] G. Leus, S. Zhou, and G. B. Giannakis. Orthogonal Multiple Access over Time- and Frequency-Selective Fading. *IEEE Trans. Inform. Theory*, 49(4):1942–1950, August 2003.

[70] Y. Li. Simplified Channel Estimation for OFDM Systems with Multiple Transmit Antennas. *IEEE Trans. Wireless Commun.*, 1(1):67–75, January 2002.

[71] Y. (Geoffrey) Li and L. J. Cimini Jr. Bounds on the Interchannel Interference of OFDM in Time-Varying Impairments. *IEEE Trans. Commun.*, 49(3):401–404, March 2001.

[72] J. Lin, J. Proakis, F. Ling, and H. Lev-Ari. Optimal Tracking of Time-Varying Channels: A Frequency Domain Approach for Known and New Algorithms. *IEEE J. Select. Areas Commun.*, 13(1):141–154, January 1995.

[73] L. Lindbom, M. Sterand, and A. Ahlén. Tracking of Time-Varying Mobile Radio Channels, Part I: The Weiner LMS Algorithm. *IEEE Trans. Commun.*, 49(12):2207–2217, December 2001.

[74] C.-L. Liu. Impacts of I/Q Imbalance on QPSK-OFDM-QAM Detection. *IEEE Trans. Consumer Electron.*, 44(3):984–989, August 1998.

[75] H. Liu and G. B. Giannakis. Deterministic Approaches for Blind Equalization of Time-Varying Channels with Antenna Arrays. *IEEE Trans. Signal Processing*, 46(11):3003–3013, November 1998.

[76] K. Liu, T. A. Kadous, and A. M. Sayeed. Orthogonal Time-Frequency Signaling for Doubly Dispersive Channels. *IEEE Trans. Inform. Theory*, 50(11):2583–2603, November 2004.

[77] X. Ma and G. B. Giannakis. Maximum-Diversity Transmissions over Doubly Selective Wireless Channels. *IEEE Trans. Inform. Theory*, 49(7):1823–1840, July 2003.

[78] X. Ma, G. B. Giannakis, and S. Ohno. Optimal Training for Block Transmissions over Doubly Selective Fading Channels. *IEEE Trans. Signal Processing*, 51(5):1351–1366, May 2003.

[79] M. Martone. Wavelet-Based Separating Kernels for Array Processing of Cellular DS/CDMA Signal in Fast Fading. *IEEE Trans. Commun.*, 48(6):979–995, June 2000.

[80] P. Monsen. Feedback Equalization for Fading Dispersive Channels. *IEEE Trans. Inform. Theory*, IT-17(1):1144–1153, January 1971.

[81] P. H. Moose. A Technique for Orthogonal Frequency Division Multiplexing Frequency Offset Correction. *IEEE Trans. Commun.*, 42(10):2908–2914, October 1994.

[82] E. Moulines, P. Duhamel, J.-F. Cardoso, and S. Mayrargue. Subspace Methods for the Blind Identification of Multi-Channel FIR Filters. *IEEE Trans. Signal Processing*, 43(2):516–525, February 1995.

[83] R. Negi and J. Cioffi. Pilot Tone Selection for Channel Estimation in a Mobile OFDM System. *IEEE Trans. Consumer Electron.*, 44(3):1122–1128, August 1998.

[84] G. Proakis. *Digital Communications*. Prentice Hall, 2nd edition, 1995.

[85] S. U. H. Qureshi and E. E. Newhall. An Adaptive Receiver for Data Transmission over Time Dispersive Channels. *IEEE Trans. Inform. Theory*, 19(7):448–457, July 1973.

[86] T. S. Rappaport. *Wireless Communications: Principles and Practice*. Prentice Hall, 2nd edition, 2001.

[87] S. Ratnavel, A. Paulraj, and A. G. Constantinides. MMSE Space-Time Equalization for GSM Cellular Systems. In *Proc. of the Vehicular Technology Conference (VTC)*, Atlanta, GA USA, April/May 1996 96.

[88] H. Sari, G. Karam, and I. Jeanclaude. Transmission Techniques for Digital Terrestrial TV Broadcasting. *IEEE Commun. Mag.*, 33(2):100–109, February 1995.

[89] A. M. Sayeed and B. Aazhang. Joint Multipath-Doppler Diversity in Mobile Wireless Communications. *IEEE Trans. Commun.*, 47(1):123–132, January 1999.

[90] P. Schniter. Low-Complexity Equalization of OFDM in Doubly Selective Channels. *IEEE Trans. Signal Processing*, 52(4):1002–1011, April 2004.

[91] B. Sklar. Rayleigh Fading Channels in Mobile Digital Communication systems, Part I: Characterization. *IEEE Commun. Mag.*, 35(7):90–100, July 97.

[92] B. Sklar. Rayleigh Fading Channels in Mobile Digital Communication systems, Part II: Mitigation. *IEEE Commun. Mag.*, 35(7):102–109, July 97.

[93] D. Slock. Blind Fractionally-Spaced Equalization, Perfect-Reconstruction Filter Banks and Multichannel Linear Prediction. In *IEEE Int. Conf. on Acoustics, Speech, and Signal Processing*, volume 4, pages IV/585 –IV/588, 1994.

[94] A. Stamoulis, S. N. Diggavi, and N. Al-Dhahir. Intercarrier Interference in MIMO OFDM. *IEEE Trans. Signal Processing*, 50(10):2451 – 2464, October 2002.

[95] A. Stamoulis, G. B. Giannakis, and A. Scaglione. Block FIR Decision-Feedback Equalizers for Filterbank Precoded Transmissions with Blind Channel Estimation Capabilities. *IEEE Trans. Signal Processing*, 49(1):69–83, January 2001.

[96] G. Stüber, J. Barry, S. McLaughlin, Y. Li, M. Ingram, and T. Pratt. Broadband MIMO OFDM Wireless Communications. *Proc. IEEE*, 92(2):271–294, February 2004.

[97] K. Tachikawa. A Perspective on the Evolution of Mobile Communications. *IEEE Commun. Mag.*, 41(10):66–73, October 2003.

[98] A. Targhiat and A. H. Sayed. On the Baseband Compensation of IQ Imbalance in OFDM Systems. In *IEEE Int. Conf. on Acoustics, Speech, and Signal Processing*, Montreal, Canada, May 2004.

[99] A. Targhiat and A. H. Sayed. MIMO OFDM Receivers for Systems with IQ Imbalance. *IEEE Trans. Signal Processing*, 2005. To Appear.

[100] E. Telatar. Capacity of Multi-Antenna Gaussian Channels. *European Transactions on Telecommunications*, 10(6):585–595, November/December 1999.

[101] L. Tong and S. Perreau. Multichannel Blind Identification: From Subspace to Maximum Likelihood Methods. *Proc. IEEE*, 86(10):1951–1968, October 1998.

[102] M. K. Tsatsanis and G. B. Giannakis. Modeling and Equalization of Rapidly Fading Channels. *International Journal of Adaptive Control and Signal Processing*, 10(2/3):159–176, March 1996.

[103] J. Tubbax, B. Come, L. Van der Perre, L. Deneire, S. Donnay, and M. Engels. Compensation of IQ Imbalance in OFDM Systems. In *IEEE Int. Conf. on Communications*, Anchorage, Alaska USA, May, 11-15 2003.

[104] J. Tubbax, A. Fort, L. Van der Perre, S. Donnay, M. Engels, M. Moonen, and H. De Man. Joint Compensation of IQ Imbalance and Frequency Offset in OFDM Systems. In *IEEE Global Communications Conference*, San Francisco, CA USA, December, 1-5 2003.

[105] J. K. Tugnait. Linear Prediction Error Method for Blind Identification of Time-Varying Channels: Theoretical Results. In *IEEE Int. Conf. on Acoustics, Speech, and Signal Processing*, Salt Lake City, UT USA, May 2001.

[106] J. K. Tugnait and W. Luo. Blind Identification of Time-Varying Channels Using Multistep Linear Predictors. *IEEE Trans. Signal Processing*, 52(6):1739–1749, June 2004.

[107] J. K. Tugnait, L. Tong, and Z. Ding. Single User Channel Estimation and Equalization. *IEEE Signal Processing Mag.*, 17(3):17–28, May 2000.

[108] T. L. Tung, K. Yao, and R. E. Hudson. Channel Estimation and Adaptive Power Allocation for Performance and Capacity Improvement of Multiple-Antenna OFDM Systems. In *Proc. Third IEEE Signal Process. Workshop Signal Process. Adv. Wireless Commun.*, March 2001.

[109] M. Valkama and V. Koivunen. Advanced Methods for I/Q Imbalance Compensation in Communication Receivers. *IEEE Trans. Signal Processing*, 49(10):2335–2344, October 2001.

[110] K. van Acker, G. Leus, M. Moonen, O. van de Wiel, and T. Pollet. Per-tone Equalization for DMT-based Systems. *IEEE Trans. Commun.*, 49(1), January 2001.

[111] K. Vanbleu. *Advanced Equalization Techniques for DMT-Based Systems.* PhD thesis, Katholieke Universiteit Leuven, Leuven, Belgium, October 2004.

[112] K. Vanbleu, G. Ysebaert, G. Cuypers, M. Moonen, and K. Van Acker. Bitrate-Maximizing Time-Domain Equalizer Design for DMT-Based Systems. *IEEE Trans. Commun.*, 52(6):871–876, June 2004.

[113] M. K. Varanasi. Parallel Group Detection for Synchronous CDMA Communication over Frequency-Selective Rayleigh Fading Channels. *IEEE Trans. Inform. Theory*, 42(1):116–128, January 1996.

[114] M. K. Varanasi. Decision Feedback Multiuser Detection: A Systematic Approach. *IEEE Trans. Inform. Theory*, 45(1):219–240, January 1999.

[115] X. Wang and H. V. Poor. Blind Multiuser Detection: A Subspace Approach. *IEEE Trans. Inform. Theory*, 44(2):677–690, March 1998.

[116] Z. Wang and G. B. Giannakis. Wireless Multicarrier Communications, where Fourier Meets Shannon. *IEEE Signal Processing Mag.*, 17(3):29–48, May 2000.

[117] B. Widrow and E. Walach. On the Statistical Efficiency of the LMS Algorithm with Non-stationary Inputs. *IEEE Trans. Inform. Theory*, 30(2):211–221, March 1984.

[118] D. Williamson, R. A. Kennedy, and G. W. Pulford. Block Decision Feedback Equalization. *IEEE Trans. Commun.*, 40(2):255–264, February 1992.

[119] G. Xing, M. Shen, and H. Liu. Frequency Offset and IQ Imbalance Compensation for OFDM Direct Conversion Receivers. In *IEEE Int. Conf. on Acoustics, Speech, and Signal Processing*, Hong Kong, 2003.

[120] G. Xu, H liu, L. Tong, and T. Kailath. A Least-Squares Approach to Blind Identification. *IEEE Trans. Signal Processing*, 43(12):2982–2993, December 1995.

[121] G. Ysebaert, K. Van Acker, M. Moonen, and B. De Moor. Constraints in Channel Shortening Equalizer Design for DMT-based Systems. *Signal Processing*, 83(3):641–648, March 2003.

[122] G. Ysebeart. *Equalization and Echo Cancellation in DMT-Based Systems.* PhD thesis, Katholieke Universiteit Leuven, Leuven, Belgium, April 2004.

[123] J. H. Yu and Y. T. Su. Pilot-Assisted Maximum-Likelihood Frequency-Offset Estimation for OFDM Systems. *IEEE Trans. Commun.*, 52(11):1997–2008, November 2004.

[124] X. Yu and S. Pasupathy. Innovations-Based MLSE for Rayleigh Fading Channels. *IEEE Trans. Commun.*, 43(2/3/4):1534–1544, February/March/April 1995.

[125] H. Zhang and Y. Li. Optimum Frequency-Domain Partial Response Encoding in OFDM. *IEEE Trans. Commun.*, 51(7):1064–1068, July 2003.

[126] Y. Zhao and S. Häggman. Intercarrier Interference Self-Cancellation Scheme for OFDM Mobile Communication Systems. *IEEE Trans. Commun.*, 49(7):1185 – 1191, July 2001.

[127] Z. Zvonar and D. Brady. Suboptimal Multiuser Detector for Frequency Selective Rayleigh Fading Synchronous CDMA Channels. *IEEE Trans. Commun.*, 43(2/3/4):154–157, February/March/April 1995.

List of Publications

Journals

1. **I. Barhumi**, G. Leus, and M. Moonen, "Optimal Training Design for MIMO OFDM Systems in Mobile Wireless Channels", *IEEE Transactions on Signal Processing*, pp. 1615-1624, VOL. 51, NO. 6, June 2003.
2. **I. Barhumi**, G. Leus, and M. Moonen, "Time Varying FIR Equalization of Doubly-Selective Channels", *IEEE Trans. on Wireless Comm.*, pp. 202-214, VOL. 4, NO. 1, Jan. 2005.
3. **I. Barhumi**, G. Leus, and M. Moonen, "Time- and Frequency-Domain Per-Tone Equalization for OFDM over Doubly-Selective Channels", *Signal Processing*, vol. 84/11, pp. 2055-2066, 2004. Special Section Signal Processing in Communications.
4. **I. Barhumi**, G. Leus, and M. Moonen, "Equalization for OFDM over Doubly-Selective Channels", *IEEE Transactions on Signal Processing*, accepted January, 2005.
5. **I. Barhumi**, and M. Moonen, "IQ Compensation for OFDM in the presence of CFO and IBI", *IEEE Transactions on Signal Processing*, submitted May, 2005.
6. **I. Barhumi**, G. Leus, and M. Moonen, "Estimation and Direct Equalization of Doubly Selective Channels", *EURASIP Journal on Applied Signal Processing*, special issue on "Reliable Communications over Rapidly Time-Varying Channels", submitted June, 2005.

Conferences

1. **I. Barhumi**, and M. Moonen, "IQ Compensation for OFDM in the presence of CFO and IBI", ICC, 2005, *to be submitted.*

2. **I. Barhumi**, G. Leus and M. Moonen, “MMSE Estimation of Basis Expansion Models for Rapidly Time-Varying Channels”, EUSIPCO 2005, *accepted*.

3. **I. Barhumi**, G. Leus and M. Moonen, “Combined Channel Shortening and Equalization of OFDM over Doubly-Selective Channels”, in the IEEE 2004 International Conference on Acoustics, Speech and Signal Processing (ICASSP 2004), May 17-21, Montreal, Canada. (Invited Paper)

4. **I. Barhumi**, G. Leus and M. Moonen, “Frequency-domain Equalization for OFDM over Doubly-Selective Channels”, in the 2004 IEEE International Conference on Communications (ICC 2004), 20-24 June, Paris, France .

5. G. Leus, **I. Barhumi**, O. Rousseaux, and M. Moonen, “ ”Direct Semi-Blind Design of Serial Linear Equalizers for Doubly-Selective Channels”, in the 2004 IEEE International Conference on Communications (ICC 2004), June 19-24, Paris, France.

6. **I. Barhumi**, G. Leus and M. Moonen, “Frequency-domain Equalization for OFDM over Doubly-Selective Channels”, in Sixth Baiona Workshop on Signal Processing in Communications, September 8-10, 2003, Baiona, Spain.

7. G. Leus, **I. Barhumi**, and M. Moonen, “Low-Complexity Serial Equalization of Doubly-Selective Channels”, in Sixth Baiona Workshop on Signal Processing in Communications, September 8-10, 2003, Baiona, Spain.

8. **I. Barhumi**, G. Leus and M. Moonen, “Time Varying FIR Decision Feedback Equalization of Doubly-Selective Channels”, in IEEE 2003 Global Communications Conference (GLOBECOM’03), San Francisco, CA, December 2003.

9. **I. Barhumi**, G. Leus and M. Moonen, “Time-Varying FIR Equalization of Doubly-Selective Channels”, in the proceedings of the IEEE 2003 International Conference on Communications (ICC’03), 11-15 May, 2003 Anchorage, AK, USA

10. G. Leus, **I. Barhumi** and M. Moonen, “MMSE Time-Varying FIR Equalization of Doubly-Selective Channels”, in The IEEE 2003 International Conference on Acoustics, Speech, and Signal Processing (ICASSP’03),Hong Kong, April 6-10, 2003.

11. G. Leus, **I. Barhumi** and M. Moonen, “Per-Tone Equalization for MIMO OFDM Systems”, in the proceedings of the IEEE 2003 International Conference on Communications (ICC’03), 11-15 May, 2003 Anchorage, AK, USA

12. **I. Barhumi**, G. Leus and M. Moonen, "Optimal Training Sequences for Channel Estimation in MIMO OFDM Systems in Mobile Wireless Channels", International Zurich Seminar on Broadband Communications, Access, Transmission, Networking (IZS02), February 18-21, 2002, Zurich, Switzerland.

13. **I. Barhumi** and M. Moonen, "Optimal Training for Channel Estimation in MIMO OFDM Systems", ProRISC, October 27-31, 2001. Veldhoven, The Netherlands.

Curriculum Vitae

Imad Barhumi was born in Kafr Zeibadd, Palestine in 1972. He received the B.Sc. degree in Electrical Engineering from Birzeit University, Birzeit, Palestine in 1996, and the M.Sc. in Telecommunications from University of Jordan, Amman, Jordan in 1999. Since 2001 he has been pursuing a PhD at the Electrical Engineering Department (ESAT) of the Katholieke Universiteit Leuven, Belgium, under the supervision of Prof. Marc Moonen. His research interests are in the area of signal processing for telecommunications, specifically, channel estimation and equalization for mobile wireless communication systems.

From 1996-1997, he was with Palestine Telecommunications Company (PALTEL) as a network engineer. From 1998-2000, he was with the Electrical Engineering department at Birzeit University, Palestine as a lecturer. During his PhD he was partially funded by the Palestinian European Academic Cooperation in Education (PEACE) programme.